The metabolism of maltose in *Arabidopsis thaliana* leaves at night

Christian Ruzanski

A thesis submitted to the University of East Anglia for the degree of Doctor of Philosophy

John Innes Centre

Norwich

September 2011

Abstract

The aim of this work was to understand how maltose is metabolised in *Arabidopsis thaliana*. Maltose is the major degradation product of starch in leaves at night. The metabolism of maltose in the cytosol of leaf cells is very complex. It is believed to involve the interaction between a 4-α-glucanotransferase (DPE2) and a soluble heteroglycan (SHG). Despite the vital importance of starch degradation (and therefore maltose metabolism) for normal plant growth, little is known about the enzymes involved in maltose metabolism and the role of the heteroglycan.

My work revealed that DPE2 possesses unique structural features and biochemical properties that might be important for the interaction with SHG and that distinguish it from other 4-α-glucanotransferases. Using a novel carbohydrate substrate screen I discovered a range of previously unknown interaction partners of DPE2. I showed that these interactions are specific to DPE2 by comparing it to its bacterial orthologue, the 4-α-glucanotransferase of *E. coli* (MalQ). Moreover I established that DPE2 and MalQ share similar active site features but differ substantially in their maltose utilisation mechanism. These results highlight common features and important differences of the two enzymes and provide new perspectives on the metabolism of maltose in both organisms.

Making use of the *in vitro* findings I established transgenic Arabidopsis plants that lack DPE2 and express MalQ. By creating these plants, I successfully engineered a bypass mechanism that circumvents the requirement for SHG as intermediate in maltose metabolism in the plant cell. This result questions the importance of the SHG-DPE2 interaction in maltose metabolism in leaves at night.

Für den gläubigen Menschen steht Gott am
Anfang, für den Wissenschaftler am Ende
aller seiner Überlegungen

Max Planck

Acknowledgements

First and foremost I would like to express my deepest gratitude to Sabrina. Her love and support unlimited patience and believe in me carried me through my studies. I could not wish for anything better than her.

I am also very grateful to Professor Alison Smith and Prof Rob Field both of whom supervised my PhD project during the last 4 years. The supervision by Alison and Rob was on a very personal level and helped me to develop and advance my personal and scientific skills. They also allowed me great freedom to develop my project while their enthusiasm was inspiring. Their guidance, advice and support were invaluable and made this PhD thesis possible.

I also wish to thank Dr. Marilyn Pike and Dr Martin Rejzek for their support, valuable suggestions and constructive advice. With great confidence I can state that both belong to the SRA (Super Research Associates) clade of RAs.

Special thanks go to Dr. Paul Barratt and Dr. Alexander Graf for help and advice in the lab. I wish to extend my thanks to all past and present members of Alison's research group, especially Doreen Feike, Alastair Skeffington and Matilda Crumpton-Taylor for a warm and friendly working environment with a lot of interesting discussions.

I would also like to thank Graeme Kettles, Nikki Hockin (with whom I could stay for a couple of months when I got kicked out of my apartment at Neville Street), Naveed Ishaque, Erika Kuchen and Katrin Geisler for the fun times in Norwich and for being there when needed.

Finally, I would like to thank my whole family and especially my mother, Uta, for her faith, encouragement and support throughout the PhD, University and school time. Without that, nothing would have become possible.

Table of contents

3 Biochemical Analysis of DPE2

4. Biochemical Differences Between DPE2 and MalQ

List of Figures

List of Tables

Abbreviations

G3P	Glyceraldehyde-3-phosphate
ADP	Adenosine 5' diphosphate
ATP	Adenosine 5' triphosphate
cDNA	Complementary DNA
CER	Controlled environment room
DPE2	Disproportionating enzyme
DNA	Deoxyribonucleic acid
dNTP	2'-deoxyribonucleoside 5'-triphosphate
DP	Degree of polymerisation
DTT	Dithiothreitol
EDTA	Ethylene diaminetetraacetic acid
F6P	Fructose-6-phosphate
FPLC	Fast protein liquid chromatography
FW	Fresh weight
G1P	Glucose-1-phosphate
G6P	Glucose-6-phosphate
Glc3,4,5,6,7	Maltotriose, maltotetraose, maltopentaose, maltohexaose, maltoheptaose
HEPES	4-(2-hydroxyethyl)piperazine-1-ethanesulphonic acid
HILIC	Hydrophilic interaction chromatography
HPAEC-PAD	High-Performance Anion-Exchange Chromatography with Pulsed Amperometric Detection
IMAC	Immobilized metal ion affinity chromatography
mRNA	Messenger RNA
MOS	Malto-oligosaccharide
MW	Molecular weight
NAD	Nicotinamide adenine dinucleotide
NADP	Nicotinamide adenine dinucleotide phosphate
PAGE	PolyAcrylamide Gel Electrophoresis
PCR	Polymerase chain reaction
P_i	Inorganic phosphate
RNA	Ribonucleic acid
s.d.	Standard deviation
SDS	Sodium dodecyl sulphate
s.e.m.	Standard error of the mean
SHG	Soluble Heteroglycan
TBS	Tris buffered saline
T_m	Melting temperature of primers
Tris	Tris(hydroxymethyl)aminomethane
v/v	Volume by volume
w/v	Weight by volume

1 Introduction

1.1 Aim

This thesis considers the metabolism of maltose in the model plant *Arabidopsis thaliana*. Maltose is the major product of leaf starch degradation in plants. Starch is the primary energy reserve in most plants and is the second most abundant carbohydrate in the biosphere after cellulose. Plants accumulate and mobilise starch in both non-photosynthetic storage tissues (such as tuber and seed endosperm) and photosynthetic tissue (leaves). In storage tissues, starch is degraded during seed germination and during sprouting after dormancy in vegetative storage organs (roots, rhizomes, turions, etc.). In leaves, transitory starch is synthesised during the light period and subsequently degraded to maltose during the dark period. Maltose is the primary source of carbon for cellular metabolism and heterotrophic growth during the night when de-novo synthesis of sugars from CO_2 via photosynthesis is not possible. Several lines of evidence suggest that cytosolic maltose metabolism in Arabidopsis leaves requires a unique transglucosidase (DPE2) and involves a highly complex pool of soluble heteroglycans (SHG).

Although it has been shown that maltose metabolism is essential for efficient mobilisation of leaf starch and normal plant growth, little is known about the key players DPE2 and SHG that are required to metabolise maltose in the cytosol of plant cells. DPE2 was discovered following recognition of maltose as the major product of starch degradation exported from the chloroplast (Niittyla *et al.* 2004), in the search for Arabidopsis genes likely to encode enzymes of maltose metabolism (Chia *et al.,* 2004, Lu and Sharkey 2004). Originally SHG was reported simply as an unusual cytosolic polysaccharide. Its possible importance in maltose metabolism was first recognised after the discovery of DPE2 (Fettke *et al.,* 2006a).

There are obvious similarities between the DPE2 pathway of maltose metabolism in plants and the way in which maltose is metabolised in *Escherichia coli*. In this thesis I provide new information about maltose metabolism in plants, making use of these similarities between the plant and the *Escherichia coli* system. This will aid *in vitro* comparisons of DPE2 and MalQ and *in vivo* experiments with mutant and transgenic plants.

In the introduction to this thesis I will summarize the current knowledge about starch metabolism in *Arabidopsis thaliana*, focussing on the enzymatic pathway of starch degradation and especially maltose metabolism. I will then move on to introduce the metabolism of maltose

in *Escherichia coli* and describe similarities to plant maltose metabolism. Finally I will discuss my experimental approach and introduce the results chapters.

1.2 The composition and structure of the starch granule

Storage of energy in the form of biopolymers is widespread in nature. Animals primarily use fatty acid (lipid) deposits as long term energy storage in their adipose tissues. Glycogen is mainly used in bacteria, fungi and archaea as primary energy storage. Plants and related organisms like some algae use starch as their energy reserve. At some stage or stages of development nearly all land plants and many algal species accumulate starch.

Starch is composed of two polymers of glucose; amylose and amylopectin (Hassid, 1969). Amylose is a predominantly linear polymer consisting of approximately 500 to 10,000 α-1,4 linked glucosyl residues. The glucosyl residues of amylopectin are linked via α-1,4-bonds to form chains of between 6 and >100 glucosyl residues in length. Similar to glycogen, the α-1,4-linked chains in amylopectin are connected by α-1,6-bonds (branch points). However, amylopectin has less branch points and therefore a less dense pattern of glucan branches than glycogen. This branching pattern of amylopectin allows for the formation of the secondary and higher-order glucan structures that make up the matrix of the starch granule.

The exact molecular architecture of the starch granule is not yet known. It is thought that the combination of chain lengths, branching frequency, and branching pattern in amylopectin give rise to a treelike structure (Figure 1.1, a) in which clusters of glucose chains occur at regular intervals along the axis of an amylopectin molecule. Adjacent glucose chains in these clusters form double helices (Hizukuri 1986). They pack together in organised arrays giving rise to concentrically-arranged, crystalline lamellae in the granule matrix (Buleon *et al.,* 1998). The crystalline lamellae alternate with amorphous lamellae that contain the branch points. From the alternating crystalline-amorphous lamellae with a repetitive periodicity of approximately 9 nm, the next level of organisation of starch granules occurs at the scale of 200 to 500 nm in the form of growth rings (Jenkins et a. 1993). Growth rings can be observed in starch granules by both light and electron microscopy. It was proposed that growth rings may arise from zones of more and less-highly packed amylopectin or possibly from alternating large and small blocklets which again consist of alternating crystalline and amorphous lamella (Buleon *et al.,* 1997, Buttrose 1960, Buttrose 1962).

The exact role of amylose in the organisation of the starch granule is not yet known. It is thought that the linear α-1,4 linked glucan amylose is embedded in the amylopectin matrix. The examination of amylose-free mutants of various species has shown that amylose is not crucial for the characteristic semi-crystalline structure of starch. The *waxy* mutants of cereals (Nakamura *et al.,* 1995, Shure *et al.,* 1983), the *lam* mutant of pea (Smith *et al.,* 1995) and the *amf* mutant of potato (van der Leij *et al.,* 1991) all lack or have severe reductions in amylose but still contain starch granules of normal morphology and higher level structure. However, amylose can influence the organisation of short chains of amylopectin and plasticity of the starch granule. Analysis of normal and low amylose lines of maize and pea indicated that an increase in amylose to amylopectin ratio increases the size of the crystalline lamella relative to the amorphous lamella while the 9 nm periodicity remains unchanged (Jenkins and Donald 1995). It was proposed that amylose reduces the packing of amylopectin chains in the crystalline lamellae leading to a reduced density and a relative increase in size of the crystalline lamellae.

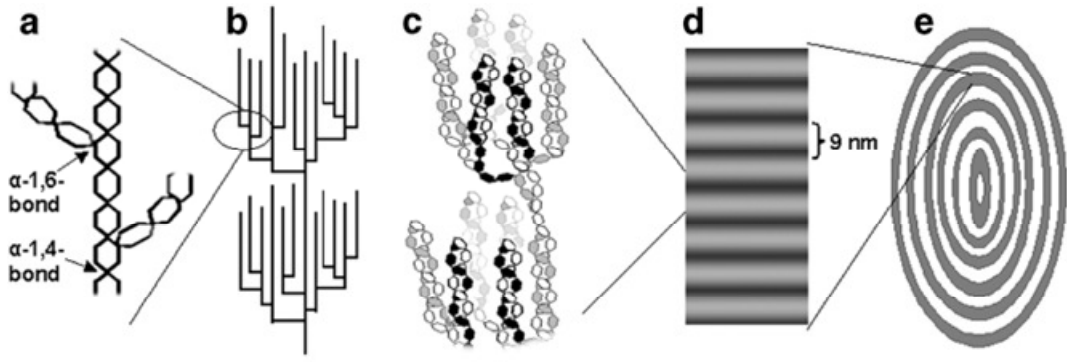

Figure 1.1 The arrangement of starch polymers within a starch granule (from Zeeman *et al.* 2004)

(a) Chains of α-1,4- and α-1,6-linked glucosyl residues within amylopectin. (b) Schematic drawing of the cluster structure of amylopectin. (c) Cartoon of the double helices formed by neighbouring chains and their ordered packing. (d) Formation of semicrystalline lamellae (containing ordered double helices) and amorphous lamellae (containing the branched regions), which alternate with 9-nm periodicity. (e) 'Growth ring' structure of a storage starch granule (Zeeman *et al.,* 1998a).

In plant storage organs, starch synthesis and degradation are usually developmentally separated (e.g. in the developing and germinating cereal grain and in developing and sprouting potato tubers). Starch in storage organs (called storage starch) represents one of the two types of starch occurring in nature. The other type, called transitory starch, is mainly found in leaves and in unicellular green algae. Transitory starch accumulates in chloroplasts during the day and is broken down during the subsequent night as a carbon supply for heterotrophic growth (Smith *et al.*, 2005; Smith and Stitt, 2007).

Storage and transitory starch granules differ significantly. Whereas storage starch is synthesised over many days or weeks, transitory starch is the immediate product of a single photoperiod. The size and shape of the two types of granules are also different. Storage starch granules can be from 0.3 to over 100 μm across in length (Lindeboom 2004). The shape varies from the smooth, oval potato starch to the irregular polygonal shaped granules of the Chinese taro (Jane *et al.,* 1994). In contrast, transitory starch granules from leaves are mostly flattened and disc like and on average between 1 and 2 μm in diameter, regardless of species (Grange *et al.,* 1989b; Santacruz *et al.,* 2004; Steup *et al.,* 1983; Wildman *et al.,* 1980). The conservation in size and shape of granules in leaves may imply that these parameters are important in diurnal starch turnover in plants in general.

Storage and transitory starch granules also differ in structure and composition. Both types of starch are composed of amylose and amylopectin but the ratios of the two polymers vary considerably. Storage starch granules consist of 20-30% amylose and 70-80% amylopectin, whereas the ratio of amylose to amylopectin varies in transitory starch granules amongst different plant species. In *Arabidopsis thaliana* (a small flowering plant native to Europe, Asia, and north-western Africa) the amylose content of leaf starch was approximately 6% (Zeeman *et al.*, 2002). A significantly higher amylose content of 15 to 20% was observed tobacco leaves (Matheson 1996) while rice leaf starch contains only 3.6% amylose (Taira *et al.,* 1991).

During the day carbohydrates produced directly by photosynthesis serve as substrates for the biosynthesis of all major cellular components. However, the growth of plants at night, when photosynthesis is not possible, is underpinned by carbohydrates derived from transitory starch degradation (Nozue and Maloof 2006, Smith and Stitt 2007). The products of this degradation are transported into the cytosol of the plant cell, where they are further metabolised.

The main aim of my research was to elucidate the cytosolic metabolism of maltose, the primary product of transitory starch degradation. My experimental research focused on the model plant

Arabidopsis thaliana. In the next two sections I will explain the importance of studying transitory starch degradation and why I used Arabidopsis as an experimental system.

1.3 The importance of transitory starch

Transitory starch provides carbon for the plant during periods of darkness, such as during the night. It may also act as an overflow sink for newly assimilated carbon when assimilation of CO_2 exceeds the demand for sucrose (Caspar *et al.,* 1985, Ludewig *et al.,* 1998, Schulze *et al.,* 1991) which would allow the rate of photosynthesis to exceed that of sucrose synthesis. Therefore, transitory starch represents an integral part of the global carbon cycle. Understanding the nature and control of transitory starch metabolism will underpin attempts to modify and improve carbon fixation. This goal is essential if we are to cope with the increasing atmospheric CO_2 concentration and the strongly increasing demand for food.

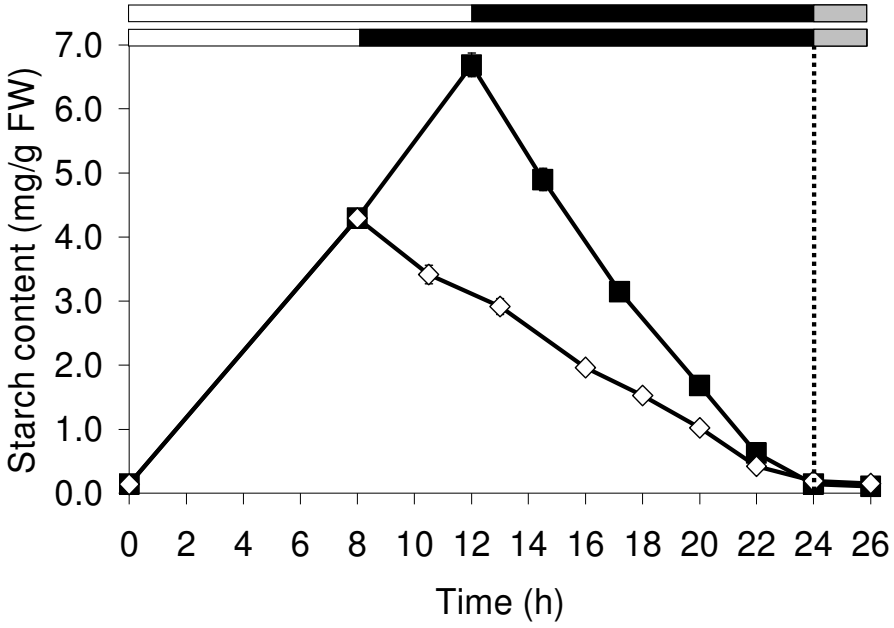

Figure 1.2 Linear starch degradation in leaves at night (Graf *et al.* 2010)

In wt plants that are grown under a 24-h days for 4 weeks and subsequently subjected to an unexpected early night starch degradation continues to operate in a linear fashion. Black cubes show normal night. White diamonds show an early night.

Wt plants degrade nearly all of their leaf starch reserves during the night (under controlled conditions, see Figure 1.2). The rate of starch degradation progresses at a linear rate which is controlled by the circadian clock so that reserves last almost precisely until dawn (Graf *et al.,* 2010). An unexpected early darkness does not disrupt the linear pattern of starch degradation (Gibon *et al.*, 2004). Plants that are grown all their life under a constant 12-hour light/12-hour dark photoperiod and suddenly subjected to an early night immediately adjust their starch degradation mashinary so that starch researves last until the expected dawn after 24 hours (Figure 1.2).

The importance of transitory starch for the plant is revealed in Arabidopsis mutants that cannot accumulate starch (e.g. *adg1, pgm*, see Section 1.5.1), or degrade it only very slowly (e.g. *dpe2*, *gwd*, *mex1*, see Section 1.7.2). All of these mutants have lower growth rates than wt plants during the night. The overall rate of growth is reduced except in continuous light or very long days (Gibon *et al.,* 2004, Smith and Stitt 2007, Usadel *et al.,* 2008). The reductions in growth rate in severe starch metabolism mutants during the night and in wt plants during extended night periods are accompanied by large transcriptional changes indicative of carbon starvation (Smith and Stitt, 2007; Usadel *et al.*, 2008).

Taken together, these observations show that the temporary storage of carbon as starch in leaves is essential for maintaining plant metabolism and growth during the night in Arabidopsis plants.

1.4 Why is *Arabidopsis thaliana* used for studying transitory starch degradation?

The first mention of Arabidopsis in the scientific literature was a paper in 1873 by Alexander Braun in which he described an Arabidopsis mutant with a double flower phenotype he had found in a field near Berlin. In 1907 Friedrich Laibach commenced the first experimental studies on Arabidopsis. During his PhD at the University of Bonn in Germany he carried out cytological studies of various plants, including Arabidopsis. But it was not until 1943, a time that could be regarded as being unsuitable for bright ideas, when the same Friedrich Laibach outlined the suitability of Arabidopsis as a model for genetic and developmental biological research (reviewed in Meyerowitz 2001).

A few of the advantages of Arabidopsis over other plants are the small diploid genome, the short life cycle, the fact that it self-fertilises and the production of several thousand seeds per plant, making it an ideal subject for mutagenesis experiments. The discovery of the simplicity of

transformation of Arabidopsis with foreign genes via *Agrobacterium tumefaciens* mediated gene transfer (Chilton *et al.,* 1977) further benefited the use of this plant as model organism later on. But perhaps one of the most important advantages in recent history is the availability of the genome sequence provided be the Human Genome Project (HGP) 2000). The vast efforts among the scientific community to provide the best genomic tools and resources available for any plant (for example TILLING - Targeting Induced Local Lesions IN Genomes (McCallum *et al.,* 2000)) have greatly advanced the use of Arabidopsis as model to study the plant system.

Fortunately, Arabidopsis is also a very good system to study transitory starch metabolism. Its genetic tractability has made large pools of Arabidopsis mutants available that are impaired in either starch synthesis or degradation (Caspar *et al.,* 1985, Lin *et al.,* 1988a, Yu *et al.,* 2000). Mutants of Arabidopsis that are impaired in starch degradation accumulate starch over time. The result is a so called starch excess (*sex*) phenotype. A simple and straight forward screening protocol allows for the identification of these mutants. The protocol involves destaining of leaves with ethanol at the end of night (EoN), followed by staining with iodine solution. A *sex* mutant is identified when the leave turns black (due to the interaction of iodine with starch in the leaf). Wt plants do not turn black upon iodine staining, as they used all leaf starch reserves during the night. Similarly, mutants impaired in starch synthesis can be identified with the same simple screening protocol. Leaves of wt plants harvested at the end of day (EoD) stained with iodine should turn black, since starch has accumulated during the day as reserve for the subsequent night. Mutants that can not synthesise starch would not stain and therefore be revealed as starchless mutants.

Similarly, the analysis of starch in Arabidopsis leaves is straight forward. Starch is made in relatively large amounts. Up to 50% of the carbon assimilated through photosynthesis in a single photoperiod is stored as starch (Zeeman *et al.,* 2002). This makes it possible to analyse the composition, structure and amount of starch produced over a period of few hours. In addition, the rate of starch synthesis can be controlled by changing environmental conditions such as light intensity, day length and CO_2 concentration.

There are good reasons to think that Arabidopsis also is a suitable model to understand important aspects of transitory starch degradation of commercially important crop species. Genes encoding enzymes responsible for leaf starch degradation in Arabidopsis can also be found in important industrial crops such as rice, potato, wheat and grape. Experimental evidence suggests that these

enzymes are the basis for a similar or identical pathway in these organisms (Fettke *et al.,* 2009b, Fettke *et al.,* 2008, Lutken *et al.,* 2010).

Mutations affecting starch metabolism have provided the ground for the enormous progress that has been made during the last decade using new and enhanced genetic approaches stemming from the publication of the Arabidopsis genome sequence ((HGP) 2000). In the next few sections I will provide an overview of current understanding of the pathways leading to and from starch in leaves. In the first section I will discusses the biosynthesis of ADP-glucose (ADPGlc), the activated glucose donor for starch synthesis. In subsequent sections I will describe the biosynthesis of the starch granule and the pathways of starch degradation.

1.5 The synthesis of transitory starch

1.5.1 The production of the precursors

The Calvin cycle (also called Calvin–Benson-Bassham cycle or reductive pentose phosphate cycle) arguably represents the most important set of enzymatic reactions on this planet. The cycle is a series of biochemical reactions that take place in the stroma of chloroplasts in photosynthetic organs. In general, photosynthesis in the chloroplast of plant cells occurs in two separate stages. Firstly, in so called light-dependent reactions in the thylakoid membrane light energy is captured and used to form ATP and NADPH. The light-independent Calvin cycle in turn requires the energy from ATP and the reducing power of NADPH. The initial carboxylation step in the Calvin cycle is catalysed by the key enzyme of the cycle: ribulose-1,5-bisphosphate carboxylase oxygenase (RuBisCO). CO_2 is combined with water and the five-carbon compound ribulose 1,5-bisphosphate (RuBP) to form two molecules of 3 phosphoglycerate (3PGA). In subsequent reactions of the Calvin cycle fructose 6-phosphate (F6P) is formed (reviewed in Zeeman *et al.,* 2007b). The autocatalytic nature of the Calvin cycle allows the removal of intermediates for the synthesis of net amount of products without compromising the rate of regeneration of the acceptor compound RuBP. 3PGA is tranformed to glyceraldehyde-3-phosphate and dihydroxyacetone phosphate. These two triose phosphates (TPs) are exported into the plant cytosol and subsequently transformed into sucrose which serves the supply of energy and building blocks for the plant catabolism and metabolism. During conditions that cause a low rate of sucrose synthesis, 3PGA export is restricted. Diversion of carbon from the stromal F6P pool into the transitory starch reserves prevents the build up of phosphorylated intermediates and

allows high rates of CO_2 assimilation to continue. It furthermore provides the plant with carbon for the subsequent night as mentioned earlier.

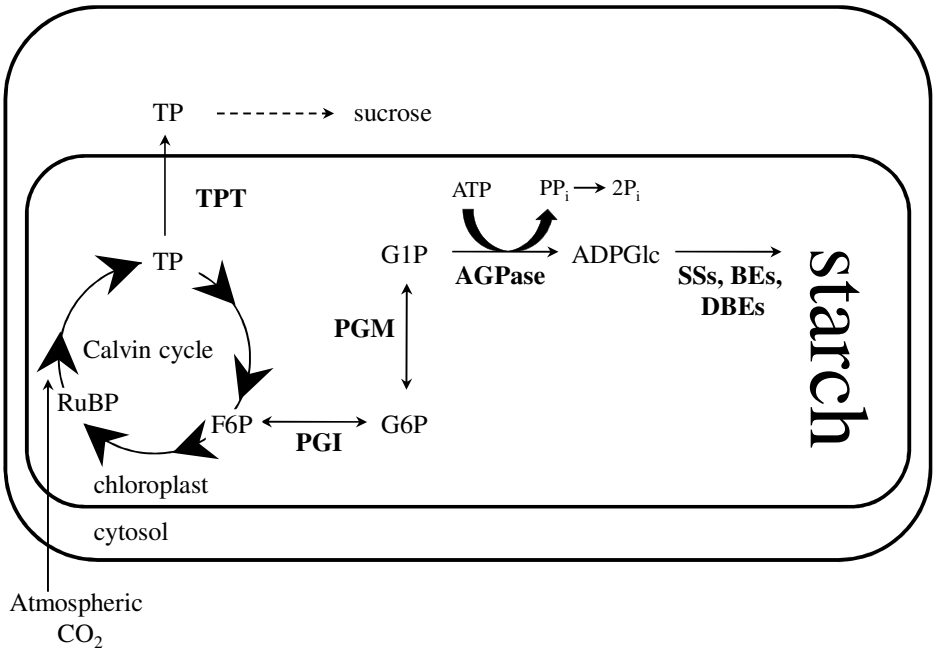

Figure 1.3 Model of the pathway of starch synthesis in chloroplasts

Carbon assimilated via the Calvin cycle is partitioned with a fraction exported as TPs to the cytosol via the triose phosphate transporter (TPT). In the cytosol the TPs are used for sucrose synthesis. A fraction is also used for starch synthesis in the chloroplast (making a total of 1/6 of carbon for product synthesis, as 5/6 have to be maintained to fuel RuBP regeneration). F6P – fructose-6-phosphate, G6P – glucose-6-phosphate, G1P – glucose-1-phosphate, ADPGlc – ADP-glucose, PGI – phosphor glucoisomerase, PGM – phospho-glucomutase, AGPase – ADP-glucose pyrophosphorylase, SS – starch synthase, BE – branching enzyme, DBE – debranching enzyme.

In the first step beyond the Calvin cycle, F6P is isomerised by phosphoglucose isomerase (PGI) to G6P which in turn is transphosphorylated by the chloroplastic isoform of phosphoglucomutase (pPGM) to G1P (Figure 1.3). G1P is the substrate for ADPGlc pyrophosphorylase (AGPase) in the first committed step of starch synthesis (Figure 1.3). AGPase converts G1P and ATP to ADPGlc and pyrophosphate (PP_i). ADPGlc is the substrate used by the starch synthases (SSs) for the extension of glucan chains at the surface of the starch granule (Leloir *et al.,* 1961, Recondo and Leloir 1961, Szydlowski *et al.,* 2009). Genetic and biochemical evidence shows that all of these steps occur within the chloroplast in Arabidopsis

and in other species. Mutations affecting pPGM, AGPase or PGI activity decrease or abolish starch synthesis in leaves (Lin *et al.,* 1988a, Yu *et al.,* 2000).

An alternative starch synthesis pathway was suggested in which ADPGlc can be produced in the cytosol via sucrose synthase (SuSy). It was proposed that ADPGlc could be imported into the chloroplast (Baroja-Fernandez *et al.,* 2004, Munoz *et al.,* 2006). However, evidence for this alternative model was criticised as being circumstantial. In addition the model is not considered consistent with existing genetic and biochemical evidence (Neuhaus *et al.,* 2005; Streb *et al.,* 2009; Zeeman *et al.,* 2007b). Any contribution by SuSy to the ADPGlc pool in leaves is minor since the study of knockout mutants lacking various combinations of Susy isoforms showed that it is not required for transitory starch synthesis in plant leaves (Barratt *et al.,* 2009).

1.5.2 The priming of starch granules

It seems unlikely that granule initiation is an important process in mature Arabidopsis leaves. Granule numbers within a single chloroplast do not change over the day-night cycle (Mathilda Crumpton-Taylor, John Innes Centre, personal communication). Granules that are degraded during the night continue to shrink until dawn, when they provide the basis of starch synthesis again. However, new granules must be initiated as chloroplasts divide during the expansion phase of leaf development. This process is not understood.

It is generally accepted that the ability of plants to synthesize semicrystalline starch granules in plastids has evolved from an ancestral capacity to make glycogen – a simpler, more highly branched polymer, which is water soluble (Ball and Morell 2003). The primer for glycogen synthesis in animals is glycogenin, a Mn^{2+}/Mg^{2+}-dependent UDPGlc-requiring glucosyltransferase (reviewed in (Alonso *et al.,* 1995, Smythe and Cohen 1991)). Glycogenin glucosylates itself to create a chain of up to eight α-1,4-linked glucose residues that are covalently linked via a tyrosine residue to the glycogenin protein (Cheng *et al.,* 1995, Lomako *et al.,* 1992, Lomako *et al.,* 1993, Whelan 1998). Complex formation with glycogenin (Pitcher *et al.,* 1987, Skurat *et al.,* 2006) allows glycogen synthase to elongate the glucan chain attached to glycogenin. Self-glycosylating proteins have been detected or purified from a number of plant tissues (Ardila and Tandecarz 1992, Langeveld 2002, Lavintman and Cardini 1973, Lavintman *et al.,* 1974, Singh *et al.,* 1995). However, evidence suggests that these proteins are involved in the synthesis of polysaccharide components of the cell wall rather than amylopectin (Delgado *et al.,* 1998, Dhugga *et al.,* 1997, Langeveld 2002), and no self-glucosylating proteins have yet been discovered that are likely to be involved in the synthesis of amylopectin.

The best characterised glycosyltransferases in the plant chloroplast are starch synthases (SSs). Plants possess multiple isoforms of SS. Based on homology studies, five classes of starch synthases can be distinguished: granule-bound starch synthase (GBSS) involved in amylose biosynthesis and soluble starch synthases (SSI, SSII, SSII, SSIV) involved in amylopectin synthesis. As opposed to the UDPGlc utilising system of glycogen generation in animals and bacteria, SSs in plants and related algae catalyse the formation of new glucosidic linkages by using ADPGlc as a donor for glycosyl transfer to the non-reducing end of an existing α-1,4-linked glucan chain, thereby elongating it. No SSs have been shown to have self-priming activity, although Szydlowski *et al.* (2009) report that SSIII is able to synthesize glucans from ADPGlc in a primer-independent manner. Recent genetic evidence suggests that the SSIV class of starch synthase (possessing a glycosyl transferase domain which is most closely related to SSIII) may have a role in granule initiation. The number of starch granules in Arabidopsis leaf chloroplasts differs and depends on the developmental stage of the leaf (Crumpton-Taylor *et al.* submitted). On average chloroplasts contain about five starch granules. In contrast, Arabidopsis *ssiv* mutants have just one large granule in each chloroplast (Roldan *et al.,* 2007). The structure of SSIV proteins differs from that of other SS isoforms in possessing an N-terminal extension containing a pair of long stretched coiled-coil motifs (200 amino acids) and a putative 14–3-3 protein binding site (Leterrier *et al.,* 2008). It is possible that features of the N-terminal extension enable SSIV to interact with other proteins and thus contribute to granule initiation. In the absence of SSIV, SSIII seems to be responsible for the initiation of the single granule per chloroplast: plants lacking both SSIV and SSIII lack starch in their leaves despite having 60% of the wt soluble SS activity (accounted for by the remaining SS isoforms (Szydlowski *et al.,* 2009).

1.5.3 The production of amylose and amylopectin

The amylose component of starch is synthesized exclusively by GBSS. GBSS is usually found bound to or embedded in starch granules (Sivak *et al.,* 1993). Mutants and transgenic plants lacking this enzyme are essentially amylose-free (Denyer *et al.* 2001). Amylose free starch possesses altered physicochemical properties that are useful for industrial applications (Zeeman *et al.,* 2010). The orchestrated interplay between SSs which operates to produce the crystallization-competent polymers is not fully understood. It is thought that SSs elongate the α-glucan chains in amylopectin, which are destined to interact with each other to ultimately form the semi crystalline matrix. Branch points within the amylopectin fraction of the starch granule

are essential for the formation and organisation of the treelike structures that are the basis of the semicrystalline lamellae in the granule (Figure 1.1, b and c)

The branch points in amylopectin are introduced by branching enzymes (BEs), which catalyze a glucanotransferase reaction whereby part of an existing α-1,4-linked chain is transferred to the C6 position of a glucosyl residue of another chain. These transferred chains are further elongated by SSs. Debranching enzymes (DBEs) may be involved in tailoring the branched glucan chains into a form capable of crystallization (Figure 1.1, a and b). Recent studies have highlighted the need for DBEs in starch biosynthesis (Streb *et al.,* 2008, Wattebled *et al.,* 2005). Plants and green algae contain two classes of DBEs: isoamylase (ISA) and limit-dextrinase (LDA). Both classes hydrolyze α-1,6-branch points but differ in their substrate specificity. The ISA class can be divided into three subfamilies designated ISA1, ISA2, and ISA3 (Hussain *et al.,* 2003). The *Arabidopsis thaliana* genome contains one gene encoding each ISA subfamily member and one gene encoding LDA. Removal of individual DBEs has different affects on transitory starch accumulation in Arabidopsis. Mutants that lack LDA or ISA3 exhibit a starch excess phenotype. Mutants that lack ISA1 or ISA2 have starch granules with altered starch structure and accumulate a soluble form of starch called (Wattebled *et al.,* 2005, Zeeman *et al.,* 1998b). Removal of all DBEs results in an essentially starch less mutant (Streb *et al.,* 2008). This suggests that DBEs trim off some of the branches introduced by BEs, making a structure able to self organise and thus crystallise.

Genetic and biochemical data indicate that each SS isoform has different properties and a distinct role in amylopectin synthesis. Analysis of the distribution of chain lengths of amylopectin in mutant and transgenic plants lacking specific isoforms has led to the idea that the SSI, SSII, and SSIII classes preferentially elongate short, medium, and long chains, respectively. SSI preferentially elongates the shortest chains of 4-10 glucosyl units, SSII medium-length chains (12-24 glucosyl units) and SSIII the longest chains (Zhang *et al.,* 2008). This suggests that SSI, SSII and SSIII work together in a synergistic fashion to determine the final amylopectin structure. This, however, does not exclude potentially redundant roles for the SSs. For example: while loss of Arabidopsis SSIII function had no impact on starch synthesis, loss of SSII function led to an increased amylose/amylopectin ratio and deficiency in amylopectin chains with a chain length (DP-degree of polymerisation) of 12 DP to 28 DP. Simultaneous loss of SSII and SSIII led to far more severe starch phenotypes than the summed changes in SSII and SSIII-deficient plants lacking only one of the two enzymes. This includes dramatically reduced starch contents and slower plant growth (Zhang *et al.,* 2008). Similarly, starch produced in transgenic potato

tubers as a result of the combined reduction of SSII and SSIII activities revealed that both SS isoforms make distinct and synergistic contributions to amylopectin synthesis (Edwards *et al.,* 1999, Lloyd *et al.,* 1999).

The precise role of SSs in producing α-glucan chains with specific lengths cannot be detected simply by analysis of an individual mutant. In fact, it is more likely that the competition between different SSs for binding to α-glucan substrates of certain lengths could in part explain the specific distribution of α-glucan chains within amylopectin. Further detailed analysis of the biochemistry and enzymology of SS is needed to elucidate the exact role in amylopectin synthesis of each enzyme.

1.6 The enzymatic pathway of starch degradation in leaves

There have been major advances in research about starch degradation during the last decade. This has been greatly facilitated by the increase of genome sequences from plants and related organisms. In Arabidopsis the major steps in the pathway have been uncovered and the genes/enzymes involved have been identified.

The initial event the starch degradation is the phosphorylation of amylopectin on the granule surface by two kinases, glucan water dikinase (GWD) and phosphor glucan water dikinase (PWD) (Baunsgaard *et al.,* 2005). Subsequently, starch is hydrolysed and maltose is released as the main degradation product. Maltose is exported from the chloroplast to the cytosol where it is further metabolised (Figure 1.4). The main challenge now is to analyse this pathway in detail so that in the future, a biotechnological use of the wealth of molecular information can be made available to society.

We currently know very little about the key processes that allow for the hydrolytic attack of amylases on the starch granule. In the following section I will summarise the initiation of starch degradation and discuss the latest findings.

1.6.1 Enzymatic attack of the starch granule surface

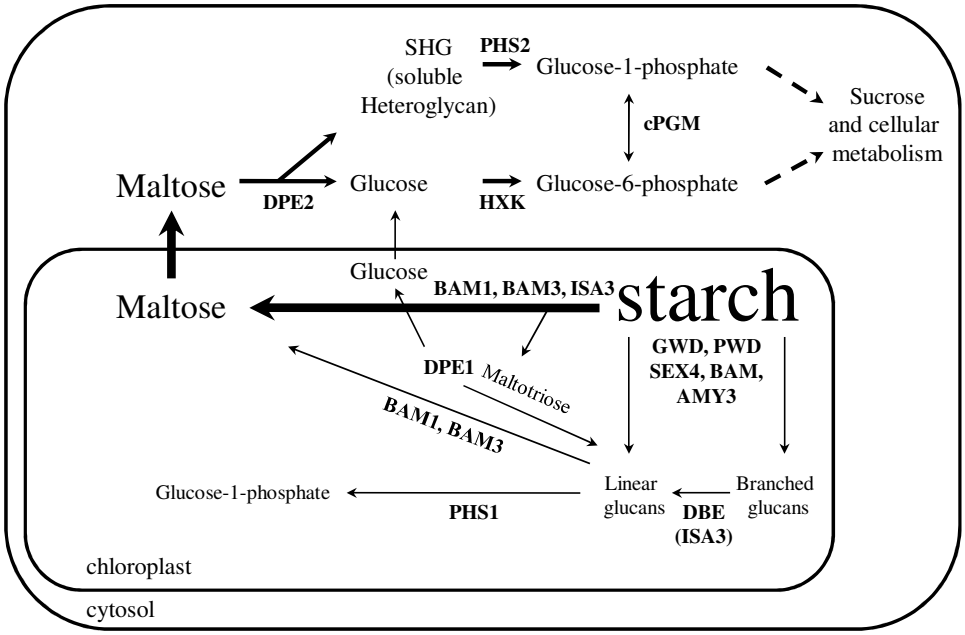

Figure 1.4 Model of the pathway of leaf starch degradation at night

Starch is directly hydrolysed to maltose and glucose during the dark. Phosphorylation of the granule surface by GWD and PWD allows the direct action of BAM3 and ISA3. Linear glucans (predominantly maltotriose [Glc3]) can be metabolised by DPE1, releasing glucose. Loss of any of these enzymes reduces starch breakdown and causes a *sex* phenotype. In addition to further degradation by BAM, PHS1 transfers glucosyl residues from linear glucans onto orthophosphate producing G1P to support chloroplast metabolism. The thickness of the arrows reflects estimates of the respective fluxes (Weise *et al.,* 2004, Zeeman *et al.,* 2007). Maltose and glucose are transported into the cytosol via specific transporters. cPGM- phospho-glucomutase, HXK – hexokinase

Starch is degraded by amylolytic enzymes that belong to the class of glycoside hydrolases. There has been wide discussion about which glycoside hydrolases are involved in degradation of transitory starch. The genomes of higher plants like Arabidopsis encode multiple exo and endo acting amylases. The Arabidopsis genome encodes nine β-amylases and three α-amylases. In the endosperm of germinating cereal seeds, the endo-amylase AMY hydrolyses α-1,4-linkages within glucan polymers exposed on the surface or in channels within granules thereby releasing soluble glucans that are substrate for further degradation. The available evidence suggests that, in leaves, AMY has a less important role in starch degradation. Of the three α-amylases, AMY3 (Yu *et al.,* 2005) and AMY2 (personal communication with Dr. Karla Simkova in the lab of Prof

Samuel, C. Zeeman at ETH Zuerich, Switzerland) were reported to be localised in the chloroplast. AMY3 was shown to be involved in release of branched glucans from the starch granule (Streb *et al.* 2008). However, loss of AMY3 function did not prevent normal rates of starch degradation (Yu *et al.* 2005). Similarly, starch metabolism was normal in *amy1/amy2/amy3* triple mutants (Yu *et al*. 2005), indicating that AMY activity is not required for starch degradation in Arabidopsis leaves under controlled environment conditions.

Data on potato tubers and Arabidopsis leaves indicate that starch granules are progressively degraded from the surface by exo-amylolysis and debranching rather than by endo-amylolysis. Out of the nine β-amylases only four are chloroplastic (BAM1,2,3,4). It was suggested that BAM and DBE play a major role in transitory starch degradation as the loss of either BAM3 or BAM4 or DBE (ISA3) results in reduced rates of starch degradation and accumulation of starch (Scheidig *et al.,* 2002; Kaplan and Guy, 2005; Wattebled *et al.,* 2005; Delatte *et al.,* 2006; Fulton *et al.,* 2008). However, recombinant BAM3 and ISA3 proteins showed very little degradation of intact starch granules *in vitro*. Elevated hydrolytic activity was only seen on soluble glucans *in vitro* when the two proteins were used in combination (Kötting *et al.* 2009). An additional step must therefore exist that allows action of β-amylases on the starch surface.

1.6.2 Phosphorylation of the starch granule surface

The phosphorylation of the starch surface is an essential step during transitory starch degradation in leaves at night. The generation of glycosyl-phosphoryl linkages is catalyzed by GWD (Ritte *et al.,* 2002) according to reaction 1.1.

$$\text{Glucan} + \text{ATP} + \text{H2O} \rightarrow \text{glucan-P}_{\beta} + \text{AMP} + \text{P}\gamma\text{i} \qquad \text{reaction (1.1)}$$

A loss of GWD in Arabidopsis (the *gwd* or *sex1* mutant) leads to an accumulation of starch in the leaves (up to 5 times elevated starch levels at end of day [EoD] and little or no loss of starch at the end of night [EoN]) (Yu *et al.,* 2001). Work *in vitro* has established that GWD phosphorylates the C6 position of glucosyl residues in amylopectin (Ritte *et al.,* 2006, Ritte *et al.,* 2002). The second glucan water dikinase, PWD, phosphorylates the C3 position of a glucose in a chain of glucosyl residues that has been previously phosphorylated by GWD on C6. PWD activity seems to be dependent on the presence of the C6 phosphate group added by GWD, or the change in glucan structure caused by the C6 phosphate (Ritte *et al.,* 2006). The presence of PWD *in vivo* is essential for normal rates of starch degradation. However, it is less important than GWD because Arabidopsis mutants that lack PWD accumulate much less starch than

mutants lacking PWD and are still capable of starch degradation at night (Baunsgaard *et al.,* 2005).

Normal rates of starch degradation also require removal of the phosphate groups added by GWD and PWD. This is catalysed by a phosphoglucan phosphatase (SEX4)(Hejazi *et al.* 2009). *In vitro*, addition of α-glucan water dikinase (GWD) and ATP to a mixture containing granular starch and BAM3 and ISA3 allowed glucan release from granular starch (Edner *et al.,* 2007). Starch degradation was however most efficient when a mix of recombinant BAM3, ISA3, GWD and SEX4 was used (Kötting *et al.,* 2009). Recombinant SEX4 can dephosphorylate glucans, including semicrystalline amylopectin. It thereby acts on phosphate groups at either the C6- or the C3- positions (Kötting *et al.,* 2009). During hydrolytic glucan release from the phosphorylated starch surface by BAM and DBE, the role of SEX4 seems to be the dephosphorylation of the phosphorylated surface of the starch granule (Kotting *et al.,* 2009). Mutants of SEX4 show a build up of phosphorylated oligosaccharides and have elevated starch contents (hence the name SEX4) because BAMs cannot act on a glucan chain carrying a phosphate group close to the nonreducing end (Kötting *et al.,* 2009). This indicates that phosphorylation and dephosphorylation of the starch granule surface catalysed by GWD and SEX4, respectively, is required for efficient degradation of starch by BAM3 and ISA3.

The model described above proposes that BAM and ISA3 are the key players in the enzymatic attack of the starch granule. However, loss of BAM or ISA3 function does not completely abolish starch degradation in Arabidopsis, indicating that other enzymes can compensate at least partly for those that are missing (Scheidig *et al.,* 2002; Kaplan and Guy, 2005; Wattebled *et al.,* 2005; Delatte *et al.,* 2006). The primary products of BAM and ISA attack on the granule surface in wt plants are probably maltose and Glc3. Glc3 was shown to be too short to act as a substrate for BAM (Chapman *et al.,* 1972) and is probably further metabolised through a glucanotransferase reaction catalysed by disproportionating enzyme 1 (DPE1). Arabidopsis mutants lacking DPE1 accumulate Glc3 during the night and have a mild *sex* phenotype (Critchley *et al.,* 2001). The disproportionation of Glc3 by DPE1 results in the release of glucose and Glc5. The latter is a substrate for BAM while glucose can be exported to the cytosol through the chloroplast envelope glucose transporter (Schafer and Heber, 1977; Weber *et al*., 2000; Servaites and Geiger, 2002).

Linear glucans can also potentially be metabolised by the chloroplast-localized *α*-glucan phosphorylase (PHS1). The preferred substrates of this enzyme are linear oligosaccharides of

five glucose residues or longer (Steup, 1981). PHS1 liberates G1P from the non-reducing ends of the chains. The exact physiological role of PHS1 in starch breakdown is still not clear. Arabidopsis plants lacking PHS1 show normal starch metabolism (Zeeman et al., 2004). However, *phs1* mutants were shown to be more sensitive to abiotic stress, especially drought. Therefore it was proposed that PHS1 might play a role in supplying substrates for the plastidial oxidative pentose phosphate pathway during stress responses (Zeeman et al., 2004).

The available evidence strongly suggests that maltose and glucose are the predominant forms in which the products of starch degradation are exported from the chloroplast (Figure 1.4). Isolated chloroplasts from different species were shown to export maltose and glucose in the dark (Stitt and Heldt 1981). Weise *et al.* (2004) showed that maltose is the main sugar exported from the chloroplast during starch degradation. However, these experiments were done on isolated chloroplasts and might therefore not necessarily reflect the *in vivo* situation. The discovery of a mutant Arabidopsis that accumulated high levels of maltose within the chloroplast strongly suggested that maltose export is essential for plant metabolism. Mutants lacking the chloroplast envelope maltose transporter MEX1 have decreased starch degradation and reduced growth (Niittylä *et al.,* 2004; Lu *et al.,* 2006).

In summary, starch degradation in Arabidopsis leaves is initiated by a cycle of phosphorylation (catalysed by GWD, PWD) and dephosphorylation (catalysed by SEX4) and occurs predominantly through combined action of exo-amylolytic BAM and the DBE ISA3 which release maltose and Glc3 from the granule surface. Glc3 is further metabolised by DPE1 and BAM to yield glucose and maltose which are exported from the chloroplast through specific transporters.

1.7 Cytosolic maltose metabolism

The last part of the introduction will focus on the metabolism of maltose in leaves at night. I will introduce the key players and set their discovery in a historic context. The pathway of maltose metabolism in prokaryotic organisms like *E. coli* has remarkable similarities with the pathway in plant leaves. I will therefore compare common features and discuss important differences.

1.7.1 Export of maltose from the chloroplast

About five years ago a long standing debate about the pathways of starch degradation in leaves was resolved with the discovery of two key proteins involved in maltose metabolism and export

from the chloroplast. The two proteins are DPE2 and MEX1. Before mutants lacking these proteins were analysed in 2004 (Chia *et al.,* 2004, Niittyla *et al.,* 2004) it was not known whether phosphorolytic or hydrolytic starch breakdown was the primary route of starch degradation in leaves at night. Many researchers thought that degradation of starch was primarily phosphorolytic and export occurred with triose phosphates or 3-phosphoglycerate via triose phosphate/phosphate translocators (TPTs) (Knappe *et al.,* 2003, Stitt and Heldt 1981). Mutants that lack TPT have drastically reduced rates of export of carbon from the chloroplast during the day, and consequently accumulate much larger amounts of starch than wt plants. In addition, the low hydrolytic activity of chloroplastic β-amylases was thought to be insufficient to catalyze the observed rate of starch degradation (Zeeman *et al.,* 1998a). Increased PHS1 activity during starch degradation in other plants like pea and spinach additionally strengthened the disbelief in a hydrolytic pathway of starch degradation in leaves at night (Hammond and Preiss 1983, Stitt *et al.,* 1978). Only the discovery of the maltose exporter MEX1 on the chloroplast envelope ended this discussion.

MEX represents a novel type of sugar transporter (Niittyla *et al.,* 2004). The protein has not been studied in detail so far but it is thought that the transport of maltose occurs passively. A sufficient gradient of maltose from inside the chloroplast to the cytosol has been proposed earlier (Weise *et al.,* 2005). The transport of maltose from the chloroplast into the plant cytosol does therefore not require energy in the form of ATP.

MEX1-deficient Arabidopsis plants are small, have a severe starch-excess phenotype and accumulate a substantial amount of maltose (100 times higher than in wt plants), indicating that MEX1 is essential in transitory starch breakdown (Niittyla *et al.,* 2004). A double knockout mutant that lacks MEX1 and DPE1 (impaired in maltose and glucose export) has a much more severe phenotype than either parent during a 12-hour light/12-hour dark photoperiod (but grows normally under continuous light). This clearly indicates that the hydrolytic pathway is the predominant pathway of starch degradation in leaves at night.

1.7.2 Metabolism of maltose in the plant cytosol

The metabolism of maltose exported from the chloroplast in the plant cytosol requires a set of enzymes that can convert it into hexose phosphates (the precursors for sucrose synthesis). This situation is somewhat analogous to that in single celled organisms that can grow on exogenous maltose as carbon source. A broad variety of mechanisms exist in nature that allow for the uptake and metabolism of maltose into cells. Figure 1.5 shows a selection of pathways from

single celled organisms like bacteria and yeasts that can use maltose taken up from the extracellular space as the sole supply of carbon for heterotrophic growth. Pathway number one in Figure 1.5, A shows a straight forward mechanism to metabolise maltose in *Saccharomyces cerevisae* involving a maltase (Barnett 1976). However, it seems unlikely that maltose would be hydrolysed via a maltase in the cytosol of leaf cells. Maltases are important for maltose hydrolysis in the endosperms of germinating cereal grains (Stanley *et al.,* 2011), but there is no evidence for their involvement in maltose metabolism in Arabidopsis.

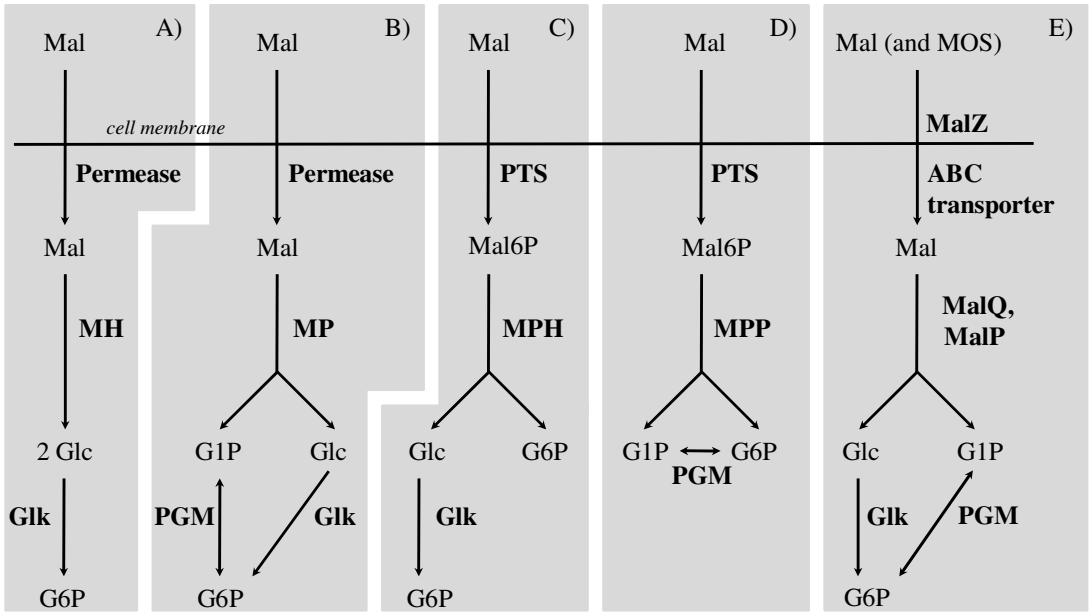

Figure 1.5 Pathways for maltose metabolism

Metabolic pathways of maltose metabolism in A) *Streptomyces cerevisiae* (Barnett 1976) B) *Lactobacillus lactis* (Levander *et al.,* 2001) and *Streptococcus bovis* (Martin and Russell 1987) C) *Fusobacterium mortiferum* (Thompson *et al.,* 1995) D) *Enterococcus faecalis* (Le Breton *et al.,* 2005) E) *E. coli* (Boos and Shuman 1998). Mal, maltose; Glc, glucose; Glk, Glucokinase; MH, maltose hydrolase (maltase; α-glucosidase); MalP, α-1,4-Glucan phosphorylase; MP, maltose phosphorylase; MPH, maltose phosphate hydrolase; MPP, maltose phosphate phosphorylase; PGM, phosphoglucomutase; MalQ, 4-α-glucanotransferase; PTS, phosphotransferase transport systems

The Arabidopsis genome encodes five enzymes classified as *α*-glucosidases. A few were shown to be apoplastic, having an acidic pH optima (Beers *et al.,* 1990). At least one of these is important for cell wall related processes like the trimming of xyloglucan oligosaccharides (AtAglu-1). Mutants lacking AtAglu-1 were shown to exhibit 70% less *α*-glucosidase activity than the wt (Iglesias *et al.,* 2006). Other *α*-glucosidases are located in the endoplasmic reticulum and seem to be involved in posttranslational processing of Asn-linked glycans of proteins

required for cellulose biosynthesis (Gillmor *et al.,* 2002) and seed development in Arabidopsis (Boisson *et al.*, 2001). It is therefore unlikely that maltose would simply be hydrolysed once it is exported into the plant cytosol.

Another way to metabolise maltose is via maltose phosphorylase (Figure 1.5, B). This enzyme is responsible for the supply of hexose phosphates in *Lactobacillus lactis* and *Streptococcus bovis* (Levander *et al.,* 2001, Martin and Russell 1987). The metabolism of maltose in pea chloroplasts was reported to occur via a maltose phosphorylase (Rees 1983, b). However, this enzyme has not been reported from Arabidopsis and the genome does not encode a protein related to the bacterial maltose phosphorylase. Similarly no genes encoding for either maltose phosphate hydrolase (MPH) or maltose phosphate phosphorylase (MPP) are found in the Arabidopsis genome (Figure 1.5, C and D).

The only remaining possibility is a pathway analogous to the one in the cytoplasm of Enterobacteriaceae like *E. coli*. In the cytoplasm of *E. coli* maltose and MOS of up to seven glucosyl residues are metabolised to G1P and G6P by the action of 4-α-glucanotransferase (MalQ), α-1,4-glucan phosphorylase (MalP) and glucokinase (Boos & Shuman 1998). Based on searches of the Arabidopsis genome for genes encoding enzymes similar to MalQ, two different research groups reported independently that a so called cytosolic D-enzyme (DPE2) is involved in the conversion of maltose to hexose phosphates (Chia *et al*. 2004; Lu & Sharkey 2004). The name DPE2 derives from its sequence similarity to the plastidic 4-α-glucanotransferase, DPE1 (25 % identity). 4-α-glucanotransferases catalyses a reaction that transfers a segment of a 1,4-α-D-glucan to a new position in an acceptor glucan, which may be glucose or another 1,4-α-D-glucan (MacGregor *et al.,* 2001).

Plants lacking DPE2 exhibited slow growth, very high levels of maltose (up to 500 times higher than in wt plant) and starch excess phenotype (Chia *et al.,* 2004). Initial experiments showed that glucose release from α-glucans by DPE2 in wt plant extracts was only detectable in the presence of maltose and glycogen (Lloyd *et al.,* 2004). Maltose alone did not trigger glucose production and therefore did not seem to be sufficient for DPE2 activity (Chia *et al.,* 2004). The presence of a pathway involving a cytosolic 4-α-glucanotransferase dependent on a complex glucosyl acceptor substrate (like glycogen) seemed puzzling at first, since no glycogen has ever been reported in the plant cytosol. It was therefore necessary to search for the cytosolic acceptor substrate of DPE2.

1.7.3 The acceptor substrate of DPE2 and PHS2 in the plant cytosol

The discovery of starch related enzymes that reside outside the chloroplast was an enigma to plant biologists for decades. The presence of extraplastidic exo- and endo-amylases (Okita *et al.,* 1979, Ziegler and Beck 1986), glucan phosphorylase (PHS2) and the discovery of DPE2 (Chia *et al.,* 2004) in so many plant species seemed to complicate the understanding of starch metabolism in leaves at night. These cytosolic enzyme isoforms cannot access the starch granules or the immediate degradation products of starch, yet often represent the major proportion of the total activity of the respective enzyme. A distinct pool of cytosolic glycans or glycoconjugates would have to be postulated if the cytosolic isoforms exert any metabolic function.

The discovery of a complex glycan substrate for the cytosolic α-1,4-glucan phosphorylase (PHS2) in peas and spinach (Steup *et al.* 1989) partially closed this gap in knowledge. It was shown that PHS2 interacts with a soluble glycan fraction that could be purified from crude extracts of spinach and pea (Steup *et al.* 1989). Incubation of recombinant PHS2 with ^{14}C-G1P and the glycan resulted in ^{14}C labelling of the glycan (Figure 1.6). Incubation of the same mixture with PHS1 (the plastidial α-glucan phosphorylase) or rabbit muscle phosphorylase (both of which have a similar primary amino acid sequence to PHS2) instead of PHS2 did not result in labelling of the substrate, indicating that the glycan is a specific substrate of PHS2 (Fettke *et al.,* 2006a).

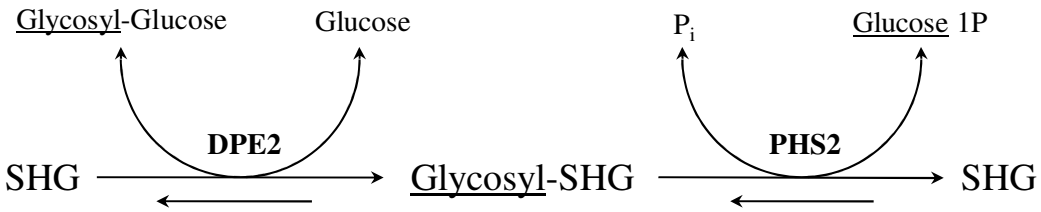

Figure 1.6 Reversible transfer reaction of glucose onto SHG by DPE2 and PHS2

In vitro labelling studies revealed that ^{14}C glucosyl residues that are transferred by DPE2 from labelled maltose to non-reducing ends of SHG (Glucosyl-SHG) can subsequently be transferred to orthophosphate (P_i) by PHS2 yielding ^{14}C G1P. Similarly, ^{14}C glycosyl residues derived from labelled G1P are transferred to SHG by PHS2. Subsequently, the labelled glucosyl residues can be transferred to glucose yielding ^{14}C maltose (glucosyl–glucose) by the action of DPE2 (Fettke *et al.* 2006)

It was not until the discovery of DPE2 15 years later that the potential significance of the interaction of PHS2 with the cytosolic glycan became apparent. The glycan fraction was now termed SHG; soluble heteroglycan. Studies with recombinant DPE2 showed that it could use the same glycan for glucosyl transfer from maltose *in vitro* (Fettke *et al.,* 2006a) (Figure 1.6). Affinity electrophoresis with immobilised glycan showed that PHS2 and DPE2 specifically interact with the glycan. Further ^{14}C *in vitro* labelling experiments with recombinant DPE2, PHS2 and the glycan showed that DPE2 can transfer glucosyl residues from maltose on the glycan and PHS2 can than transfer the same glucosyl residues from the glycan onto orthophosphate producing G1P (Fettke *et al.,* 2006a). This reaction is entirely reversible *in vitro* as shown in Figure 1.6. Thus it was suggested that maltose could be metabolised to hexose phosphates in the cytosol of plant leaves by a pathway involving DPE2, PHS2 and SHG.

1.7.3.1 Isolation and Composition of SHG

SHG is a heterogeneous pool of molecules that is localised in various cell compartments such as chloroplast, cytosol and apoplast (Fettke *et al.,* 2005a). It has been found in several plant organs including leaves, roots and storage organs such as potato tubers (Fettke *et al.,* 2009b, Malinova *et al.,* , Malinova *et al.,* 2011). However, only a specific subfraction of SHG molecules serves as substrate for DPE2 and PHS2 mediated glucosyl transfer. Fettke *et al.* (2004) have established a purification protocol that allows for separation of various subfraction of SHG. The purification procedure that leads to the active subfraction of SHG (termed SHG_{LI}) is outlined in Figure 1.7. Filtration and dialysis as well as Field-Flow-Fractionation (FFF) ensures separation of SHG_{LI} from other SHG subfractions based on molecular size. Contamination of SHG with starch derived molecules (such as soluble MOS) that could interfere in activity assays conducted with DPE2 and PHS2 is unlikely. First, no starch related linkages (1,4-Glc; 1,6-Glc) are present in SHG (Fettke *et al.,* 2006a, Fettke *et al.,* 2004). Second, SHG derived from Arabidopsis mutants that lack starch (e.g. *pgm*) has the same composition and linkage pattern as SHG derived from wt plants (Fettke *et al.,* 2009b).

The monosaccharide composition and linkage analysis of SHG have so far been determined for SHG_{LI} and SHG_{LII} isolated from Arabidopsis, spinach and pea leaves (Fettke *et al.,* 2004, Fettke *et al.,* 2005a, Fettke *et al.,* 2005b). Both glycan pools exhibit complex linkage and monosaccharide patterns. SHG is mainly composed of galactose and arabinose and minor amounts of glucose, fucose, mannose, rhamnose and xylose. Interestingly, the linkage pattern of SHG is remarkably similar to arabinogalactan (AG) from larch (Table 1.1). The occurrence of

3,6-Gal(p), 6-Gal(p), and 3-Gal(p) as well as t-Gal(p) and t-Ara(f) (Eckermann *et al.,* 2004) in SHG points to a structural similarity of the cytosolic heteroglycan to AGs (Fincher et al., 1983). This suggests a cell wall related origin of SHG. However, the high content of glucosyl residues in SHG_{LI} is not present in AGs. Glucosyl residues in SHG_{LI} are terminal as well as 2-linked and 2,4-linked. In particular, the proportion of terminal glucosyl residues considerably exceeds that of subfraction II (SHG_{LII}) and AG from larch (Table 1.1).

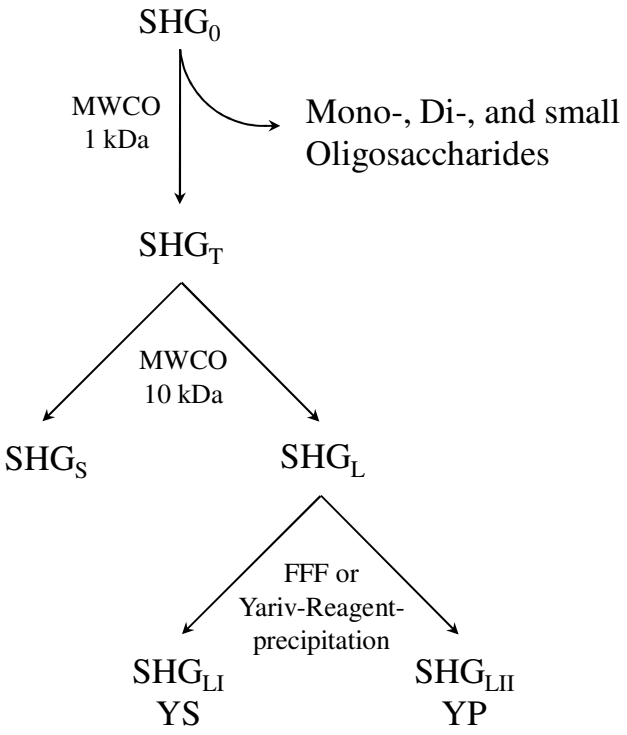

Figure 1.7 Scheme of the isolation of SHG from plant tissue (Fettke *et al.,* 2004)

Leaves are homogenised in 20% (v/v) ethanol. The soluble material remaining after centrifugation of the homogenate is termed SHG_0. Removal of all compounds having a size below 1 kD by dialysis from SHG_0 results in SHG_T. Subsequently, compounds with a size less than 10 kD (SHG_S) are separated from larger constituents (SHG_L) by membrane filtration (MWCO 10 kD). SHG_L is then separated into subfractions I and II by either field flow fractionation (FFF) or treatment with the $(\beta\text{-glucosyl})_3$-Yariv reagent. Subfraction I (SHG_{LI}) does not react with the Yariv reagent and is retained in the supernatant (YS) whereas subfraction II (SHG_{LII}) is precipitated and pelletable by centrifugation (YP). SHG_{LI} serves as substrate for DPE2 and PHS2 whereas SHG_{LII} does not (Fettke *et al.,* 2006a)

Sugar and linkage(s)	Larch AG	SHG_L Sub I	SHG_L Sub II	YP
All sugars and linkages are given in mol.%. p, Pyranose; f, furanose; Hex, unidentified hexose residue.				
Arabinose				
t-Ara*f*	2.28	3.6	5.33	4.7
t-Ara*p*	1.94	0.43	0.75	0.61
2-Ara*f*			0.56	0.25
3-Ara*f*	2.17	1.4	1.7	1.73
5-Ara*f*/4-Ara*p*		3.3	4.91	4.87
Galactose				
t-Gal*p*	30.25	8.2	7.45	6.63
3-Gal*p*	1.67	6.7	10.8	12.8
4-Gal*p*	0.13		0.34	0.25
6-Gal*p*	23	17.7	20	17.2
3,6-Gal*p*	29.4	30.2	42.57	43.7
3,4,6-Gal*p*	2.56		0.76	1.36
2,3,6-Gal*p*	6.14		0.63	1.35
Glucose				
t-Glc*p*		1.82	0.25	0.55
2-Glc*p*		2.1	0.81	
2,4-Glc*p*		2		
Mannose				
2-Man*p*		1.9	0.52	0.35
Rhamnose				
2-Rha*p*		1.24		
Fucose				
t-Fuc*p*		0.18		
3,4-Fuc*p*		0.2		
Unidentified hexoses				
2,6-Hex*p*		2	0.94	0.83
4,6-Hex*p*		2	0.31	0.3
Sum	99.54	84.97	98.63	97.48

Table 1.1 Adopted from Fettke *et al.* 2004 showing the distribution of glycosidic linkages in SHG_{LI} and SHG_{LII} compared to AG from larch

The sum shows the combined mol % of all sugar linkages. The Yariv precipitate (YP) essentially represents SHG_{LII}. Differences between the two result from the Field Flow Fractionation (FFF) on SHG_L which does not completely separate SHG_{LI} from SHG_{LII}.

The complex structure of SHG_{LI} raises questions about the mechanism of glucosyl transfer from maltose by DPE2 onto this unusual glycan acceptor substrate. DPE2 belongs to the family 77 of glycoside hydrolases (GH77). This classification is based upon similarities found between enzymes on primary amino acid sequence level and was introduced by Henrissat et al., (1997). Members of this family transfer glucose and/or fragments of a 1,4-α-D-glucan to a new position in an acceptor glycan, which may be glucose or another 1,4-α-D-glucan (MacGregor *et al.,* 2001). SHG, however, does not contain 1,4-linked glucose residues. How does DPE2 transfer glucose onto SHG?

Only one study has briefly investigated possible transfer mechanisms *in vitro*. In this study (Fettke *et al.,* 2006a) DPE2 was incubated with glycogen as glucosyl donor and various monosaccharides that are found in SHG, as acceptor molecule. Disaccharide formation was found to occur only with xylose, mannose, arabinose and galactose. Nevertheless, the study failed to analyse the linkage pattern of the disaccharide products. Crucial information is therefore lacking that could explain the complex linkage pattern in SHG_{LI}.

1.7.3.2 Subcellular location of SHG

The linkage pattern and monosaccharide composition of SHG_{LI} indicates a relationship with cell wall components like AGs (Ellis *et al.,* 2010, Fettke *et al.,* 2004). To establish whether SHG_{LI} is distinct from cell wall components, analysis of the subcellular distribution had to be done. The determination of the subcellular location of carbohydrates has some difficulties. Unlike proteins, for which fluorescent tagging facilitates intracellular distribution without disturbing their subcellular distribution, the location of intracellular carbohydrates can usually only be achieved by methods involving tissue disruption. Fettke *et al.* (2004) employed non-aqueous fractionation on whole plant extracts to determine the location of the individual SHG subfractions in the plant cell. SHG_{LI} was found to co migrate with cytosolic marker proteins, rather than with cell wall related or plastid markers, which established its cytosolic location (Fettke *et al.,* 2004). It was furthermore found that β-glucosyl)$_3$-Yariv reagent specifically precipitates SHG_{LII} whereas it does not interact with SHG_{LI}. Yariv reagent is a synthetic phenyl glycoside that specifically interacts with AG and AGPs by a mechanism yet to be identified (Yariv *et al.,* 1967). The fact that SHG_{LI} remained soluble in the presence of this reagent further strengthened the idea of a cytosolic rather than a cell wall location. Preparation of protoplasts (no cell wall present) from plant leaf cells furthermore indicated that SHG_{LI} is not cell wall associated. Whereas SHG_{LII} was

shown to be released into the buffer medium, SHG_{LI} remained inside the protoplast (Fettke *et al.,* 2009b).

Unlike SHG_{LI}, SHG_{LII} and SHG_S are believed to be apoplastic and plastidic, respectively. However, strict separation of all SHG subfractions into specific compartments cannot be achieved since the technique of non-aqueous fractionation has some limitations. The cytosol cannot be distinguished from several other cellular compartments. Therefore the location of some SHG in mitochondria, peroxisomes, endoplasmic reticulum or the Golgi apparatus cannot be excluded. Studies performed with isolated microsomal and organelle preparations however indicated that SHG_{LI} is not associated with these compartments but rather resides in the cytosol in a strict sense (Fettke *et al.* 2005a).

1.8 Metabolism of maltose in *E. coli*

Apart from the postulated involvement of SHG as an important intermediate in the metabolism of maltose in leaves, the metabolism of maltose in *E. coli* is similar to that in the plant cytosol. In this section I will introduce key players and common features of both pathways.

1.8.1 Import of maltose

The proteins of the maltose utilisation system in *E. coli* are all encoded by genes that are part of a single regulon. This regulon consists of ten genes that encode proteins necessary for the utilization of maltose and MOS. Five of these genes encode a high-affinity ABC transporter that is necessary to supply the cell with maltose and MOS. The proteins encoded comprise: LamB, a specific outer membrane diffusion porin; MalE, a high-affinity maltose/MOS binding protein in the periplasm; MalF and MalG, two tightly membrane-bound permease subunits, and MalK, the ATP-hydrolyzing subunit of the transporter (located at the cytoplasmic side of the transporter) providing the necessary energy for active transport (summarised in Boos *et al.* [1998]). It was previously shown that this system ensures extremely efficient uptake of maltose even at nM external maltose concentration. Boos *et al.* (2005) showed that *E. coli* cells are able to increase their intracellular maltose concentration from a few nM up to mM levels at initial external maltose concentration of just under 30 nM. This represents a very complex and highly efficient maltose transport system that requires the consumption of energy in form of one ATP per transported molecule of maltose.

1.8.2 Intracellular metabolism of maltose in *E. coli*

The conversion of maltose to hexose phosphates in *E. coli* proceeds via MalQ (4-α-glucanotransferase like DPE2) which acts on maltose and MOS to produce glucose. The glucose is metabolised to G6P via hexokinase (HXK). MalP (α-1,4-glucan phosphorylase like PHS2) transfers glucosyl residues from MOS onto orthophosphate producing G1P. A phosphoglucomutase catalyses the equilibrium between G1P and G6P (Figure 1.8).

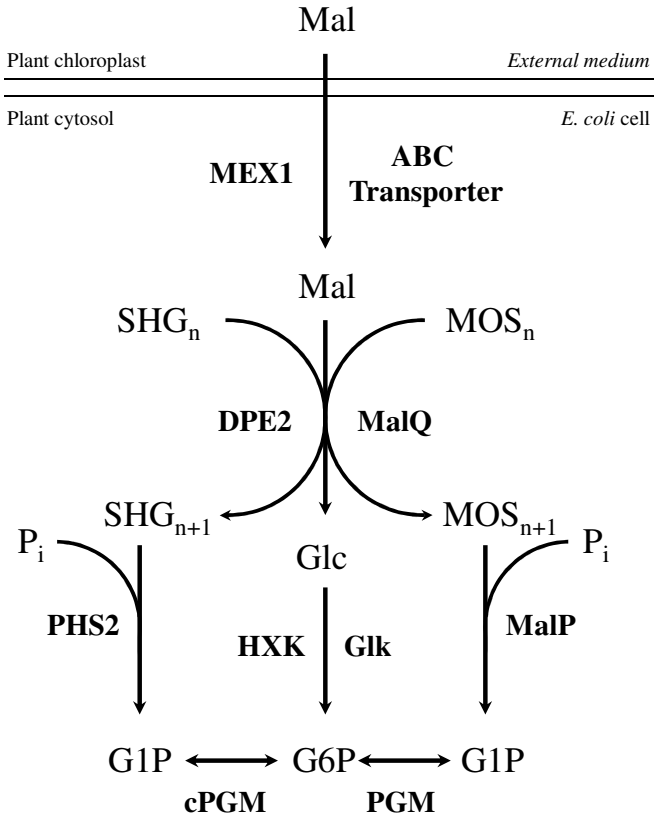

Figure 1.8 Maltose metabolism in leaf cells and *E. coli*

Comparison of maltose/MOS metabolism in *E. coli* with maltose/SHG metabolism in plant leaf cells. Mal, maltose; SHG, soluble heteroglycan; G1P, glucose-1-phosphate; G6P, glucose-6-phosphate; MalQ, 4-α-glucanotransferase; MalP, α-1,4-glucan phosphorylase; DPE2, 4-α-glucanotransferase; Pi, orthophosphate; cPGM and PGM, (cytosolic) phosphoglucomutase; HXK, Hexokinase; Glk, Glucokinase

Much research has been done to describe the maltose utilisation system in *E. coli*. The first set of publications that aimed to explain the pathway were by Monod *et al*. (1948) and Weismeyer *et*

al. (1960). It was soon discovered that MalQ is the central enzyme in maltose metabolism in *E. coli*. In the early stages of the biochemical characterisation of MalQ, a few discrepancies in its ability to act on maltose were discovered. Investigators reported that action of MalQ on maltose follows an autocatalytic reaction mechanism (Haselbarth *et al.,* 1971, Wiesmeyer and Cohn 1960). These finding were questioned later on. Palmer *et al.* (1976) proposed that MalQ cannot act on pure maltose, but rather uses longer chain MOS (DP ≥ 3) as donor molecules for glucan transfer. This implied that maltose is the acceptor substrate of the transfer reaction catalysed by MalQ. Later publications in 2005 and 2009 by Boos, Lengsfeld and colleagues rejected this mechanism in turn, stating that MalQ was able to use maltose as both, acceptor and donor substrate for glucosyl and MOS transfer (Dippel and Boos 2005, Lengsfeld *et al.,* 2009).

Important biochemical and biophysical parameters of MalQ that could answer questions about its mode of action (substrate affinity or acceptor specificity) have not been determined so far. In addition, the ongoing debate about the action of MalQ on maltose has not taken account of other systems of maltose metabolism (like that in plants) that also involve a phosphorylase and glucanotransferase. Crucial information that might help to further elucidate both plant and bacterial pathways might be gained by comparing the two.

The metabolism of maltose in plants and bacteria is remarkably conserved and essentially operates with the same set of enzymes (Figure 1.8). The only difference between the two pathways lies in the nature of the acceptor molecule. MalQ in bacteria uses simple linear MOS. DPE2 in plants however is proposed to use the complex SHG. Nothing is known about the origin, structure or enzymes involved in SHG biosynthesis. Although *in vitro* experiments are entirely consistent with a role for SHG in cytosolic maltose metabolism in plants, there is no evidence that this is the sole or major acceptor substrate for DPE2 *in vivo*.

1.9 Experimental approach

In order to shed light on the metabolism of maltose in plant leaves at night I first analysed the biochemical properties of DPE2. To achieve this I established a new purification procedure for DPE2 which allowed me to produce a large quantity of highly pure enzyme. This was used to undertake crystallisation trials and glucosyl acceptor substrate screens. This work is described in Chapter 3. I then go on to describe biochemical and enzymatic characteristics that distinguish DPE2 from its bacterial orthologue MalQ from *E. coli* (in Chapter 4). To investigate the importance of the DPE2-SHG interaction in cytosolic maltose metabolism in plants, I stably

expressed the malq gene from *E. coli* in *dpe2* knockout mutants. The generation and analysis of these transgenic plants is described in Chapter 5.

2 Materials and Methods

2.1 Bacterial strains

E. coli strains DH5α and TOP10 were used for general construction and propagation of plasmids. *E. coli* DB3.1 contains a gyrase mutation (*gyrA462*) that renders it resistant to the CcdB lethal effect (Bernard *et al.,* 1994) and therefore it finds its application in the maintenance of GATEWAY vectors (Section 2.3). *E. coli* Rosetta II was used for the overexpression of plant proteins as it provides "universal" translation where translation would otherwise be limited by the codon usage of the *E. coli* host. For transformation of *Arabidopsis thaliana* via floral dipping (Section 2.7.12.) *Agrobacterium tumefaciens* strain GV3101 was used.

Strain	**Antibiotic resistance**	**Genotype/ Properties**	**Source**
E. coli			
DH5α	-	F- φ80*lac*ZΔM15 Δ(*lac*ZYA-*arg*F)U169 *rec*A1 *end*A1 *hsd*R17(rk-, mk+) *pho*A *sup*E44 *thi*-1 *gyr*A96 *rel*A1	(Hanahan 1983)
DB3.1	Str^R	F- *gyrA462 endA1* D*(sr1-recA) mcrB mrrhsdS20* (rB-, mB-) *supE44 ara14 galK2 lacY1proA2 rpsL20 xyl5* Δ*leu mtl1*	(Hanahan 1983)
TOP10	Str^R	F- *mcr*A Δ(*mrr-hsd*RMS-*mcr*BC) φ80*lac*ZΔM15 Δ*lac*X74 *rec*A1 *ara*D139 Δ(*ara-leu*)7697 *gal*U *gal*K *rps*L *end*A1 *nup*G λ-	Invitrogen
(DE3)pLysS	Cm^R	F^- *ompT hsdS*$_B$(r_B^- m_B^-) *gal dcm* (DE3) pLysS (Cm^R)	Novagen
Rosetta(DE3)	Cm^R	F^- *ompT hsdS*$_B$(r_B^- m_B^-) *gal dcm lacY1* (DE3) pRAREII *(*Cm^R)	Novagen
Agrobacterium tumefaciens			

GV3101	RifR, GentR	pMP90 (pTiC58ΔT-DNA), genes for nopalin biosynthesis	(Van Larebeke *et al.,* 1973)

Table 2.1 Bacterial strains

All bacterial strains were stored as glycerol stocks at -80°C. Glycerol stocks were prepared from 5 ml overnight cultures by mixing 800 ml of cell culture with 800 ml of sterile 40% glycerol.

2.2 Plant material

Arabidopsis thaliana accessions Columbia (Col0; N1093), Wassilewskija (Ws; N1602) and Landsberg erecta (Ler; N1686) and the mutant lines *dpe* 2-3 (Feldmann collection pool N6486) (Chia *et al.,* 2004) and *phs* 2-1 (N169185) (Lu *et al.,* 2006b) were originally obtained from the Nottingham Arabidopsis stock centre (NASC) and are available from the seed archive of the research group of Prof. Alison Smith, John Innes Centre.

2.2.1 Plant growth conditions

For routine growth Arabidopsis seeds were sown on wet potting compost (Levington's F2, Levington Horticulture, Suffolk, UK) in single pots of 9 to 11 cm diameter. Pots were covered with black lids and placed in a cold room (4°C) for 3 to 4 days to break seed dormancy.

After the cold treatment plants were transferred to SANYO cabinets (Sanyo GallenKamp). The diurnal cycle consisted of 12 h light and 12 h dark unless otherwise stated. The quantum irradiance was 160 $\mu mol \cdot m^{-2} \cdot s^{-1}$ and temperature was maintained at 20ºC. Seedlings were generally transferred to 40- or 60-cell trays (21 x 35 cm) when 9 days old. After transfer trays were covered with propagator lids for 5 to 7 days. For seed production, plants were grown in a controlled environment room (CER) (12 h light/12 h dark, 20ºC, 200 $\mu mol \cdot m^{-2} \cdot s^{-1}$) and seeds were harvested by bagging inflorescences before the siliques ripened and split open.

2.3 Plasmids

Empty vectors used for cloning or as controls during this study are listed in Table 2.2. Gateway vectors were transformed into *E. coli* DB3.1 for propagation and maintenance using the antibiotic resistance(s) shown. *E. coli* DH5α or Top10 cells were transformed with the plasmid carrying the gene of interest.

Vector	Resistance	Description	Source
pCR8/GW/TOPO TA	Spc^R	Vector for cloning DNA fragments with terminal 3' A-overhangs.	Invitrogen
pET151	Amp^R	Overexpression vector with N-terminal TEV-His_6 tag. TOPO cloning facilitated via 5' CACC overhang. Under control of T7 promoter.	Invitrogen
pGWB11	bar, Hyg^R	Gateway binary vector for cloning DNA fragments with terminal 3' A-overhangs. Provides N-terminal FLAG tag Expression of proteins in plant host.	Invitrogen
pEarleyGate202	Bar, Hyg^R	Gateway binary vector for cloning DNA fragments with terminal 3' A-overhangs. Provides C-terminal FLAG tag.	Invitrogen
pET-28a (+)	Kan^R	Overexpression vector with C-terminal His_6 tag.	Invitrogen

Table 2.2 Vectors used during this study

2.3.1 Oligonucleotides

Oligonucleotide primers were ordered from Sigma-Aldrich Ltd (Haverhill, UK) and resuspended in dH_2O to obtain a 100 µM stock solution. To obtain a working solution for the standard polymerase chain reaction (PCR), primers were diluted to 5 µM. For sequencing reactions a dilution to 1.25 µM was made. The most important oligonucleotides used in this work are listed in Table 2.3.

Oligonucleotide	Oligonucleotide sequence
For cloning of protein mutants into pET151	
FwDPE2TOPO	5'- CACCATGATGAATCTAGGA-3'

Oligonucleotide	Oligonucleotide sequence
RevDPE2TOPO	5'- TTATGGGTTTGGCTTAGT-3'
For cloning of DPE2 mutants	
FwDPE2coiledcoilLPAGS	5'-CTGCCGGCGGGCAGCCTGGACAAGAATGAT-3'
RevDPE2coiledcoilLPAGS	5'-GCTGCCCGCCGGCAGTTGATTCTTCGCCTT-3'
FwDPE2deltaCC	5'-CTCTCTGAACGTCTGATCTTTGACATAGAG-3'
RevDPE2deltaCC	5'-CTCTATGTCAAAGATCAGACGTTCAGAGAG-3'
RevDPE2D563N_1st	5'-TCCCAATATATGATTAATCCTGTATGC-3'
FwDPE2d563N_2nd	5'-GCATACAGGATTAATCATATATTGGGA-3'
RevDPE2D563A_1st	5'-TCCCAATATATGTGCAATCCTGTATGC-3'
FwDPE2d563A_2nd	5'-GCATACAGGATTGCACATATATTGGGA-3'
RevDPE2D810N_1st	5'-CAGGGTAGAGCAATTGTGGCATGAAGG-3'
FwDPE2D810N_2nd	5'-CCTTCATGCCACAATTGCTCTACCCTG-3'
RevDPE2D810A_1st	5'-CAGGGTAGAGCATGCGTGGCATGAAGG-3'
FwCBM201st	5'-GCTAGCTAGCATGATGAATCTAGGATCTC-3'
RevCBM201st	5'-ATATGGATCCTTAATCGAAACTGTGGTGGA-3'
FwCBM202nd	5'-GCTAGCTAGCAAAGTAGAAAAACCTCTAG-3'
RevCBM202nd	5'-TATAGGATCCTTATACAGAGAACATGGGAAC-3'
FwCBM20tandem	5'-TATAGCTAGCATGATGAATCTAGGATCTC-3'

Oligonucleotide	Oligonucleotide sequence
RevCBM20tandem	5'-TATAGGATCCTTATACAGAGAACATGGGAAC-3'
FwCDDPE2	5'-ATATGCTAGCGTTCCCATGTTCTCTGTA-3'
RevCDDPE2	5'-ATATGGATCCTTATGGGTTTGGCTTAGT-3'
FwDPE2delta1stCBM20	5'-TATAGCTAGCAAAGTAGAAAAACCTCTAGGG-3'
RevDPE2delta1stCBM20	5'-ATATGGATCCTTATGGGTTTGGCTTAGT-3'
FwDPE2deltainsert	5'-TATAGCTAGCATGATGAATCTAGGATCTC-3'
RevDPE2deltainsert	5'-ATATGGATCCTTATGGGTTTGGCTTAGT-3'
FwDPE2flpET28	5'-TATAGCTAGCATGATGAATCTAGGATCTC-3'
RevDPE2dlpET28	5'-ATATGGATCCTTATGGGTTTGGCTTAGT-3'
FwDPE2noinsert2	5'-CCTTTAAGTCAGGAAGCTCTGTTGAATTCA-3'
RevDPE2noinsert2	5'-TGAATTCAACAGAGCTTCCTGACTTAAAGG-3'
FwCBM20-MalQ1st	5'-ATGATGAATCTAGGATCT-3'
RevCBM20-MalQ2nd	5'-TCACTTTTTCTTAGCAGC-3'
RevCBM20-MalQ1st	5'-TCTCTTAGATTCCATTTCTGACCTTACAGAGA-3'
FwCBM20-MalQ2nd	5'TTCTCTGTAAGGTCAGAAATGGAATCTAAGAG-3'

Table 2.3 Oligonucleotides used during this study

2.4 Bacterial culture and media

Compositions of bacteria and plant media are described in Table 2.4.

Medium	Composition
Bacterial growth media	
Luria-Bertani Broth (LB) medium	10 g/l Bacto-tryptone, 5 g/l bacto-yeast extract, 10 g/l NaCl, adjust to pH 7.0, for solid medium Bacto agar (Difco) was added to a final concentration of 1.5%
Super Optimal broth with Catabolite repression (SOC)	20 g/l Bacto-tryptone, 5 g/l bacto-yeast extract, 10 mM NaCl, 2.5 mM KCl, pH was adjusted to pH 7.0, medium was autoclaved prior to addition of glucose to a final concentration of 20 mM and $MgCl_2$ to a final concentration of 2 mM.
Plant growth medium	
MS medium	0.5 x Murashige and Skoog plant salt mixture (Duchefa Biochemie, Ipswich, UK), 50 mg/l *myo*-inositol, 0.5 mg/l thiamine, 0.25 mg/l pyridoxine, 0.25 mg/l nicotinic acid, 0.25 g/l 2-[N-morpholino]-ethanesulphonic acid (MES), 0.8% (w/v) Bacto agar (Difco), pH was adjusted to 5.7 with 1 M KOH, sucrose was added to a final concentration of 30 mM for selection of transgenic plants

Table 2.4 Media used for bacteria and plants

Antibiotics were used for growth selection of *E. coli* and Agrobacterium and during selection of transgenic Arabidopsis lines. The final concentrations of antibiotics used are listed in Table 2.5.

Antibiotic	Final concentration	Dissolved in	Effect on
Ampicillin (Amp)	100 $\mu g \cdot ml^{-1}$	dH_2O	Gram-negative bacteria

Kanamycin (Kan)	50 µg·ml^{-1} (*E. coli*) 30 µg·ml^{-1} (*A. thaliana*)	dH_2O	Bacteria, fungi and plants
Gentamycin (Gm)	50 µg·ml^{-1}	dH_2O	Gram-negative bacteria
Rifampicin (Rif)	10 µg·ml^{-1}	methanol	Bacteria
Spectinomycin (Spc)	100 µg·ml^{-1}	dH_2O	Bacteria
Hygromycin (Hyg)	50 µg·ml^{-1}	dH_2O	Bacteria, fungi and plants
Basta (Glufosinate)	100 µg·ml^{-1}	dH_2O	Bacteria, fungi and plants
Chloramphenicol (Cm)	34 µg·ml^{-1}	ethanol	Gram-negative and Gram positive bacteria

Table 2.5 Antibiotic concentrations in selection media

2.5 Chromatography systems

For automated protein purification the ÄKTA® FPLC chromatographic system (Amersham Biosciences, Uppsala, Sweden) was used. The machine, including all pumps and buffer systems, was located in a refrigerator at 4 °C to prevent any protein aggregation or degradation during the purification process.

Separation of MOS and other soluble sugars was done with an automated HPAEC system (DIONEX DX-300) with pulsed amperometric detection (detector model PAD-II, Dionex Corp., Sunnyvale, CA). For analytical purposes, CarboPAC PA-100 and CarboPAC PA-1 columns (4·250 mm) (DIONEX, UK Ltd.) were used.

2.6 Biochemistry methods

2.6.1 Preparation of protein extracts

Approximately 1 g fresh weight leaf tissue was harvested onto ice midway through the light period (unless stated otherwise) and weighed immediately. The samples were homogenised with liquid N_2 in a pestle and mortar. The powder extract was suspended in the presence of 5 ml extraction buffer (see below) at 4 ºC and further prepared in a glass homogeniser. Complete cell disruption was achieved when the cell debris pellet appeared white after centrifugation of the homogenized extract (30.000 g).

100 mM	MOPS (pH 7.0)
150 mM	NaCl
10% v/v	Glycerol
0.1% v/v	Triton X-100
50 µM	DTT
10 $\mu l \cdot ml^{-1}$	Protease inhibitor Roche

2.6.2 Enzyme activity assays

2.6.2.1 Activity on APTS labelled acceptor substrates

Active site mutants of DPE2 were analysed for their ability to transfer glucose from maltose onto APTS-derivatised maltoheptaose (APTS-Glc7). The products of the reaction were transferred mixed with an equal amount of 6 M urea to allow settling into precast wells and separated on 30% polyacrylamide gels in a Tris-borate buffer system run at 450 V for 45 min at room temperature. Once run, the gels were scanned on a phosphorimager (Fuji BAS5000, GE) using reusable imaging plates at emission wavelength of 502 nm and excitation wavelength of 426 nm.

2.6.2.2 Initial rate kinetics of DPE2 and MalQ

To compare the disproportionation rates of DPE2 and MalQ on various MOS, two methods were used. In the first, glucose production was monitored using an NADP(H)-linked assay as described in 2.8.1.3 with maltose as glucose donor and Glc7 and glucose acceptors. The initial reaction rate was monitored as glucose production at increasing maltose concentrations. This

was plotted as a function over the rate of reaction. The K_m and V_{max} values were deduced from the reciprocal plot of both coordinates. The program used was Sigma plot (Section 2.9.3).

The second method was based on initial product analysis. The initial rate of formation of disproportionation products was analyzed using MOS with a degree of polymerization (DP) of 3-7 as substrates. Products of the reactions were analysed on HPAEC-PAD (Section 2.8.4). Standards were included at the beginning, middle, and end of the detection series to correct for a minor detector drift. An approximation of the detector response for G8, G9 and G10 was achieved by calculating the slope of the declining detector response over the applied MOS concentration.

2.6.3 Native PAGE

2.6.3.1 Protein oligomeric state

Non-denaturing gel electrophoresis, also called native gel electrophoresis, was used for activity assays and to obtain information about the oligomeric state of the proteins. The proteins migrate according to their size and charge properties, while maintaining their enzymatic active and native conformation.

Gel recipes were based on those published in "Protein Methods" (Bollag *et al.,* 1996). The rest of the procedure was as described in "Current Protocols in Protein Science" (Gallagher 2001).

Gels were run in Mini PROTEAN III gel tanks (Bio-Rad) using discontinuous electrophoresis, i.e. the running buffer is different from those used for preparing the acrylamide gels. The standard Laemmli running buffer (see 2.2.1.6.1) was used, without SDS and the reducing agent (β-mercaptoethanol). The sample buffer (native sample buffer) added to the protein samples did not contain SDS or β-mercaptoethanol, and the samples were not boiled before loading.

2.6.3.2 Activity gels

To identify specific activities in crude plant extracts, extraction-buffer soluble and insoluble fractions of extracts were loaded onto native gels. Samples of 2.5 µg of protein were mixed with native sample buffer and loaded onto the gel. Electrophoresis was at 4 ºC 30 mA and was stopped when the bromophenol blue dye reached the bottom of the gel.

After washing the gel twice with 40 ml of 100 mM Tris-HCl, pH 7.0, 1 mM $MgCl_2$, 1 mM EDTA and 1 mM DTT for 15 min the gels were incubated for 2 h at 37°C in 20 ml of this medium plus the appropriate substrate. The gel was stained with an aqueous solution of 0.67% (w/v) I_2 and 3.33% (w/v) KI.

2.6.4 Immunoblotting

Soluble protein fractions (prepared as in section 2.6) were separated by SDS PAGE and then transferred onto PVDF membranes by electro blotting. Equal loading was achieved by measuring the protein content of samples via Bradford assay prior to loading onto gels. After transfer, the membranes were blocked with 5% (w/v) BSA in TBS, and then incubated with either anti-MalQ (1:3000) or anti-DPE2 (1:1000) antisera. The secondary antibody was alkaline phosphatase conjugated anti-rabbit antibody (1:5000). Each incubation and blocking step was followed by extensive washing steps in TBST (TBS with 0.05% (v/v) Tween 20).

2.6.4.1 Antibody purification

Polyclonal antibodies targeted against recombinant DPE2 and MalQ (purified as described below) were raised in rabbits by immunisation with purified protein preparations (rabbit immunisation was done by Eurogentec, Southampton, Hampshire, SO45 1FJ, UK). The resultant blood sera were used to purify anti-DPE2 and anti-MalQ antibodies. For this purpose, purified DPE2 and MalQ proteins were covalently coupled to aldehyde-activated beaded agarose (Piercenet Aminolink Plus) in columns. The efficiency of protein immobilisation onto the beads was approximately 90% as judged by Bradford analysis of protein content in the column flow through. The blood serum was mixed with TBS and applied to the column. After extensive washing of the column with TBS buffer, a low pH glycine (50 mM pH 2.5) elution buffer was used to elute bound antibodies. Eluted fractions were used to develop immunoblots of plant extracts from lines with or without DPE2 and MalQ proteins. The fraction with the highest titre was used in immunoblots in this study. The purification and evaluation of the purified fraction is further described and shown in Appendix 4.

2.6.5 Linkage Analysis of disaccharide products

Sugar linkage analyses were performed by Martin Rejzek (laboratory of Prof Rob Field, John Innes Centre) and Alan Jones (Metabolite service, JIC) as described previously (Ciucanu *et al.* 1984) using a standard protocol (Oxley *et al.* 2006). Briefly, samples of disaccharides (10 µg)

were per-*O*-methylated using 50 µl of NaOH/DMSO (120 mg·ml^{-1}) followed by 40 µl of methyl iodide. The resulting per-*O*-methylated samples were hydrolysed using 500 µl of 2.5 M trifluoroacetic acid at 110 °C for 4 h, reduced using 50 µl of 1 M $NaBD_4$ in 2 M NH_4OH, and per-*O*-acetylated using 250 µl of acetic anhydride for 2.5 h at 110 °C. The resulting alditol acetates were solubilised in dichloromethane before analysis by gas chromatography/mass spectrometry (GC/MS) (Alderwick *et al* 2005).

The analyses were performed on an Agilent GC 6890N coupled to a Mass Selective Detector 5973*inert* (Agilent Technologies, Wilmington, Delaware, USA). Automated splitless injections (3 µl) were made using an Agilent 7683 automatic sampler. Conditions of chromatography were as follows: inlet temperature 250 ^{o}C, the carrier gas was helium at a flow rate of 0.9 ml/min, nominal inlet pressure of 8.70 psi, the oven temperature program was: 80 ^{o}C for 2 min, 20 ^{o}C/min to 380 ^{o}C then hold for 3 min, giving a total run time of 20 minutes. The column was a Zebron ZB-1ht (7HG-G014-02, Phenomenex, Torrance, California, USA) 30 mm x 0.25 mm ID x 0.10 µm film.

The mass spectrometer parameters were as follows: electron ionisation in positive mode (70eV), with a source temperature of 230 ^{o}C and a quad temperature of 150 ^{o}C set to the manufacturer's defaults. Total ion scans were made from 50 to 500 amu and all data processed via the Agilent GC Chemstation software (D.03.00) in conjunction with the NIST Mass Spectral Library, V8.0 (National Institute of Standards and Technology, Gaithersburg, Maryland, USA).

2.6.6 Protein purification and preparation

For the analysis of enzyme activity and protein properties, various mutants of AtDPE2, AtPHS2 and *E. coli* MalQ were produced in *E. coli* and purified via fast protein liquid chromatography (FPLC). Recombinant expression and purification of proteins were as follows.

2.6.6.1 Cell culture and protein expression

Starter cultures were grown overnight in 5 ml LB supplemented with the appropriate antibiotics at 37 ºC. These were used as inoculate (100 µl) for 100 ml cultures that were grown until OD_{600nm} ~0.6. These cultures were used to inoculate 1 l cultures plus suitable antibiotics in 2 l flasks, and grown at 37 ºC until early log phase (OD_{600nm} ~0.3). The cultures were transferred in shakers at 16 ºC for one hour, at which point they had an optical density of OD_{600nm} ~0.6. IPTG was added to a concentration of 1 mM, then cultures were grown overnight at 16 ºC with

constant shaking at 225 rpm. In the case of MalQ, expression was leaky and induction with IPTG was not necessary for overnight cultures at 28 ºC or more. In all cases, lower temperatures (< 37°C) were tried to improve protein folding and increase the yield of soluble protein. Cells were harvested by centrifugation at 5,500 *g* for 20 min at 4 ºC, and the cell pellets stored at -20 ºC until required.

2.6.6.2 Cell lysis

The pellets were thawed on ice and resuspended in 10 ml of lysis buffer (buffer A; see 2.6.5.3.) for each 1 l of original culture. The lysis buffer was supplemented with DNAase, Lysosyme and one tablet of Complete Protease Inhibitor EDTA-free (Roche). Cells were lysed with a cell disrupter (FAI BIO, Johnson & Johnson, USA). The cell debris was removed by centrifugation at 25,000 *g* for 30 min at 4 ºC, and the supernatant filtered through a 0.45 µm filter, then through a 0.22 µm filter before injecting in the chromatography column.

2.6.6.3 Nickel chelating affinity chromatography

HiTrap Chelating columns (Amersham Biosciences, Uppsala, Sweden) of 1 ml and 5 ml were used for the affinity purification of the proteins. The purifications were automated using an ÄKTA® FPLC chromatographic system (Amersham Biosciences, Uppsala, Sweden). The columns were washed with 5 column volumes of filtered, degassed MilliQ water, charged with half a column volume of 0.1 M $NiCl_2$ and washed again with 5 column volumes of filtered degassed MilliQ water before being equilibrated with 5 column volumes of washing buffer (buffer A).

The clarified lysate obtained as described in 1.13.2 was injected using a SuperLoop™ (Amersham Biosciences, Uppsala, Sweden), and the protein eluted using a gradient from 0 to 100% elution buffer (buffer B) over 10 column volumes. Fractions of 2-5 ml were collected and analyzed using SDS-PAGE.

Composition of buffers used during cell lysis and Ni^{2+}-affinity chromatography:

Buffer A: 100 mM HEPES pH7.5, 500 mM NaCl, 2 mM DTT, Protease inhibitor cocktail (one tablet; without EDTA), 60 mM imidazole

Buffer B: As buffer A, but with 500 mM imidazole.

Proteins produced with the TOPO 151 vector system were cleaved with TEV protease after a first purification step with HiTrap Chelating columns. The prepared samples were reloaded onto a HiTrap Chelating column where the flow through (proteins lacking His_6) was collected and further processed.

2.6.6.4 Size exclusion chromatography

Typically, size exclusion chromatography was performed (1 ml·min^{-1})using a HiLoad Superdex 200 16/60 prep grade column (Amersham Biosciences), pre-equilibrated with buffer C. Prior to loading, the protein sample was concentrated to 2-5% of the geometric column volume (2.5-6 ml) and filtered through a 0.22 μm filter. Fractions of 2 ml were collected and analysed using SDS-PAGE.

Buffer C: 25 mM HEPES pH 7.5, 50 mM NaCl

Size exclusion chromatography was also used to estimate the oligomeric state of the protein. A series of proteins of known molecular weight was used to construct a standard curve as described in the product literature (Gel Filtration HMW Calibration Kit, GE Healthcare). The molecular size of the protein of interest was estimated by extrapolation from the standard curve.

The proteins listed in the table on the next page were injected at a flow-rate of 1 ml·min^{-1} into a HiLoad Superdex 200 16/60 prep grade column pre-equilibrated with 25 mM Tris-HCl pH 7.5, 0.2 M NaCl. Blue dextran 2000 was also injected to determine the void volume of the column (V_o).

Knowing the molecular weight (M_r) and the elution volume (V_e) of the calibrating proteins, the K_{av} was calculated as shown in formula 2.1 and plotted against log M_r. The molecular size of the protein of interest was then estimated from the regression line of the plot for the column, expressed in formular 2.2.

$$K_{av} = \frac{(V_e - V_o)}{(V_t - V_o)}$$ formular 2.1

$$K_{av} = -0.3686 \cdot \text{LogM}_r + 2.2005; R^2 = 0.9994$$ formular 2.2

Total volume of the column: $\mathbf{V_t}$ = 112.6 ml

Void volume of the column: $\mathbf{V_o}$ = 42.91 ml

	Mr (Da)	**log Mr**	**Ve (ml)**	**K_{av}**
Ovalbumin	43,000	4.633468	77.08	0.490352
Conalbumin	75,000	4.875061	71.32	0.407694
Aldolase	158,000	5.198657	62.46	0.280549
Ferritin	440,000	5.643453	51.7	0.12614
Thyroglobulin	669,000	5.825426	46.34	0.049222

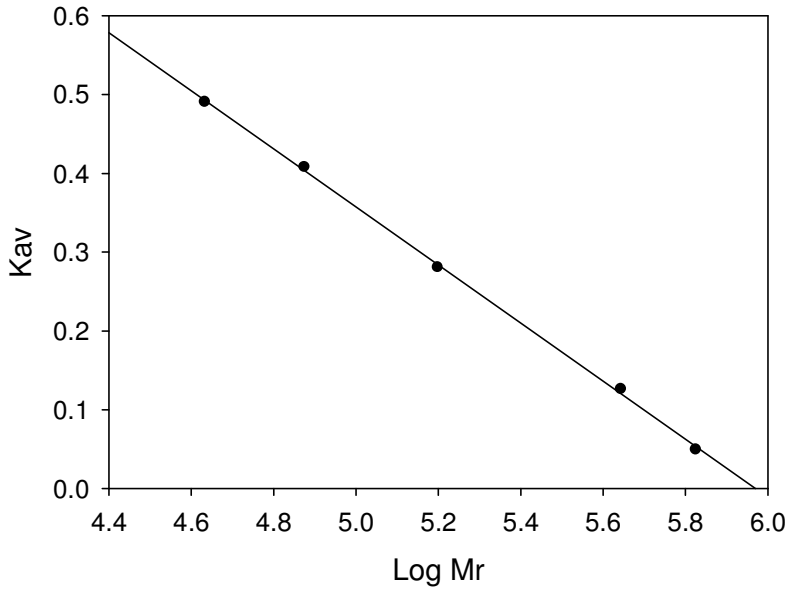

Figure 2.1 Standard curve for the calibration of the Superdex 200 16/60 column used for the experiments described in this work

2.6.6.5 Dialysis

Dialysis was performed using dialysis tubing with a molecular weight cut-off (MWCO) of 10,000 Da (snake skin pleated dialysis tubing, Thermo Scientific). Dialysis was against 100 times the volume of the protein sample, generally overnight with gentle stirring at 4 ºC.

2.6.6.6 Protein concentration and quantification

Where necessary, protein solutions were concentrated using centrifugal concentrators (Amicon™ Centricon™, Millipore), typically of 10,000 MWCO.

Protein concentration was estimated using the Bradford Reagent (Sigma) (Bradford 1976). Generally, 1 µl of protein solution was diluted with 999 µl of MilliQ water (with adjustments if estimated protein concentration lay outside the linearity range of the assay, which is between 0.1-1.4 $mg \cdot ml^{-1}$). Then 1 ml of Bradford Reagent was mixed with the sample by inverting 3-4 times and incubated at room temperature for 3 min. The OD_{595nm} was measured in a spectrophotometer within 5 min of mixing and the protein concentration calculated against a bovine serum albumin (BSA) standard curve.

2.6.7 Protein analysis

2.6.7.1 SDS-PAGE

The reagents and SDS-polyacrylamide gel preparation methods were based on the discontinuous buffer system of Laemmli (Laemmli 1970). Gels were run in Mini PROTEAN III gel tanks (Bio-Rad) filled with Tris-glycine electrophoresis buffer (25 mM Tris-HCl, 250 mM glycine pH 8.3, 0.1% SDS). Gel electrophoresis was performed at 200-250 V.

Prior to loading, samples were mixed with 5x SDS reducing buffer (60 mM Tris-HCl, pH 6.8, 25% glycerol, 2% SDS, 0.1% bromophenol blue, and 5% β-mercaptoethanol), boiled for 5 min at 100°C then centrifuged briefly. Samples were then loaded into the gel wells. Electrophoresis was continued until the bromophenol blue dye reached the bottom of the gel.

2.6.7.2 Dynamic Light Scattering

Dynamic light scattering was routinely used to assess the oligomeric state of the proteins after purification and/or prior to crystallization trials. Samples of 20 µl of protein were filtered

through a 0.1 μm membrane by centrifuging for 1 min in an Ultrafree-MC centrifugal filter (Millipore Co., Bedford, USA), then loaded into a 12 μl quartz cuvette (Wyatt) and count measurements taken in a dynamic light scattering device (DynaPro, Wyatt) at 25 ºC every 5-10 s. Data were analyzed using the Dynamics™ software package.

2.6.7.3 Circular Dichroism

Circular dichroism was used to examine the folding states of DPE2 mutant and wild-type proteins, purified as described above.

The samples were contained in a 0.1 mm quartz cuvette. CD measurements were taken at room temperature in a Jasco J-715 spectropolarimeter at the wavelengths normally used to study the conformation of the peptide backbone, i.e. between 260-185 nm, in 0.5 nm steps. Three measurements were taken per sample, the spectra averaged and the background (CD spectrum of the dialysis buffer) subtracted.

Subsequent data analysis was performed using the software available in the DICHROWEB server (http://www.cryst.bbk.ac.uk/cdweb/html/), (Whitmore and Wallace 2004)

2.6.7.4 Surface Plasmon Resonance (SPR)

Protein solutions of DPE2, MalQ and CBM20-MalQ were adjusted to 2 $mg \cdot ml^{-1}$. A 20 mM solution of the EZ-link Sulfo NHS-LC Biotin (Pierce) was also made. A 20-fold molar ratio of the biotin was added to the protein and incubated at room temperature for 30 minutes. Excess biotin reagent was removed by passing the reaction mixture through a G20 gel filtration spin column (GE) twice. The purified protein was then diluted to 100 $\mu g \cdot ml^{-1}$ for use in the immobilization.

The protein was immobilized on a Series S Sensor chip SA (GE), using 10 mM HEPES pH 7.0 with 150 mM NaCl as the running buffer. The chip surface was prepared by washing with 50 mM NaOH 1 M NaCl. The biotinylated protein was then applied to the surface at a flow rate of 10 $\mu g \cdot ml^{-1}$ until a target of 3000 bound Response Units (RU) was reached.

For the results for MalQ with Glc3, Glc4 and β-cyclodextrin immobilization was performed on a Series S Sensor chip CM5 (GE). In this case the protein was not biotinylated first and was instead directly coupled to the chip. In this case the protein was diluted to 100 $\mu g \cdot ml^{-1}$ using 10 mM sodium acetate (NaOAc) pH 5.0 with 150 mM NaCl. The protein was then immobilized

using the amine coupling kit from GE healthcare (life sciences). The CM5 surface was activated using a mixture of 1-ethyl-3-(3-dimethylaminoproplyl)-carbodiimide (EDC) and N-hydroxysuccinimide (NHS). The protein was then applied to the surface until an immobilization level of 6000 RU was reached (the higher binding level was needed to increase the sensitivity). The surface was then quenched with ethanolamine.

In all binding experiments analytes were applied to the chip at a flow rate of 30 $\mu l \cdot min^{-1}$ at 25 °C with the same running buffer as above. The contact time was 90 seconds, followed by a dissociation time of 30 seconds and regeneration using 10 mM HEPES pH 7.0 with 1 M NaCl for 90 seconds. All measurements were performed in triplicate on one chip and then repeated on another chip. In all cases a blank flow cell was measured at the same time. This cell is treated exactly the same as the others except protein is never immobilized. This blank, as well as a 0 concentration blank (a buffer only solution run over the flow cells with protein immobilized) is subtracted from the measured results for each analyte.

Analyte concentrations ranged from 50 nM to 10 mM for the oligosaccharides Glc3, Glc4, Glc5, Glc6 and Glc7 and from 25 µM to 3 mM for β-cyclodextrin.

All experiments were performed on a Biacore T100 (GE).

2.7 General molecular methods

2.7.1 Purification of plasmid DNA from *E. coli*

Plasmid DNA was isolated from *E. coli DH5α* cells using the QIAprep Miniprep system (Qiagen). This kit utilizes the method of alkaline lysis of bacterial cells followed by adsorption of DNA to silica in high osmotic conditions. Buffers mentioned below were supplied as part of the kit.

Typically 5 ml of overnight bacterial culture were centrifuged for 5 min at 3,200 *g* at 4 ºC and the supernatant discarded. The cell pellet was resuspended in 250 µl of buffer "P1" containing 100 $\mu g \cdot \mu l^{-1}$ RNase A, lysed by addition of 250 µl of buffer "P2" followed by gentle mixing, and neutralized by thorough mixing with 350 µl of buffer "N3". The white precipitate was removed by centrifugation at 13,000 rpm for 10 min. The supernatant was applied to a QIAprep spin column and centrifuged for 30-60 s at 13,000 rpm. The column was washed with 500 µl of buffer "PB" and centrifuged for further 30-60 s. The column was finally washed with 750 µl of

buffer "PE" and centrifuged twice for 30-60 s, discarding the flow-through after each spin. DNA was eluted by application of 50 µl of buffer "EB" on the centre of the filter. After 1 min, the column was centrifuged for 1 min. When the expected yield of DNA was low, or simply in order to obtain a higher DNA concentration, elution was performed with 30 µl of "EB" buffer warmed to 30-37 ºC.

2.7.2 Digestion of DNA with restriction enzymes

In the process of genotyping or confirmation of successful cloning, DNA was digested using restriction enzymes. Conditions depended on the origin and purity of the DNA and on the restriction enzyme used. In general, 1 U of enzyme was added to a 20 µl reaction to cut about 500 ng of DNA. Invitrogen (Buffer A to M) or New England Biolabs (NEBuffer 1 to 4 buffers) were used for all restriction enzyme digestions. Restriction enzyme digestions were performed according to the manufacturer's instructions, which usually recommend an incubation time of 1 to 2 h at 37°C. BSA was added to some of the digestion reactions as required.

2.7.3 Agarose gel electrophoresis of DNA

DNA fragments and PCR products were analyzed by agarose gel electrophoresis. Gels (1% agarose) were prepared by heating 1 g agarose in 100 ml TAE buffer (40 mM Tris, 20 mM acetic acid, 1 mM EDTA) with gentle agitation until just reaching boiling temperature. After cooling, ethidium bromide was added to a concentration of 1 $\mu g \cdot ml^{-1}$, and the solution was used to form horizontal gels. The DNA solutions were mixed with 6x loading dye (10 mM Tris-HCl pH 7.6, 0.03% bromophenol blue, 60% glycerol, 60 mM EDTA) prior to loading. The gel was run in TAE buffer at 100 V, monitoring the migration by following the bromophenol blue band. The DNA was visualized under UV light.

2.7.4 DNA sequencing

DNA was sequenced by cycle sequencing using the chain termination method, which takes dideoxynucleotide triphosphates (ddNTPs) as DNA chain terminators (Sanger *et al.,* 1977). A final volume of 10 µl contained about 100 ng of template DNA, 1.6 µl of 2 µM sequencing primer, 1.5 µl Big Dye sequencing buffer and 1 µl ABI BigDye version 3.1 sequencing mix (Applied Biosystems, Foster City, USA). Samples were run as described below.

Step	Temperature	Time
1	96°C	10 s
2	55°C	5 s
3	60°C	4 min

Repeat steps 1 to 3 25 times

Cool down to 10°C

Automated DNA sequencing was performed on AbiPrism 3730XL and 3730 capillary sequencers (Applied Biosystems,Warrington, UK) by the DNA Sequencing Service at the John Innes Centre. DNA sequences were analysed using ContigExpress (Vector NTI Advance 11, Invitrogen).

2.7.5 Site directed mutagenesis/overhang PCR

Site-directed mutagenesis of DPE2 and creation of chimeric proteins and truncated proteins was performed by overhang PCR, using a two-step protocol in which desired gene fragments were fused or substituted.

Internal mutagenic primers were designed to either introduce desired amino acid substitutions at specific amino acid position or to introduce a whole gene fragment. The internal forward 5'-primer and reverse 3'-primer contained complementary sequences surrounding the mutated bases. Two PCR reactions were set up using the internal mutagenic primers and Pfu Ultra (Stratagene) high-fidelity polymerase (Figure 2.2). The following thermal cycling conditions were used:

1) 95 °C,	30 sec
2) 70 °C,	1 min (-1 °C per cycle)
3) 68 °C,	1 min/kb
4) Repeat 1) to 3),	15 times

5) 95 °C, 30 sec

6) 50 °C, 1 min

7) 68 °C, 1 min/kb

8) Repeat 5) to 7), 10 times

The extension phases were sufficiently long to amplify the whole sequence. After identification via agarose gel electrophoresis products were mixed with the appropriate forward and reverse primers of the desired whole gene fragment.

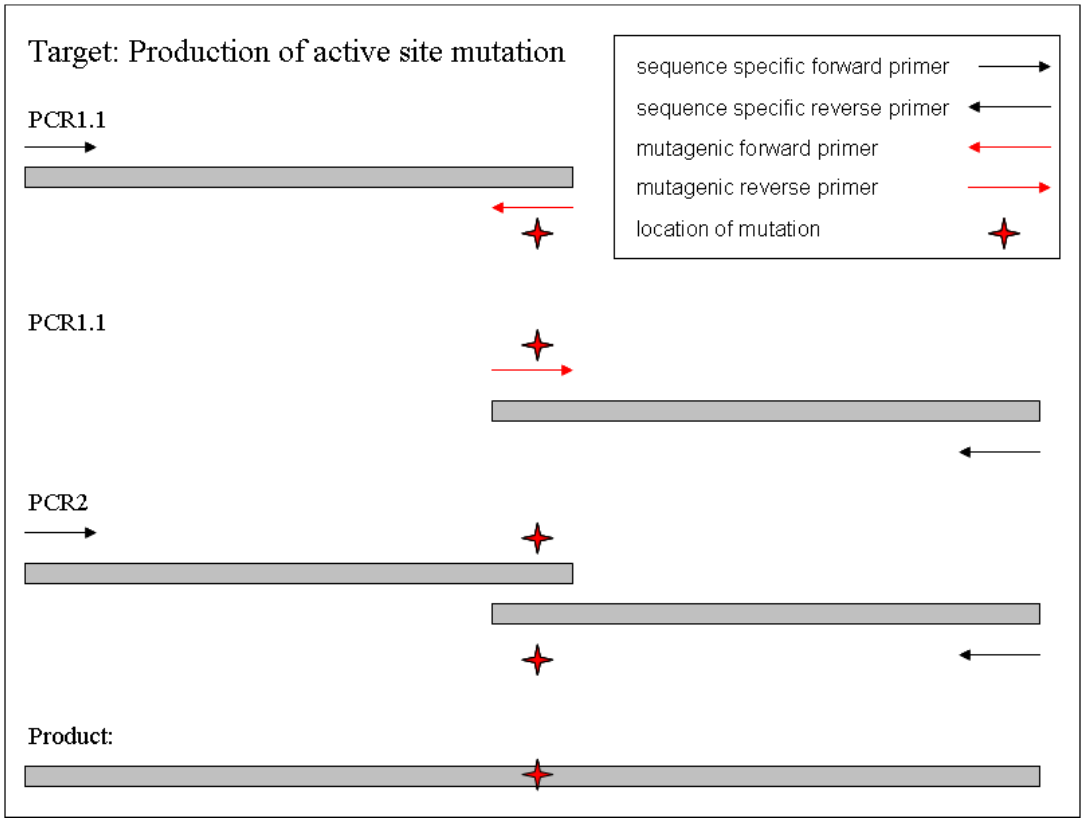

Figure 2.2 Outline of the two-step PCR protocol for the production of truncated protein, chimeric proteins (e.g. CBM20-MalQ) and active site mutants of DPE2

2.7.6 TOPO cloning

The TOPO cloning Technology utilises the inherent biological activity of DNA topoisomerase I. The TOPO cloning kit was used to clone PCR products with 5' CACC overhang into TOPO

vectors (TOPO® TA Cloning® Kit, Invitrogen). TOPO vectors are designed in such a way that they carry a specific sequence 5´-(C/T)CCTT-3' at the two linear ends. The linear vector DNA already has the topoisomerase enzyme covalently attached to both of its strands' free 3' ends. This is then mixed with PCR products that carry a 5' CACC sequence. The CACC sequence of the PCR product attaches the topoisomerase 3' end. The result is a directional cloning product.

2.7.7 Standard polymerase chain reaction (PCR)

Either the GoTaq Flexi Kit (Promega) or the Phusion High-Fidelity DNA polymerase (New England Biolabs Ltd) was used for colony-PCR and genotyping. For amplification of difficult products 3% (v/v) DMSO was added to the reaction. Negative and positive control samples were run together with the other samples to ensure correct handling and mixing of the components.

Final concentration	**Component**
1 pg – 50 ng 50 – 500 ng	plasmid DNA or genomic DNA
1 x 1 x	GoTaq Flexi Buffer or Phusion HF Buffer
500 µM	Deoxyribonucleotides (dNTPs)
0.4 µM	Oligonucleotide A
0.4 µM	Oligonucleotide B
0.1 U 0.05 U	GoTaq Flexi polymerase or Phusion polymerase

Table 2.6 Standard PCR used for DNA amplification conditions used during this study

All PCR amplifications were conducted in a DYAD Thermal Cycler (Bio-Rad) using the program displayed in Table 2.7.

Step	**Temperature**		**Time**	
	GoTaq	Phusion polymerase	*Taq/Pfu* polymerase	Phusion polymerase
1	95°C	98°C	1 min (10 min for colony PCR)	1 min
2	94°C	98°C	30 s	20 s
3	T_m-3°C	T_m	30 s	20 s
4	72°C		1 min/ kb	15 to 30 s/ kb
5	*Repeat steps 2 to 4 29 to 34 times*			
6	72°C		2 to 10 min	
7	*Cool down to 10°C*			

Table 2.7 Standard PCR program used for DNA amplification conditions used during this study

2.7.8 A-tailing of PCR products

Cloning of a PCR product into the GATEWAY-ready pCR8/GW/TOPO TA plasmid (Invitrogen) requires 3' A-overhangs at the end of the DNA double strand. Standard Taq polymerase enzymes like GoTaq (Promega) produce DNA fragments with such overhangs. Proofreading function of Phusion taq (New England Biolabs Ltd) removes 3' A-overhangs resulting in blunt-end PCR fragments. To allow cloning of Phusion taq amplified PCR products into pCR8/GW/TOPO an A-tailing reaction was performed using the following reaction mix.

Final concentration	Component
---	5 µl PCR product
1 x	GoTaq Flexi Buffer
1 mM	Deoxyadenosinetriphosphate (dATPs)

1 mM MgCl2

0.1 U GoTaq Flexi polymerase

dH2O to 10 µl total volume

Samples were incubated for 10 min at 72°C then used for agarose gel electrophoresis and subsequently purified from the gel.

2.7.9 Cloning of PCR fragments into pCR8/GW/TOPO TA

Cloning of PCR fragments into pCR8/GW/TOPO TA (Invitrogen) was performed using the following reaction mix in Table 2.8.

Amount	**Component**
0.5 to 3.5 µl	PCR product
1 µl	Salt solution (1.2 M NaCl, 60 mM $MgCl_2$)
0.5 µl	Vector (pCR8/GW/TOPO TA)
x µl	dH_2O to 5 µl

Table 2.8 Standard reaction conditions for TOPO cloning

Samples were incubated 10 min to 1 h at room temperature and transformed into chemically competent Top10 *E. coli* cells (Section 2.1). Successful cloning was confirmed by colony-PCR (Section 2.7.7).

2.7.10 LR reaction

The gene in the pCR8 entry plasmid (Section 2.7.9) is flanked by attL sites, whereas the GATEWAY cassette in the destination plasmid is flanked by attR sites. These sites are recombined by the clonase enzyme thereby exchanging the sequences within the attL and attR sites (LR reaction).

For the LR reaction, 50 to 150 ng of pCR8 plasmid containing the fragment of interest were mixed with the same amount of destination vector. TE buffer (10 mM Tris-HCl, 0.1 mM EDTA, pH 8.0) was added to 4.5 µl of total volume. LR Clonase II (Invitrogen Ltd.) (0.5 µl) was added followed by vigorous mixing. The samples were left at room temperature for 4 h to 16 h. To terminate the LR reaction, 0.5 µl of proteinase K solution was added to each sample followed by incubation at 37°C for 10 min. Subsequently, *E. coli* Top10 or DH5α cells were transformed with 2.5 µl of each LR reaction (Section 2.7.11.1) and the successful recombination was confirmed by colony-PCR (Section 0).

2.7.11 Transformation of living cells

2.7.11.1 Transformation of *E. coli*

In each *E. coli* transformation, 15 to 30 µl of frozen competent cells were mixed with 1 to 3 µl of LR recombination reaction (Section 2.7.10) or 0.5 µl of vector DNA isolated using the QIAprep Spin Miniprep Kit (Section 2.7.1). The mix was incubated on ice for 20 to 30 min. The cells were then heat shocked at 42°C for 40 s and chilled on ice for 2 min. One ml of SOC medium was added and the cells were incubated in a shaker at 37°C and 200 rpm for 1 h. Cells were collected by centrifuging at 5,500 *g* for 5 min. The supernatant was removed and the pellet was resuspended in 100 µl of LB broth. Cells were plated on LB agar medium containing the appropriate antibiotics and the plates were incubated upside down at 37°C for about 16 h. To isolate bacteria with the correct insert, colony PCR was used to screen bacterial colonies after transformation (Section 0).

2.7.11.2 Transformation of *Agrobacterium tumefaciens*

A. tumefaciens strain GV3101 was grown in 200 ml LB to an OD_{600} of 0.8 to 1.0. Cells were collected by centrifugation and washed in subsequent steps with 200 ml and 2 ml of ice-cold $CaCl_2$ to generate freeze/ thaw competent cells. Fifty µl competent cells were thawed on ice and 5 µl of plasmid DNA isolated with the QIAprep Spin Miniprep Kit (Section 2.7.1) was added and mixed carefully. Cells were incubated on ice for 5 min, followed by 5 min in liquid nitrogen and 5 min at 37°C. One ml of LB medium was added to the cells followed by incubation at 28°C with shaking for 2 h then centrifugation at 5,500 *g* for 5 min. The cell pellet was resuspended in 100 µl of LB broth and plated on selective LB medium. Plates were incubated upside down at 28°C. Colonies appeared after 48 h and were tested by colony PCR (Section 0).

2.7.12 Agrobacterium mediated transformation of Arabidopsis by floral dipping

Arabidopsis plants were planted 5 per 121 cm^2 pot and grown in a CER until they flowered. The primary inflorescence was removed and plants were infiltrated when most secondary inflorescences were 3 to 15 cm tall. *A. tumefaciens* strains transformed with the appropriate plasmid were grown in 400 ml LB broth medium at 28ºC shaking at 250 rpm to an OD_{600} of 1.0 to 1.4. Cells were harvested by centrifugation for 10 min at room temperature at 5,500 *g* then resuspended into infiltration medium (5% (w/v) sucrose, 0.05% Silwet). The Agrobacterium inoculate were transferred to beakers and plants were inverted into the suspension such that all above-ground tissues were submerged while moving the plants in the infiltration medium for 1 to 2 min. Infiltrated plants were placed in trays and covered with clear plastic to maintain humidity then left in low light or dark overnight and returned to the glasshouse the next day and allowed to set T_0 seed.

2.8 Plant metabolic biology methods

2.8.1 Measurement of starch content

To determine the starch content in Arabidopsis leaves, insoluble material was extracted from plant tissue using the perchloric acid method. Starch was then enzymatically digested to glucose which was subsequently assayed using an NADP(H)-linked assay. The original method as described earlier (Hargreaves and ap Rees 1988) was modified to allow high throughput sample preparation, as follows.

2.8.1.1 Extraction of starch and soluble carbohydrates from Arabidopsis rosettes

From a single rosette, 50 – 150 mg of plant material comprising a representative mixture of rosette leaves of all growth stages was harvested in 2 ml tubes containing a steel ball (4 mm diameter) and immediately frozen in liquid nitrogen. The tissue was ground using a Genogrinder (SPEX Sample Prep) at 500 strokes per minute for 35 s, constantly keeping the material frozen. Perchloric acid (1.5 ml of 0.7 M) was added and vigorously mixed. Samples of 400 µl were transferred to two replicate 96-well plates on ice. To each sample 300 µl of 95% (v/v) ethanol was added. The 96-well plate was sealed and the contents briefly mixed by inversion, followed by centrifugation at 3260 g for 10 min using a swing out rotor. Part of the supernatant was removed for analysis of soluble sugars and MOS. The remainder was discarded and 600 µl of 80% (v/v) ethanol was added to the residue in each well followed by shaking in the Genogrinder

at 500 to 700 strokes per minute for 20 s. Plates were centrifuged as before and the washing step using 80% ethanol was repeated. The supernatant was discarded and 150 µl of dH_2O was added to each sample. To solubilise starch, plates were sealed with thermo-stable 96 cap mats (Thermo scientific) and heated at 90 to 95°C for 15 min. Samples were cooled and 600 µl 95% (v/v) ethanol was added. Plates were sealed, inverted twice and centrifuged as before. The supernatant was discarded and samples were air-dried for 10 min to allow residual ethanol to evaporate. Pellets were resuspended in 300 µl dH_2O and either used immediately for enzymatic starch digestion (Section 2.8.1.2) or stored at -20°C.

2.8.1.2 Enzymatic digestion of starch

For one of the two replicate plates (Section 2.8.1.1) starch was enzymatically digested to glucose by addition of 290 µl NaOAc (0.2 M, pH 4.8) and 10 µl of a 9:1 (v/v) mixture of amyloglucosidase (10 $\mu g \cdot \mu l^{-1}$, Roche, Basel, Switzerland) and α-amylase (1 $U \cdot \mu l^{-1}$Megazyme, Bray, Ireland) to each well. The second plate was used as a negative control: 300 µl NaOAc (0.2 M, pH 4.8) was added to each well. The contents of the plates were placed mixed by briefly shaking in the Genogrinder at 500 strokes per minute. Plates were incubated over night at 37°C. Samples were then used for glucose measurement or stored at -20°C.

2.8.1.3 Glucose assay

The replicate plates containing the negative control and the enzymatic digest of starch were centrifuged at 3,260 *g* for 10 min using a swing out rotor. To measure glucose content, 5 to 20 µl supernatant of each sample was transferred in triplicate (technical repeats) to 96-well microtitre plates and the following assay mixture was added to a total volume of 198 µl.

Final concentration	Component
25 mM	HEPES (pH 7.9)
1 mM	MgCl2
1 mM	ATP (Roche)
1 mM	NAD (Roche)
0.003 $U \cdot \mu l^{-1}$	Hexokinase (Roche)
x µl	dH2O (add to 198 µl)

The OD_{340} was measured as using a plate reader (SPECTRAmax 340PC, Molecular Devices). Two µl (1 U) glucose-6-phosphate dehydrogenase (G6PDH) (*Leuconostoc mesenteroides*,

Roche) was added to each sample. Following an incubation of 15 min at room temperature to allow the completion of the enzymatic reaction, a second OD_{340} measurement was made. The glucose content was calculated as described before (Hargreaves and ap Rees 1988).

2.8.2 Measurement of soluble sugars in pH neutralised extracts

To determine the soluble sugar content in Arabidopsis leaves, soluble carbohydrates were extracted from plant material using the perchloric acid method described above (2.8.1.1.).

2.8.2.1 Measurement of glucose, fructose and sucrose

To measure glucose content, 5 to 20 µl of neutralised extract were transferred in triplicate (technical repeats) to 96-well microtitre plates. Glucose was assayed as in 2.8.3. To measure the fructose content, 2 µl of phosphoglucoisomerase (1 U) (yeast, Roche) were added to each well following the incubation with G6PDH and a third reading was taken at OD_{340} nm.

To measure the sucrose content, the neutralised extract was incubated with or without ß-fructosidase overnight at 37°C as displayed in Table 2.9. This was followed by assay for glucose as in section 2.8.3. Glucose derived from sucrose was calculated from the difference in OD values between assays of samples incubated with and without ß-fructosidase.

amount	**Component**
200 µl	Acid extracted soluble fraction (neutralized)
100 µl	0.22 M NaOAc pH 4.8
2.5 µl	5 $mg \cdot ml^{-1}$ ß-fructosidase solution

Table 2.9 Reaction conditions for sucrose quantification

2.8.2.2 Measurement of maltooligosaccharides (MOS)

2.8.2.2.1 Sample preparation

Samples of soluble perchloric acid extracts prepared as in 2.8.1.1 were neutralised to pH 5 with neutralisation buffer:

Final concentration	Component
2 M	KOH
0.4 M	MES
0.4 M	KCl

Table 2.10 Neutralisation buffer for MOS extraction

The neutralisation volume was recorded and the samples were centrifuged for 10 min at 4,500 *g* and 4 °C. The resultant supernatant was used for all subsequent steps.

2.8.2.2.2 Ion exchange chromatography on neutralised samples

The neutralised samples were subjected to anion/cation exchange chromatography. Dowex 50 and Dowex 1 resins were charged with 2 M HCl and 1 M NaOAc respectively, then poured into 2 ml columns (1.5 ml of resin) consisting of syringe barrels from 2 ml syringes with the plunger rods removed. To keep the resin slurry inside the syringe barrel, 3 mm glass balls were used to block the needle exit. The columns were assembled in series, so that extract passed through the Dowex 50 then the Dowex 1 column. Columns were loaded with, 100 µl of neutralised sample then washed 10 times with 100 µl water followed by 4 times with 500 µl water. The eluate was freeze dried, then dissolved in 100 µl of water and filtered with a 0.1 µm filter prior to HPAEC-PAD analysis.

2.8.2.2.3 High-performance Anion-Exchange Chromatography with Pulsed Amperometric Detection (HPAEC-PAD) analysis

High-performance Anion-exchange Chromatography (HPAEC) was carried out on a Dionex DX-300 system with a pulsed amperometric detector (Model PAD-II, Dionex (UK) Ltd, Albany Court, Camberley, Surrey), using a CarboPAC PA-100 column. A sample (50 µl) prepared as above was injected and eluted with 150 mM NaOH.

Linear gradient for separation of MOS on DIONEX CarboPAC PA-100

Time (min)	**% A**	**% B**
0	100	0
5	100	0
25	30	70
30	0	100
35	0	100
40	100	0

Solution A: 100 mM NaOH

Solution B: 100 mM NaOH,
1 M NaOAc

Table 2.11 Gradient for HPAEC separation on CarboPAC PA-100

For the analysis of monosaccharide and disaccharide products from enzyme assays carried out on AtDPE2 and *E. coli* MalQ (chapter 4 Section 4.2.1) a CarboPAC PA-1 column (4 · 250 mm) was used. Samples of 25 µl were injected and eluted with 150 mM NaOH.

2.9 Software tools

2.9.1 DNA and protein sequence analysis

Sequences were aligned using the AlignX function of the Vector NTI Advance Suite 11 (Invitrogen). Protein alignments were done with ClustalW or Prankster with the default settings on NCBI. The alignments were manually modified where necessary with BioEdit. The graphical output was performed with BioEdit and Power Point. Coiled coil prediction based on primary amino acid sequences was done with Paircoil II (http://groups.csail.mit.edu) and Coils (http://www.ch.embnet.org). The phylogenetic tree and protein sequence alignments were constructed with Mega5 (http://www.megasoftware.net/). The sequences were assigned with the John Taylor Thornton algorithm and a bootstrap value of 1000 was used for the calculations and assembly of the tree.

2.9.2 Quantifying band intensities in immunoblots and activity gels

Gels and blots were scanned (Epson perfection V750 pro) or photographed (Andrew Davies, John Innes Centre, photography department) and saved as .png files. These were analysed in Image J 1.44p (Wayne Rasband, National Institute of Health, USA). The band intensities corresponded to band area and pixel density that were normalised to a standard. This allowed approximate quantification of the data.

2.9.3 Linear regression and curve fitting

Various datasets collected in this study were based on regression analysis of standards. For Bradford assay of protein quantification linear regression of standard BSA sample data was used. For data on protein kinetics, Michaelis Menten curve fitting was used. For analysis of MOS derived from plant material or enzyme assay on the DIONEX system, global curve fitting was used to determine the standard values. The programs used for linear and global curve fitting were Microsoft Excel and Sigma plot respectively.

3 Biochemical analysis of DPE2

3.1 Introduction

The conversion of starch derived maltose to hexose phosphates in plants requires a complex pool of soluble heteroglycans (SHG) that serves as substrate for the transglucosidase DPE2 and the glucan phosphorylase PHS2. The action of DPE2 on maltose and SHG represents the key step in this pathway. The unique structural and enzymatic features of DPE2 will be discussed below.

3.1.1 The unique multimodular domain arrangement of DPE2

DPE2 belongs to family 77 of glycoside hydrolases as classified based on primary amino acid sequence (Cantarel *et al.,* 2009). GH77 enzymes catalyse a chemical reaction that transfers a segment of a 1,4-α-D-glucan to a new position in an acceptor glycan, which may be glucose or another 1,4-α-D-glucan (MacGregor *et al.,* 2001). There are many synonyms in the literature for enzymes belonging to this class of glycoside hydrolases. A few are: amylomaltase, transglucosidase, disproportionating enzyme (D-enzyme), glucanosyltransferase or glucosyltransferase and even incorrectly glycosyltransferase (Chia *et al.,* 2004, Critchley *et al.,* 2001, Dippel and Boos 2005, Fettke *et al.,* 2006a, Palmer *et al.,* 1976). In this and the following chapters, I shall refer to these enzymes as GH77 enzymes.

There are currently 1130 protein sequences (22.06.2011) annotated as GH77 enzymes in the CaZy database of carbohydrate active enzymes (http://www.cazy.org/GH77.html)(Cantarel *et al.,* 2009). Approximately 90% of these are single domain proteins like MalQ from *E. coli* (orthologue of DPE2 in bacteria) which possesses only a single GH77 domain (see next page, Figure 3.1, A). DPE2 in contrast is much more complex. It is the only GH77 enzyme that contains a starch binding domain (SBD). The SBD is located at the N-terminus and is made up of two carbohydrate binding modules that belong to family 20 (CBM20) (see next page, Figure 3.1, B). It furthermore contains a large insertion (approximately 170 amino acids) within its GH77 domain. This insertion is unique to DPE2-like GH77 enzymes and does not share any sequence similarity with other proteins (Steichen *et al.,* 2008). In the following paragraphs these unusual structural aspects of DPE2 are described in further detail.

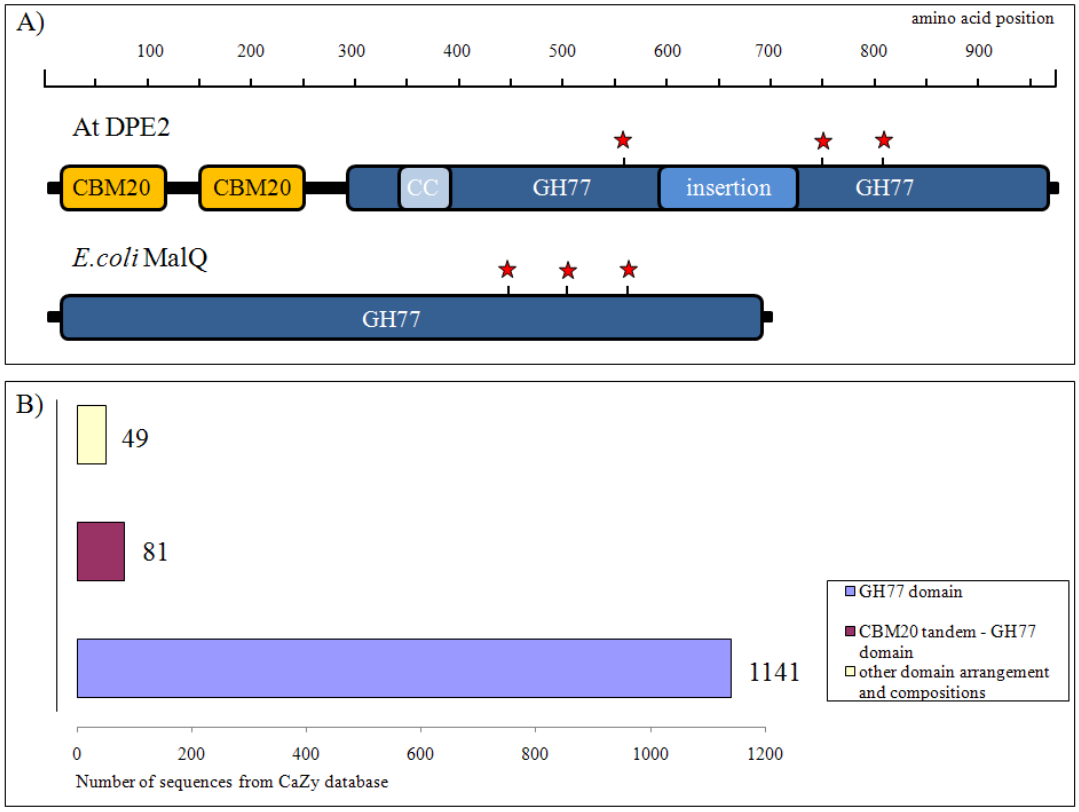

Figure 3.1 Multimodular domain arrangement of DPE2

A) DPE2 and MalQ are shown with the prediction of their domain boundaries. The top numbers indicate the positions of the amino acids. The red stars indicate the position of the active site residues. CBM20; carbohydrate binding module family 20, GH77; glycoside hydrolase family 77, CC; coiled coil motif 20 B) The bar chart shows the distribution of the domain arrangements amongst GH77 enzymes. X-axis indicates the number of sequences as of June 2011 (Origin: CaZy database; http://www.cazy.org/)

3.1.2 The amino acid insertion and the active site

GH77 enzymes are found in archaea and bacteria as well as in plants and other eukaryotes (Janecek *et al.,* 2007). They are involved in the metabolism of MOS, glycogen or starch (Boos and Shuman 1998, Lu *et al.,* 2006b). The common catalytic machinery is the same for all members of this class of enzymes and involves a catalytic triad. Two aspartate and one glutamate residue are essential for the catalytic activity. The two aspartates act as catalytic nucleophile and transition state stabiliser respectively. The role of the acid base catalyst is carried out by the glutamate (Przylas *et al.,* 2000b). This catalytic triad is not only conserved in GH77 enzymes, but also in members of the GH70 and GH13 class of glycoside hydrolases. Together these three families form the ClanH of glycoside hydrolases (more than 10,000

predicted protein sequences) (Cantarel *et al.,* 2009). DPE2 is the only enzyme in this clan that contains the large amino acid insertion within the active site on primary amino acid level. This insertion is found in all DPE2-like enzymes (Steichen *et al.,* 2008) and no specific function has yet been assigned to it. However, it was proposed that the insertion would have little impact on catalysis (Steichen *et al.,* 2008). This proposal was based on the crystal structure of potato DPE1 (pdb file: 1X1N; Figure 3.2). In this template structure of DPE1, the insert of DPE2 replaces a segment which makes up the α-4 helix and the β-5 strand of the $(\alpha/\beta)_8$ barrel. Figure 3.2 shows the location of the segment (green).

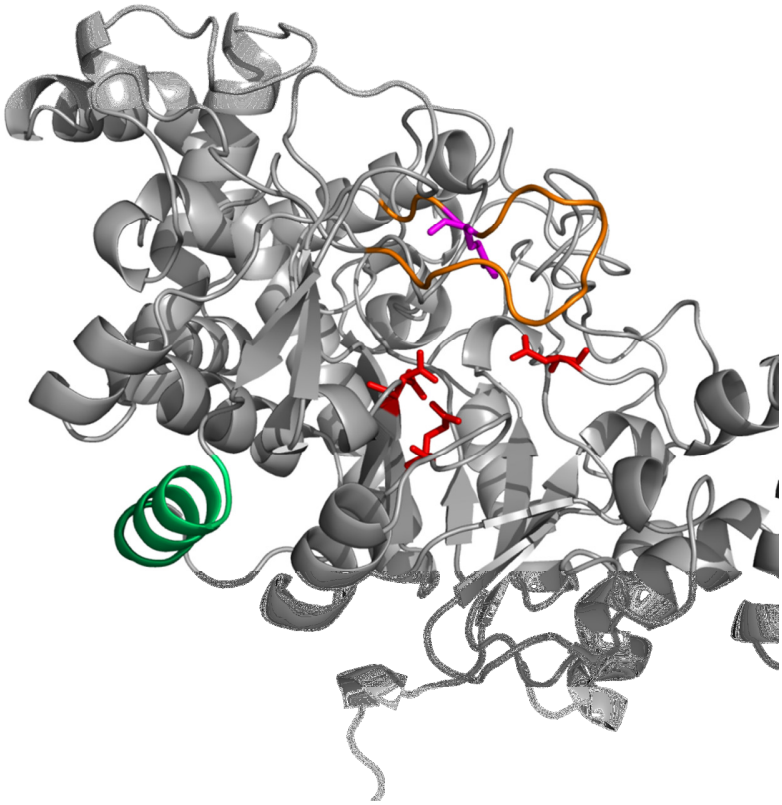

Figure 3.2 Structure of DPE1 (1X1N)

Shown is the location of the α-helix that has been replaced by the 170 amino acid-insertion in the DPE2 type enzymes. The red sticks show the active site residues and the orange loop shows the flexible loop typical for GH77 enzymes, shielding the active site. The magenta stick shows the position of a glutamine residue that was proposed to control the hydrolysis to transfer ratio in GH77 enzymes. The structure was downloaded from the PDB database (http://www.pdb.org) and displayed with PyMOL. The final picture was rendered in ray1200, 1200.

The segment is at the surface of the enzyme directly opposite the active site (the three active site acidic residues are shown in red). It was suggested that there is no obvious way in which the insertion could directly interact with substrate at the active site. DPE2 and DPE1 however, are not closely related proteins (Figure 3.3) and share only 26% sequence identity (CBM20 tandem and amino acid insertion of DPE2 excluded). A complete analysis of the active site has not been done yet and data on the function of the insertion are lacking.

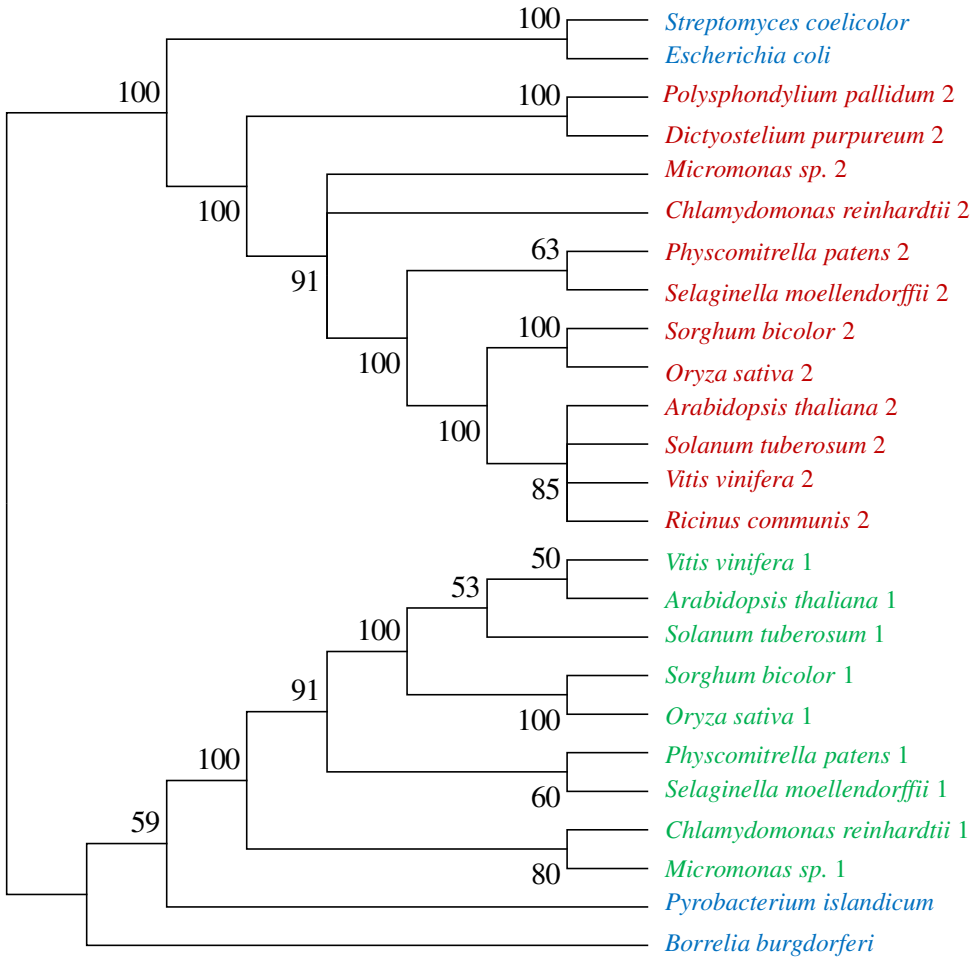

Figure 3.3 Phylogenetic analyses of the evolutionary relationships of DPE1, DPE2 and MalQ

The protein sequences were aligned by Prankster (Goldman Group Software) and analyzed by Mega4. Numbers on the branches are bootstrap values. The CBM20 tandem and amino acid insertion of DPE2 were excluded in the alignment. For plant enzymes, 1 (in green) refers to the plastidial GH77 enzyme DPE1, while 2 (in red) refers to the cytosolic GH77 enzyme DPE2. Blue refers to MalQ from prokaryotes.

3.1.3 The CBM20 tandem

Enzymes containing CBM20 modules that form the basis of an SBD are widespread among bacteria, archaea and eukaryota (Machovic *et al.,* 2005). The role of these enzymes is diverse. For instance, R-47 from *Thermoactinomyces vulgaris* hydrolyses storage starch extracellularly (Tonozuka *et al.,* 1993). In contrast, PWD from *Arabidopsis thaliana* modifies the surface properties of transient starch granules in chloroplasts of photosynthetically active leaf cells (Baunsgaard *et al.,* 2005). However, the function of the SBD unit in both enzymes is the same: binding to starch (Abe *et al.,* 2004, Christiansen *et al.,* 2009b). It is surprising to find a protein like DPE2 that contains such a SBD in the plant cytosol as there is no evidence for starch or starch-like molecules in this cellular compartment (Zeeman *et al.,* 2010). DPE2 was even shown to bind to starch *in vitro* (Steichen *et al.,* 2008). The proposed substrate of DPE2 *in vivo* (SHG) does not share any of the physicochemical characteristics that can be found in a starch granule. As mentioned previously in Chapter 1, SHG is water soluble, contains glucose only to a very limited extent and does not seem to contain any 1,4-glucose linkages as judged from linkage analysis (Fettke *et al.,* 2004, Fettke *et al.,* 2005a, Fettke *et al.,* 2005b). Nevertheless, it cannot be excluded that the N-terminal CBM20 tandem targets DPE2 to SHG. However, experimental data supporting this possibility are lacking.

The role of the two CBM20 modules of DPE2 may be different from those of CBM20s in other enzymes. DPE2 mutant proteins lacking the first of the CBM20 modules lose the ability to bind to starch. The same mutant also shows an altered enzyme activity on small carbohydrate substrates (Steichen *et al.,* 2008). This suggests a role of the CBM20 tandem not only in binding of complex polysaccharides like starch but also in the determination of substrate specificity. How these findings translate to the interaction of DPE2 with the proposed *in vivo* substrate SHG is difficult to assess and requires further experimental investigation.

3.1.4 The proposed *in vivo* acceptor SHG

Work so far has established that the monosaccharide composition of SHG differs between wt plants and mutants lacking DPE2 (Fettke *et al.,* 2006a), PHS2 (Fettke *et al.,* 2005b) or the cytosolic phosphoglucomutase (cPGM) (Fettke *et al.,* 2008). However, SHG is not only restricted to photosynthetically active leaf cells. It is also found in Arabidopsis roots (Malinova

et al., , Malinova *et al.,* 2011), potato tubers (Fettke *et al.,* 2009b) and Arabidopsis seeds (fettke, 2006). (Fettke *et al.,* 2006b). Thus, it appears to be widely distributed in plant tissues. It was furthermore found that there is a diurnal turn over of SHG in plants. The size of the total SHG pool and the glucose composition of specific subfractions of SHG changes throughout the day and night cycle (Fettke *et al.,* 2006a). Taken together, these analyses are consistent with a role of SHG in the mobilisation of starch to sucrose. However, information about the biochemical origin and more importantly any structural information on SHG are lacking. Furthermore, the similarity to cell wall components like AGs, as discussed in Chapter 1, is striking and analysis of this relationship is lacking.

It seems possible that the structural complexity of DPE2 is related to its use of SHG as glucosyl acceptor substrate. However, relatively little is known about the structure-function relationship of DPE2 and SHG.

The aim of this chapter was to further explore the unique properties of DPE2 in relation to its proposed use of SHG as an acceptor substrate. In order to achieve this I did the following experiments:

- Production of DPE2 active site mutants and analysis of their activity
- Production of a range of DPE2 truncation mutants and their biochemical analysis
- Extensive protein crystallisation trials with DPE2 and truncated mutants thereof
- Bioinformatic analysis of the DPE2 sequence to further investigate the multimodular domain arrangement and evolutionary relationship to other GH77 enzymes
- Screening of DPE2 and PHS2 for enzymatic activity on a range of potential plant cell wall polysaccharide substrates to explore enzyme-substrate interactions

3.2 Results

3.2.1 Protein expression and purification

All of the work in this and the following result chapters required the purification of recombinant AtDPE2 and AtPHS2. In this section I describe how these proteins were generated.

3.2.1.1 Expression and purification of full length DPE2

The initial construct for expression of DPE2 in *E. coli* was already available in a Gateway compatible vector, pDest17 (Chia *et al.,* 2004). This construct encodes DPE2 with a non-cleavable C-terminal His_6-tag that is linked to the protein via a long amino acid linker region. When overexpressing and purifying the protein with this construct I achieved only very low yields of soluble protein and I repeatedly observed contaminants that co-purified with DPE2 when performing Nickel Immobilized Metal Affinity Chromatography (IMAC). The contaminants could not be separated from DPE2 with a size exclusion chromatography (SEC) step, as they were of similar molecular size as DPE2. It is likely that the contaminants are C-terminal degradation products of DPE2 because of their high affinity for nickel resin. To be able to remove the His_6-tag during the purification process I re-cloned the DPE2 gene into pET151. This construct encodes His_6-tagged DPE2 protein in which the N terminus of the protein is separated from the His_6-tag by a TEV protease cleavage site.

To improve the solubility and yield of DPE2 from expression in *E. coli* cells I experimented with different growth temperatures and *E. coli* strains. I found that yields of soluble DPE2 were highest when *E. coli* cells were grown over night at 16°C. Prior to induction with 1 mM isopropyl-β-D-thio-galactoside (IPTG), the *E. coli* cells were cooled down from 37°C to 16°C. An *E. coli* strain containing two extra plasmids for the expression of rare codons yielded best expression levels at these low temperatures (Section 2.1).

Using this new system I was now able to modify the purification procedure appropriately. The purification scheme described by Fettke *et al*. (2006) started with nickel IMAC and finished with SEC. I added a new step in which the His_6-tag was cleaved from the DPE2 protein by over night incubation with TEV protease (N-terminal His_6-tag). The combined purification procedure for DPE2 was as follows:

1. Nickel IMAC

This purification step was performed with a high stringency washing buffer that contained 80 mM imidazole. However, the elution from the nickel IMAC column with 500 mM imidazole yielded only partially purified DPE2 (Figure 3.4, B; lane 4).

2. TEV protease cleavage and second nickel IMAC

TEV protease was added to the eluate from the first nickel IMAC step. This mixture was dialysed over night against 20 mM imidazole at 4°C and then centrifuged (35,000 g). The supernatant was applied to a second nickel IMAC column. The stringency of this second purification step was reduced (only 20 mM imidazole in the washing buffer). The flow through fractions were pooled and concentrated (via spin concentration). Most of the contaminants remained on the column together with the His_6-tagged TEV protease, while DPE2 passed through the column (Figure 3.4, B; lane 8).

3. SEC

As in the original procedure (Fettke *et al.,* 2006a), SEC was used to remove any remaining contaminants from the DPE2 preparation. The concentrated protein flow-through fraction from the second nickel IMAC step was applied to a 16/60 S-200 SEC column. Fractions derived from the second major OD_{280} nm peak around 59 ml contain pure DPE2 protein as judged by SDS PAGE analysis (Figure 3.4, A and B; lane D to K).

Dynamic light scattering (DLS) was done to check the purity and dispersity of the DPE2 protein preparation (Bernstein *et al.,* 1998). Compared with a DPE2 preparation that was purified according to the original purification procedure (Fettke *et al.,* 2006a), the value for the polydispersity decreased dramatically (24.5% vs. 9.5%) (Figure 3.4, C [new procedure] and D [old procedure]). Any protein solution that has a polydispersity of less than 13% is regarded as being monodisperse and therefore free of any higher molecular weight aggregates and impurities (Bernstein *et al.,* 1998). This level of purity was important for crystallisation of the protein, as will be explained later in this chapter.

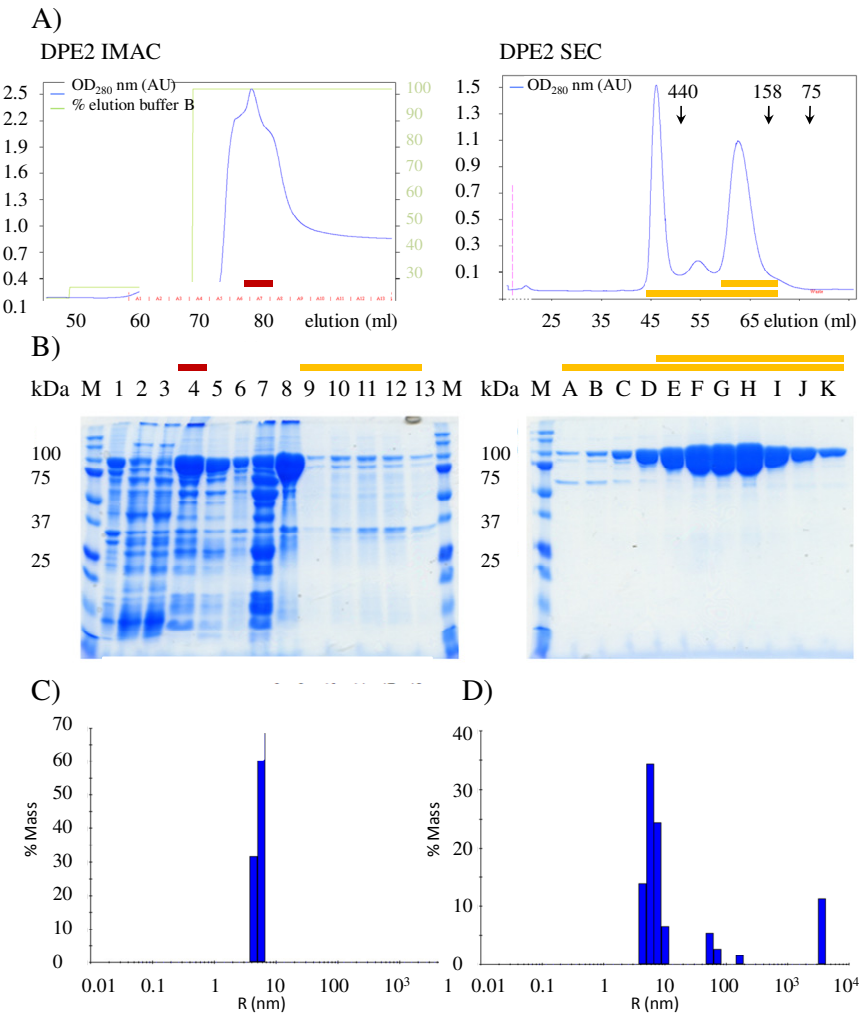

Figure 3.4 Purification procedure for DPE2

A) Elution profile of DPE2 from nickel IMAC and 16/60 Sephacryl S-200 columns. The red and orange bars indicate the position of the chromatography fractions in the acrylamide gels shown in B. The orange double bar highlights the position of the `DPE2 peak` as judged from specific activity. B) SDS PAGE analysis of DPE2 fractions from purification steps (12.5% acrylamide gels). "M" molecular weight marker, 1 insoluble protein extract, 2 soluble protein extract, 3 flow through, 4 protein eluate from 1st IMAC step, 5 overnight cleavage with TEV protease, 6 aggregated protein from cleavage, 7 eluate from 2nd IMAC step, 8 flow through from 2nd IMAC step (loaded onto S-200), 9-13 first peak from S-200 column, A-K second peak from S-200 column. C) and D) DLS histogram of DPE2 derived from pET151 (new purification procedure) and pDest17 (old purification procedure) respectively. 10mg·ml^{-1} DPE2 was used for each DLS analysis. The protein preparation was monitored for a period of 10 seconds at a laser intensity of 25% (which equalled approximately 3,000,000 counts per seconds). The histogram shows an average of 10 readings.

3.2.1.2 Cloning, expression and purification of full length PHS2 from *Arabidopsis thaliana*

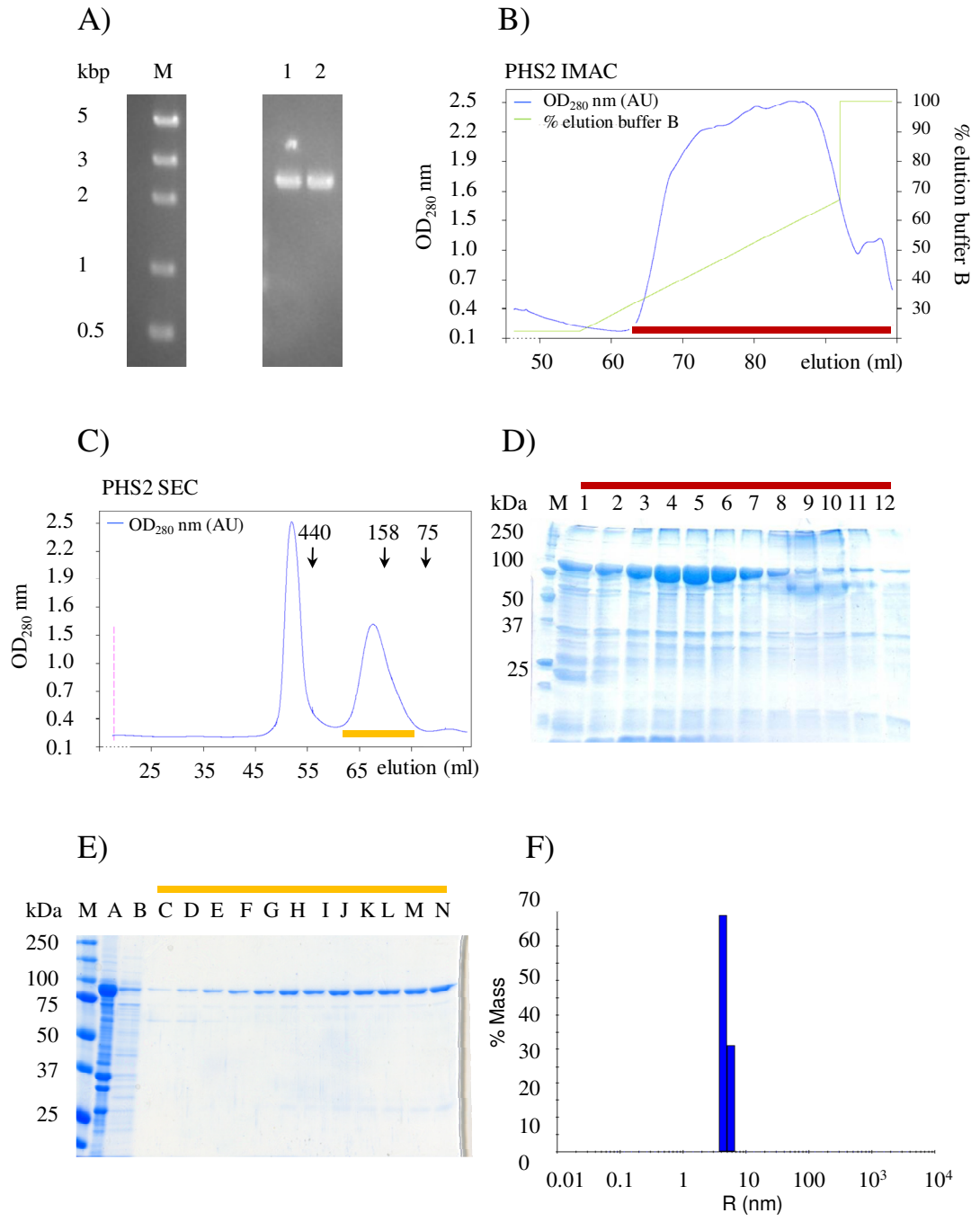

Figure 3.5 Cloning, expression and purification of PHS2

A) Agarose gel (1% [w/v]) of the PCR product of PHS2 cDNA amplification. Col0 cDNA from plants grown for 28 days was used as the basis for cloning PHS2. Band 1 and 2 show the correct cDNA size of PHS2 (2523bp)

B) Nickel IMAC elution profile of PHS2. The orange bar indicates the position of the fraction on the nickel IMAC elution profile

C) 16/60 S-200 elution profile of PHS2. The red bar indicates the position of the fraction on the SEC elution profile. The arrows indicate the position of molecular weight markers (in kDa).

D and E) SDS PAGE analysis of chromatography fractions from nickel IMAC and SEC loaded on 12.5% acrylamide gel. Lanes 1-12 in D are eluate fractions (1 ml) from nickel IMAC. Lanes C-N in E are eluate fractions from SEC 16/60 S-200.

F) DLS histogram of purified PHS2, 10 $mg \cdot ml^{-1}$ PHS2 was monitored for a period of 10 seconds. The laser intensity was 25% (which equalled approximately 3,000,000 counts per seconds). The histogram shows an average of 10 readings.

PHS2 is the second enzyme in the maltose uitilisation pathwayin plants. It acts on SHG downstream of DPE2 and produces G1P as mentioned in chapter 1 (see figure 1.8). Later on in this chapter the activity of PHS2 on a broad range of complex polysaccharides will be compared to DPE2.

I cloned PHS2 from *Arabidopsis thaliana* Col0 cDNA with the primers published in Lu *et al.* (2006) (Figure 3.5, A). The PHS2 cDNA was subcloned into pET151 and transferred in *E. coli* Rosetta II cells by Ellis O'Neil (PhD student laboratory Prof Rob Field, John Innes Centre). I produced the protein over night at 16° C after induction with 1mM IPTG when cell density reached an OD_{600} of 0.6. The protein purification procedure comprised an initial nickel IMAC purification step that was followed by a gel chromatography step on a 16/60 Sephacryl S-200 column (Figure 3.5, C and D). The final PHS2 protein preparation was judged by SDS PAGE and DLS to be highly pure and monodisperse (Figure 3.5, E and F). The predicted molecular weight of PHS2 according to its amino acid composition is 95 kDa. SEC and DLS on the purified PHS2 preparation showed a molecular weight for PHS2 of 185 kDa and 165 kDa respectively (Figure 3.5, C and F). This fits close to a calculated dimer weight of 190 kDa. This is in agreement with the estimated dimeric molecular weight for phosphorylases from other plant species (Albrecht *et al.,* 1998).

3.2.1.3 Cloning, expression and purification of truncated DPE2 proteins

To analyse the active site and identify structural properties and function of the individual domains in DPE2, I produced a range of active site and truncated mutant proteins. The active site residues aspartate at amino acid position 563 and aspartate at amino acid position 810 were mutated to the respective amide and alanine. The N-terminal CBM20 tandem was individually produced and purified as well as the individual CBM20 modules (Figure 3.6).

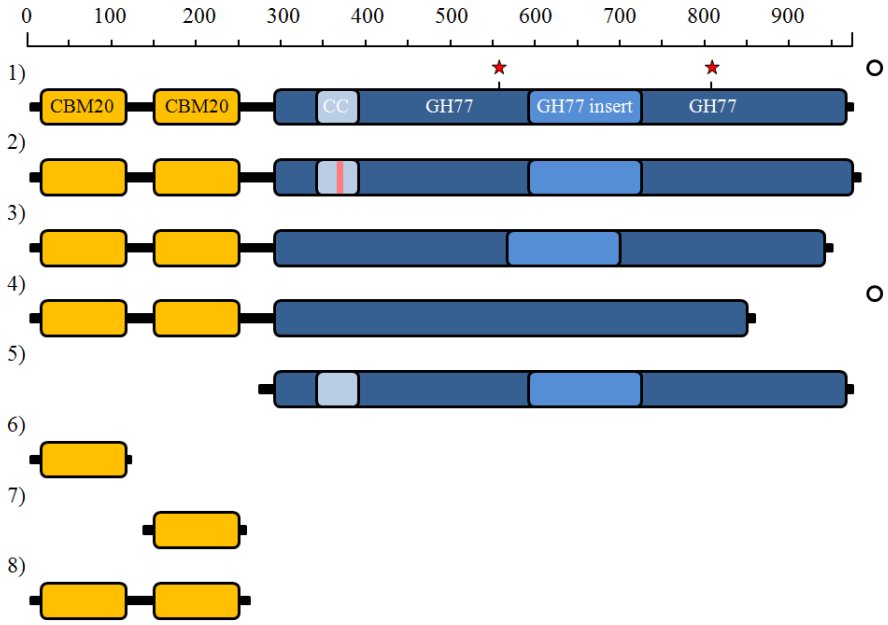

Figure 3.6 Overview of truncated DPE2 proteins produced during this study

The top numbers indicate the positions of the amino acids. Red stars indicate the place of active site point mutations, empty circles indicate where CD was used to check the protein folding state. The individual domains and modules have been coloured yellow (Carbohydrate binding module family 20; CBM20) and blue (glycoside hydrolase domain GH77). The grey box labelled CC shows the position of the newly identified coiled coil motif. The red horizontal bar in number 2 indicates an insertion of a beta-turn motif. 1) DPE2; full length protein 2) $DPE2_{\Delta CC1}$; coiled coil motif interrupted by beta-turn motif 3) $DPE2_{\Delta CC2}$; coiled coil motif deleted 4) $DPE2_{\Delta insert}$; insertion deleted 5) $DPE2_{\Delta CBM20}$; CBM20 tandem deleted 6) CBM20-1 7) CBM20-2 8) CBM20 tandem

I also produced and purified DPE2 mutants that lacked the insert and the proposed coiled coil motif. In addition I produced and purified MalQ from *E. coli* and a chimeric version of MalQ

containing the N-terminal CBM20 tandem of DPE2 at the N-terminus (the rationale for this will be explained later in this chapter). The purification procedures for all of these were similar to the ones described above for DPE2 and PHS2. Proteins were produced in *E. coli* and purified with nickel IMAC followed by SEC. The protein preparations were judged highly pure by SDS PAGE and DLS analysis (Appendix 1).

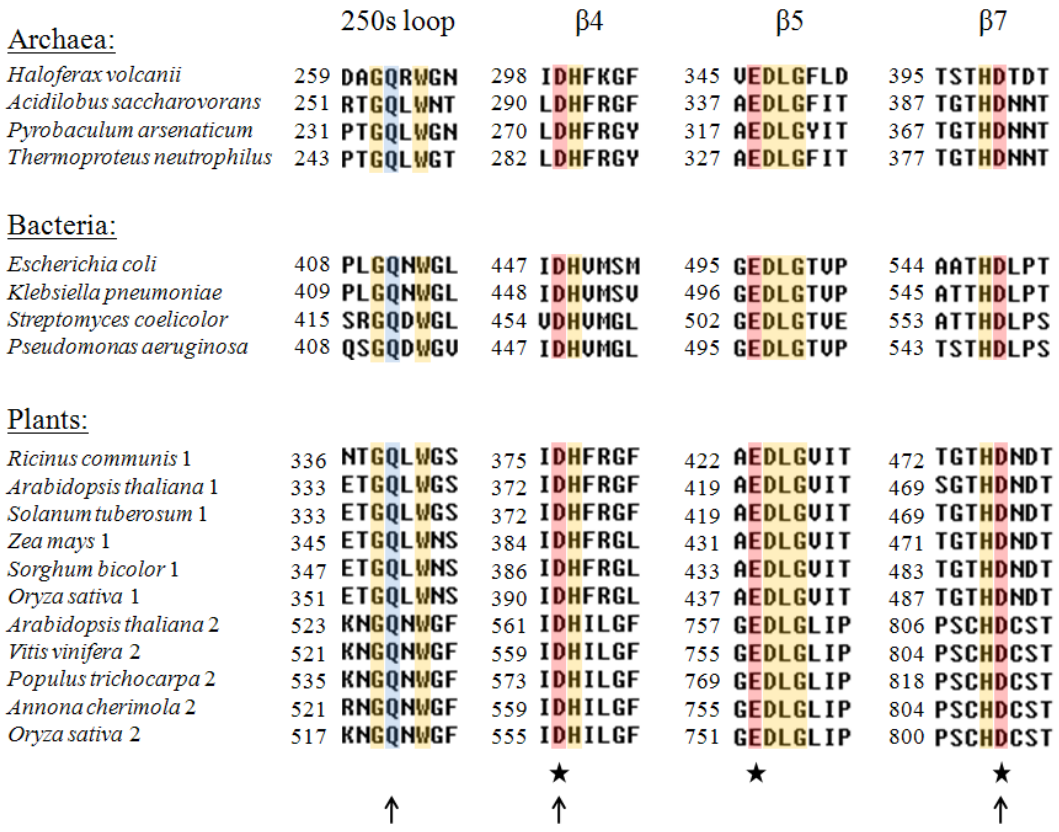

Figure 3.7 Sequence alignment of active site residues of a diverse group of GH77 enzymes

The sequence alignment shows the four conserved regions that form the active site of a GH77 class enzyme. Each column represents part of the $(\alpha/\beta)_8$-barrel that forms the active site of GH77 enzymes; the 250s loop is exclusively found in GH77 enzymes and shields the active site of the enzymes (pdb file: 1X1N; Figure 3.1). The yellow highlighted positions are conserved amongst GH77 enzymes; the red highlighted positions show the only three invariant residues in the ClanH of glycoside hydrolases. The stars highlight the three residues forming the catalytic triad. The arrows indicate the positions of point mutations that have been produced and analysed in this study. The group of plant enzymes are designated as 1 for the plastidial DPE1 and 2 for the cytosolic DPE2. The sequences were aligned with Prankster (http://www.ebi.ac.uk/goldman-srv/prank/). The graphical output was done with BioEdit (http://www.mbio.ncsu.edu/bioedit/bioedit.html).

3.2.2 Mechanism of the 4-α-glucanotransferase reaction

The active site architecture of GH77 from plants and bacteria is very similar (MacGregor *et al.,* 2001). Several amino acid residues are invariant and mutation leads to a loss of catalytic activity (Przylas *et al.,* 2000a) (see previous page, Figure 3.7). In DPE2 these invariant residues are the predicted catalytic residues Asp563 (nucleophile, β4), Glu758 (general acid/base catalyst, β5), and Asp810 (third catalytic residue, β7). The large amino acid insertion that is conserved amongst all DPE2-like enzymes lies between the predicted active site residues on primary structure level. The glutamate at position 758 was analysed previously and it was shown that substitution to glutamine causes a loss of catalytic activity of DPE2 (Steichen *et al.,* 2008). To verify the importance of the remaining residues, they were substituted with their respective amide derivative and alanine.

The analysis of the mutant enzymes was done in two different ways. First, 3-aminopropyltriethoxysilane-derivatised Glc7 (APTS-Glc7) was used as acceptor substrate for DPE2 mediated glucosyl transfer. The formation of reaction products was visualised with fluorophore-assisted carbohydrate electrophoresis (FACE). Second, non-derivatised Glc7 was used as an acceptor substrate to monitor the initial rate of glucose production with an NADP-linked assay. In both cases, maltose served as the donor substrate.

The mutant enzymes exhibited greatly reduced disproportionation activity (see next page, Figure 3.8, A and B). DPE2 active site mutants with the alanine substitutions (D563A and D810A) gave no apparent disproportionation of the APTS-derivatised Glc7 acceptor substrate. DPE2 active site mutants with the amide substitution (D563N and D810N) exhibited little enzyme activity, and this was seen only when the reaction was left for 24 hours. The enzyme activities obtained from the initial rate kinetics agreed with the data obtained with the APTS-derivatised Glc7 acceptor substrate. The mutant enzymes showed an approximately 2000 fold decrease in activity with unlabelled Glc7 as acceptor substrate. To assess the folding state of the mutants, a CD spectra of the far-UV spectral region was taken (Figure 3.8 C). At the spectral region from 180 nm to 250 nm the chromophore is the peptide bonds of the protein backbone, and a signal arises when it is located in a regular, folded environment (Oakley *et al.,* 2006). Folded polypeptides have a distinctive spectral signature in the far-UV, with local maxima at 190 nm and minima at 208 nm and 222 nm (Whitmore and Wallace 2008). All mutants showed a similar spectral pattern to the wt. Therefore structural integrity was not disrupted in these mutants.

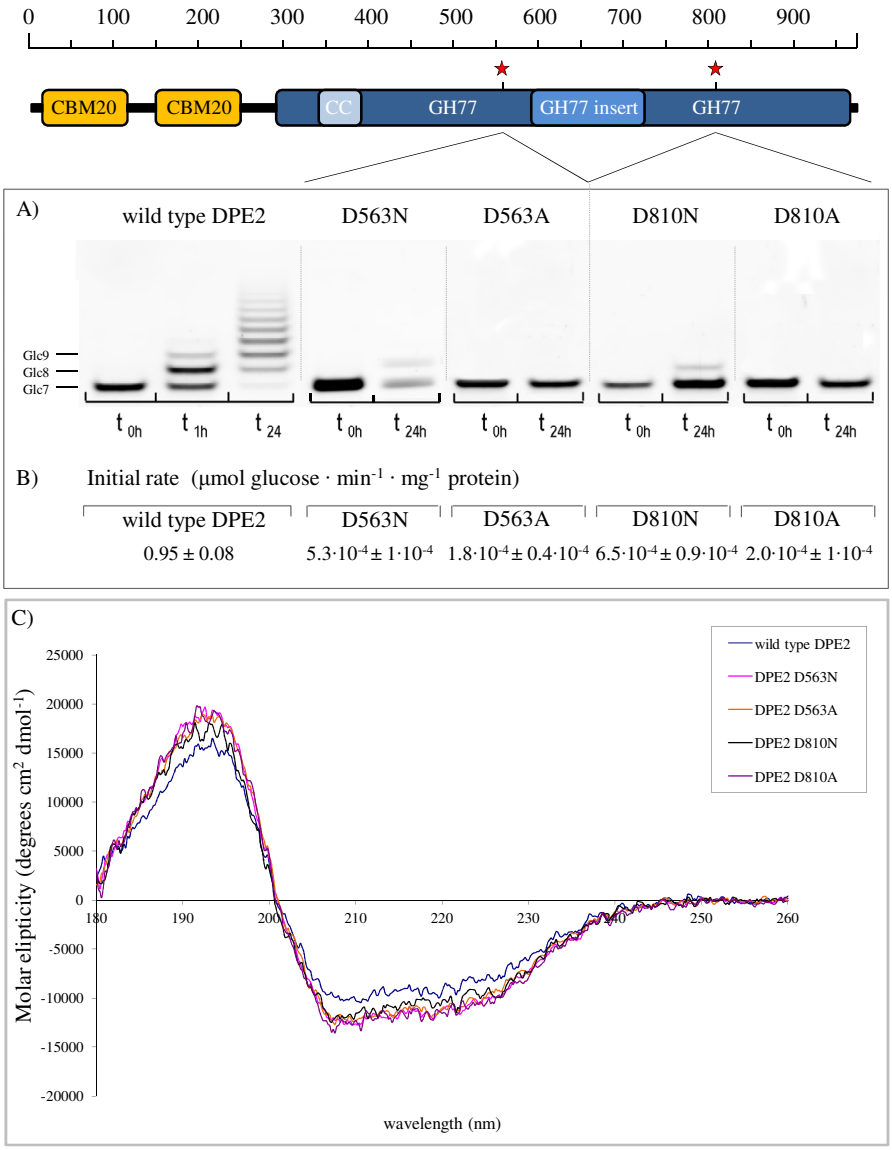

Figure 3.8 wt and active site mutant activity of DPE2

DPE2 and mutants D563N, D563A, D810N or D810A (1.5 µg) were incubated with two different acceptor substrates. A) Fluorophore-assisted carbohydrate electrophoresis (FACE) of reaction products of DPE2 with 1 mM APTS-derivatised Glc7 and 5 mM maltose. Separation was done on 35% acrylamide Tris-Borate slab-gel. B) Incubation of DPE2 with 10 mM Glc7 and 2 mM maltose. The initial rate of glucose production was measured using an NADP(H)-linked assay as described in Chapter 2. Values are mean ± S.D. (n = 3). C). Wt DPE2 and active site mutants were analysed on a circular dichroism polarimeter. The secondary structure of wt DPE2, active site mutants and delta insertion were monitored over the far-UV spectral region from 180 nm to 260 nm. Values were recorded to calculate the molar elipticity.

3.2.3 Identification and analysis of a putative coiled coil motif in DPE2

SEC and DLS data on the purified DPE2 preparation suggest that DPE2 forms homodimers (Figure 3.4, A and C). To confirm this I did native PAGE analysis of a boiled and a native sample of DPE2. The migration pattern of the two samples was different. Whereas the native sample migrated slowly with standards around 250 kDa, the boiled sampled co-migrated with standards that are around 100 kDa (Figure 3.11). Together with data from the DLS and SEC analysis, this suggests that DPE2 forms active homodimers in solution.

The self association of proteins to form dimers is mostly achieved by so-called coiled coil motifs (Mason and Arndt 2004). A repeated pattern of hydrophobic (h) and charged (c) amino-acid residues referred to as heptad repeats, forms the basis for coiled coils. The positions in such a repeat are usually labelled abcdefg where a and d are the hydrophobic and e and g are the charged positions forming the pattern hxxhcxc (Marianayagam *et al.,* 2004). A repeated pattern of this sequence when folded into an alpha-helical secondary structure causes the hydrophobic residues to be presented as a stripe that coils around the helix in a left-handed fashion, forming an amphipathic structure (Gruber *et al.,* 2006, Marianayagam *et al.,* 2004, Mason and Arndt 2004). In a polar environment like the cytosol of a plant cell, the most favourable way for two such helices to arrange themselves is to wrap the hydrophobic strands against each other, sandwiched between the hydrophilic amino acids.

There are two major algorithms that predict such structural folds from the primary amino acid sequence (COILS (Lupas 1996) and Paircoil2 (Berger *et al.,* 1995)). Both algorithms search the submitted protein sequence for heptad repeat that have the characteristic residue distribution and score the coiled-coil-forming propensity of the sequence by its match to a position-specific scoring matrix. Repeats that have been rated significant in supporting coiled coil formation will appear as positive hits (Gruber *et al.,* 2006). Both algorithms predict formation of a coiled coil structure at the N-terminal end of the GH77 domain of DPE2 between residue 348 and 386 (Figure 3.9). The insertion that spans the active site also gives a positive hit for a coiled coil formation which is less strong. GH77 enzymes involved in maltose metabolism in bacteria like the *E. coli* MalQ do not contain such a motif. The same pattern and distribution of coiled coil motifs in the DPE2 sequence can be observed when submitting the amino acid sequence from DPE2-like proteins from potatoes, poplar, barley and apple (Figure 3.10). The occurrence of a

coiled coil motif in this region in DPE2 from the lycophyte *Selaginella moellendorffii* and the green alga *Ostreococcus lucimarinus* shows that it is evolutionarily conserved. This points to an important function of the coiled coil motif within DPE2.

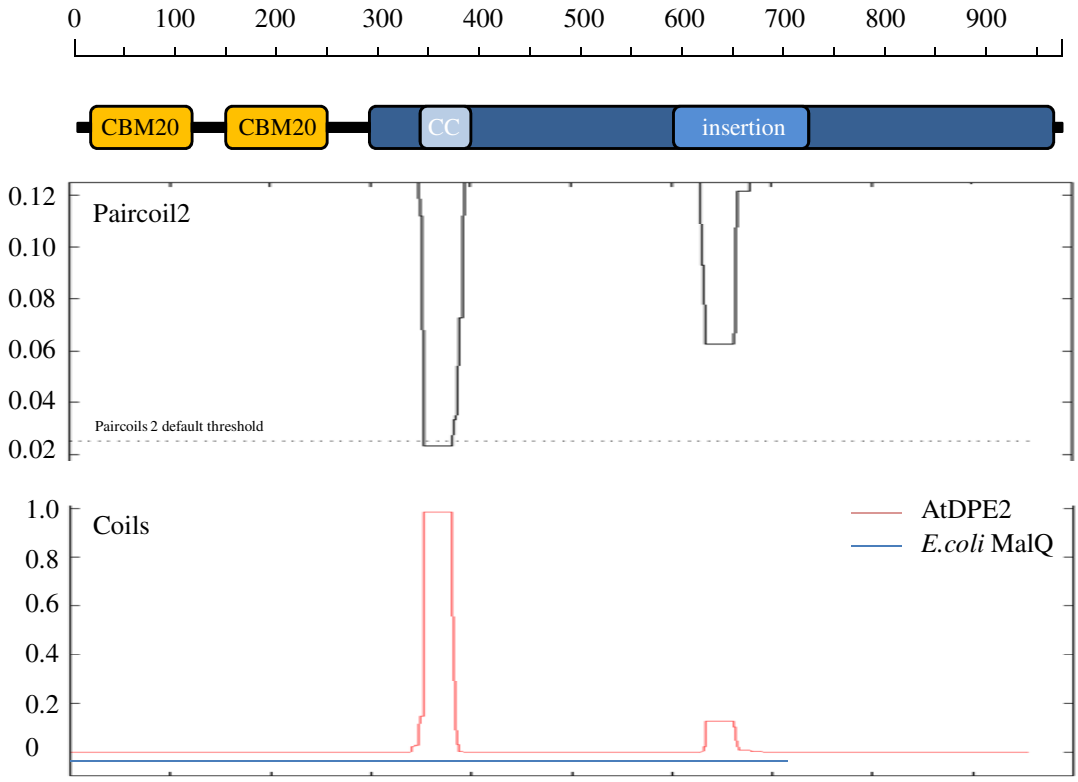

Figure 3.9 Prediction of coiled coil motif from primary amino acid sequence

Primary amino acid sequence of DPE2 was submitted to online servers running the coiled coil prediction programs Paircoil2 and Coils. A window frame of 28 (at least four heptad repeats) was chosen. The top numbers indicate the positions of the amino acids. The y-axis numbering is algorithm specific and dimensionless. The `Coils` window shows prediction for DPE2 (red) and MalQ from *E. coli* (blue).

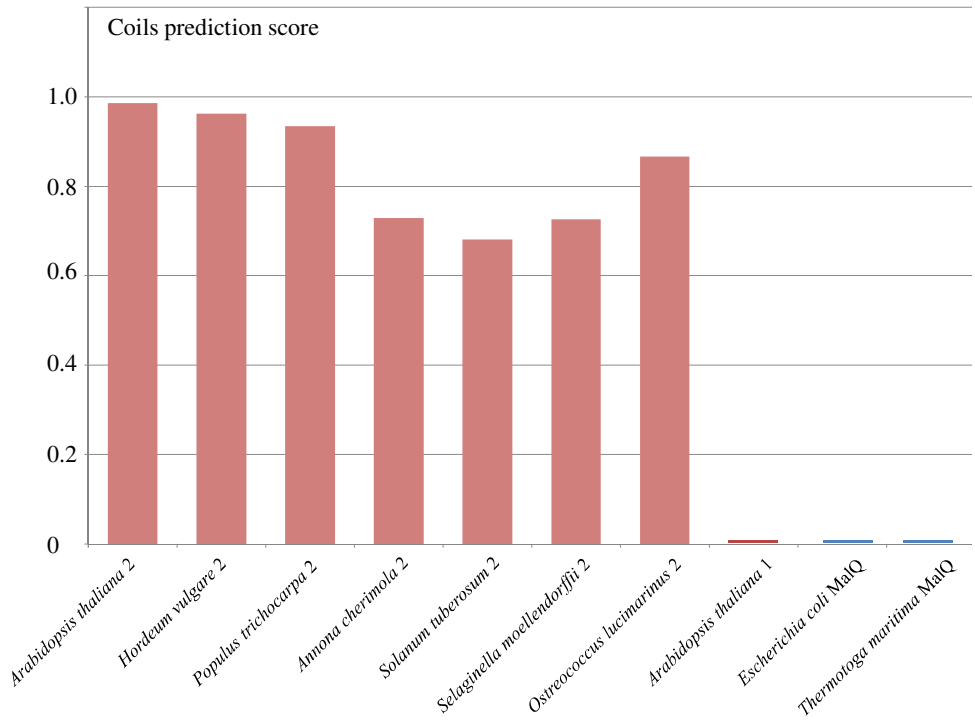

Figure 3.10 Presence of coiled coil motif in DPE2 in a range of organisms

DPE2 sequences from monocots, dicots and algae as well as DPE1 from *A. thaliana* and MalQ from prokaryotes were submitted to the `Coils` prediction server. The x-axis shows the score obtained for prediction of the coiled coil motif over a window frame of 28.

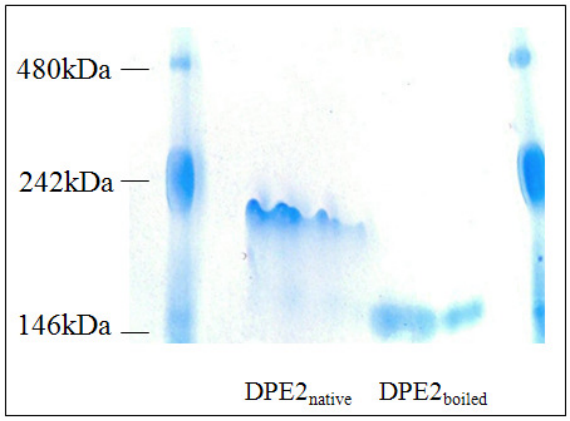

Figure 3.11 Native PAGE of DPE2

DPE2 (2.5 ug) was loaded onto acrylamide gel (7.5%) that did not contain SDS. $DPE2_{native}$ is the native sample; $DPE2_{boiled}$ is the boiled and therefore denatured sample. Native protein standards are designated (NativeMark™, Invitrogen); ferritin, 480 kDa; β-phycoerythrin, 242 kDa; lactate dehydrogenase, 146 kDa.

To investigate the functional significance of this newly identified motif I produced two DPE2 mutants that lack a functional coiled coil motif. $DPE2_{\Delta CC1}$ lacks the coiled coil domain completely and $DPE2_{\Delta CC2}$ has an inserted beta-turn located within the predicted coiled coil motif. The beta-turn motif was shown to disrupt formation of coiled coil motifs in other proteins in earlier studies (Cheng *et al.,* 1999). Neither DPE2 mutants could be purified as both formed insoluble inclusion bodies during synthesis in *E. coli*. Optimisation of the overexpression conditions did not yield soluble protein. Any structural disruption in this region seems to impair the overall structural stability of DPE2.

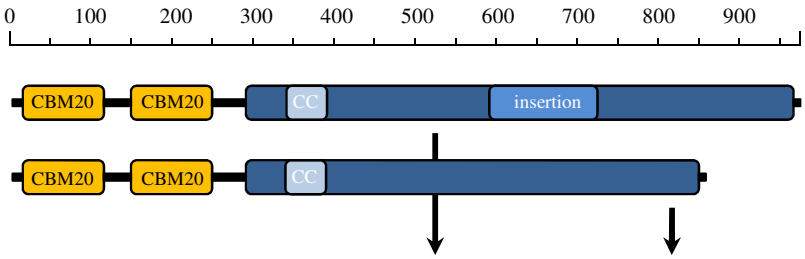

acceptor substrate	donor substrate	wild-type DPE2 OD_{340} nm		$DPE2_{\Delta insert}$ OD_{340} nm
Glc2	Glc2	0.005	0.001	< 0.001
Glc3	Glc2	0.053	0.012	< 0.001
Glc4	Glc2	0.089	0.014	< 0.001
Glc5	Glc2	0.154	0.013	< 0.001
Glc6	Glc2	0.227	0.019	< 0.001
Glc7	Glc2	0.290	0.015	< 0.001
Glycogen	Glc2	0.953	0.106	< 0.001

Figure 3.12 Enzyme activity of $DPE2_{\Delta insert}$

Wt DPE2 and $DPE2_{\Delta insert}$ were incubated with maltose (Glc2) and glycogen or MOS (Glc2-Glc7). The glucose release was monitored with a NADH coupled assay (Chapter 2) and the OD340nm was recorded after incubation of 100 nM enzyme and 5 mM maltose and 2 mM acceptor substrate (100 µg of type II oyster glycogen).

As mentioned above, a second putative coiled coil motif is located within the amino acid insertion of DPE2 (Figure 3.9). Based on three-dimensional structure of DPE1, Sharkey *et al.* (2008) suggested that the insertion in DPE2 is surface-exposed. It is thus potentially a good site for protein-protein interaction via a coiled coil motif. It was also proposed that the insertion does not have any impact on the catalytic activity of DPE2 since it is located at the opposite site of the beta-barrel fold from the sequence containing the active site residues (pdb file: 1X1N; Figure 3.1). I produced and purified a DPE2 mutant protein that lacks the insertion, $DPE2_{\Delta insert}$. In

contrast to DPE2$_{\Delta CC1}$ and DPE2$_{\Delta CC2}$, DPE2$_{\Delta insert}$ was soluble. The purification yielded a single band and was judged pure. However, no enzyme activity could be seen when DPE2$_{\Delta insert}$ was tested on various substrates (Figure 3.12).

To assess the folding state of DPE2$_{\Delta insert}$ a CD spectra of the far-UV spectral region was taken. At the spectral region from 180 nm to 250 nm the chromophore is the peptide bonds of the protein backbone, and a signal arises when it is located in a regular, folded environment (Oakley *et al.,* 2006). Folded polypeptides have a distinctive spectral signature in the far-UV, with local maxima at 190 nm and minima at 208 nm and 222 nm (Whitmore and Wallace 2008). The far-UV spectrum of DPE2$_{\Delta insert}$ shows an altered signature around 190 nm and around 220 nm when compared to the wt protein (Figure 3.13). DPE2$_{\Delta insert}$ might be partially unfolded and still possess sufficient hydration to stay soluble. A partial unfolding of the active site containing domain could account for the loss of catalytic activity.

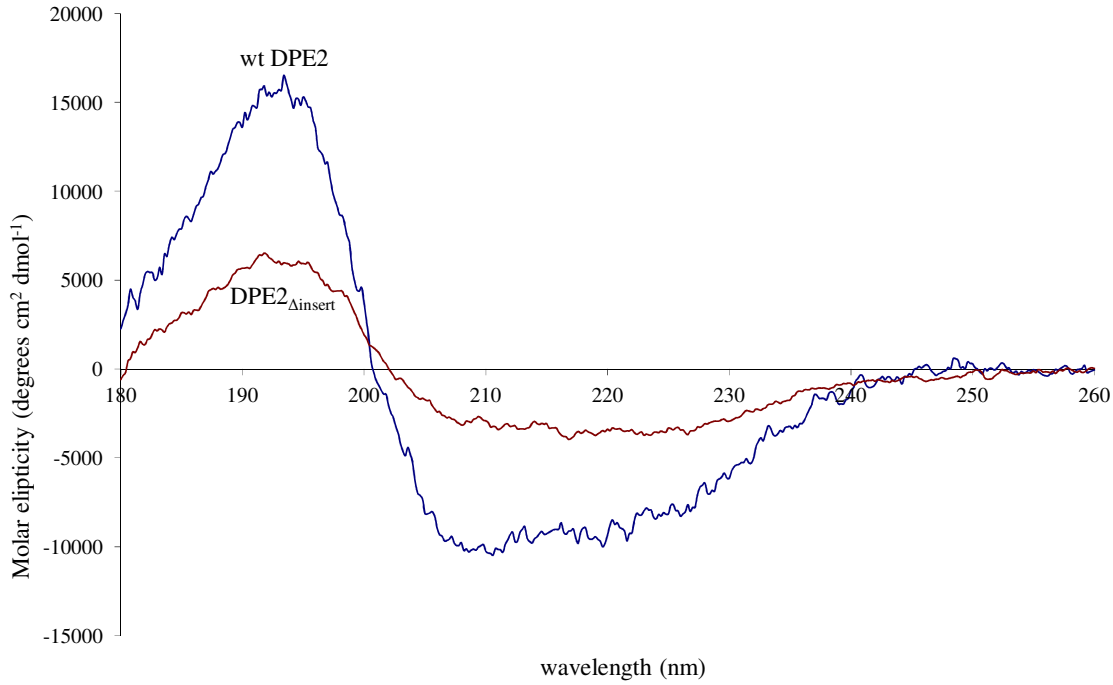

Figure 3.13 CD analysis of DPE2 mutant proteins

Wt DPE2, active site mutants and DPE2$_{\Delta insert}$ proteins were analysed on a circular dichroism polarimeter. The secondary structure of wt DPE2, active site mutants and delta insertion were monitored over the far-UV spectral region from 180 nm to 260 nm. Values were recorded to calculate the molar elipticity.

3.2.4 The role of the CBM20 tandem in carbohydrate binding of DPE2

As shown by Steichen *et al.* (2008), DPE2 binds to starch *in vitro* and deletion of CBM20-1 causes loss of starch binding ability (Steichen *et al.,* 2008). To further investigate the role of the N-terminal CBM20 tandem of DPE2 in carbohydrate binding I produced and purified the individual CBM20 modules of DPE2, CBM20-1 and CBM20-2. To compare carbohydrate binding of DPE2 to other maltose metabolising enzymes I also produced MalQ from *E. coli* and a chimeric protein composed of MalQ from *E. coli* fused to the CBM20 tandem of DPE2 which will be called CBM20-MalQ. All proteins were produced in soluble form and purified to homogeneity (as judged by SDS-PAGE and DLS analysis).

Binding of CBM20-1, CBM20-2, DPE2, MalQ and CBM20-MalQ to starch, amylose and amylopectin was done in 100 mM PIPES buffer pH 6.8 at 4°C. Starch (wheat, potato or quinoa), amylose and amylopectin was washed with 100 mM PIPES buffer (pH 6.8), and then 20 µM of protein was added to 20 mg of starch in 500 µl of PIPES buffer. The mixture was shaken for 30 min on ice and then spun at 22,000 *g* for 5 min, and the supernatant was removed. To extract protein bound to the starch, amylose or amylopectin, the pellet was incubated at 100°C for 10 min in 500 µl of SDS PAGE loading buffer. The fractions were analyzed by 4–12% SDS-PAGE and stained with 0.1% Coomassie Brilliant Blue (see next page, Figure 3.14)

Figure 3.14, B shows binding of full length DPE2 to starch, amylose and amylopectin. Binding to amylose was stronger than to amylopectin as all of the protein located in the pellet fraction when DPE2 was incubated with amylose. When incubated with amylopectin, some of the protein localised in the supernatant. MalQ in contrast did not bind to starch or the starch components amylopectin and amylose (Figure 3.14, B and C). However, the chimeric protein CBM20-MalQ bound to starch from wheat and quinoa and to amylose (see next page, Figure 3.14, D). This suggests that binding of DPE2 to starch and starch components is a property conferred at least in part by the N-terminal CBM20 tandem.

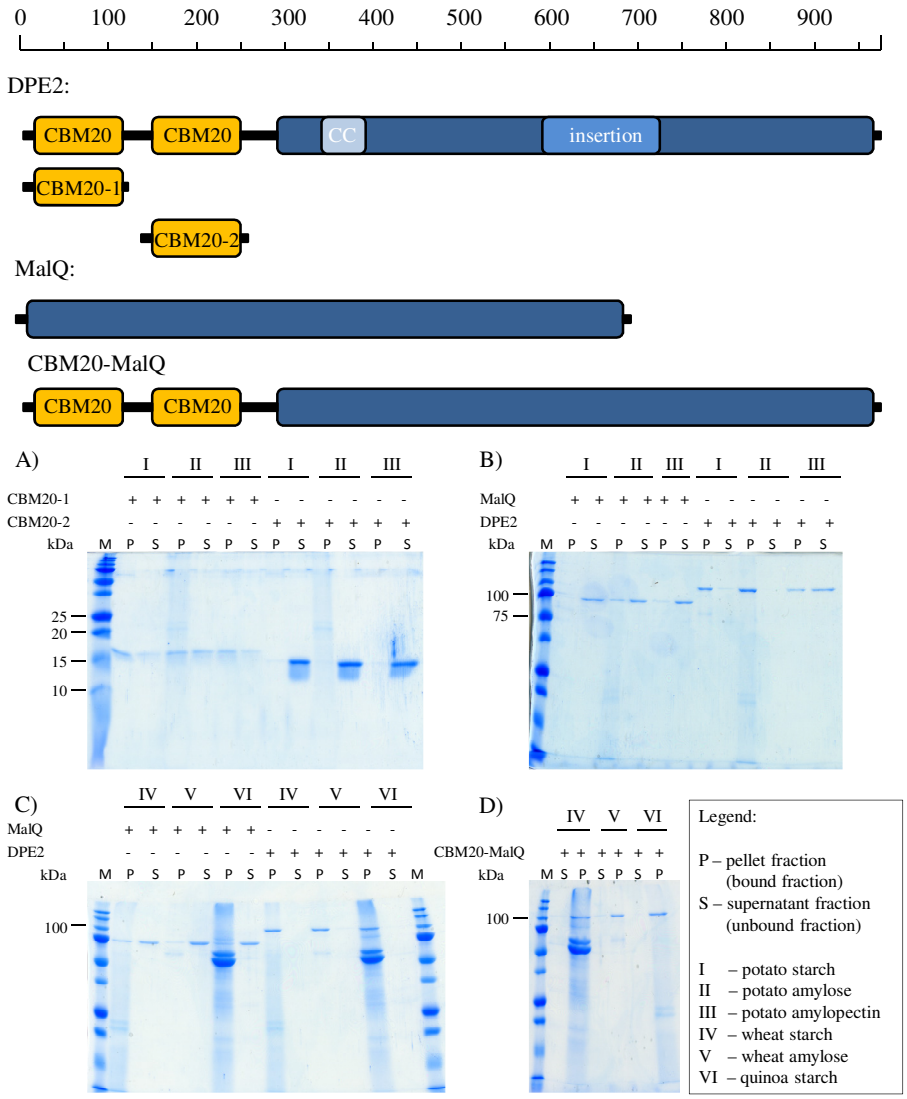

Figure 3.14 Starch binding assay of wt DPE2, MalQ from *E. coli*, CBM20-1, CBM20-2 and chimeric protein CBM20-MalQ

Granular starch, amylose and amylopectin (30 mg each) were added to a total assay volume of 500 µl PIPES buffer (pH 6.8). Recombinant proteins were added to a final protein concentration of 20 µM. The pellet samples were loaded onto SDS PAGE after extensive washing with phosphate buffered saline (PBS). The extra protein bands that appear in the quinoa starch sample are starch bound proteins that could not be washed off the starch preparation. A) CBM20-1 and CBM20-2 binding to starch, amylose and amylopectin of potato; B) and C) MalQ and DPE2 binding to starch, amylose and amylopectin from potato and from wheat respectively D) CBM20-MalQ binding to starch (IV, VI) and amylose (V) from wheat and quinoa respectively.

Starch binding of the individual CBM20 modules differed from one another. While CBM20-1 partially bound to starch, amylose and amylopectin, CBM20-2 did not. CBM20-2 exclusively located in the soluble fraction and therefore has no measurable affinity for starch, amylose or amylopectin (Figure 3.14 A). Taking all data together, this *in vitro* study suggests that the starch binding site in DPE2 is located in the N-terminal CBM20 tandem.

3.2.5 DPE2 crystallisation trials

To gain further insight into the structural organisation of DPE2 I did protein crystalisation trials on wt and truncated DPE2 mutant proteins. Preliminary crystallization trials of full length protein, the catalytic domain and the CBM20 tandem (#1, #5, #8 in Figure 3.6) were performed using the sitting drop-vapour diffusion method in a 96-well plate format. The protein preparations had a concentration of approximately 10 $mg \cdot ml^{-1}$, and were filtered through a 0.1 µm filter prior to crystallization set-up.

A range of commercial and "in house" screens were used: Classics Suite, JCSG+, PEGs Suite, PACT Suites (all from Qiagen), Johan-Zeelen Screens 1 and 2, and Clear Strategy Screens (CSS) 1 and 2, in addition to other "in house" screens. The CSS screens were tested in a range of pH between 6 and 10.

After 4 days about 80% of conditions showed either amorphous precipitate or denatured protein, about 10% showed clear drops, and the remainder precipitate, phase separation or pseudocrystalline structures. Crystallization screens were also set up at 5, 7 and 15 $mg \cdot ml^{-1}$, with similar results (with higher number of clear drops, resulting from more diluted protein samples or only precipitation with higher protein concentration). Crystallizations trials were done at 20 ºC and at 4 ºC, although no significant differences were apparent.

DPE2 was set up with maltose, Glc3, Glc4 or Glc7 (10 mM each) as protein-cocrystallising agent. Protein crystals of DPE2 were first obtained when 7.5 $mg \cdot ml^{-1}$ DPE2 were incubated with 10 mM Glc7 on ice for 30 min and subsequently transferred into 20% PEG 6000 (w/v). Optimization allowed for a certain control of the crystal number and size, but very often they grew as long and thin crystals (30·20·50 µm; Figure 3.15, A). A few crystals were assessed at the Diamond synchrotron beamlines (Oxford, UK). Diffraction data were obtained (Figure 3.15,

B) but crystal quality proved to be too poor for further diffraction analysis. Both macroseeding and microseeding were used to better the crystal quality but no improvement of crystal quality and size was achieved

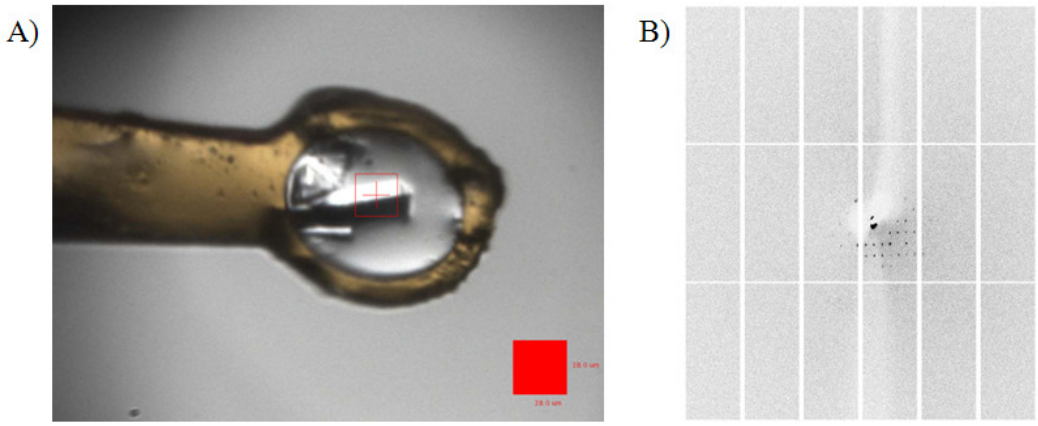

Figure 3.15 DPE2 crystal mounting and corresponding diffraction image

A) DPE2 crystal co crystallised with Glc7 (30x20x50 µm) was mounted on a 0.5 mm cryoloop. B) Diffraction image of the crystal recorded on the diamond beamline in Oxford.

3.2.6 DPE2 acceptor substrate screen

The lack of structural information about DPE2 hampers analysis of its molecular interaction with SHG. Analyses have revealed that DPE2 and PHS2 act on the same acceptor sites on SHG (Fettke *et al.,* 2006a) and that SHG can only be found in organisms that contain DPE2 and PHS2-like enzymes (Fettke *et al.,* 2009b). However, there are no structural data about SHG that could explain its recognition by two completely different classes of carbohydrate active enzymes.

With no structural information of DPE2 and SHG available I decided to do a large scale screen with potential acceptor substrates that resemble the proposed *in vivo* substrate SHG with respect to its linkage pattern and monosaccharide composition (Chapter 1, Table 1.1) (Fettke *et al.,* 2005a). For this purpose I used a technique that has been developed for screening carbohydrate binding proteins and antibodies for binding to polysaccharides derived from plant cell walls (Moller *et al.,* 2007, Sorensen *et al.,* 2009). Nitrocellulose membranes are used to immobilise polysaccharides that mainly derive from plant cell wall components (Sorensen *et al.,* 2009).

A)

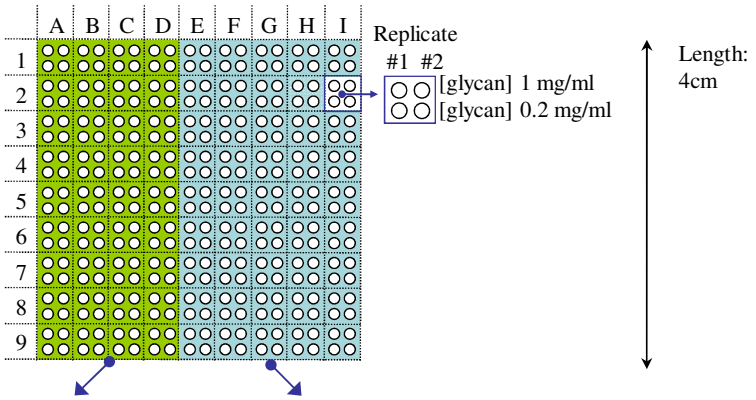

B)

sample list - BSA conjugated:

	Epitope displayed in BSA-conjugate
A1	α-(1→4)-D-heptagalacturonate (DE 0%)
B1	α-(1→4)-D-pentagalacturonate (DE 0%)
C1	β-D-galactose
D1	β-(1→4)-D-galactotetraose
A2	α-L-arabinose
B2	α-(1→5)-L-arabinobiose
C2	α-(1→5)-L-arabinotriose
D2	α-(1→5)-L-arabinotetraose
A3	α-(1→5)-L-arabinopentaose
B3	α-(1→5)-L-arabinohexaose
C3	α-(1→5)-L-arabinoheptaose
D3	β-(1→4)-D-glucopentaose
A4	β-D-mannose
B4	β-(1→4)-D-mannotriose
C4	β-(1→4)-D-mannotetraose
D4	β-(1→4)-D-mannopentaose
A5	β-D-xylose
B5	β-(1→4)-D-xylotriose
C5	β-(1→4)-D-xylotetraose
D5	β-(1→4)-D-xylopentaose
A6	Conjugate of Xyloglucan heptamer XXX(G)-
B6	Conjugate of Xyloglucan octamer XXL(G)-
C6	Conjugate of Xyloglucan nonamer XLL(G)-
D6	6^1-α-D-galactosyl-β-(1→4)-D-mannobiose
A7	(1→3),(1→4)-β-D-glucotriose [G4G3G(G)-]
B7	(1→3),(1→4)-β-D-glucotetraose [G3G4G4G(G)-]
C7	(1→3),(1→4)-β-D-glucopentaose [G3G4G3G4G(G)-]
D7	6^3,6^4-*di*galactosyl-β-(1→4)-D-mannotetraose
A8	α-(1→4)-D-glucobiose
B8	α-(1→4)-D-glucopentaose
C8	α -(1→6)-D-glycosyl-α-(1→4)-D-maltotriose G6G4G
D8	α-(1→6)-D-glycosyl-α-(1→4)-D-maltosyl-maltose G6G4G4G6G4G
A9	β-D-glucose
B9	β-(1→3)-D-glucotriose

sample list:

E1	Lime pectin, DE 11% (Danisco #F11)
F1	Lime pectin, DE 43% (Danisco #F43)
G1	Lime pectin DE 0% (Danisco #B00)
H1	Lime pectin, DE 16% (Danisco #P16)
I1	Sugar beet pectin (Danisco #SBP6232)
E2	Pectic galactan #1 (lupin, INRA/Nantes)
F2	Pectic galactan #2 (potato, INRA/Nantes)
G2	Pectic galactan #3 (lupin, Megazyme)
H2	Pectic galactan #4 (tomato, J. Paul Knox)
I2	RGII enriched pectin (red wine)
E3	RGI #1 (soy bean, Megazyme)
F3	RGI #2 (carrot, INRA/Nantes)
G3	RGI #3 (sugar beet, INRA/Nantes)
H3	RGI #4 (Arabidopsis, INRA/Nantes)
I3	Seed mucilage (Arabidopsis, INRA/Nantes)
E4	Arabinan (sugar beet, Megazyme)
F4	Arabinan, de-branched (sugar beet, Megazyme)
G4	(1→5)-alpha-L-arabinan (sugar beet, Megazyme)
H4	RGI #5 (potato, Megazyme)
I4	Xylogalacturonan, XGA (apple, INRA/Nantes)
E5	Xylan (birch wood, Sigma-Aldrich)
F5	Arabinoylan (wheat, Megazyme)
G5	4-Methoxy-glucoronoarabinoxylan (birch, Sigma-Aldrich)
H5	Xyloglucan, non fucosylated (tamarind seed, Megazyme)
I5	Xyloglucan, fucosylated (pea, INRA/Nantes)
E6	Carboxymethyl-cellulose, CM-cellulose (Avicel)
F6	Hydroxymethyl-cellulose, MeO-cellulose (Avicel)
G6	Hydroxyethyl-cellulose, EtO-cellulose (Avicel)
H6	(1→6),(1→3)-β-D-glucan (laminarin, Sigma-Aldrich)
I6	(1→3)-β-D-glucan (pachyman)
E7	β-glucan #1 (lichenan, icelandic moss, Megazyme)
F7	β-glucan #2 (barley, Megazyme)
G7	β-glucan #3 (oat, Megazyme)
H7	β-glucan #4 (yeast)
I7	(1→6),(1→4)-α-D-glucan (pullulan)
E8	Glucomannan
F8	Galactomannan
G8	Gum guar
H8	Gum Arabic (Sigma-Aldrich)
I8	Locust bean gum (Megazyme)
E9	Xanthan gum (Danisco #R80)
F9	Carrageenan #1 (Danisco #100)
G9	Carrageenan #2 (Danisco #201)
H9	Alginate, sodium salt (Danisco #FD-155)
I9	Sugar beet arabinan (Megazyme)

Figure 3.16 Layout of carbohydrate array type II

A) Blue print of carbohydrate membrane. Half of the membrane has BSA conjugated oligosaccharides printed on it, the other contains non-conjugates polysaccharides. Two concentrations of carbohydrates have been printed in quadruples onto nitrocellulose as indicated B) Listing of printed carbohydrates and their origin.

The membranes were produced by Henriette Lodberg Pedersen in the laboratory of William G. T. Willats, department of plant biology and biotechnology, University of Copenhagen, DK. Figure 3.16 and 3.17 show a blue print of the two membranes used during this study. The polysaccharides were non-covalently spotted onto the nitrocellulose using a microarray printer. The three-dimensional micro-porous structure of the nitrocellulose provides a high binding capacity (Sorensen *et al.,* 2009). Polysaccharides on the membranes are presented in duplicates at two different concentrations. Membrane type I and half of membrane type II were spotted with polysaccharides obtained either by enzymatic fragmentation of large cell wall polymers followed by purification or by chemical synthesis of various glycans (Moller *et al.,* 2007, Sorensen *et al.,* 2009). The other half of membrane II was spotted with polysaccharides that are reductively aminated onto BSA. This type of carbohydrate array on basis of a nitrocellulose membrane has not been used for enzymatic screens before. My study provides the first example of its use as a substrate screen for carbohydrate active enzymes.

I incubated the membranes with recombinant DPE2 or PHS2 in buffer containing ^{14}C labelled maltose or G1P respectively. After shaking in a small petri-dish (4.5 cm diameter) for 4 hours at 25°C I washed the membrane three times for 5 min with ^{14}C-free PBS buffer. A sample from a fourth and fifth wash was taken and analysed in a scintillation counter. When no radioactivity was detected, the membrane was dried and exposed to a phosphorimager plate.

A large number of carbohydrates was labelled by both enzymes. Substrate used by both, DPE2 and PHS2, were sulphated carbohydrates like carrageenan (Figure 3.18, array type I: A,B,C,D, line 8 and array type II F and G in line 9), Rhamnogalacturonan I (RGI) from carrot ($A_1$3), RGI from Arabidopsis ($C_1$3) fucosylated xyloglucan ($D_1$4), cellulose ($D_1$5), glucomannan ($D_1$6) and 1,3-β-D-glucan ($E_1$5) on array type I and Rhamnogalacturonan II (RGII) enriched pectin from red wine ($I_2$2), enriched pectin ($I_2$6), 1,3-β-D-glucan ($E_2$5) and glucomannan ($E_2$8) on carbohydrate array type II. Overall, DPE2 and PHS2 seem to use the same carbohydrates as acceptor molecules for glucosyl transfer. The only exception is BSA conjugated maltose ($A_2$8 Figure 3.18) which was only used by DPE2.

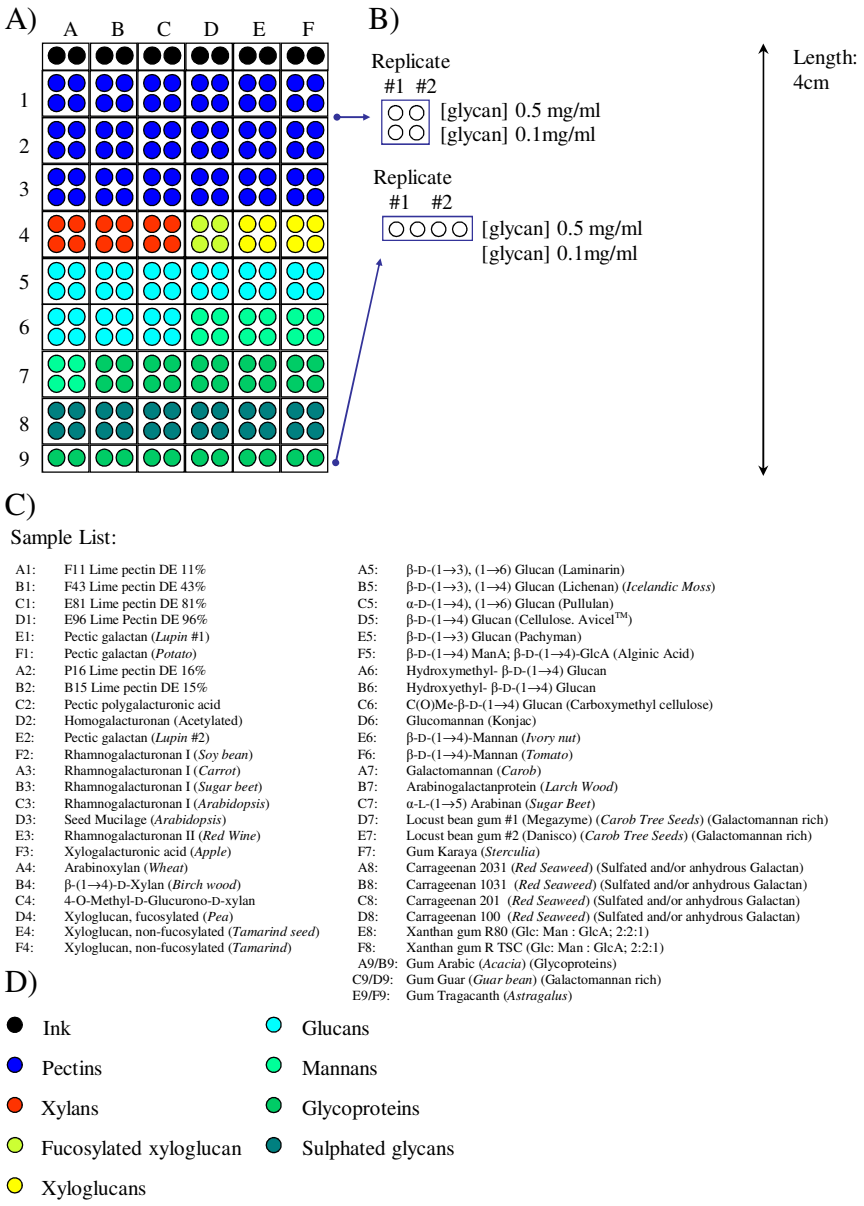

Figure 3.17 Array layout of carbohydrate array type I

Based on the result of the first screen with DPE2 and PHS2 on array type II, I designed membrane type I. The membranes were produced by Henriette Lodberg Pedersen in the laboratory of William G. T. Willats, department of plant biology and biotechnology, University of Copenhagen, DK. A) and B) Dilutions of carbohydrates have been printed in quadruples onto nitrocellulose. C) Listing of carbohydrates on the array D) colour code designating the chemical nature of the carbohydrates on the membrane

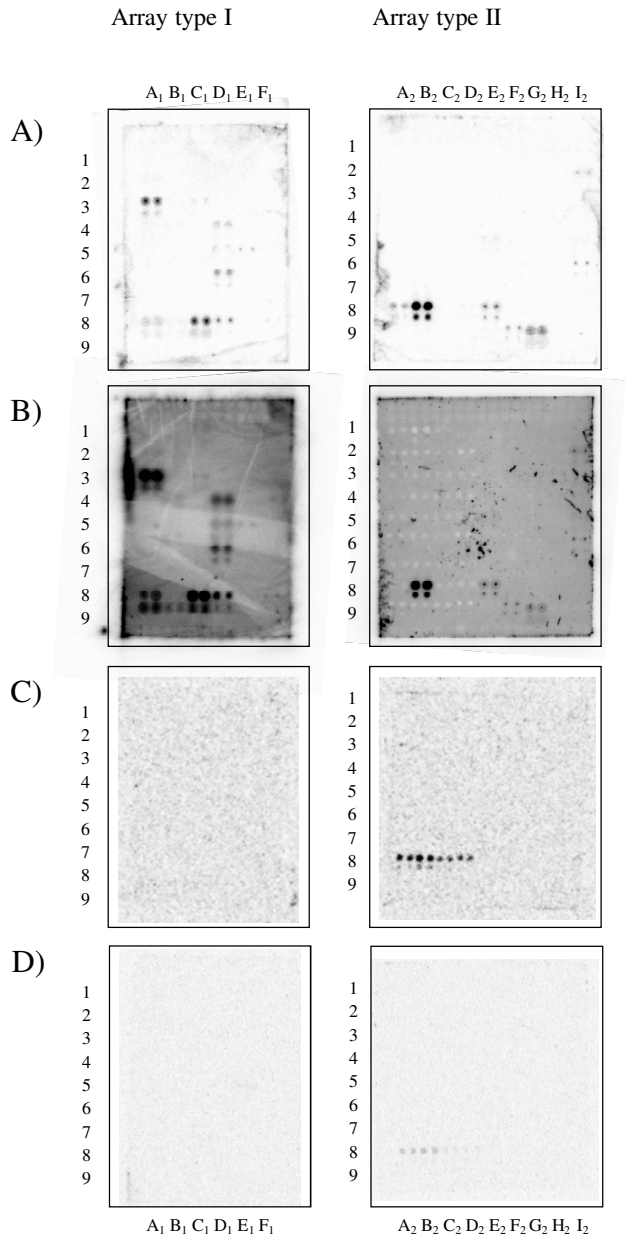

Figure 3.18 Acceptor substrate screen for DPE2 and PHS2

Plant cell wall polysaccharides and MOS were printed onto nitrocellulose membranes (membrane type I: 4cm·2cm; membrane type II: 4cm·3cm). The membranes were incubated with recombinant proteins in a volume of 5 ml buffer. A) 1 mg·ml^{-1} DPE2 and [^{14}C] maltose, B) 1 mg·ml^{-1} PHS2 and [^{14}C]-G1P) 1 mg·ml^{-1} MalQ and [^{14}C] maltose, D) 1 mg·ml^{-1} CBM20-MalQ and [^{14}C] maltose. After 4 hour incubation at 25°C the membranes were washed three times with PBS and two times PBST. After drying the membranes, the ^{14}C labeling on the membranes was imaged on a phosphorimager system.

A direct quantification of glucosyl transfer is possible only to a limited extent. The orientation on the carbohydrate array and the accessibility to the solvent might differ amongst the polysaccharides. Additionally, the time the membranes were exposed on the phosphoimager plate varied. However, it is clear that conjugated Glc5 ($B_2$8) was the most effective substrate for PHS2 and DPE2. The only difference in labelling on both membranes is position $A_2$8, which is maltose conjugated to BSA. Maltose was shown to be a very poor substrate for DPE2 in earlier experiments (Steichen *et al.,* 2008). When incubated for a longer time, maltose seems to serve as a weak acceptor substrate for glucosyl transfer by DPE2. In contrast, PHS2 strictly uses MOS that are larger than DP4 as substrates (Steup 1981).

The similar pattern of labelling of carbohydrates on both carbohydrate arrays (array type I and array type II) by DPE2 and PHS2 is consistent with the proposal that both proteins share the same acceptor molecule SHG *in vivo*.

The wide range of substrates used by DPE2 and PHS2 was unexpected. To discover whether or not this is a general feature of GH77 enzymes, I did the same experiment with MalQ from *E. coli*, which represents the orthologue of DPE2 in bacteria. None of the plant cell wall derived carbohydrates, previously labelled by DPE2 and PHS2 were labelled by MalQ. However, MalQ labelled maltose, Glc5, α-(1,6)-D-glycosyl-α-(1,4)-D-Glc3 and α-(1,6)-D-glycosyl-α-(1,4)-D-maltosyl-maltose. The latter two were not labelled by DPE2 or PHS2. Maltose and Glc5 were shown previously to be efficient acceptor molecules for glucosyl and MOS transfer by MalQ (Palmer *et al.,* 1976). It has not been previously shown that α-(1,6)-D-glycosyl-α-(1,4)-D-Glc3 and α-(1,6)-D-glycosyl-α-(1,4)-D-maltosyl-maltose can serve as substrates for MalQ. However, a recent study suggests that MalQ is involved in glycogen metabolism in *E. coli* (Park *et al.,* 2011). MalQ may thus have some activity on α-(1,6)- branched MOS. On the other hand, DPE2 was shown to act on glycogen *in vitro* (Lu *et al.,* 2006b). The activity on glycogen was even higher when compared to SHG (Steichen *et al.,* 2008). Nevertheless, the α-(1,6)-branched MOS on the membranes ($C_2$8 and $D_2$8) might be too small in comparison to glycogen to serve as acceptor substrates for DPE2.

The big difference between MalQ and DPE2 in the range of carbohydrates that act as acceptors is surprising. The differing substrate specificities might be due to the CBM20 tandem. The CBM20 tandem could bind to the SHG-like cell wall components on the carbohydrate

membrane and therefore allow DPE2 to use these as acceptor substrates. To discover whether MalQ can be at least partially targeted to some of the substrates identified for DPE2, I incubated the two carbohydrate membranes with the chimeric protein CBM20-MalQ. The result obtained was the same as with MalQ: only MOS at position $A_2$8 to $D_2$8 were labelled (Figure 3.18, D).

This result shows that DPE2 has a more relaxed substrate specificity than MalQ. It furthermore shows that substrate specificity of DPE2 is not determined by its N-terminal CBM20 tandem since the chimeric protein CBM20-MalQ does not act on any of the substrates that were labelled by DPE2. It also provides confidence that there are no substantial amounts of MOS contamination in the plant cell wall preparations spotted onto the membrane, as MalQ would have labelled other carbohydrate spots on the membrane if this was the case.

3.3 Discussion

3.3.1 DPE2 contains the catalytic triad of GH77 enzymes

My study has completed the analysis of the active site residues of DPE2 that are crucial for catalysis. I found that aspartate D563 and aspartate D810 are indispensible for the function of the protein. Substitution of these amino acids yielded enzymes with low but detectable activities, similar to the activity of the E528Q substitution studied by Steichen *et al.* (2008) (Figure 3.8). The outcome of this experiment was not obvious since DPE2 harbours a large amino acid insertion in the active site which could have potentially altered the principle reaction mechanism.

It may seem surprising that even when the catalytic nucleophile is substituted by the respective amide, some residual activity is observed. Several explanations can be given for this observation. First, the residual activity may be caused by a possible low degree of spontaneous deamidation of the D563N mutant (Reissner and Aswad 2003). Second, destabilization of the maltose bound in subsite -1 may allow it to react directly with an incoming acceptor even in the absence of the nucleophilic aspartate. This property has been exploited in the design of artificial "glycosynthases" (McKenzie *et al.* 1998). Finally, the residual activity may result from errors in translation and protein synthesis (Fersht, 1999). I conclude that DPE2 belongs to the ClanH of

glycosyl hydrolases and follows the same reaction mechanism that was proposed for other enzymes of the GH77 class of enzymes.

The insertion that spans the active site on primary amino acid level might form an extra subdomain that does not have impact on the catalytic triad and could be involved in the binding of the unusual acceptor substrate SHG. Deletion of the insertion did not affect protein solubility and DPE2 lacking the insertion could be purified to homogeneity. However, CD analysis of $DPE2_{\Delta insert}$ showed reduced signal intensity in the far-UV spectral region when compared to the wt protein (Figure 3.13). A reason for this could be a partial unfolding of the protein that does not affect its solubility. This disruption of the structural integrity of the $DPE2_{\Delta insert}$ could have caused the observed loss of catalytic activity. Therefore, information that might have shed light on the function of this insertion in catalysis could not be obtained.

After extensive trials I was able to obtain protein crystals of DPE2. Unfortunately they did not yield sufficient diffraction data when assessed on the X-ray source at the Diamond synchrotron in Oxford, UK. A refinement of the crystallisation conditions could help to produce better quality crystals that eventually yield a sufficient diffraction pattern. A three-dimensional structure of DPE2 would not only help to identify possible roles of the large amino acid insertion it could also point to possible surface binding sites on DPE2 that might explain its ability to use SHG as a substrate.

3.3.2 DPE2 contains a coiled coil motif that is important for structural integrity

Using a variety of approaches I established that purified DPE2 is a dimer. Based on the data presented in this chapter, I propose that dimer formation of DPE2 is facilitated by a coiled coil motif that I found to be located in the linker region between the active-site containing domain and the CBM20 tandem (Figure 3.9). Attempts to produce a soluble DPE2 mutant with a disruption in this motif were unsuccessful. Both mutant proteins ($DPE2_{\Delta CC1}$ and $DPE2_{\Delta CC2}$) formed inclusion bodies when produced in *E. coli*.

DPE2 from *Arabidopsis thaliana* was shown to exist in two high molecular weight states, one at approximately 220 kDa and one larger than 1000 kDa (Fettke *et al.,* 2009a). The occurrence of a 220 kDa state shows that dimer formation of DPE2 might also occur *in planta*. The formation of

dimers could be in equilibrium with the formation of large molecular weight complexes. However, I did not obtain evidence of the existence of such high molecular weight complexes with recombinant DPE2. The structure and function of these complexes is unknown, but they seem to be a common feature of DPE2 activity not only in *Arabidopsis thaliana* but also in maize (Fettke *et al.,* 2009a). This is in agreement with my experiments that show that DPE2 from multiple plant sources contains a coiled coil motif at the same position which could facilitate formation of dimers and/or high molecular weight oligomers (Figure 3.10). On the other hand, these complexes found in Arabidopsis and maize could also be an artefact that occurs during the purification procedure used in the respective study. The buffer used for SEC in the study by Fettke *et al.* (2009 a) did not contain any NaCl and the buffer concentration was 100 mM (Fettke *et al.,* 2009a). Under these conditions proteins like MalQ from *E. coli* also start forming high molecular weight complexes (Palmer *et al.,* 1976). In Chapter 5 I show evidence of the formation of multiple and catalytically active high molecular weight forms of recombinant purified MalQ (Cahpter 5,Figure 5.4, B). In future, *in vivo* information about the oligomeric state of DPE2 could be obtained by bimolecular fluorescence complementation (BiFC, also referred to as "split YFP"). This has been shown to be a useful tool to study protein-protein interactions in living cells. It could confirm the nature of a possible oligomeric state of DPE2 *in planta.*

The only three–dimensional molecular structure with a similar domain arrangement to DPE2 has been published very recently (Lammerts van Bueren *et al.,* 2011). The crystal structure of the glycogen degrading virulence factor (SpuA) from *Streptococcus pneumoniae* contains an N-terminal CBM41 tandem that is connected to a GH13 domain via a linker region. This linker region is partially unstructured and surface exposed. In DPE2 this position is occupied by the coiled coil motif that could be the point of protein dimerisation. Swapping this coiled coil motif with another one from an unrelated protein might confirm its role in protein dimerisation.

3.3.3 DPE2 binding to starch is conferred by its N-terminal CBM20 tandem repeat

My data confirm an earlier report (Steichen *et al.,* 2008) that showed binding of DPE2 to granular starch. In addition I showed that the N-terminal CBM20 tandem transfers the ability to bind starch when fused to MalQ from *E. coli* that by itself cannot bind to starch. This shows that the site of starch binding lies in the CBM20 tandem of DPE2. It is intriguing that DPE2 binds to

starch since it is a cytosolic protein (Chia *et al.,* 2004, Li *et al.,*) and starch is located in the plastid of the plant cell. The optimal acceptor substrate for DPE2 *in vitro* was found to be glycogen (Lu *et al.,* 2006b, Steichen *et al.,* 2008) which is also not found in the plant cytosol. The unusual properties of DPE2 discovered *in vitro* might reflect its complex role in the metabolism of maltose and SHG *in vivo*.

When produced and purified individually, the CBM20 modules from DPE2 showed different binding capabilities with respect to starch or the starch components amylose and amylopectin. Whereas CBM20-1 bound to starch, amylose and amylopectin, CBM20-2 did not bind to any of these molecules. There are several explanations that can account for this observation. One is that both modules together act as a single functional domain rather than acting individually. This, however, is not consistent with present knowledge as all CBM20s characterised so far (and STBs in general for that matter) are organised as independent structural units (Christiansen *et al.,* 2009a, Christiansen *et al.,* 2009b). Another explanation is that CBM20-2 is part of a linker region that connects CBM20-1 with the catalytic domain of DPE2. This was shown to be the case in the crystal structure of SpuA. In the structural model of the glycogen degrading enzyme from *Streptococcus pneumoniae* (Lammerts van Bueren *et al.,* 2011), the first CBM module makes contact with the active site containing GH13 domain. This creates a binding site for the MOS substrate. The second CBM in SpuA does not seem to have any function, other than extending the linker region. This is the first study that directly shows active involvement of a CBM in providing subsites in the substrate binding pocket of an active site. The similarity of the domain organisation of SpuA with that of DPE2 is striking and favours the idea that the structural organisation of DPE2 is similar to that of SpuA. Deletion of CBM20-1 in an earlier study showed that the substrate specificity of DPE2 changes from a preference for long and complex substrates like glycogen to short MOS like Glc3 and Glc4 (Steichen *et al.,* 2008). This finding could be accounted for by a loss of contact between the CBM20-1 and the GH77 domain of DPE2.

3.3.4 DPE2 can act on plant cell wall polysaccharides *in vitro*

To gain further insight into the interaction of DPE2 and SHG I did a substrate screen for DPE2 on a range of plant cell wall derived polysaccharides. In contrast to MalQ, DPE2 and PHS2 acted on a broad range of different polysaccharides. This is surprising as other studies have shown that DPE2 is specific in its choice of SHG substrate. It was proposed that DPE2 only acts on one specific subfraction of SHG (SHG_{LI}) (Fettke *et al.,* 2006a). Another subfraction, SHG_{LII}, is not used by DPE2 even though SHG_{LI} and SHG_{LII} are very similar in composition and glycosidic linkages (Chapter 1, Table 1.1). I found that PHS2 labelled essentially the same range of acceptor substrates with ^{14}C glucose. Taking these results together I propose that the shape and structure of the potential acceptor substrate rather than monosaccharide composition might be the determining factor that allows for successful glucosyl transfer catalysed by DPE2 and PHS2. The shape of polysaccharides is still poorly understood. However, some polysaccharides were found to form helices (Rees, D *et al*. 1977). Such helix formation has also been reported for many types of carrageenans (van de Velde *et al.,* 2001, van de Velde *et al.,* 2002) and for cellulose and xyloglucan (Hayashi, T *et al.* 1994). DPE2 might be able to recognise the helical conformation of carbohydrates in some way. This could be achieved by the N-terminal CBM20 tandem. However, the transfer of the CBM20 tandem to *E. coli* MalQ did not alter its substrate specificity. This could be for a number of reasons. First, the CBM20 tandem may target MalQ towards those polysaccharides that were used by DPE2 as substrate, but MalQ does not have the enzymatic capacity to subsequently act on these. Second, the CBM20 tandem may not target MalQ to the appropriate substrates. The latter is less likely since I showed that the CBM20 tandem transfers starch binding ability to MalQ. The first assumption will be investigated further in Chapter 4 by comparing the monosaccharide acceptor specificity of DPE2 and MalQ.

4. Biochemical Differences Between DPE2 and MalQ

4.1. Introduction

DPE2 and MalQ are tranglucosidases that belong to family GH77 of glycoside hydrolases. Both enzymes metabolise maltose, in plants and bacteria like *E. coli* respectively. In the previous chapter I have shown some unique structural features and enzymatic properties of DPE2 that are not present in MalQ. In this chapter I will further analyse and compare biochemical and enzymatic features that distinguish the two proteins. Below I discuss important aspects of the catalytic activities of DPE2 and MalQ that are not fully understood but are potentially relevant to their distinct biological roles.

4.1.1. Same family but different substrate specificities

The classification of enzymes by specialist databases into families and clans is entirely based on their primary amino acid sequence (Cantarel *et al.,* 2009, Sonnhammer *et al.,* 1997). This is advantageous in the post genome era, since myriads of sequences originating from automated sequencing projects need to be automatically annotated. The CaZy database is such a specialist database dedicated to the display and analysis of genomic, structural and biochemical information on carbohydrate-active enzymes (Cantarel *et al.,* 2009). This provides an excellent tool for the comparison and analysis of enzyme sequences. According to CaZy, enzymes such as DPE2, DPE1 and MalQ belong to family GH77 and therefore have the same enzyme specificity - the amylomaltase (EC 2.4.1.25). However, this classification is no indication of actual substrate specificity, which can vary dramatically. For instance: Incubation of DPE1, DPE2 and MalQ with Glc3 leads to the formation of a different range of products (Figure 4.1). Whereas DPE1 transfers maltosyl residues onto Glc3 forming glucose and Glc5 (Critchley *et al.,* 2001), DPE2 cannot use Glc3 as a substrate (only in combination with maltose). MalQ in contrast completely disproportionates Glc3, yielding glucose and MOS (Lengsfeld *et al.,* 2009). This shows that thorough biochemical analysis of all enzymes is required to make valid predictions about their biological role and catalytic capacity.

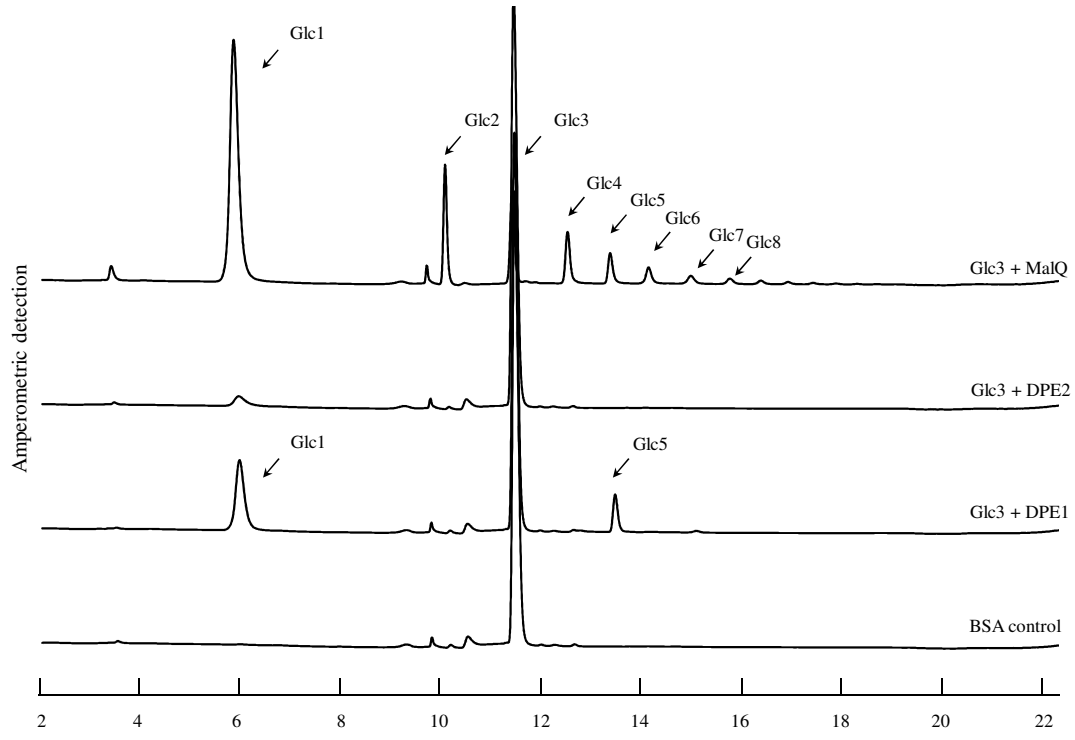

Figure 4.1 Disproportionation of Glc3 by DPE1, DPE2 and MalQ

In a final volume of 100 µl, 15 µg recombinant DPE1, DPE2 or MalQ were incubated with 10 mM Glc3 for 15 min at 37°C. Following incubation, the reaction mixtures were analysed with HPAEC-PAD. BSA (15 µg) incubated with 10 mM Glc3 served as a protein control. DPE1 was produced and purified by Krit Tantanarat (JIC, laboratory of Prof Rob Field).

4.1.2. The acceptor substrate of DPE2 and MalQ

DPE2 is able to use the complex heteroglycan SHG as a substrate (Fettke *et al.,* 2006a, Fettke *et al.,* 2009a). The substrate screen reported in Chapter 3 showed that it can also use a wide range of other polysaccharides as opposed to MalQ which can only use MOS (Figure 4.2). However, it is not known how DPE2 transfers glucose onto SHG. It was previously shown that DPE2 is able to transfer glucose from glycogen as an efficient (but non-physiological) glucose donor onto various monosaccharides that are components of SHG (Fettke *et al.,* 2006a). Disaccharide formation and therefore glucosyl transfer was shown to occur with glucose, mannose, xylose, fucose and galactose. Thus DPE2 may be able to transfer glucose from maltose onto a variety of

terminal residues of SHG, and not simply onto terminal glucosyl residues. It is not known whether this broad acceptor specificity is unique to DPE2 or whether other GH77 enzymes like MalQ can also use acceptors other than glucose. In addition, the linkage of the disaccharides formed by transfer onto sugars other than glucose was not analysed. Vital information about the properties of DPE2 relevant to its biological role is therefore lacking.

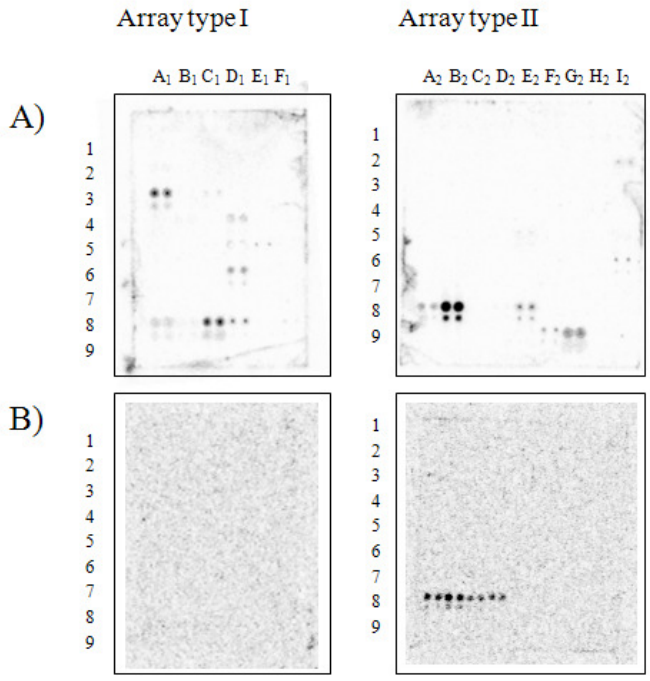

Figure 4.2 Acceptor substrate screen for DPE2 and MalQ

Reaction as described in Chapter 3, Figure 3.18. A) membranes incubated with DPE2 B) membranes incubated with MalQ.

4.1.3. Maltose as donor and acceptor substrate for DPE2 and MalQ

The pathway of maltose metabolism in Arabidopsis and *E. coli* is similar (Lu and Sharkey 2006). Maltose enters the cytosol from the chloroplast in plants and from the extracellular space in bacteria like *E. coli*. Once transferred into the cytosol maltose is acted on by a GH77 enzyme and the products of this reaction are further processed to hexose phosphate via phosphorylase and hexokinase (Chapter 1, Figure 1.7). As discussed in Chapter 1, the complexity of the proposed acceptor substrate of DPE2 (SHG) and MalQ (MOS) differs greatly in terms of

composition and glycosidic linkage. In addition however, the exact role of maltose as substrate is also still under debate und not entirely clear (Boos and Shuman 1998, Lengsfeld *et al.,* 2009, Palmer *et al.,* 1976, Wiesmeyer and Cohn 1960). Based on experimental data, Palmer *et al.* (1976) suggested that maltose cannot act as glucose donor substrate for MalQ and therefore only serves as acceptor substrate of glucose and MOS transfer. It was therefore stated that reaction (4.1) cannot be catalysed by MalQ.

Glc2 + Glc2 = Glc3 + Glc reaction (4.1)

However, in later studies it was shown that MalQ indeed can produce glucose and MOS from chromatographically pure maltose (Dippel and Boos 2005, Lengsfeld *et al.,* 2009). Studies on recombinant DPE2 have mainly focussed on the proposed acceptor substrate SHG, rather than on the donor substrate maltose. Contradictory reports on MalQ action on maltose and the lack of experimental data on the action of recombinant DPE2 on chromatographically pure maltose demands further investigation.

4.1.4. Affinity of DPE2 and MalQ for MOS

The reaction kinetics of amylomaltases belonging to GH77 family of glycoside hydrolases are usually compared by monitoring the glucose release from action on MOS (Kaper *et al.,* 2007, Kaper *et al.,* 2005). In earlier studies, DPE2 and MalQ were shown to use MOS as substrate for glucose and glucan transfer *in vitro* (Palmer *et al.,* 1976, Steichen *et al.,* 2008, Weise *et al.,* 2005). A direct comparison of the reaction kinetics of DPE2 and MalQ however is not practical, as the two proteins are thought to use maltose and MOS differently. Whereas MalQ was shown to transfer a range of MOS and glucose from MOS onto glucose and MOS (Palmer *et al.,* 1976), DPE2 is thought to only transfer single glucose molecules from maltose onto an acceptor molecule (Steichen *et al.,* 2008). The kinetic parameters of GH77 enzymes are usually compared and studied on single MOS substrates (Kaper *et al.,* 2007, Kaper *et al.,* 2005). DPE2 however was shown not to act directly on MOS as it strictly requires maltose as donor substrate (Fettke *et al.,* 2006a). Therefore DPE2 activity on MOS needs to be reanalysed.

Palmer *et al.* (1976) inferred an autocatalytic reaction mechanism for MalQ. Glc3 and higher MOS at catalytic concentrations were thought to 'prime' enzyme action on chromatographically pure maltose. However, in later studies MalQ was shown to act on pure ^{14}C-labelled maltose

even after extensive dialysis was done on highly pure MalQ preparations (Dippel and Boos 2005, Lengsfeld *et al.,* 2009). It would require very strong binding (K_d in the low nM range) of small MOS by MalQ to be able to retain these molecules in catalytic concentrations throughout the purification process. The affinity of neither DPE2 nor MalQ for MOS has been previously assessed. Comparing the binding constants of the two proteins for MOS would provide information about the efficiencies of the two enzymes for potential substrates and therefore shed light on the activity of MalQ and DPE2 on pure maltose and MOS.

4.1.5. Hydrolytic activity

Although they share a similar fold and catalytic machinery (MacGregor *et al.,* 2001), the members of ClanH of glycoside hydrolases are able to perform a range of different reactions, such as hydrolysis, transglycosylation, condensation and cyclization (Nahoum *et al.,* 2000). GH77 enzymes, which are part of the ClanH, exhibit very high transglucosylation activity (Kaper *et al.,* 2007). When compared to the only two other members of ClanH (family GH13 and GH70), GH77 enzymes have the lowest hydrolysis to transfer ratio (down to 1 to 5000; hydrolysis to transfer) (Fujii *et al.,* 2005, Kaper *et al.,* 2005, Kuriki and Imanaka 1999, Leemhuis *et al.,* 2002). This property has been exploited for industrial applications like large scale production of cycloamyloses (Fujii *et al.,* 2005) but its biological significance has not yet been assessed. MalQ was reported to have no hydrolytic activity towards maltose, MOS and amylopectin (Palmer *et al.,* 1976). The hydrolytic activity of DPE2 has not yet been measured.

In this chapter I further examine biochemical and enzymatic characteristics that distinguish the maltose metabolising enzymes DPE2 and MalQ. In the light of the deficiencies in understanding described above, I analysed the following features to achieve this:

- Potential monosaccharide acceptors
- MOS binding using SPR
- Action on maltose and MOS as sole substrate
- Capacity to hydrolise maltose

4.2 Results

4.2.1 Selectivity of the DPE2-, and MalQ-catalyzed glucosyl transfer

As discussed above (Figure 4.2) and shown in Chapter 3, DPE2 catalysed glucosyl transfer is not strictly dependent on glucose as acceptor. Earlier *in vitro* studies have shown that (when providing glycogen as glucose donor substrate) DPE2 utilizes glucose as an acceptor substrate yielding maltose. Mannose and xylose, however, were similarly efficient acceptors. Fucose and galactose also acted as glucosyl acceptors, although less efficiently than glucose, mannose and xylose (Fettke *et al.,* 2006a). My results in Chapter 3 show that DPE2 can utilise acceptors polysaccharides that do not contain glucose. To extend this study on other potential acceptors I incubated recombinant DPE2 with various hexoses or pentoses as potential glucose acceptors. Glycogen was used as a highly effective (but non-physiological) glucose donor. Following incubation, the reaction mixture was boiled, filtered and then analyzed by HPAEC-PAD.

The occurrence of additional peaks eluting in the disaccharide region of the chromatogram indicates that under *in vitro* conditions the respective monosaccharide can act as a glucose acceptor (Figure 4.3 A). It could be confirmed that glucose, mannose and xylose serve as acceptor of glucosyl transfer by DPE2. In addition, no disaccharide formation s occurred with rhamnose and arabinose as reported by Fettke *et al.* (2006). However, fucose and galactose (that were previously shown to serve as acceptor of glucosyl transfer by DPE2 [Fettke *et al.* 2006]) did not yield the respective disaccharide Glc-Gal and Glc-Fuc in my experiment. To test whether the C_2 and C_3 position of the hydroxyl group in the monosaccharide acceptor are important for catalysis I also tested 2,3-deoxy-D-glucose, N-acetyl-D-glucosamine and D-allose for their ability to serve as acceptor for glucosyl transfer with DPE2. Table 4.1 shows that disaccharide formation occurs with these substrates and summarises the results for all potential acceptors. These data support the idea that DPE2 exhibits a relaxed specificity towards modifications at C_2 and C_3. In addition, the presence of C_6 does not seem to be critical (Figure 4.12). However, the C_4 hydroxyl group must be in equatorial position for glucosyl transfer by DPE2 to occur.

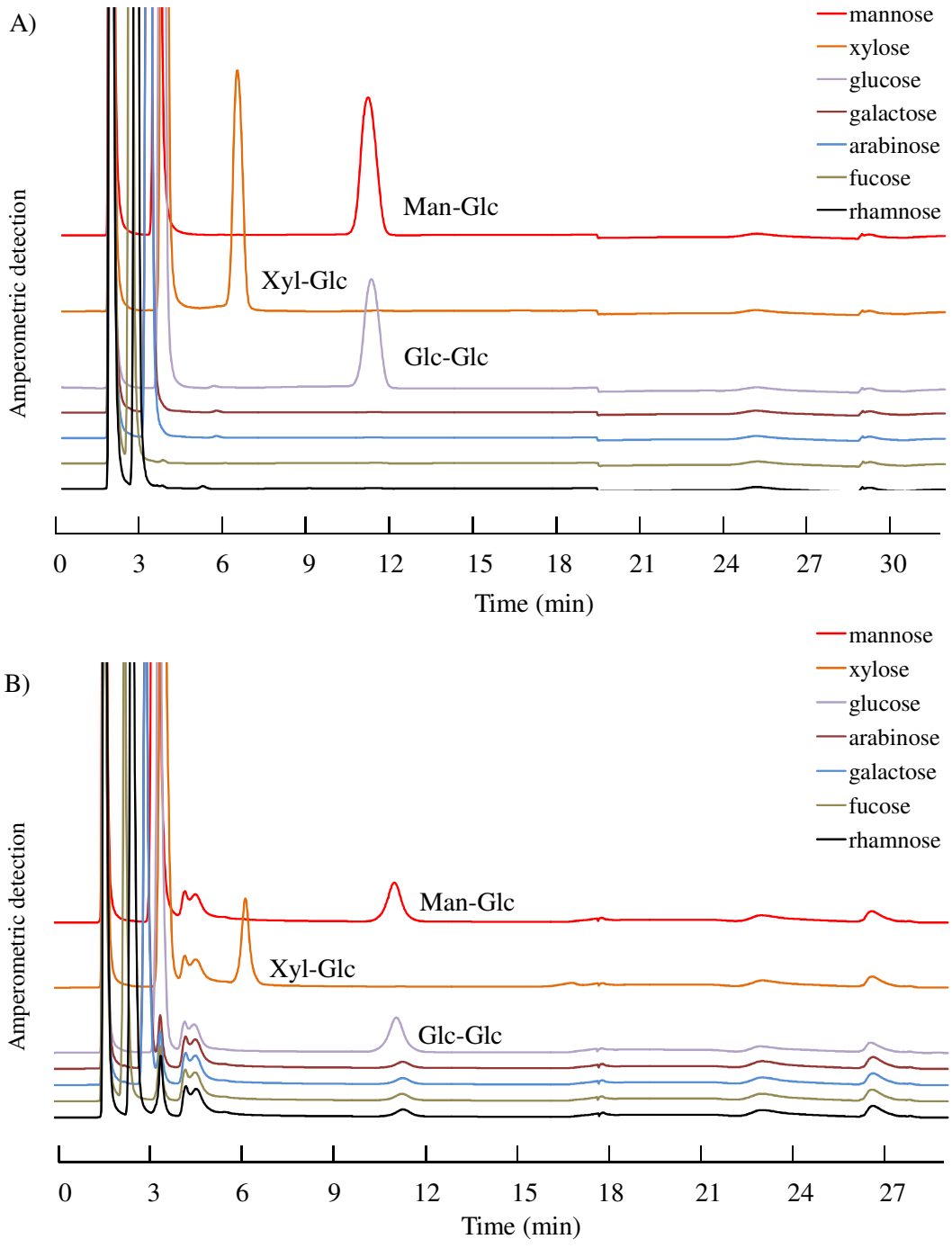

Figure 4.3 Glucosyl transfer from glycogen to various monosaccharides

Recombinant DPE2 (A) and MalQ (B) (2.5 µg each) were incubated for 90 min at 37°C with glycogen and various monosaccharides (30 mM each). Following incubation, the reaction mixtures were passed through a 10 kDa filter and the resulting filtrates were analyzed by HPAEC-PAD.

To test whether or not MalQ also shows this relaxed substrate specificity I incubated MalQ with the same set of monosaccharides and followed formation of disaccharides upon transfer of glucosyl residues from glycogen. Monosaccharides that were used as acceptor by DPE2 also yielded disaccharide formation with MalQ (Figure 4.3, B and Table 4.1). The amperometric detection of the disaccharides gave a lower response when compared to the DPE2 reaction. This may be because glycogen is a better donor substrate for DPE2 than it is for MalQ (Fettke *et al.,* 2006a, Palmer *et al.,* 1976). Nevertheless, in this experiment it was advisable to use glycogen instead of Glc7 as the product range with Glc7 and MalQ would have been much larger with MalQ than with DPE2 due to the disproportionation activity of MalQ on single MOS.

The glycosidic linkage of Glc-Xyl and Glc-Man produced by DPE2 and MalQ were analysed as described in Chapter 2 section 2.6.5. In brief, the disaccharides were per-O-methylated and subsequently further derivatised to give the corresponding partially methylated alditol acetates (PMAAs). The PMAAs were then analysed using Gas Chromatography coupled with Electron Impact Mass Spectrometry (GC-EIMS). Standards were kindly provided by Prof Birte Svensson (Denmark Technical University, Denmark) (Nakai *et al.,* 2010). As expected all tested disaccharides had a 1,4 glycosidic linkage (Table 4.1 and Appendix 2). This agrees with the proposed reaction mechanism of GH77 enzymes forming α-1,4- linked glucans.

Acceptor	DPE2	MalQ
D-Glucose	+	+
D-Mannose	+	+
D-Xylose	+ (1,4)	+ (1,4)
N-Acetyl-D-glucosamine	+	+
2,3-Dideoxy-D-glucose	+	+
D-Allose	+	+
L-Rhamnose	-	-
L-Arabinose	-	-
D-Galactose	-	-
D-Fucose	-	-

Table 4.1 Summary of the acceptor specificity of DPE2 and MalQ

Experiments were those shown in Figure 4.3. + indicates product formation; - indicates no product formation. Where stated, (1,4) indicates the linkage of the disaccharide formed.

4.2.2 Disproportionation activity of DPE2 and MalQ on pure maltose

I assessed the ability of recombinant DPE2 and MalQ to act on chromatographically pure maltose. For this purpose I incubated the enzymes with maltose and followed the production of glucose by monitoring NADH production from NAD in a hexokinase/glucose 6-pohosphate dehydrogenase coupled assay (Chapter 2, Section 2.8.1.3). Recombinant MalQ released glucose from maltose after an initial lag phase (Figure 4.4 A). In contrast, DPE2 did not release glucose from maltose. Only the addition of Glc7 allowed release of glucose from maltose by DPE2 presumably as a result of glucosyl transfer from maltose onto Glc7 (Figure 4.4 B).

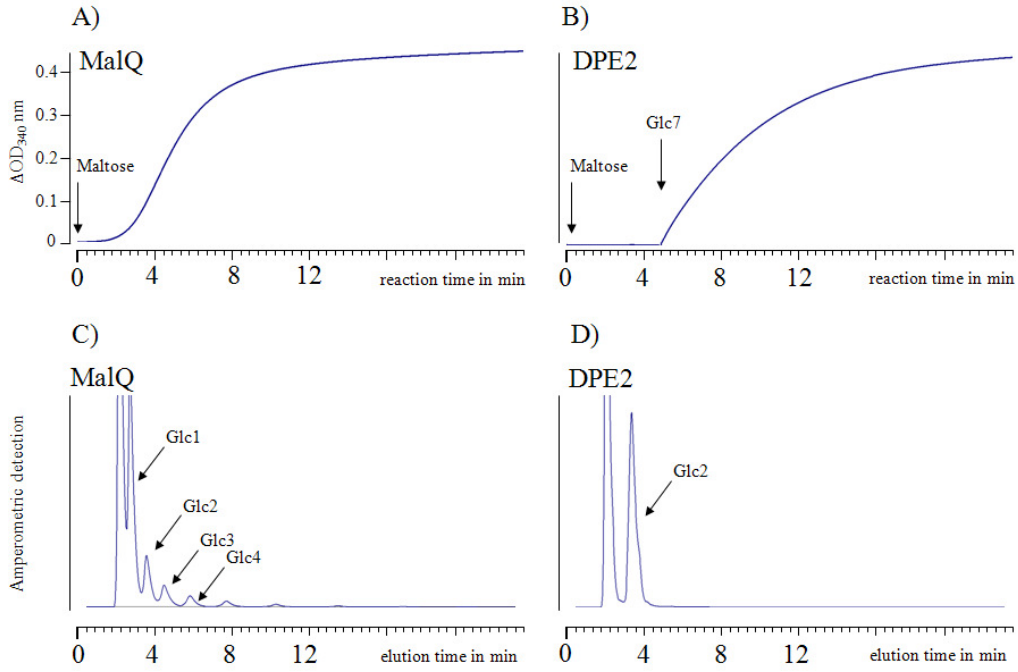

Figure 4.4 Reaction of MalQ and DPE2 on chromatographically pure maltose

A,B: Recombinant MalQ (A) and DPE2 (B) were incubated with 0.05 mM maltose in a continuous, coupled assay in which glucose release was monitored as conversion of NAD to NADH in the presence of hexokinase, G6PDH, ATP and magnesium at pH 7.9. Glc7 (0.25 mM) was added to B after 5 min.

C,D: Recombinant MalQ (A) and DPE2 (B) were incubated with 0.05 mM maltose (10 min) and the reaction products were analysed with HPAEC-PAD.

To identify additional reaction products other than glucose I analysed both reaction mixtures with HPAEC-PAD. The reaction mixture containing MalQ and maltose contained a range of

MOS (up to DP 8) and glucose (Figure 4.4 C). The reaction mixture containing DPE2 and maltose as sole substrate (without added Glc7) contained only maltose (Figure 4.4 D). No accumulation of MOS or glucose was observed.

4.2.3 SPR analysis of MOS binding to DPE2, MalQ and CBM20-MalQ

The existence of a long lag phase (Figure 4.4, A - 4 min) in the reaction mixture containing MalQ and maltose suggests that the MalQ reaction could be autocatalytic. Another explanation for the direct activity of MalQ on maltose could be the presence of catalytic quantities of MOS present in the MalQ enzyme preparation that could serve as primers for the initial reaction (Boos and Shuman 1998, Palmer *et al.,* 1976). If this was true, molecules like Glc3 would have to bind to MalQ in the low nM range. Analysis of the affinity of MalQ to MOS however is lacking. Therefore I analysed the affinity of DPE2 and MalQ (and CBM20-MalQ) on various MOS. The experiments were run by Dr Darrell Cockburn (Denmark Technical University in Copenhagen, Denmark)

The SPR procedure is described in Chapter 2, Section 2.6.7.4. Briefly, protein solutions were biotinylated and immobilised on a Series S Sensor chip SA (GE). The biotinylated protein was applied to the surface at a flow rate of 10 $\mu l \cdot min^{-1}$ until a target of 3000 bound Response Units (RU) was reached. For the results for MalQ with Glc3, Glc4 and β-cyclodextrin immobilization was performed on a Series S Sensor chip CM5 (GE). In this case the protein was not biotinylated first and was instead directly coupled to the chip. The protein was applied to the surface until an immobilization level of 6000 RU was reached (the higher binding level was needed to increase the sensitivity). In all binding experiments analytes were applied to the chip at a flow rate of 30 $\mu l \cdot min^{-1}$ at 25 °C. The contact time was 90 seconds, followed by a dissociation time of 30 seconds and regeneration using 10 mM HEPES pH 7.0 with 1 M NaCl for 90 seconds. All measurements were performed in triplicate on one chip and then repeated on another chip. Blanks were included as stated. Analyte concentrations ranged from 50 nM to 10 mM for the oligosaccharides Glc3, Glc4, Glc5, Glc6 and Glc7 and from 25 μM to 3 mM for β-cyclodextrin (β-CD).

The affinity of MalQ for Glc3 (K_d = 0.26 μM ± 0.03) and Glc4 (K_d = 0.41 μM ± 0.02) was approximately 20 times higher than its affinity for maltopentaose (Glc5) (K_d = 7.43 μM ± 0.87), maltohexaose (Glc6) (K_d = 11.03 μM ± 1.05) and Glc7 (K_d = 12.07 μM ± 0.1)(Figure 4.5). The strong binding of Glc3 and Glc4 to MalQ could account for the activity of the MalQ preparation on maltose. A K_d in the nanomolar range as observed for MalQ could be enough for Glc3 or

A)

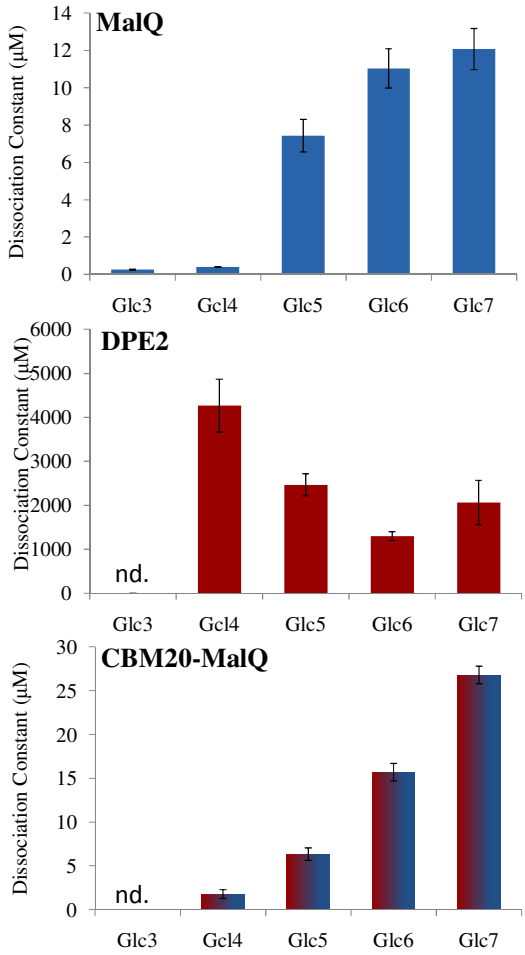

B)

	MalQ	DPE2	CBM20-MalQ
Glc3	0.26 +/- 0.03		
Glc4	0.41 +/- 0.02	4.27×10^3 +/- 0.60×10^3	1.77 +/- 0.50
Glc5	7.43 +/- 0.87	2.47×10^3 +/- 0.25×10^3	6.33 +/- 0.71
Glc6	11.03 +/- 1.05	1.30×10^3 +/- 0.10×10^3	15.70 +/- 1
Glc7	12.07 +/- 1.10	2.07×10^3 +/- 0.50×10^3	26.80 +/- 1

K_d in µM

Figure 4.5 Surface Plasmon Resonance analysis of MOS binding of DPE2, MalQ and CBM20-MalQ

The SPR experiments were done by Dr Darrell Cockburn (Denmark Technical University in Copenhagen, Denmark). Surface plasmon resonance sensorgrams of the binding of 50 nM to 10 mM linear MOS (DP 3–7) and 25 µM to 3 mM β-CD to biotinylated protein (3000 RU on Series S Sensor chip SA (GE)) were recorded (except for MalQ on Glc3 and Glc4 – direct coupling of MalQ on Series S Sensor chip CM5 (GE)). K_d values were calculated by steady-state affinity fitting (BIAevaluation 1.1 software) to the response after subtracting the reference cell signal. Y-axis values are in mM (DPE2) and µM (MalQ and CBM20-MalQ).Nd. = not done

Glc4 to bind to the enzyme in catalytic amounts during purification of the enzyme. However, extensive dialysis performed on the enzyme preparation (Boos and Shuman 1998, Dippel and Boos 2005) should eliminate any binding of Glc3 or Glc4.

To check whether the strong binding of small MOS is specific to MalQ I analysed binding of DPE2 to Glc4, Glc5, Glc6 and Glc7. The affinity of DPE2 for Glc4 was at least 10,000 times lower than that of MalQ (K_d of 4.27 mM as compared to a K_d of 0.41 μM). A strong difference in affinity between MalQ and DPE2 can also be seen with Glc5 (K_d = 2.47 mM ± 0.25), Glc6 (K_d = 1.3 mM ± 0.1) and Glc7 (K_d = 2.07 mM ± 0.5). A further difference between the two proteins is the reversed substrate length preference. Whereas MalQ prefers to bind to small MOS with a DP of less than 5, DPE2 seems to have an increased affinity for longer MOS up to Glc6.

The difference between DPE2 and MalQ in the binding of small MOS with a DP up to 7 is striking. To investigate the impact of the CBM20 tandem domain of DPE2 on binding of MOS, the chimeric protein CBM20-MalQ was tested on Glc4, Glc5, Glc6 and Glc7. The affinity of the chimeric protein to MOS resembled more that of MalQ, than that of DPE2 (Figure 4.5). However, the values of the dissociation constants were slightly lower with CBM20-MalQ than with MalQ. Binding of Glc4 to CBM20-MalQ was 5 times less strong (Glc4: K_d = 1.77 μM ± 0.5) and binding of Glc5, Glc6 and Glc7 was approximately half that of MalQ (Glc5: K_d = 6.33 μM ± 0.71, Glc6: K_d = 15.7 μM ± 1 and Glc7: K_d = 26.7 μM ± 1). The decrease in affinity of MalQ on increasing DP seems to start levelling off at a DP of 6 and 7. In contrast, CBM20-MalQ shows a linear decrease in affinity throughout.

In the previous chapter I confirmed that DPE2 can bind to starch. To investigate this property further I analysed binding of DPE2 to the starch mimic β-CD. The affinity of DPE2 to β-CD is in the μM range and therefore stronger than to linear MOS. MalQ also bound to β-CD. Its binding was even stronger than that of DPE2 (K_d of 0.26 mM compared to 0.35 mM) (Figure 4.6). This is surprising as MalQ was shown not to bind to granular starch in the previous chapter. However, its binding to β-CD was much weaker than to linear MOS (20 times than when compared to Glc7).

A)

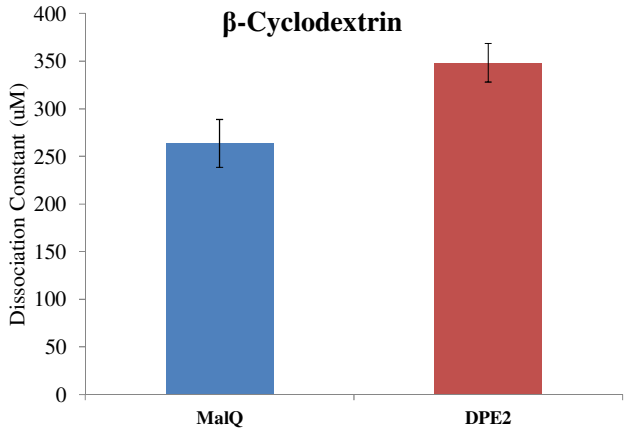

B)

264 +/- 25	MalQ
348 +/- 20	DPE2

K_d in µM

Figure 4.6 SPR analysis of β-cyclodextrin binding to DPE2, MalQ

Experiments were done as described in Figure 4.5.

4.2.4 Disproportionation of MOS

It was previously shown that DPE2 cannot fully disproportionate single MOS (Steichen *et al.,* 2008). It is only able to transfer glucose to MOS when maltose is added as a donor substrate (Figure 4.4, B). In contrast, MalQ is able to produce a range of MOS and glucose when incubated with a single MOS substrate. However, when I incubated large quantities of DPE2 (1 µM) with Glc2 to Glc7 (25 mM) over 12 h at 37°C formation of products was observed (Figure 4.7, A). When I repeated the experiment with MalQ, the reaction reached an equilibrium producing glucose and a wide range of MOS (Figure 4.7, B). Therefore a conclusion about initial product formation by MalQ cannot be assessed, since the initial products themselves seemed to have served as substrate for disproportionation, masking the initial reaction products. The reaction mixtures containing DPE2 however showed appearance of two main products. Glc7 was predominantly converted into Glc6 and Glc8. Glc5 was mainly converted to Glc4 and Glc6 and so on (Figure 4.8). Product formation by DPE2 therefore seems to follow reaction (2).

$Glc_n = Glc_{n+1} + Glc_{n-1}$ reaction (4.2)

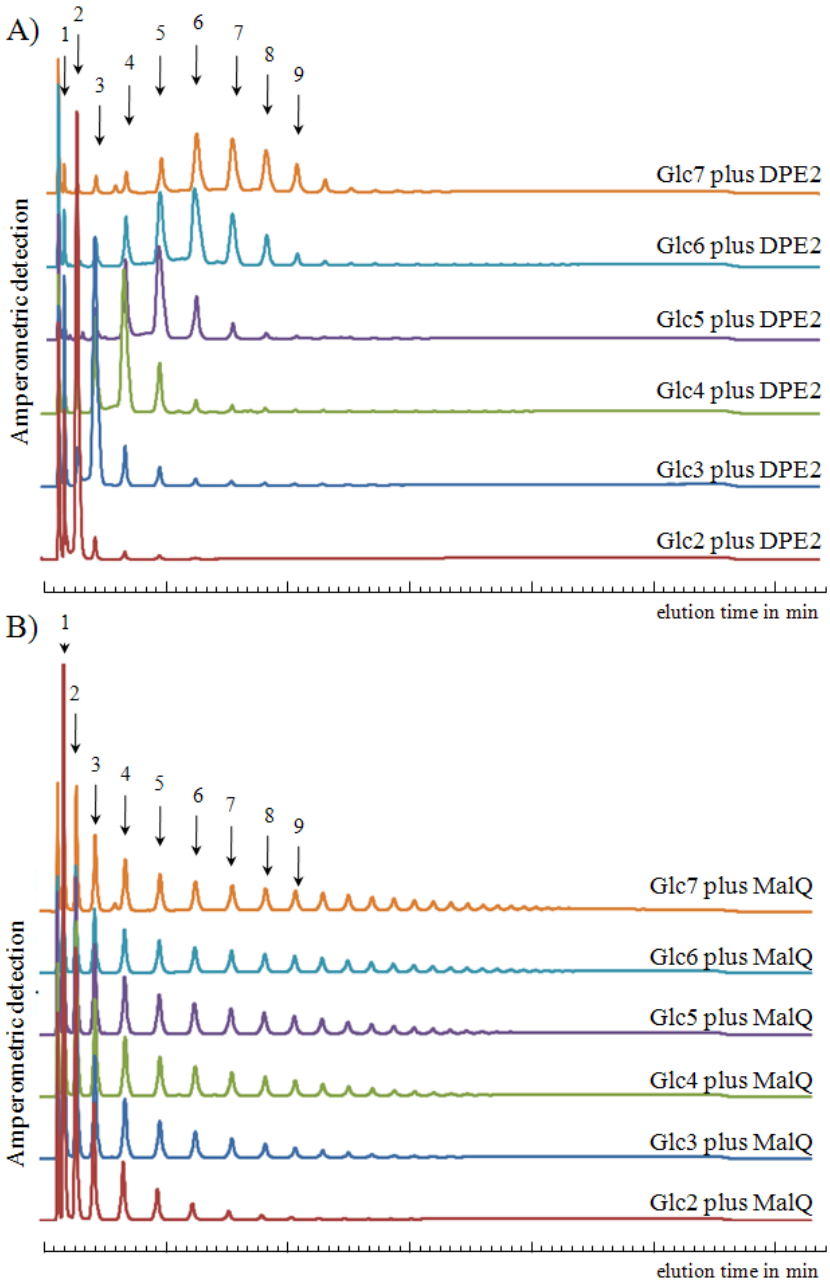

Figure 4.7 Disproportionation of linear MOS by DPE2 and MalQ

DPE2 (A) and MalQ (B) were incubated with Glc2-Glc7 (25 mM) for 12 h at 37°C. Reactions were performed in 100 mM HEPES (pH 7.0) at 37 °C with 1 µM enzyme The reaction mixture was boiled, spun down and filtered before loading onto PA-100 CarboPAC column (DIONEX). The numbers above the peaks show degree of polymerization of the eluting MOS products.

During the initial disproportionation of MOS via GH77 enzymes, equal amounts are produced, of two oligosaccharides that typically differ in length by twice the transferred saccharide unit (Albenne *et al.,* 2002, Kaper *et al.,* 2007, Kaper *et al.,* 2005). My results indicate that DPE2 transfers single glucosyl residues and therefore products are formed that differ twice by the size of the transferred molecule glucose. With these data it is therefore possible to deduce the binding modes of substrate binding in the active site of DPE2.

One of the two major products in the DPE2 reaction is slightly more abundant than the other. The more abundant product is likely to correspond to the saccharide that is released when the covalent enzyme substrate reaction intermediate is formed, since it has to leave the active site before the bound part of the substrate is released by an incoming acceptor. The deduced dominant binding mode of substrate with DPE2 shows a restriction of substrate binding beyond subsite -1 (Figure 4.8, B). Beynding beyond the -1 subsite is only acchieved in the case of Glc3 as substrate since formation of maltose is less dominant than formation of glucose. However, maltose was one of the least abundant products in all reactions. This is possibly because DPE2 uses newly formed maltose molecules as donor substrate for glucosyl transfer onto MOS. Therefore maltose could have been the major product in the initial reaction with DPE2 and Glc3 but was used efficiently by DPE2 to transfer glucose onto Glc3 producing glucose and Glc4.

Maltose by itself is a poor substrate for DPE2. Very small amounts of reaction products were formed and glucose was the most abundant. This indicates that substrate binding in only subsites -1 and +1 is insufficient for promotion of catalysis (in the absence of an external acceptor molecule like SHG). The production of glucose is likely due to the transfer of glucosyl residues from maltose onto newly formed MOS. The product of this reaction is approximately one mol of glucose per one mol of newly formed MOS.

A)

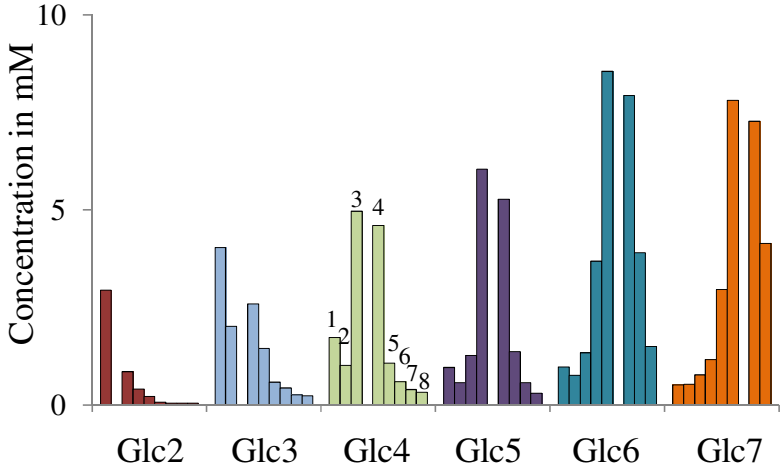

B)

substrate	-5 -4 -3 -2 -1 +1 +2 +3 +4 +5 +6	main products
Glc2	○ ∅	Glc1, Glc3
Glc3	○ ○ ∅	Glc2, Glc4
Glc4	○ ○ ○ ∅	Glc3, Glc5
Glc5	○ ○ ○ ○ ∅	Glc4, Glc6
Glc6	○ ○ ○ ○ ○ ∅	Glc5, Glc7
Glc7	○ ○ ○ ○ ○ ○ ∅	Glc6, Glc8

Figure 4.8 Product formation of DPE2 on 25 mM MOS

Experiment is the same as in Figure 4.7

A) Numbers above the bars correspond to the degree of polymerization of MOS products. Assays were performed in 100 mM HEPES (pH 7.0) at 37 °C with 1 µM enzyme. The amount of the MOS products was determined with standards. The amount of Glc8 and Glc9 were approximated from values obtained for Glc7 standards.

B) Dominant binding modes of substrates in the active site of DPE2. The numbering of substrate binding subsites is that of Davies (Davies *et al.,* 1997).The glycosidic linkage is broken between subsites -1 and +1. The main products that were released upon formation of the covalent intermediate are as indicted. Ø, reducing end of MOS. The arrows indicate the site of cleavage.

4.2.5 The hydrolysis activity of DPE2 and MalQ

Even small amounts of hydrolysis might have important implications for the biological role of DPE2 and MalQ. To discover whether maltose is hydrolysed by MalQ or DPE2 I analysed both enzymes for their hydrolytic capacity on maltose using two different approaches.

In the first approach I incubated DPE2 or MalQ with maltose in ^{18}O labelled water. The rationale for this experiment was that if hydrolysis occurred, the transfer of glucosyl residues onto a water molecule via the GH77 enzyme specific double displacement reaction should result in ^{18}O labelled glucose (Figure 4.9). In the case of a DPE2 catalysed reaction, the acid base catalyst glutamate-758 protonates the α-1,4 glycosidic oxygen in maltose while aspartate-563 simultaneously attacks C_1 of the non-reducing end glycosyl unit, forming a covalent bond. The glucose that formed the reducing end of maltose then leaves the active site. This allows the carboxylate glutamat-758 to deprotonate either the C4-hydroxyl group of an incoming acceptor glucan or (in case of hydrolysis) to deprotonate ^{18}O water. The latter would yield ^{18}O-labelled product. To detect ^{18}O glucose formation the reaction mixture was analysed with Hydrophilic Interaction Liquid Chromatography-Mass Spectrometry (HILIC-MS). The presence of a glucose peak with an additional molecular weight of 2 would identify a labelled glucose molecule that can only derive from hydrolysis of maltose (Figure 4.9, B).

In the second approach I analysed the amount of reducing ends in the reaction mixture. During disproportionation reactions, the number of glycosidic linkages is maintained. For every broken α -1,4- glycosidic linkage, a new one is formed. If hydrolysis takes place, the generation of glucose by transfer onto water would increase the total number of reducing ends in the freaction mixture. The increase in reducing values for the production of glucose by hydrolysis was determined by the 2,2′-bicinchoninate assay (BCA). The extent of Cu^{2+} reduction was monitored by spectrophotometric measurement of Cu^{+}/2,2′-bicinchoninate complexes.

To detect hydrolysis via ^{18}O labelling of the reaction product a solution of maltose dissolved in ^{18}O-labelled water was incubated with DPE2 or MalQ. As negative control I used boiled enzyme samples and bovine serum albumin (BSA). Yeast α-glucosiadase (YAG) served as positive control (which should yield 50% labelling and therefore 100% hydrolysis; see Figure 4.9). The analytes were detected as sodium adducts and the monitored masses for the unlabelled and labelled glucose fragments were 179 *m/z* and 181 *m/z* respectively.

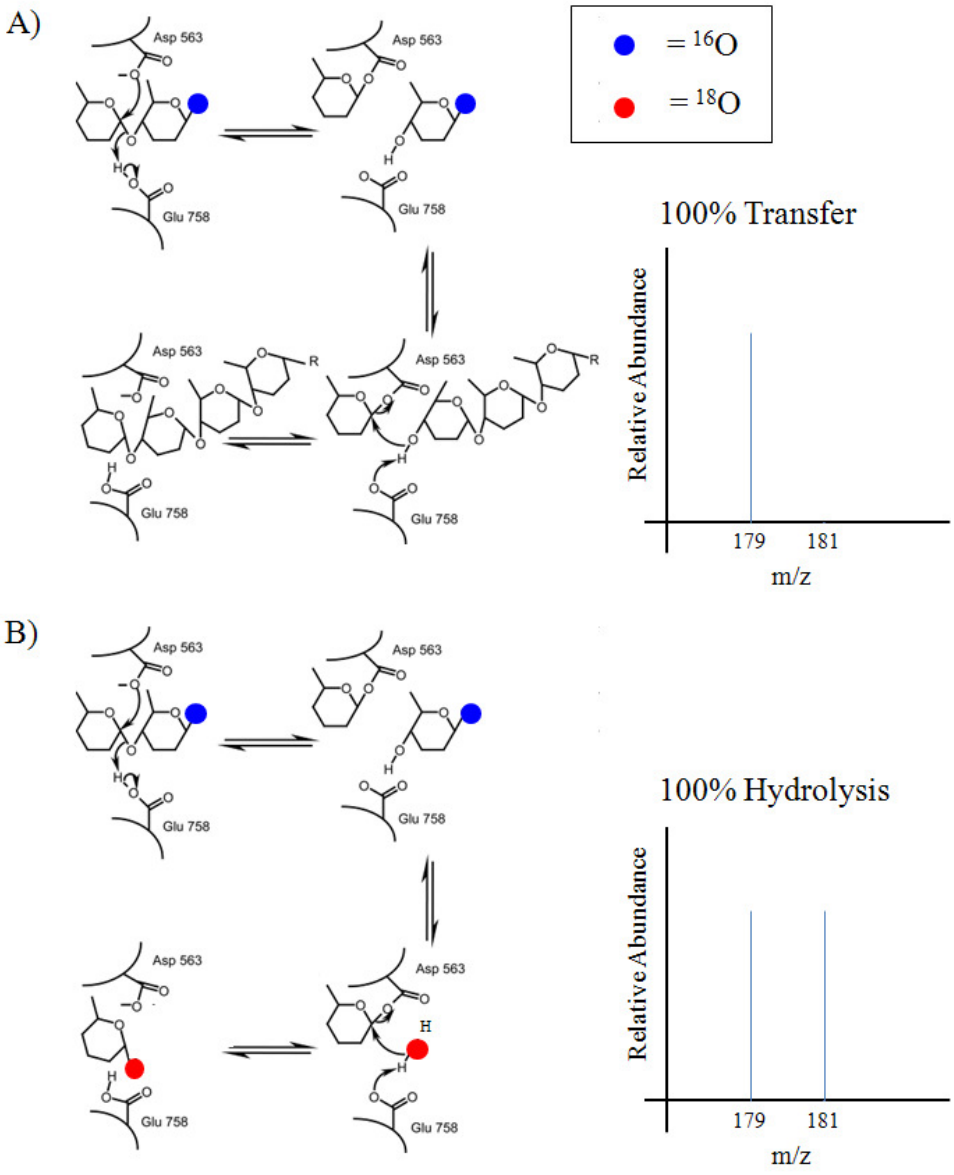

Figure 4.9 Double displacement reaction catalysed by DPE2 in ^{18}O water

A) Transfer of one glucosyl residue from maltose to an α-glucan polymer yielding one free glucose. The cartoon MS spectrum shows only occurrence of unlabelled glucose (179 m/z). This would indicate 100% transfer reaction has taken place.

B) Transfer of one glucosyl residue from maltose to water (H_2O^{18} in this case). A transfer onto O^{18} labelled water results in labelling of the second reaction product (hydrolysis). The cartoon MS spectrum shows occurrence of labelled glucose (181 m/z). 50% labelling would indicate 100% hydrolysis has taken place.

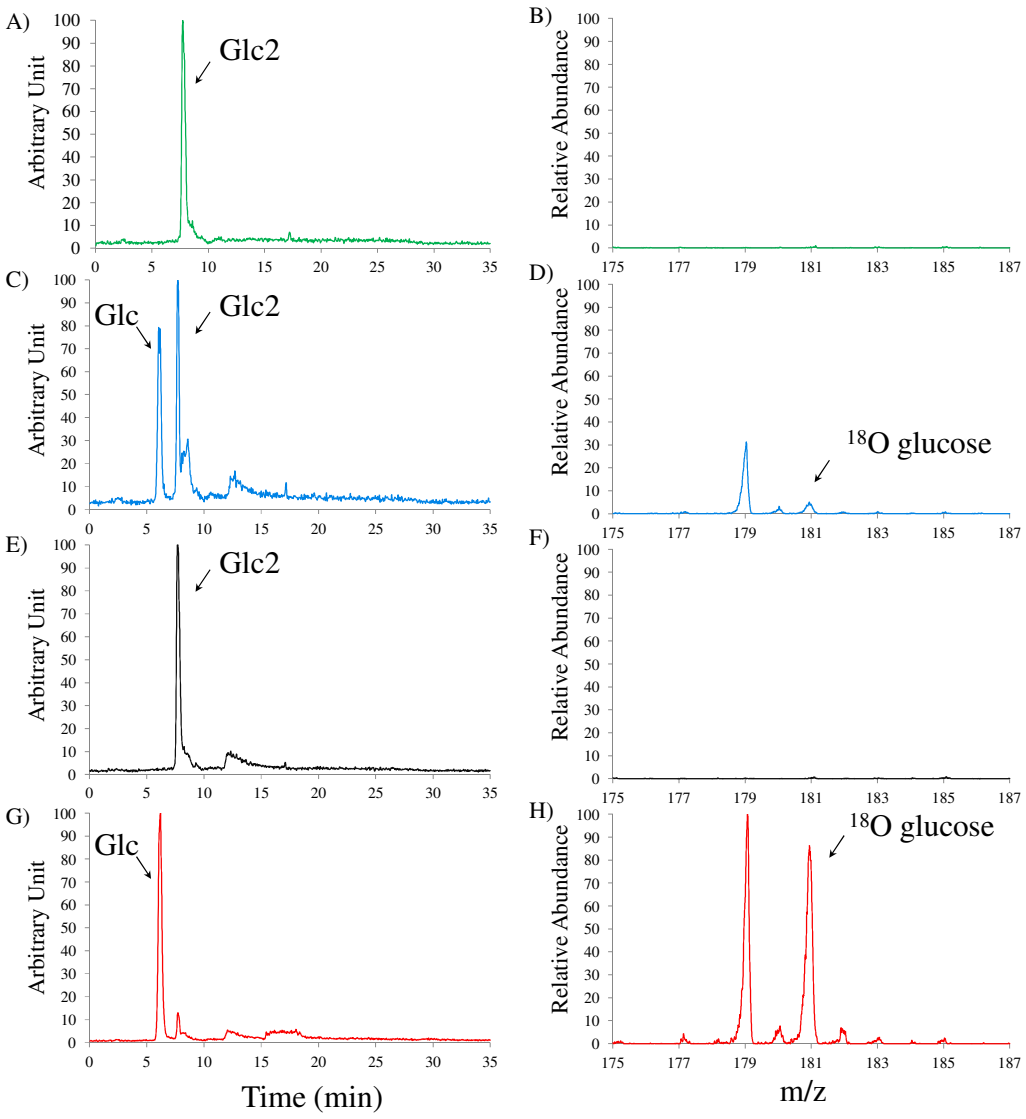

Figure 4.10 Hydrophilic Interaction Chromatography- Mass spectrometry (HILIC-MS) analysis of reaction mixtures

Maltose (5 mM) was incubated for 5 min at 37 °C with A,B) 1 µl DPE2 (1mg·ml^{-1}), C,D) 1 µl MalQ (1mg·ml^{-1}), E,F) 1 µl BSA (1mg·ml^{-1}) or G,H) 1 µl YAG (1mg·ml^{-1}) in ^{18}O water. The Reaction mixture was boiled and analysed with HILIC. Separation was on a 100×2mm Luna NH2 column (Phenomenex) run in HILIC mode, at 200µL·min^{-1} and 30ºC using a gradient of acetonitrile versus 20mM ammonium acetate pH 9.45 (90% to 10% over 15 min). Glc, glucose; Glc2, maltose. In A,C,E,G, the y-axis values are based on peak area of the starting material maltose. Detection of ^{18}O-labelled glucose was by electrospray MS. The ^{18}O labelled glucose product of the reaction is shown with arrow. In B,D,F,H, data are expressed relative to the unlabelled peak in H.

DPE2 did not produce any detectable glucose from maltose during the course of the reaction (15 min at 37°C). MalQ and YAG however produced glucose (Figure 4.10). In the MS spectra for the DPE2 reaction, no glucose was detected that carried a plus two mass/charge ratio (^{18}O-label). Only the MalQ and the YAG reaction mixture contained ^{18}O-labelled glucose. However, the MalQ reaction contained much less ^{18}O-labelled glucose than the YAG reaction (Figure 4.10).

To provide an independent check on the findings from the ^{18}O water experiment the reducing end assay was employed. DPE2 or MalQ were incubated with maltose and the increase of reducing ends in the reaction mixture was monitored over time. The largest increase in Cu^{2+} reduction (ΔOD_{540} nm) can be seen with YAG which served as positive control exhibiting 100% maltase activity. The reaction mixture containing MalQ and DPE2 only show a slight increase in ΔOD_{540} nm (Figure 4.11). The MalQ reaction contained slightly higher levels of reducing ends as indicated by the increase in ΔOD_{540} nm, than the DPE2 reaction. This finding agrees with the results from ^{18}O experiment, which also point to a slightly higher hydrolytic activity of MalQ than DPE2 on maltose.

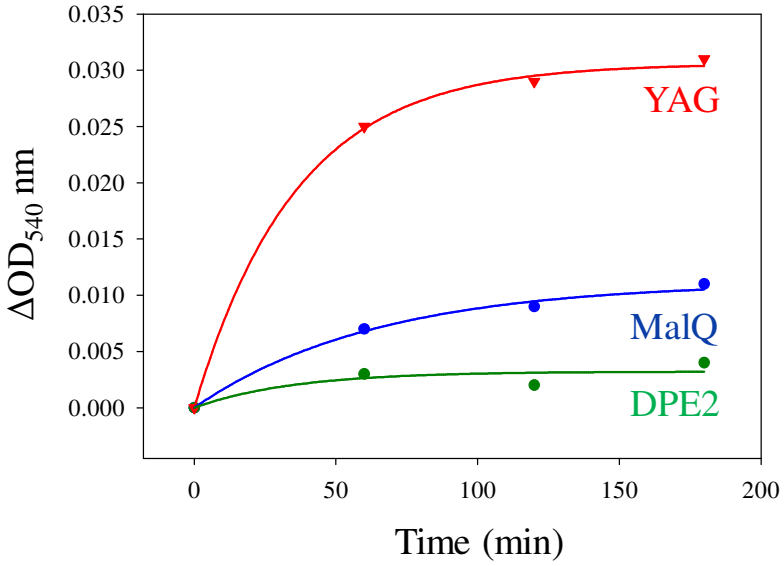

Figure 4.11 Reducing end assay for the hydrolytic activity of MalQ and DPE2 on maltose

Enzymes (10 µM) were incubated with 200 µM maltose at 37°C in 100 mM MOPS pH 7.0. At time points 35 µl of the reaction were quenched in 3,5-dinitrosalicylic acid (DNS-reagent), boiled for 12 min, cool in water bath and then analysed at OD_{540} nm. Values were substracted from a BSA control. Curves were fitted with global curve fit using sigma plot. YAG – yeast α-glucosiadase

4.3 Discussion

4.3.1 DPE2 and MalQ use the same monosaccharides as acceptor molecules

My study has shown that DPE2 and MalQ use the same monosaccharide acceptors (Table 4.1). The capacity to act on a broad range of monosaccharides is therefore not exclusive to DPE2. Interestingly, MalQ also catalysed the transfer of glucosyl units from glycogen onto xylose and mannose. These two carbohydrates are components of SHG. However, no SHG or SHG like carbohydrate material has been found in *E. coli* so far (personal communication Prof Steup, University of Potsdam, Germany).

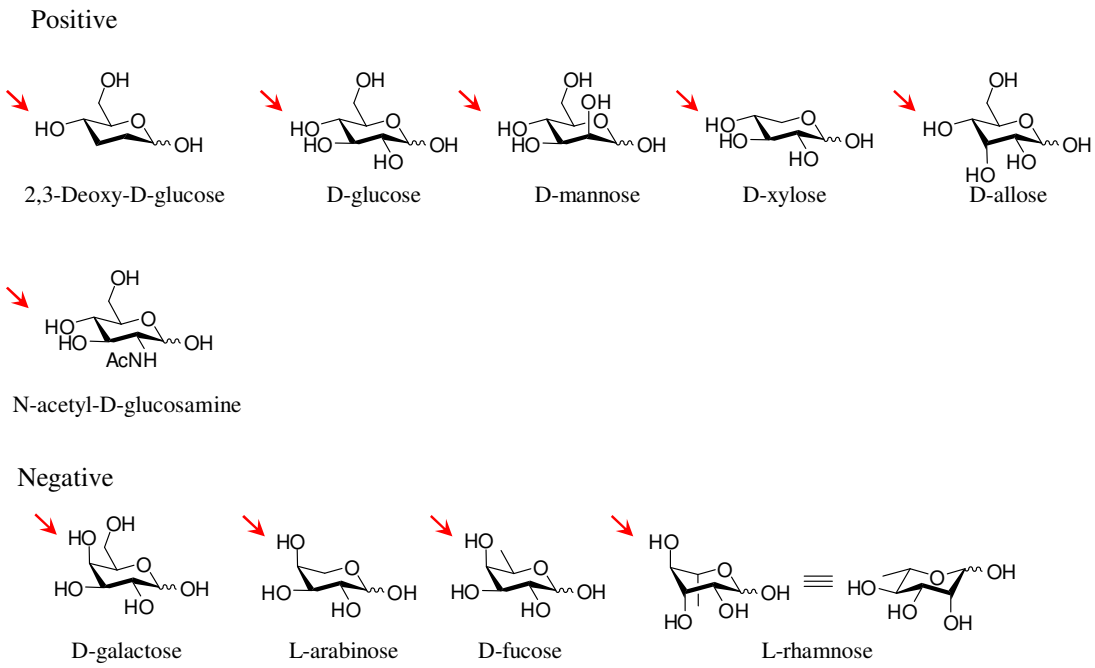

Figure 4.12 Overview of tested monosaccharides

Red arrows indicate positions that may determine whether the molecules are DPE2 and MalQ substrate as discussed in the text. `Positive` and `Negative` show monosaccharides from which disaccharides were formed or not formed respectively. The chemical structures were created with Chemdraw.

It is reasonable to assume that DPE2 and MalQ share some features of their active site that allow them to use the same monosaccharides as acceptor molecules. It appears that two features of a monosaccharide are important for an efficient acceptor function by both enzymes: first, a

pyranose ring having a configuration similar to that of glucose and second, the axial orientation of the hydroxyl group at C_4 (Figure 4.12). In contrast, both the presence and orientation of the hydroxyl group at C_2 and C_3 and the presence or absence of C_6 appear to be of little relevance. The crystal structure of the GH77 enzyme from *Thermus thermophillus*in complex with 4-deoxyglucose showed that a glutamate at position 256 established hydrogen bonds to O_5 and the O_6 hydroxyl group of the 4-deoxyglucose at subsite -1 (Barends *et al.,* 2007). Substitution of glutamate to glutamine in this position decreased disproportionation activity on small acceptor substrates (Kaper *et al.,* 2007). My data show that in DPE2 and MalQ the possible interaction of the corresponding glutamate (Q526 in DPE2 and Q411 in MalQ – Figure 3.7 in Chapter 3) with O_6 of monosaccharide acceptors might not be crucial, since xylose served as acceptor substrate in both cases. However, the O_4 hydroxyl group of xylose in this case presumably has to be oriented towards the glutamate (equatorial position) to make contact to the glutamate and allow for catalysis.

The capacity to use a broader range of monosaccharide acceptors is not unique to DPE2 and MalQ. StDPE1 from potato and the MalQ homologue from *Pyrococcus kodakaraensis* (KOD1) also used various acceptors (Peat et al. 1957; (Tachibana *et al.,* 2000). However, StDPE1 and KOD1 did not accept mannose and N-acetyl-D-glucosamine as substrate. This shows that MalQ and DPE2 might have a more relaxed substrate specificity than other GH77 enzymes. Nevertheless, only DPE2 was able to transfer glucose onto a broad range of polysaccharides when probed with carbohydrate arrays (Chapter 3). Therefore, the ability of DPE2, to act on monosaccharides that are components of SHG might not have implications in a possible enzymatic interaction with SHG.

Future studies could focus on the molecular recognition of substrates like maltose in DPE2 and MalQ. In earlier studies, a series of deoxy-maltoside compounds was used to assess substrate/transition state binding by a high pI barley α-glucosidase (Frandsen *et al.,* 2000). Depending on the site of hydrogen bond formation to the deoxy-maltoside in the high pI barley α-glucosidase active site, product formation was comparable with maltose or worse. The resulting data were used to calculate the binding energy contributed by the individual deoxy-maltoside OH-groups to transition-state stabilization. It would be possible to do similar experiments with fluoromaltose compounds that were recently produced with DPE2, glycogen (glucose donor) and fluoroglucose (acceptor substrate) (personel communication, Krit Tantarrat, laboratory of Prof Rob Field, John Innes Centre). Bound in the active site of the enzyme, the substituted fluoride would abolish any hydrogen bond formation that was previously established

with the respective hydroxyl group. In this case product formation and therefore rection kinetics would be slowed down. These data could then be used to calculate the binding energy contributed by the individual fluoromaltosides F-groups to transition-state stabilization.

4.3.2 DPE2 and MalQ have different abilities to act on maltose and MOS

My results show that DPE2 and MalQ have different capacities to act on maltose and MOS. I confirmed that DPE2 is strictly dependent on maltose as donor substrate for glucosyl transfer since maltose by itself is not a substrate. MalQ in contrast acts on individual MOS and even on pure maltose. Reaction with the latter however showed a biphasic reaction-curve when glucose release was monitored (Figure 4.4, A). It was suggested that the lag phase during the first minutes of the reaction could be due to a slow build up of potent donor molecules by MalQ (Boos and Shuman 1998, Palmer *et al.,* 1976). Hereby, an appropriate concentration of Glc3 as smallest donor substrate would have to be reached before the rate of glucose release continues exponentially. The assumption was that maltose acts as acceptor molecule rather than a donor for transfer of glucosyl units onto MOS by MalQ (Boos and Shuman 1998, Palmer *et al.,* 1976). This assumption however is based on results obtained with an excess of radioactively labelled glucose as acceptor molecule for MalQ transfer. The study by Palmer *et al.* (1976) did not take into account that MalQ activity is inhibited by glucose concentrations higher than 0.02 mM (Lengsfeld *et al.,* 2009). Therefore it cannot be excluded that MalQ can act on pure maltose by transferring glucose onto maltose producing Glc3 and longer MOS (Reaction 2).

My analysis of the affinity constants of MalQ with a range of MOS revealed very tight binding of MalQ to Glc3 and Glc4 (260 ± 20 nM and 410 ± 30 nM respectively)(Figure 4.5, B). Binding with this affinity could account for potential carry over of MOS material in catalytic concentrations during the MalQ purification process. However, thorough dialysis of purified MalQ preparations as described by Dippel and Boos (2005) and Lengsfeld et al. (2009) should eliminate any binding of Glc3 in catalytic concentrations. This should therefore eliminate action of MalQ on maltose if MalQ was not able to use maltose as glucose donor. Yet my data have shown that MalQ fully disproportionates maltose (Figure 4.7, B). Consequently, action of MalQ on maltose indeed could be autocatalytic as proposed by Wiesmeyer et al. 1960 and Dippel and Boos (2005).

The binding constants of DPE2 and MalQ for β-CD were very similar (0.26 mM for MalQ and 0.34 mM for DPE2). This was unexpected since β-CD is traditionally used as a starch mimic (Christiansen *et al.,* 2009b, Glaring *et al.,* 2011) and DPE2 was earlier shown to bind to starch

whereas MalQ did not (Chapter 3; Figure 3.14, B and C). There are two reasons for this discrepancy; first: β-CD is not an optimal mimic to study potential protein-starch interactions, second: β-CD binds to the active site of MalQ, rather than to a surface binding site.

Binding of small MOS like Glc4 to DPE2 was up to 10,000 times weaker than their binding to MalQ (Figure 4.5, B). This difference in binding of MOS between MalQ and DPE2 could reflect the different nature of the *in vivo* substrates of the two enzymes. The putative DPE2 substrate SHG is a pool of highly branched glycans and has no evident similarity to MOS other than its water solubility.

Binding of MOS to the chimeric protein CBM20-MalQ is dominated by MOS binding to the MalQ part of the chimeric protein. The CBM20 tandem that is fused to the N-terminus of MalQ does not enhance but rather negatively effects binding of MOS to MalQ. This result is consistent with a potential role of the CBM20 tandem in subside restriction rather then binding of MOS in DPE2 (this chapter and results from Sharkey *et al.* (2008).

My results about the enzymatic action on maltose and MOS binding to DPE2 and MalQ support earlier data from the literature about the biological role and enzymatic capacity of the two enzymes. It was shown that MalQ uses Glc3 as efficient substrate for disproportionation (Dippel and Boos 2005, Palmer *et al.,* 1976). The MAL gene cluster in *E. coli* is switched on by Glc3 (Ehrmann and Boos 1987). In the absence of MalQ, *malQ* strains appear constitutive (Decker *et al.,* 1993). My data show that MalQ is able to bind nM concentrations of Glc3. This might provide the basis for efficient disproportionation of Glc3 by MalQ in *E. coli*. As a consequence, endogenous induction of the MAL gene cluster is prevented.

MalQ binds MOS larger than DP4 with a much weaker affinity than Glc3 or Glc4 (approximately 20 times smaller K_d). This large drop in K_d value could be explained by the presence of MalP in *E. coli*. MalP only acts on MOS larger than DP4 (Dippel and Boos 2005). Therefore there seems to be no need for MalQ to tightly bind MOS with a ≥ DP5, as MalP metabolises sugars with ≥ DP5 to G1P. DPE2 in contrast showed an increase in binding efficiency with longer MOS until DP6. This corresponds with data from Fettke *et al.* (2006). They isolated SHG from *dpe2* knockout mutants ($_{dpe2}$SHG). The glucose content in $_{dpe2}$SHG is higher than in SHG derived from wt plants ($_{wt}$SHG). When $_{dpe2}$SHG and $_{wt}$ SHG were probed with DPE2 and maltose, $_{dpe2}$SHG was the better acceptor for glucosyl transfer. This was thought to be due to a built up of MOS on $_{dpe2}$SHG which presumably served as more efficient substrate

for DPE2 than the MOS free $_{wt}$SHG. Consequently the difference in the biological role of DPE2 and MalQ in maltose metabolism in plants and *E. coli* might be reflected by their different ability to process maltose and MOS.

4.3.3 DPE2 does not bind substrates beyond subsite -1

My results indicate that substrate binding in DPE2 is prevented beyond subsite -1. To show this I chose reaction conditions that allowed DPE2 to convert MOS by incubating DPE2 at high concentration (1 µM) for a longer period of time (12 hours at 37 °C) with various MOS (DPE2-DP7). This resulted in formation of two dominant products (Figure 4.8, A). These two products are likely corresponding to the MOS that were released from the active site after the covalent enzyme substrate reaction intermediate was formed and the glucan transfer had taken place (Figure 4.8, B)(Albenne *et al.,* 2002, Kaper *et al.,* 2007). Steichen *et al.* (2008) argued that the CBM20 tandem of DPE2 somehow restricts binding of substrates beyond subsite -1. My data support this by showing subsite restriction beyond subsite -1 in the full length DPE2 enzyme.

My data support the hypothesis that DPE2 uses maltose exclusively as donor substrate. Longer MOS cannot be used as substrate unless they are incubated with large quantities of the enzyme over a longer period of time or when maltose is added as donor substrate. This agrees with previous reports that showed no enzymatic activity of DPE2 on SHG or Glc4 as sole substrate (Fettke *et al.,* 2006a). MalQ in contrast disproportionates longer MOS as well as maltose (Figure 4.7 B)(Dippel and Boos 2005, Lengsfeld *et al.,* 2009). If DPE2 was able to disproportionate maltose, like MalQ, the pathway of maltose metabolism in plants would be modified. Longer MOS produced from maltose would become substrate for PHS2 and SHG as acceptor substrate would possibly be bypassed making SHG as acceptor substrate redundant. The restriction in the use of maltose as only glucose donor ensures that SHG is maintained as acceptor substrate for DPE2.

The underlying biological function of MalQ in *E. coli* seems very different to the one of DPE2 in Arabidopsis. MalQ can freely disproportionate MOS and does not have a substrate binding subsite beyond -1 as opposed to Arabidopsis. By disproportionating MOS of any length MalQ degrades as well as synthesizes Glc3, ensuring induction of the MAL gene cluster when the bacteria are grown on any MOS (Dippel *et al.,* 2005, Dippel and Boos 2005). The difference in the disproportionation activity of MalQ and DPE2 might therefore mirror the substantial

difference between the two organisms. Whereas bacteria have to constantly adjust to the present availability of carbon derived from glycogen and other sources outside the cell system, the plants have a regular pattern of carbon flow from the chloroplast to the cytosol.

4.3.4 MalQ and DPE2 hydrolyse maltose

Although low in comparison to YAG, the hydrolytic activity of DPE2 and MalQ detected with the ^{18}O labelling is surprising and contradictory to earlier results published in the literature about the hydrolytic activity of other members of the GH77 family and MalQ (Kuriki and Imanaka 1999, Leemhuis *et al.,* 2002, Palmer *et al.,* 1976). MalQ seemed to hydrolyse maltose to a greater extent than DPE2 in both assays. However, only very small amounts of maltose were metabolised to glucose by DPE2 (Figure 4.10, 4.11). The presence of an appropriate acceptor like SHG or glycogen in the reaction mixture might abolish any hydrolysis activity as DPE2 was shown to efficiently transfer glucose from maltose onto complex glucans and glycans like glycogen and SHG (Fettke *et al.,* 2006a, Steichen *et al.,* 2008). In contrast to DPE2, MalQ efficiently disproportionates maltose into glucose and MOS. This high disproportionation activity of MalQ with maltose might result in the occasional transfer of glucosyl residues onto water. This however might be overrepresented in the assays employed during this study as the accumulation of ^{18}O-labelled glucose or increase in reducing ends is non reversible. To compare the result from the ^{18}O labelling experiment, the more traditional reducing end assay was employed. The data show that both DPE2 and MalQ exhibit hydrolytic activity on maltose. However, this activity was just above the baseline value that was recorded when BSA was incubated with maltose. The disadvantage of the reducing end assay in this case is the strong reducing activity of maltose itself. All recorded data only represent a small increase in absorbance.

Nevertheless, both assays conclude that DPE2 and MalQ have relatively little hydrolytic activity. Combined with the previous experiments in this chapter, these data show that DPE2 and MalQ exhibit a slight hydrolytic activity *in vitro,* but in general can be considered to have a tight control over their hydrolysis to transfer ratios.

DPE2 and MalQ are typical members of the family GH77 with respect to active site residues (this study and Sharkey *et al* 2008) and sequence conservation (Chapter 3, Figure 3.7). Members of the family 77 of glycoside hydrolases were shown to have a high ratio (up to 5000:1) of

transglucosylation over hydrolysis (Fujii *et al.,* 2005, Kaper *et al.,* 2005, Kuriki and Imanaka 1999, Leemhuis *et al.,* 2002). There are three possible explanations that could account for the tight control of tranglucosylation over hydrolysis. First, in the hypothesis put forward by Davies *et al.* 2003 and Numao *et al.*2003, transglucosylases use a low energy $^4C_1$ chair conformation to stabilize their covalent intermediates. In glycosidases (that perform hydrolysis reactions) however, the covalent intermediate adopts a more strained conformation, such as a skew boat. Second, during formation of the enzyme bound intermediate, the acid/base catalyst glutamate was found to have moved out of a productive position in the covalent intermediate crystal structure of the GH77 enzyme of *Thermus thermophilus*. This precludes the glutamate from activating undesired acceptor molecules like water, thus protecting the intermediate from hydrolysis (Barends *et al.,* 2007). Third, Barends *et al.* (2007) proposed that the plane of the ester bond between the nucleophile aspartate and the sugar is perpendicular to the plane of the sugar ring. This could serve to make the C_1 atom less accessible to an incoming nucleophile like water, because of a possible steric hindrance and charge repulsion by the partially negative O_2. This three-way-stabilisation should also ensure that GH77 enzymes like DPE2 and MalQ do not hydrolyse their substrate but rather perform tranglucosylation reactions.

The biological implications for the presence of such tight enzymatic control might lie in the efficiency of maltose metabolism in Arabidopsis and *E. coli*. Hydrolysis of maltose would result in two glucose molecules that are substrate for hexokinase (glucokinase in bacteria). The conversion of glucose to G6P requires one molecule of ATP. Transfer of glucosyl residues from SHG via PHS2 in plants (or from MOS via MalP in *E. coli*) only requires free orthophosphate and therefore would save consumption of one ATP as the interconversion of G1P to G6P is energy free via phosphoglucomutase. Therefore, a tight control of transglucosylation over hydrolysis (reducing hydrolytic activity to a minimum) might give the organism an energetic advantage, that would not occur if hydrolytic activity was present. Under favourable growth conditions (minimum of biotic and abiotic stress factors), ATP availablitlity might not be a limiting factor, but it could be crucial in conditions of biotic or abiotic stress (Arora and Pedersen 1995, Jang and Sheen 1994).

The proposed *in vivo* acceptor of DPE2 mediated glucosyl transfer SHG is a very complex pool of molecules that was shown to contain at least 8 different sugars that are linked by at least 20 different glycosidic linkages (Fettke *et al.,* 2006a, Fettke *et al.,* 2009b). The synthesis of such glycans would require at least 20 different glycosyl transferases since these class of enzymes are very specific for the reaction catalysed (Henrissat and Davies 2000), and would also require the

synthesis of at least 8 different activated sugar donors. In light of this potentially high energy demanding process of producing and maintaining SHG, the energetic advantage by saving one molecule of ATP per processed molecule of maltose might not be important even under stressful environmental conditions. Only in the case of a stable pool of SHG molecules with a very long half life (several days/weeks) would there be any benefit of one extra ATP per maltose molecule since several µmol of maltose are being processed per plant per day. There is however no information about the production, origin or half life of SHG available.

In the next chapter I will further analyse and question the necessity and importance of SHG in maltose metabolism in *Arabidopsis thaliana*.

5 Expression of *E. coli* MalQ in *dpe2 Arabidopsis thaliana*

5.1 Introduction

In the previous two chapters I have addressed the unique structural and enzymatic features of DPE2 from *Arabidopsis thaliana* that are not present in MalQ from *E. coli*. Although both enzymes catalyse the metabolism of maltose to hexose phosphates in their respective organisms, they possess striking biochemical differences. However, all of these differences have only been identified *in vitro*. Their biological implications are not clear and demand analysis of maltose metabolism *in vivo*. In this chapter I will focus on the interchangeability of DPE2 from Arabidopsis and MalQ from *E. coli* by creating transgenic *dpe2* knockout lines of Arabidopsis that express MalQ from *E. coli*.

DPE2 is the key enzyme in maltose metabolism in plants. It represents the first committed step to metabolise the maltose derived from starch degradation to hexose phosphate (Chapter 1, Figure 1.3). Plants that lack DPE2 accumulate large amounts of maltose (up to 500 times higher maltose levels in *dpe2* knockout mutants than in wt plants) and exhibit a reduced growth phenotype (Chia *et al.,* 2004, Lu and Sharkey 2004). *E. coli* that lack the MalQ have a similar phenotype. These cells are Mal^- (not able to grow on maltose as sole carbon source) (Pugsley and Dubreuil 1988) and therefore accumulate large levels of maltose intracellularly when grown on complex media and grow more slowly than wt *E. coli* (Szmelcman *et al.,* 1976). Complemented *E. coli* strains that lack MalQ but express DPE2 from Arabidopsis regained the ability to grow on maltose as sole carbon source and did not accumulate maltose intracellularly. However, the complementation was not complete since the transgenic *E. coli* lines had very long cell sizes and a slower growth compared to the wt strain (Lu *et al.,* 2006b). These experiments indicate that the role of DPE2 in plants might be analogous to that of MalQ in bacteria but the exact molecular function of the two enzymes could be different.

My *in vitro* results from the previous two chapters and data from the literature indicate that MalQ and DPE2 process maltose differently *in vivo*. MalQ uses maltose as acceptor substrate for glucosyl transfer onto MOS and onto maltose itself. DPE2 in contrast uses maltose exclusively as donor substrate for glucosyl transfer onto SHG (and onto MOS *in vitro*). In addition, DPE2 possesses structural features that are not present in MalQ. The physiological function of the CBM20 tandem and the insertion of DPE2 is unknown and has not been examined previously.

Chapter 5 – Expression of *E. coli* MalQ in *dpe2* knockout mutants

To understand better the function of DPE2 *in vivo* and the importance of its complex domain architecture, I decided to introduce the relatively simple MalQ from *E. coli* into the Arabidopsis *dpe2* knockout mutant and observe the extent to which the mutant phenotype was complemented. Based on the results obtained from the previous two chapters I envisaged one of the following outcomes:

1. MalQ can complement the phenotype of the *dpe2* knockout mutants. It could act like DPE2 by transferring glucosyl residues from maltose onto SHG. The carbohydrate array experiment in Chapter 3 showed that MalQ does not act on any of the substrates that were used by DPE2 as glucosyl acceptors. However, MalQ can use the same monosaccharide acceptors as DPE2 and therefore may transfer glucosyl residues onto SHG at these potential sites.

2. MalQ fails to complement because it cannot use SHG or lacks other features of DPE2 essential for the conversion of maltose to hexose phosphates in the plant cytosol. If this is the case, valuable information about DPE function can be obtained by introducing MalQ-DPE2 chimeras (like CBM20-MalQ) into a *dpe2* knockout mutants to discover which features of DPE2 are required for normal maltose to hexose phosphate conversion in Arabidopsis.

3. MalQ can complement the phenotype of the *dpe2* knockout mutants by bypassing SHG. This could occur by direct disproportionation of maltose by MalQ. The products of this reaction would be glucose and MOS. Glucose can be converted to G6P via HXK and MOS could be used by PHS2 to produce G1P.

To achieve the aim of this chapter I did the following experiments:

- Stable transfer of *E. coli* MalQ into *Arabidopsis thaliana* lacking a functional DPE2
- Checking transgenic lines for expression of *E. coli* MalQ and lack of DPE2 via immunoblot analysis with anti-MalQ and anti-DPE2 antibodies
- Assaying MalQ and DPE2 activity in transgenic lines
- Analysing the starch, SHG, MOS and sugar content in the transgenic lines

5.2 Results

5.2.1 Transfer of *E. coli* MalQ into *Arabidopsis thaliana dpe2* knockout mutants

The gene sequence encoding MalQ from *E. coli* MC 4100 (Lu *et al.,* 2006b) was optimised for expression in *Arabidopsis thaliana* by Geneart (Appendix 3). Cis-acting sites (such as splice sites, poly(A) signals, TATA boxes etc), which may negatively influence expression, were eliminated wherever possible. Codon usage was adapted to the bias of *Arabidopsis thaliana* resulting in a CAI (codon adaptation index) value of 0.93 (1.00 = perfect; ≥ 0.9 = very good). The optimised gene should therefore allow high and stable expression rates in *Arabidopsis thaliana*. The optimised gene sequence was then cloned into the vector plasmid pEarleyGate 202. This added a 35S-promoter and a FLAG sequence tag to the N-terminus of the protein and contained a glufosinate resistance gene cassette (Earley *et al.,* 2006). The vector plasmid encoding the MalQ protein under control of the 35S promoter was then stably transferred into *dpe2-3 Arabidopsis thaliana* via Agrobacterium mediated transformation. The *dpe2-3* mutant has a T-DNA insertion in exon 7 of the DPE2 coding region that was shown to disrupt expression of a functional DPE2 protein (Chia *et al.,* 2004). The T_0 generation of plants was sprayed with glufosinate. Plants that survived the treatment were likely to express the *bar* gene that confers tolerance to glufosinate (Abdeen and Miki 2009). These plants were allowed to self-fertilise and taken to the T_3 generation. No further segregation was observed in any of the lines in the T_3 generation. All plants analysed in this chapter are therefore homozygous. As control, wt and *dpe2* Arabidopsis were transformed with an empty vector plasmid. To compare any impact on MalQ expression in *dpe2* knockout mutant I also stably transferred full length DPE2 and $DPE2_{\Delta CBM20}$ into the *dpe2-3* mutant. To prepare for the second outcome mentioned in the introduction to this chapter, I furthermore stably transferred CBM20-MalQ into *dpe2-3* Arabidopsis. All lines express the genes under control of the 35S promoter. Plants that lack DPE2 and are transformed with any pEarleyGate contruct will be called *dpe2* knockout line from now on (unless stated otherwise).

5.2.2 Presence of DPE2 and MalQ in transgenic *dpe2* lines

To detect the presence of MalQ and CBM20-MalQ in *dpe2* knockout lines transformed with the vector plasmid encoding MalQ and CBM20-MalQ I did immunoblot analysis on soluble protein extracts from whole rosettes that were grown for 28 days in 12-hour light/12-hour dark photoperiod. Proteins were separated via SDS-PAGE and blotted on nitrocellulose membranes.

Recombinant DPE2 and MalQ were used to raise antisera in rabbit (Appendix 4). The sera were enriched for anti-DPE2 and anti-MalQ antibodies respectively. This was done by the immobilisation of recombinant DPE2 and MalQ on resin beads via reductive amination and application of each antiserum to the respective resin bound protein. After several rounds of washing the resins, the eluted fraction with the highest anti-DPE2 or anti-MalQ antibody was used for all immunoblots described this chapter.

The anti-DPE2 antibody strongly recognised a band of about 100 kDa on immunoblots of crude extracts of wt rosettes (Figure 5.1, A – lane with extract from wt control line). This mass corresponds well with the predicted molecular mass of 110 kDa for DPE2, based on its primary amino acid sequence. Extracts of transgenic *dpe2* knockout lines expressing MalQ or CBM20-MalQ did not contain any DPE2 as shown by the lack of a similar band in lanes containing these extracts. The anti-MalQ antibody recognised a band of approximately 75 kDa in lanes containing soluble extracts from *dpe2* knockout lines expressing MalQ. This mass matches the predicted molecular weight of the MalQ protein (75 kDa) based on its primary amino acid sequence. The anti-MalQ antibody furthermore recognised a band of approximately 100 kDa in lanes containing extracts of *dpe2* knockout lines expressing the chimeric protein CBM20-MalQ. This corresponds with the predicted mass of CBM20-MalQ (105 kDa). This shows that MalQ and CBM20-MalQ were successfully produced in the transgenic lines.

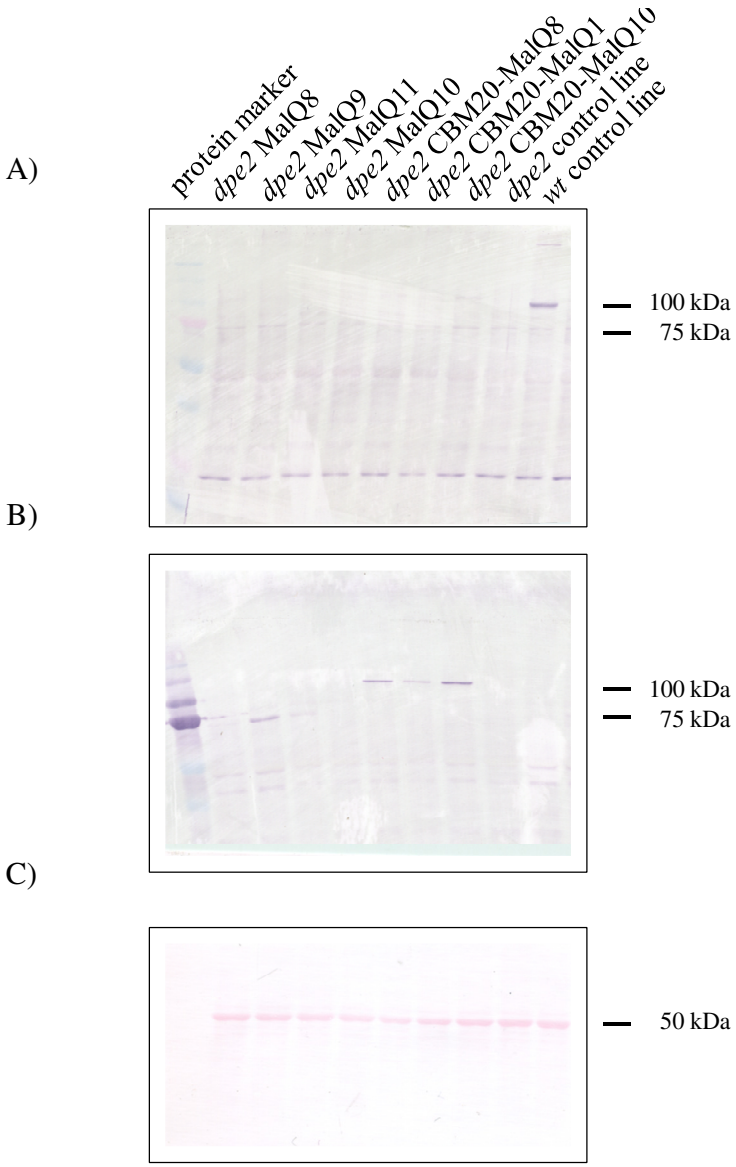

Figure 5.1 Immunoblot of selected transgenic lines probed with anti-MalQ and anti-DPE2 antibodies

A sample of 5 µg of soluble protein extract was subjected to SDS PAGE and blotted onto nitrocellulose membrane. Lanes 2-8 contain protein extracts from transgenic lines of *dpe2* that express MalQ or CBM20-MalQ. Lanes 9 and 10 contain protein extract from control lines. A) Nitrocellulose membrane probed with anti-DPE2 antibody B) Nitrocellulose membrane probed with anti-MalQ antibody C) loading control, nitrocellulose membrane was developed with Ponceau S solution (0.1% w/v). The band appearing at 50 kDa represents the large subunit of ribulose-1,5-bisphosphate carboxylase oxygenase (RuBisCO).

5.2.3 Starch content and fresh weight of transgenic *dpe2* lines

dpe2 knockout mutants possess a starch excess phenotype. Measuring the starch content at the end of night (EoN) gave a first indication about the carbon status of the transgenic plants. Wt Arabidopsis plants utilise their starch reserves efficiently and metabolise nearly all of the starch that was synthesised during the light period by the end of the subsequent night. The EoN starch content of a wt Arabidopsis plant is typically not more than 1 $mg \cdot g^{-1}$ fresh weight. Arabidopsis plants lacking DPE2 contain EoN starch of up to 15 $mg \cdot g^{-1}$ fresh weight (Figure 5.2, A). The MalQ expressing *dpe2* lines show a varying degree of starch excess at EoN. A few lines have EoN starch values close to the dpe2 control line. However, EoN starch levels in others are much lower and more like those of wt. Two of these lines are *dpe2* MalQ9 (EoN starch of 3 $mg \cdot g^{-1}$ fresh weight) and *dpe2* MalQ11 (EoN starch of 3.5 $mg \cdot g^{-1}$ fresh weight) (Figure 5.2, A). Four lines contain EoN starch comparable to the *dpe2* knockout line (*dpe2* MalQ,4,5,1 and 7; EoN starch values around 15 $mg \cdot g^{-1}$ fresh weight). Transgenic lines expressing CBM20-MalQ show a similar range of starch phenotype as the lines expressing MalQ with EoN starch levels ranging from 3.5 $mg \cdot g^{-1}$ fresh weight to 15 $mg \cdot g^{-1}$ fresh weight. Wt plants expressing MalQ and CBM20-MalQ have the same amount of EoN starch and fresh weight as wt control lines (around 1 $mg \cdot g^{-1}$ fresh weight). *dpe2* lines that express $DPE2_{\Delta CBM20}$ (dpe2 CD in Figure 5.2, A) have EoN starch levels comparable with the *dpe2* control line (EoN starch of 15 $mg \cdot g^{-1}$ fresh weight). Transgenic lines of *dpe2* that express the full length DPE2 protein have an EoN starch content comparable to the wt control line.

The growth of the transgenic lines seems to correlate with the amount of starch present at the EoN. Plants that contain less starch at the EoN have higher fresh weight than plants that exhibit a starch excess phenotype (Figure 5.2, B). Plants that lack DPE2 grow more slowly and are small when compared with wt plants. The wt control line (fresh weight of up to 150 mg per individual rosette) grows better than the *dpe2* control line (only 30 mg). The best growing MalQ expressing *dpe2* lines are those that had the lowest amount of EoN starch (*dpe2* MalQ9: 140 mg and *dpe2* MalQ11: 120 mg). Lines with EoN starch values of around 6-7 $mg \cdot g^{-1}$ fresh weight also only had a fresh weight of around 60-80 mg (*dpe2* MalQ12 or *dpe2* CBM20-MalQ1)

It was surprising to see that the simple bacterial GH77 enzyme MalQ can complement the growth and starch excess phenotype of an Arabidopsis plant that lacks DPE2. To further analyse this interesting result I will now focus on two transgenic lines (*dpe2* MalQ9 and *dpe2* MalQ11)

that lack DPE2 and express MalQ. These two lines exhibit a growth phenotype and EoN starch phenotype that is closest to the wt control line (Figure 5.3).

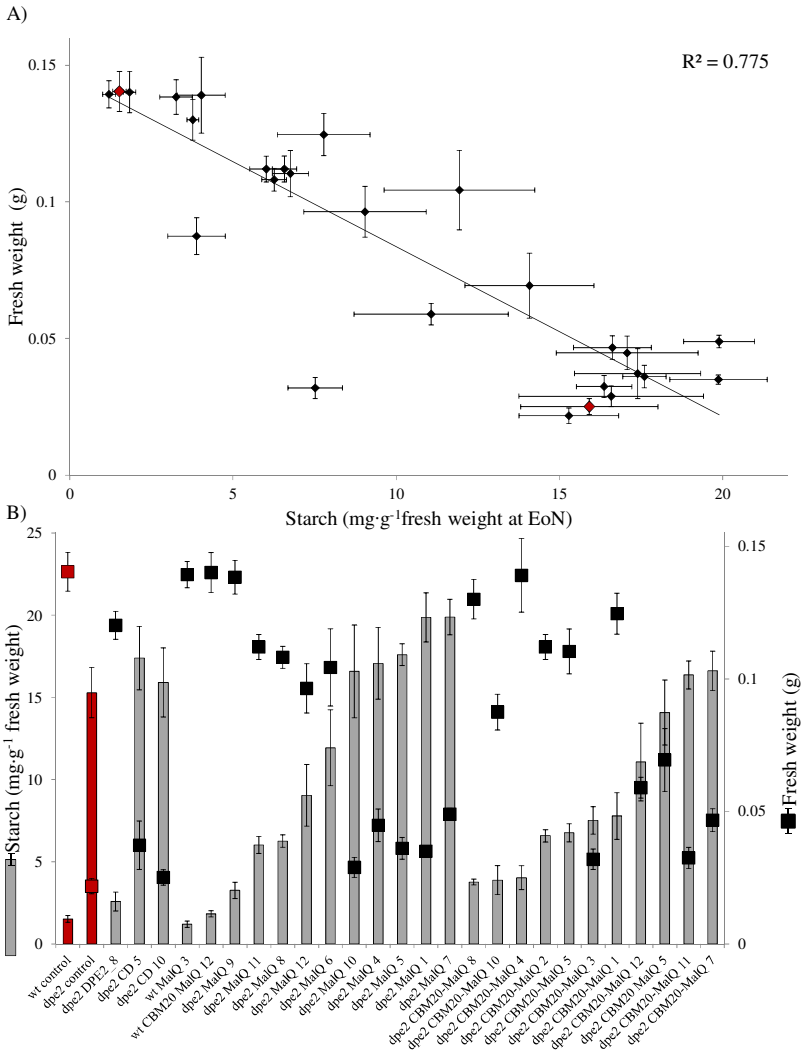

Figure 5.2 End of night starch and fresh weight of transgenic Arabidopsis lines

A) *dpe2* knockout mutants were stably transformed with vector plasmids designed to express MalQ, CBM20-MalQ, DPE2 and DPE2$_{\Delta CBM20}$ (dpe2 CD) under control of a 35S-promoter. *dpe2* knockout mutants and wt plants transformed with empty vector plasmids served as control lines (red data points and bars). Lines with a wt background expressing MalQ and CBM20-MalQ are designated wt MalQ and wt CBM20-MalQ. Plants were grown for 21 days in a 12-hour light/12-hour dark photoperiod. A) At the end of night, the starch content and weight was analysed (starch in mg·g^{-1} fresh weight). Values are means of measurements made on five plants. The error bars represent the standard error. B) The end of day starch content plotted against the fresh weight. The data points were basis for the linear regression.

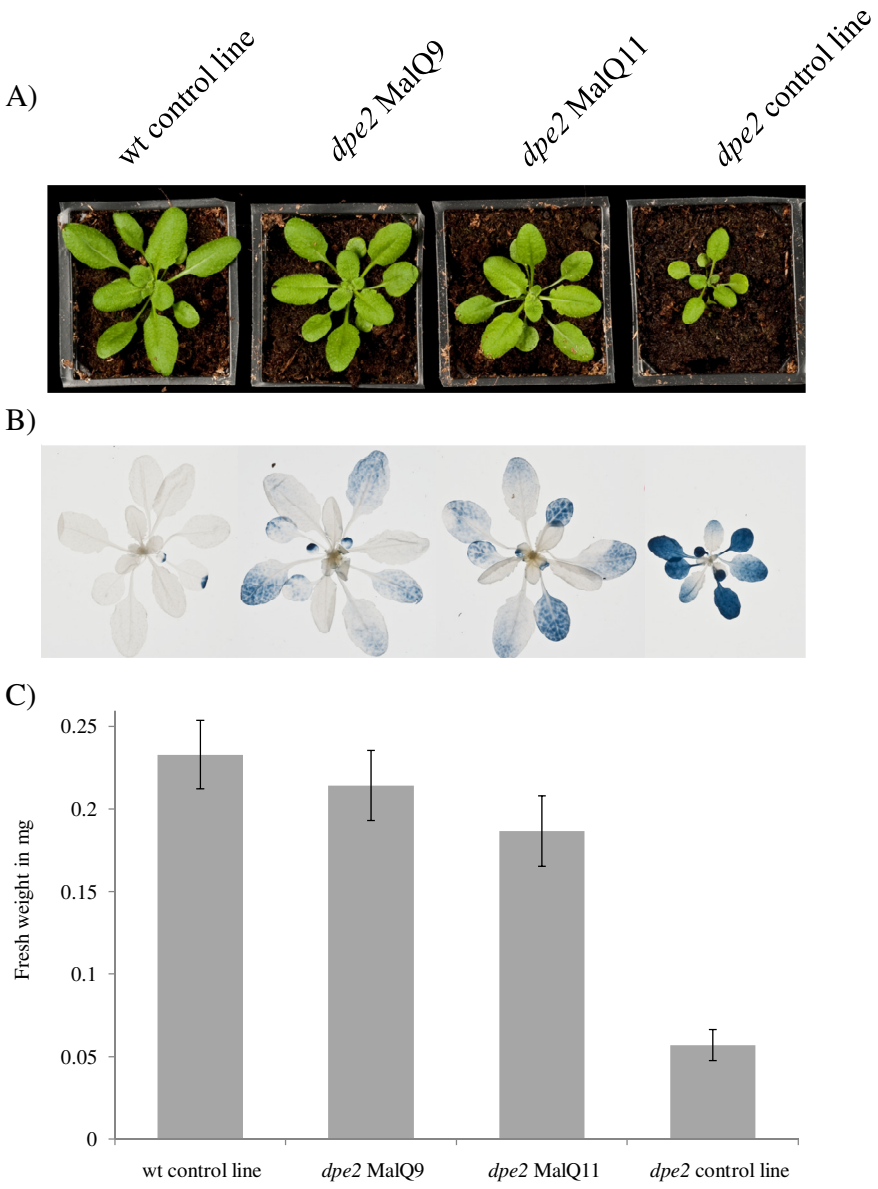

Figure 5.3 Starch excess and growth phenotype of transgenic Arabidopsis lines

A) Two independent lines of transgenic *dpe2* knockout mutants expressing MalQ and *dpe2* control and wt control were grown together in a 12-hour light/12-hour dark photoperiod. The photograph was taken 21 days after stratification. B) Plants harvested at the end of a 12 hour dark period (end of night) were harvested and decolourised with 80% ethanol solution and stained with iodine solution. The presence of starch is revealed by dark staining of the leaves. C) Plants that were grown for 26 days in a 12-hour light/12-hour dark photoperiod were weighed. Values are means of measurements made on ten plants.

5.2.4 Activity of DPE2 and MalQ in transgenic *dpe2* lines

To check for DPE2 and MalQ activity in *dpe2* MalQ11 and *dpe2* MalQ9 I performed native PAGE analysis. I homogenised whole rosettes in liquid N_2 until complete cell disruption was achieved. The resulting powder was suspended in buffer (Chapter 2, Section 2.6.3.2) and the soluble proteins of this extract were separated on native gels containing glycogen. Incubation of this gel with buffer containing maltose allows glucosyl transfer from maltose onto glycogen by DPE2. The product of this in-gel reaction is an insoluble form of hydrogel (Izawa *et al.,* 2009) that can be stained with iodine solution (Chia *et al.,* 2004). Therefore, any DPE2 activity will appear as a band when the glycogen containing native gel is stained with iodine after incubation with maltose (Fettke *et al.,* 2006a).

Only the soluble protein extract from the wt control line and the recombinant DPE2 protein preparation contained DPE2 activity (Figure 5.4, A). This activity is visible as a band on the very top of the separation gel. The very slow migration of DPE2 into the gel is probably due to very strong interaction of DPE2 with glycogen in the gel. No additional bands were visible in the lanes containing extracts from *dpe2* MalQ9 and *dpe2* MalQ11. There was also no band in the lane containing the recombinant MalQ protein. Nonetheless, immunoblots showed the presence of MalQ in these transgenic lines (Figure 5.5, B). I therefore searched for a different disproportionation substrate that can be used to check for MalQ activity in native gels.

My results in Chapter 4 showed that MOS are excellent substrates for MalQ. Long chain MOS (up to DP 20 as shown in Figure 4.7, B in Chapter 4) and glucose are the main products of disproportionation of MOS with MalQ. The rationale was that MalQ activity should be visible when the native gel containing the *dpe2* MalQ extracts is incubated with MOS as substrate. MalQ should disproportionate the MOS substrate, release glucose as well as MOS. During the reaction of MalQ with (for example) Glc7, any resulting glucose can potentially be used by MalQ as acceptor (Palmer *et al.,* 1976). However, glucose is likely to dissociate from the gel into the surrounding buffer medium. Glucose therefore cannot be used as acceptor by MalQ in the gel and thus disproportionation will probably result in long chain MOS molecules (Park *et al*. 2011) that could be visualised with iodine solution. DPE2, in contrast, is not able to directly act on MOS and therefore MalQ activity might be distinguishable from DPE2 activity using native PAGE.

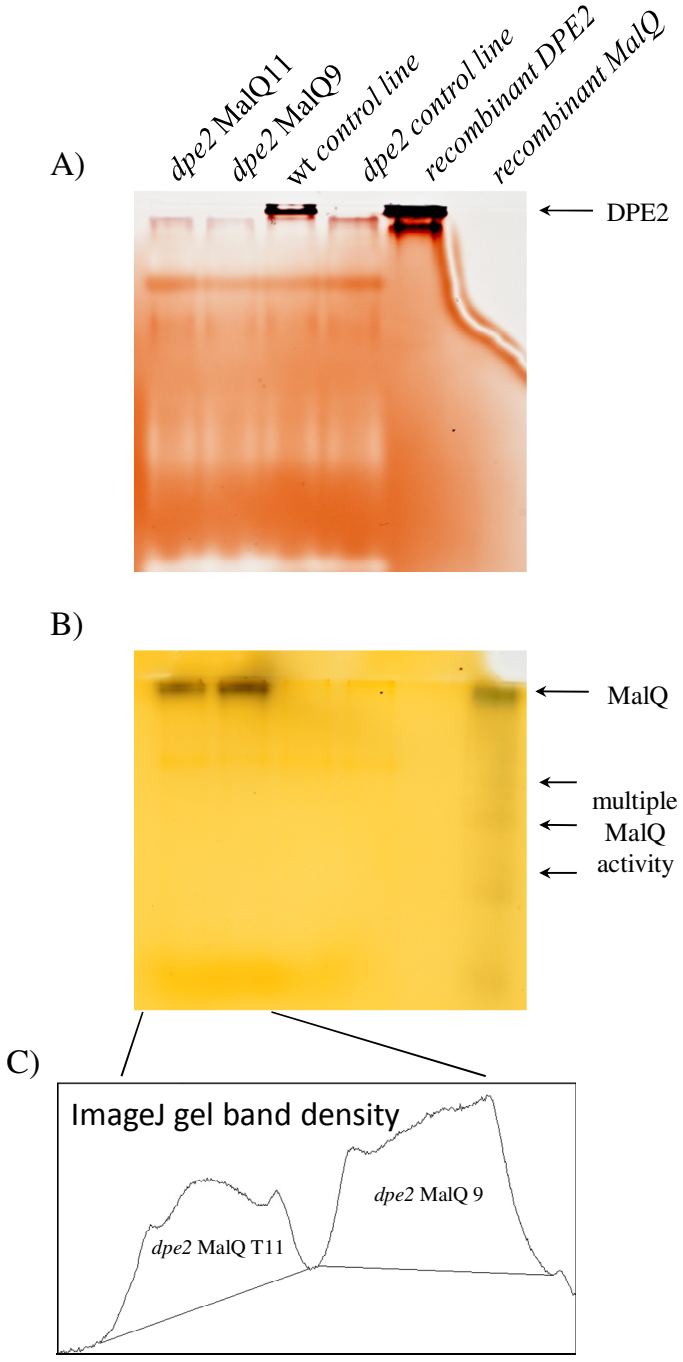

Figure 5.4 Native PAGE of MalQ and DPE2 activity in transgenic Arabidopsis lines

To detect A) DPE2 or B) MalQ activity, soluble proteins were extracted from whole rosettes and separated in polyacrylamide gels containing A) 1% (w/v) glycogen, B) no glycogen. The gels were incubated in the presence of A) 5 mM maltose or B) 5 mM Glc7 for 2 h at 37°C, and then stained with an iodine solution. C) Analysis of band intensities in lane one and two with imageJ. The graph shows the area under the curve.

Soluble protein extracts from whole rosettes of the control lines, *dpe2* MalQ9 and *dpe2* MalQ11 were separated on glycogen free native gels. After incubation with Glc7 the gel was stained with iodine. Lanes containing extracts of *dpe2* MalQ9 and *dpe2* MalQ11 had one band each. Neither of the two control lines nor the recombinant DPE2 lane showed any activity on Glc7 (Figure 5.4, B). This shows that disproportionation activity must be due to the presence of MalQ and that MalQ produced in *dpe2* knockout lines is active. Comparison of the intensity of the MalQ band shows that *dpe2* MalQ9 contains higher MalQ activity than *dpe2* MalQ11. This also correlates with the protein band intensity obtained from the immunoblot analysis of the two lines with anti-MalQ antibodies (Figure 5.5, B). The band appearing on immunoblots of *dpe2* MalQ9 extracts is more intense than the band in *dpe2* MalQ11 extracts. This again correlates with higher fresh weight and lower EoN starch levels of *dpe2* MalQ9 when compared to *dpe2* MalQ11 (Figure 5.3).

The lane containing recombinant MalQ shows multiple activity bands (Figure 5.4, B). The most prominent band does not fully migrate into the gel. The multiple bands might correspond to different oligomeric states of MalQ. Consistent with this idea, Palmer *et al.* (1976) reported the existence of interconvertible low-molecular-weight (apparent molecular weight 71 kDa) and high-molecular-weight (apparent molecular weight 370 kDa) forms of MalQ. Transgenic plants that expressed the malq gene only seem to contain the high-molecular-weight form of MalQ visible as a single band on the top of the gel.

Taken together, these results confirm that complementation of the slow growth and starch excess phenotype of the *dpe2* knockout lines is caused by expression of active MalQ.

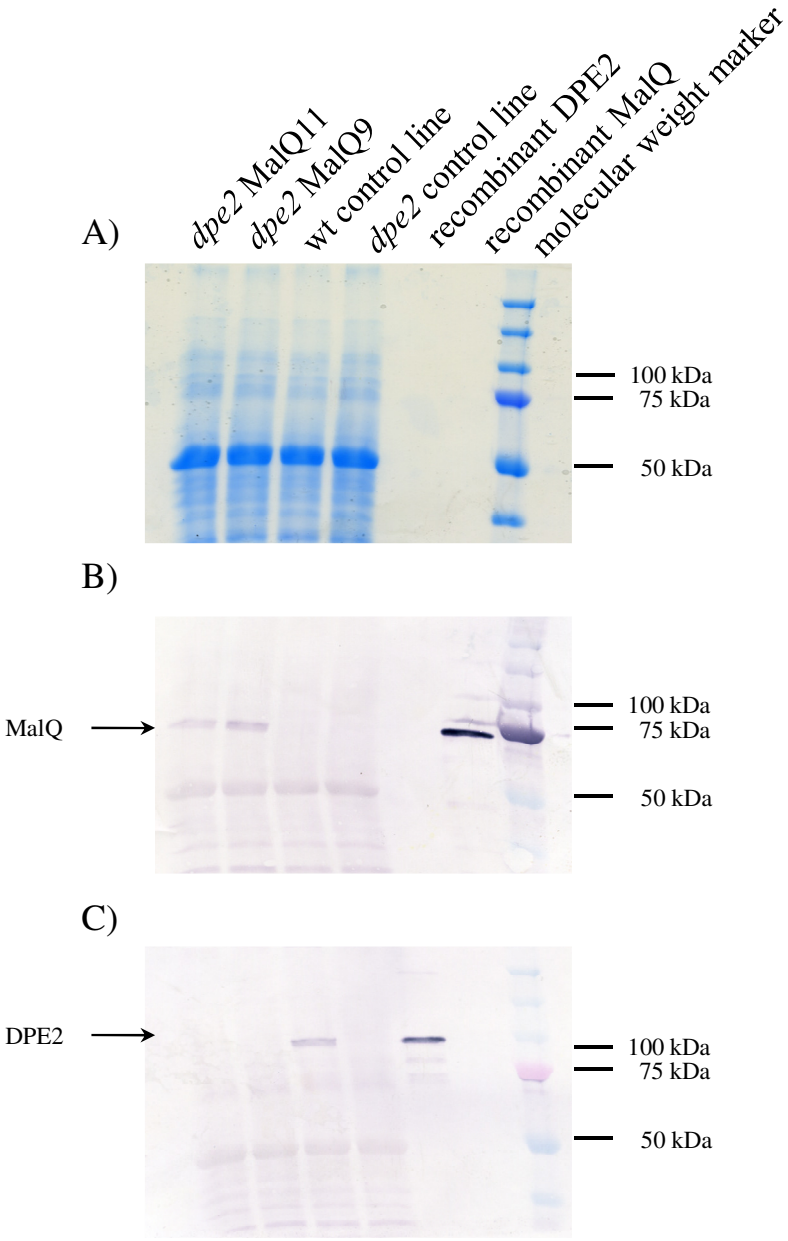

Figure 5.5 Immunoblot analysis of transgenic Arabidopsis lines

The plant material used is the same as in Figure 5.4. Soluble protein from whole rosettes (2.5 µg) from *dpe2* MalQ11 and *dpe2* MalQ9 (lane 1,2), wt control and *dpe2* control (lane 3,4) and purified recombinant DPE2 and MalQ (lane 5,6 – 0.01 µg) were separated by SDS-PAGE, blotted onto nitrocellulose membrane and probed with B) anti-MalQ antibody and C) anti-DPE2 antibody. Mass of molecular weight markers and mobility of DPE2 and MalQ are shown. A) SDS PAGE with soluble extracts stained with coomassie blue solution to show equal protein loading of each lane.

5.2.5 Analysis of carbohydrate content in transgenic *dpe2* lines

To provide more detailed information about the impact of the substitution of DPE2 with MalQ on plant carbohydrate metabolism, I determined the maltose, starch, MOS and hexose content of whole rosettes of the transgenic lines throughout a 24-h period.

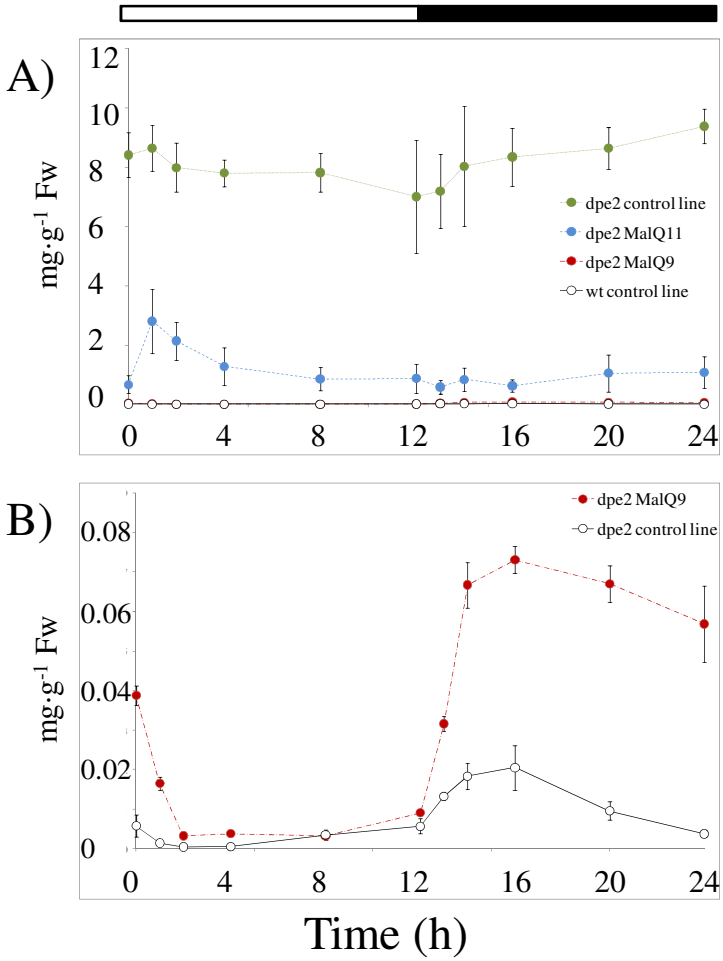

Figure 5.6 Maltose content of transgenic Arabidopsis lines

For each graph, measurements were made on plants grown over a single 24-h period. Values for maltose were obtained by HPAEC-PAD. Maltose standards of known concentrations served for calculations of the total maltose content. A) Open circles with black lines indicate wt control line. Closed circles represent *dpe2* control lines. The green line shows the *dpe2* control line. The blue and the red line show the *dpe2* MalQ11 and *dpe2* MalQ9 line respectively. Values are means of measurements made on 5five plants. The error bar shows the standard error values. B) Graph shown is a zoom out of values for the wt control and *dpe2* MalQ9 line shown in A.

Maltose levels in the *dpe2* control line were up to 500 times higher than those of the wt over a 24-h period (Figure 5.6). The data correspond with previous reports on maltose accumulation in *dpe2* knockout muants (Chia *et al.,* 2004, Lu and Sharkey 2004). The levels of maltose in *dpe2* MalQ11 were approximately 10 times lower than those in the *dpe2* control line but approximately 50 times higher than in the wt control line. Maltose levels in *dpe2* MalQ9 line were very similar to wt levels (Figure 5.6, B). The maltose concentration in this line was up to 4 times higher during the dark period than in the wt control line. During the first 2 hours of the light period however, levels of maltose in *dpe2* MalQ9 dropped to wt levels.

The starch accumulation of the wt control line was linear throughout the light period. Almost complete degradation of starch was achieved during the subsequent 12 h in the dark. The *dpe2* control line had much higher levels of starch at the EoN than the wt control line. The rate of accumulation during the light period and the rate of degradation in the dark were less than half of the wt rates. This diurnal pattern of starch content in wt and *dpe2* control lines is very similar to that reported previously (Chia *et al.,* 2004). Overall, *dpe2* MalQ11 and *dpe2* MalQ9 showed a rate of starch degradation and synthesis that was similar to that of the wt control line. Both MalQ expressing *dpe2* knockout lines had slightly elevated levels of starch at the end of day (EoD) relative to the wt control line. The rate of starch synthesis and degradation in *dpe2* MalQ9 was faster than that observed for *dpe2* MalQ11 (Figure 5.7, A).

The increase of maltose in the cytosol of plants lacking DPE2 causes an increase of maltose in the chloroplast as well (Lu *et al.,* 2006a). In *dpe2* knockout mutants, the decline in maltose during the light period is accompanied by elevated levels of longer MOS (Chia *et al.,* 2004). Since some of the maltose is in the chloroplast (Lu *et al.,* 2006a) it is reasonable to assume that maltose may be used by starch synthases as glycosyl acceptor for glucose transfer from ADPGlc during the day. The result of this would be an accumulation of MOS in the chloroplast.

Whereas MOS levels were barely detectable in the wt control line, they were much higher in the *dpe2* control lines (Figure 5.8, A and D). This was most pronounced during the light. The pattern of MOS build up in *dpe2* MalQ11 (Figure 5.8, C) was similar to that in the *dpe2* control line (Figure 5.8, B). MOS levels in *dpe2* MalQ11 increased during the light period and fell during the dark period. The total amount of MOS in *dpe2* MalQ11 was only 30% of that in the *dpe2* control line. The *dpe2* MalQ9 line had MOS levels that were similar to levels in the wt control line. The MOS levels were barely detectable during the light period and rose slightly during the dark period.

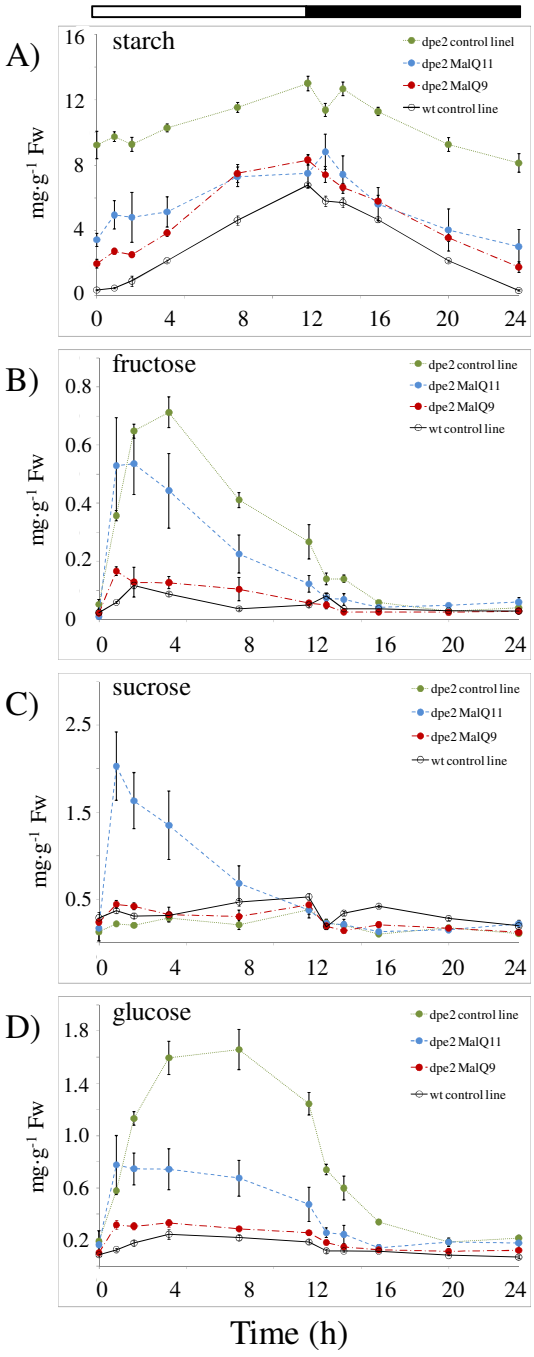

Figure 5.7 Starch and sugar content of transgenic Arabidopsis lines

For each graph, measurements were made on plants grown over a single 24-h period. Open circles with black lines indicate wt control line. Closed circles represent *dpe2* control lines. The green line shows the *dpe2* control line. The blue and the red line show the *dpe2* MalQ11 and *dpe2* MalQ9 line respectively. Values are means of measurements made on five plants. The error bars show the standard error values.

Hexoses, especially glucose, were more abundant in the *dpe2* control line than in the wt line during most of the 24-h period (Figure 5.7, D) (up to 10 times more glucose). The two MalQ expressing lines had less glucose and fructose than the *dpe2* control line. Sucrose levels were comparable in wt and *dpe2* control lines during the light period, but whereas the sucrose in wt showed a characteristic fall and recovery (Zeeman *et al.,* 1998a) at the start of the dark period, the level in the *dpe2* line fell and remained low throughout the dark period.

Sucrose levels in the two MalQ expressing *dpe2* knockout lines were very different. While sucrose levels in *dpe2* MalQ11 increased dramatically during the first hour of the light period, levels in *dpe2* MalQ9 were similar to wt and *dpe2* control lines. During the light period, sucrose levels in *dpe2* MalQ11 reduced slowly. Throughout the dark period, the levels of sucrose in *dpe2* MalQ9 and *dpe2* MalQ11 more resembled the sucrose levels of the *dpe2* control line (Figure 5.7, C).

Combined, the data show that MalQ is processing maltose efficiently. In the two transgenic lines, *dpe2* MalQ9 and *dpe2* MalQ11, MalQ seems to complement for the loss of DPE2. Metabolite levels in *dpe2* MalQ9 are very similar to wt levels.

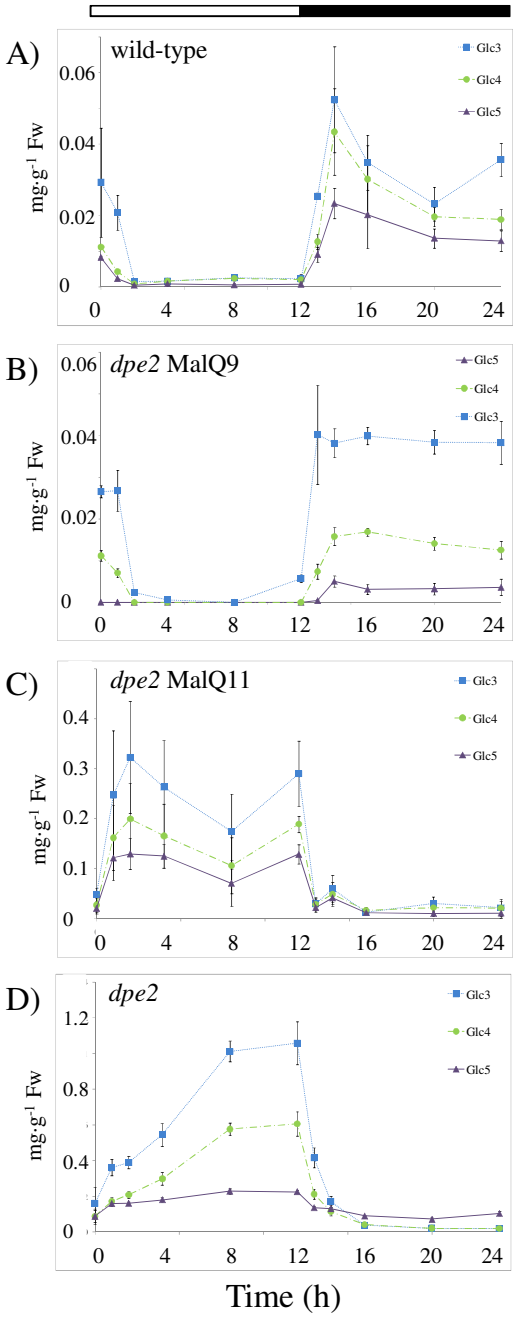

Figure 5.8 MOS content of transgenic Arabidopsis lines

For each graph, measurements were made on plants grown over a single 24-h period. Values are means of measurements made on five plants. The error bar shows the standard error values. Soluble sugar extracts of A) wt control line B) *dpe2* MalQ9 C) *dpe2* MalQ11 D) *dpe2* control line were analysed by HPAEC-PAD. Notice the difference on the y-axis. The closed square with the blue lining shows Glc3; the closed circle with the green lining shows Glc4; the closed triangle with the violet lining shows Glc5.

5.2.6 Analysis of phosphorylase activity and SHG composition in transgenic *dpe2* lines

The proposed *in vivo* substrate of DPE2 and PHS2 is SHG. The available *in vitro* evidence suggests that DPE2 transfers glucosyl residues from maltose onto SHG. PHS2 in turn transfers these glucosyl residues onto orthophosphate producing G1P (Fettke *et al.,* 2006a). The glucosyl content in SHG from plants that lack DPE2 ($_{dpe2}$SHG) however is elevated when compared to SHG from wt plants ($_{wt}$SHG) (Fettke *et al.,* 2006a). This seems contradictory to the role of DPE2 in the plant cytosol, as smaller amounts of glucose in $_{dpe2}$SHG should be expected if DPE2 is lacking. It was proposed that an altered carbon flux from starch to sucrose occurs in plants lacking DPE2 that is causing an increase of glucose in $_{dpe2}$ SHG (Kunz *et al.* 2011). The main route of flux from starch to sucrose in *dpe2* knockout mutants was suggested to be via glucose which is transported into the cytosol via glucose specific transporters (Fettke *et al.,* 2008, Weber *et al.,* 2000). In the cytosol glucose is converted to G6P and G1P via the combined action of HXK and cPGM (Chapter 1, Figure 1.3). In a *dpe2* knockout mutant, PHS2 possibly uses G1P made in this route as glycosyl donor to transfer glucose onto SHG and therefore increase the glucose content of SHG in *dpe2* knockout mutants (Fettke *et al.,* 2008). Indeed, elevated levels of phosphorylase activity have been observed in *dpe2* knockout mutants (Chia *et al.,* 2004, Fettke *et al.,* 2008). I therefore decided to analyse the SHG composition and phosphorylase activity in the *dpe2* MalQ lines.

To provide information about how the SHG composition is affected in *dpe2* lines expressing MalQ, SHG derived from these lines was analysed. The SHG extraction and analyses were done by collaborators at the University of Potsdam in Golm, Germany (Julia Smirnova in the laboratory of Prof Martin Steup and Joerg Fettke, University of Potsdam). The total SHG pool (SHG_T) was separated into SHG_L and SHG_S (Chapter 1, Figure 1.7) and the composition was analysed by acid hydrolysis and subsequent separation of the monosaccharides on HPAEC-PAD. Equal amounts of SHG were separated on HPAEC-PAD and the data were normalised to the galactose content, which remains constant in SHG derived from wt and *dpe2* control lines (Fettke *et al.,* 2006a). SHG_L derived from *dpe2* control lines had a remarkable increase in glucose, xylose and fucose when compared to SHG derived from the wt control line. This corresponds with earlier reports (Fettke *et al.,* 2006a). In contrast, the *dpe2* lines expressing MalQ do not contain elevated levels of glucose. In SHG_L derived from *dpe2* MalQ9 and *dpe2* MalQ11, the amount of glucose decreased to wt levels (Figure 5.9). Xylose and fucose levels also decreased in *dpe2* MalQ9 and *dpe2* MalQ11 when compared to the *dpe2* control line.

To analyse the phosphorylase activity in the transgenic lines, native PAGE was performed (Julia Smirnova in the laboratory of Prof Martin Steup and Joerg Fettke, University of Potsdam). The phosphorylase activity of wt and *dpe2* control lines was compared to different transgenic lines that lack DPE2 and express either; MalQ (*dpe2* MalQ9), the chimeric protein CBM20-MalQ (*dpe2* CBM20-MalQ8), the catalytic domain of DPE2 lacking the CBM20 tandem (*dpe2* $DPE2_{\Delta CBM20}$) or the full length DPE2 protein (*dpe2* DPE2_8).

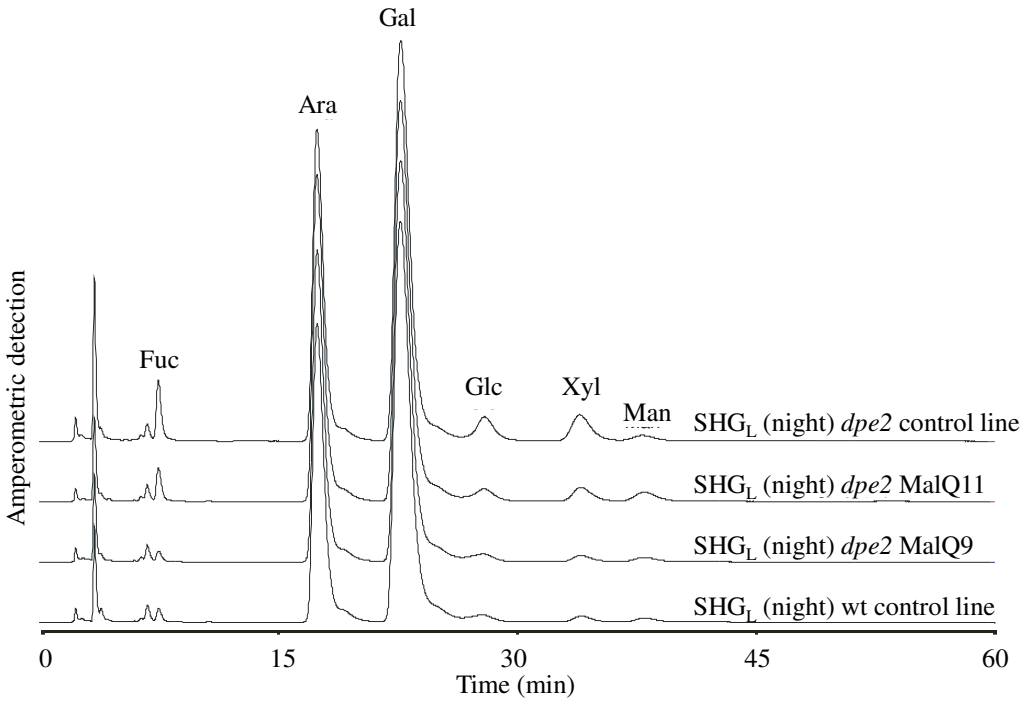

Figure 5.9 Monosaccharide patterns of SHG from leaves of transgenic Arabidopsis lines

SHG_T was isolated from leaves of *dpe2* control lines, wt control lines, *dpe2* MalQ9 and *dpe2* MalQ11 at EoN. Aliquots of the unhydrolysed SHG_T preparations were separated into SHG_S (A) and SHG_L (B) (the proposed substrate for DPE2). Following hydrolysis, 3 µg glucose equivalents SHG_L was analysed by HPAEC-PAD. All chromatograms were normalised to galactose. Fuc, fucose; Rha, rhamnose; Ara, arabinose; Gal, galactose; Glc, glucose; Xyl, xylose; Man, mannose. SHG analysis done by Julia Smirnova in the laboratory of Prof Martin Steup and Joerg Fettke, University of Potsdam.

The phosphorylase pattern (Figure 5.10) consists of three bands of activity all of which are strictly dependent upon G1P. Band one and two correspond to PHS2 activity whereas the most mobile band corresponds to PHS1 activity (Fettke *et al.,* 2005b, Schupp and Ziegler 2004). As expected from previous work, the activities of PHS1 and PHS2 were higher in the *dpe2* control line than in the wt control line. The expression of $DPE2_{\Delta CBM20}$ (which is the catalytic domain of DPE2 only) did not affect phosphorylase activities and PHS1 and PHS2 activities remained elevated. The expression of full length DPE2 in *dpe2* restored wt PHS1 and PHS2 activity. Expression of MalQ and the CBM20-MalQ reduced phosphorylase activities which remained similar to the wt control.

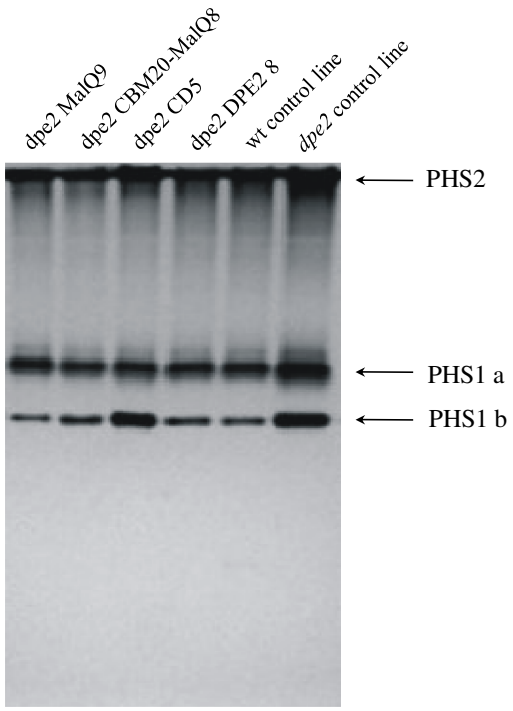

Figure 5.10 Native PAGE of phosphorylase activity in transgenic Arabidopsis lines

Soluble proteins (5 µg total protein per lane) were extracted from whole rosettes and separated in polyacrylamide gels containing 1% (w/v) glycogen. The gels were incubated with 5 mM G1P for 2 h at 37°C, then stained with an iodine solution Phosphorylase bands having high, medium, and low apparent affinity toward glycogen are marked with I, II (PHS2) and III (PHS1), respectively (Fettke *et al.,* 2005b). *dpe2* CD5, *dpe2* knockout line expressing the catalytic domain of DPE2 ($DPE2_{\Delta CBM20}$); *dpe2* DPE2_8, *dpe2* knockout line expressing the full length version of DPE. Native PAGE done by Julia Smirnova in the laboratory of Prof Martin Steup and Joerg Fettke, University of Potsdam.

5.3 Discussion

The metabolism of maltose in bacteria and plant leaves at night is very similar. The first committed step to metabolise maltose is catalysed by DPE2 in plants and by MalQ in bacteria. The two proteins belong to family 77 of glycoside hydrolases but exhibit different biochemical properties and structural features. DPE2 is a large protein (110 kDa) containing a starch binding CBM20 tandem at its N-terminus and a unique amino acid insertion in its active site containing GH77 domain. MalQ, in contrast, possesses a single domain architecture and does not contain any of the features that are present in DPE2. The previous two chapters have dealt with the biochemical properties of DPE2 and MalQ and what enzymatic features distinguish the two proteins. To investigate the importance of the unique and conserved multi domain architecture of DPE2 *in vivo* I decided to express the relatively simple bacterial MalQ from *E. coli* in Arabidopsis lacking DPE2.

5.3.1 *E. coli* MalQ can complement for the loss of DPE2 in Arabidopsis

My data show that the growth defect of Arabidopsis lacking DPE2 was complemented by MalQ. Plants that lack DPE2 and express MalQ (*dpe2* MalQ lines) form larger rosettes and have more fresh weight than the *dpe2* control line (Figure 5.3). This was a surprising finding, as the two proteins were shown to use different acceptor substrates to metabolise maltose (Decker et al., 1993; Fettke et al., 2006 and my work). Whereas DPE2 was proposed to use SHG *in vivo*, MalQ was shown to use linear MOS. As of yet, no MOS were found in the plant cytosol that could potentially serve MalQ as acceptor or donor substrate to metabolise maltose. However, maltose levels in *dpe2* MalQ9 and *dpe2* MalQ11 were well below levels found in the *dpe2* control line. Especially in *dpe2* MalQ9 the diurnal maltose levels very closely resembled those of the wt control line.

Data from the literature together with results obtained in Chapter 4 suggest that MalQ can directly act on maltose to produce MOS. This would enable MalQ produced in a *dpe2* knockout mutant to produce MOS from chloroplast derived maltose during the night. However, MOS levels in *dpe2* MalQ lines were lower than in the *dpe2* control line. The levels of MOS in *dpe2* MalQ9 were comparable to the wt control line, indicating a high turn over of any MOS derived from action of MalQ on maltose. Therefore, the metabolism of maltose in *dpe2* MalQ at night could occur in two steps. First, maltose and MOS are acceptor and donor substrate for MalQ in *dpe2* MalQ. Second, PHS2 could act on MOS to generate G1P. Earlier studies on PHS2 support

this hypothesis. It was shown that PHS2 can use MOS with a DP ≥ 4 as substrate for the production of G1P *in vitro* (Steup 1981). In combination MalQ and PHS2 could metabolise any MOS that are formed by the action of MalQ on maltose.

The carbohydrate analysis of *dpe2* MalQ suggests that the carbon flux from starch to hexose phosphates in the *dpe2* MalQ lines has normalised to wt levels. Levels of starch, glucose and fructose are more similar to those in wt control lines, rather than those in the *dpe2* control line. The effective metabolism of maltose prevents a built up of maltose in the cytosol (Lu *et al.,* 2006a) and therefore diminishes a potential built up of maltose and MOS in the chloroplast which in turn may be responsible for the inhibition of starch degradation observed in *dpe2* (Chia *et al.,* 2004). In summary, plants that express MalQ instead of DPE2 seem to be able to process maltose derived from starch efficiently and are therefore able to produce carbohydrates needed for plant metabolism and heterotrophic growth at night.

5.3.2 Complementation of *dpe2* Arabidopsis by MalQ generates a bypass to the conserved SHG pathway

As pointed out earlier, the elevated glucose content in $_{dpe2}$SHG is thought to be associated with the increase in phosphorylase activity in plants lacking DPE2 (Fettke *et al.,* 2008). The data presented in this chapter support this idea. The activity of PHS1 and PHS2 (Figure 5.10) as well as the glucose content of SHG_L in the *dpe2* control line are elevated (Figure 5.9). In the *dpe2* MalQ lines the glucose content of SHG dropped to wt levels. The PHS2 activities in these lines are also close to wt levels. This indicates that metabolism of maltose via MalQ in *dpe2* MalQ is adequate to allow for a normal rate of maltose turn over in the plant cytosol. Any disturbances to carbohydrate metabolism that were caused by the lack of DPE2 have been abolished with the introduction of MalQ.

But how does MalQ metabolise maltose in the plants? MalQ could act on SHG, using it as donor or acceptor of glucosyl or MOS transfer from or onto maltose. Preliminary and very recent data from collaborators suggest that MalQ is able to use SHG as substrate *in vitro* (Julia Smirnova in the laboratory of Prof Martin Steup and Joerg Fettke, University of Potsdam). However, the activity of MalQ on SHG *in vitro* was at least one order of magnitude lower than that of DPE2. In addition, my data from the carbohydrate array (Chapter 3, Figure 3.18) suggest MalQ only has a very low affinity (if any) for carbohydrates other than MOS. This would rule out the possibility that MalQ could use a MOS chain attached to SHG. However, 1,4 Glc linkages were not found in SHG so far (Fettke *et al.,* 2004, Fettke *et al.,* 2009a, Fettke *et al.,* 2005b). Alternatively, MalQ

could bypass the SHG pathway. Based on data from the previous two chapters, MalQ does not seem to require an external acceptor substrate since it can form MOS and glucose from pure maltose.

As first test of the credibility of this idea I examined whether recombinant MalQ, HXK and PHS2 could convert pure maltose to hexose phosphate *in vitro* (Figure 5.11). I found that MalQ alone converted maltose to glucose and MOS. In the presence of PHS2 and HXK and MalQ, maltose in coverted to G1P and G6P. If this pathway operated *in vivo* it would eliminate the need for SHG by creating a MOS utilisation system similar to that in bacteria like *E. coli* (Boos and Shuman 1998). PHS2 would be required in *dpe2* MalQ to act on long chain MOS (DP ≥ 4) produced by MalQ. HXK would use glucose produced by MalQ to produce G6P. Glucose, however, is a potent acceptor substrate for MOS transfer via MalQ itself (Palmer *et al.,* 1976). The constant removal of glucose by HXK would force MalQ to use long chain MOS as acceptors producing long chain MOS with DP ≥ 19 (Park *et al.* 2011). These long chain MOS would then be metabolised by PHS2. Without the action of PHS2, the *dpe2* MalQ plant would probably accumulate large amounts of long chain MOS. To test whether or not this is the case, *dpe2* MalQ lines were crossed into *phs2* knockout mutants. The selection and analysis of these lines is in progress. If MalQ indeed bypasses the conserved SHG pathway as I suggest here, the *dpe2/phs2* double knockout mutants expressing MalQ could potentially accumulate long MOS that can be visualised by HPAEC-PAD.

The identification of MOS potentially generated via MalQ in a *dpe2/phs2* MalQ plant could be further complicated by the presence of amylase activity. The plant genome encodes three α-amylases (AMY) and nine β-amylases (BAM) (Fulton *et al.,* 2008). AMY3 and AMY2 are localised in the chloroplast (Streb *et al.* (2008) and personal communication with Dr. Karla Simkova in the lab of Prof Samuel, C. Zeeman at ETH Zuerich, Switzerland) and AMY1 outside the cell in the apoplastic space (Doyle *et al.,* 2007). Most β-amylases (BAM) are either localised in the chloroplast (BAM1,2,3,4,6 and 9) (Fulton et al., (2008)and personal communication with Dr. Karla Simkova in the lab of Prof Samuel, C. Zeeman at ETH Zuerich, Switzerland) or in the nucleus (BAM7 and BAM8) (Reinholdt *et al*. 2011). Only BAM5 could not be identified in photosynthetically active mesophyll cells of the plant leaves. Little is known about the physiological role of BAM5. Up to 80% of total β-amylase activity in Arabidopsis was attributed to this enzyme (Lin *et al.,* 1988b). However, earlier reports suggest BAM5 is localised in the phloem (Wang *et al.,* 1995). It is therefore not likely that MOS generated by MalQ could be metabolised by amylolytic enzymes in the cytosol.

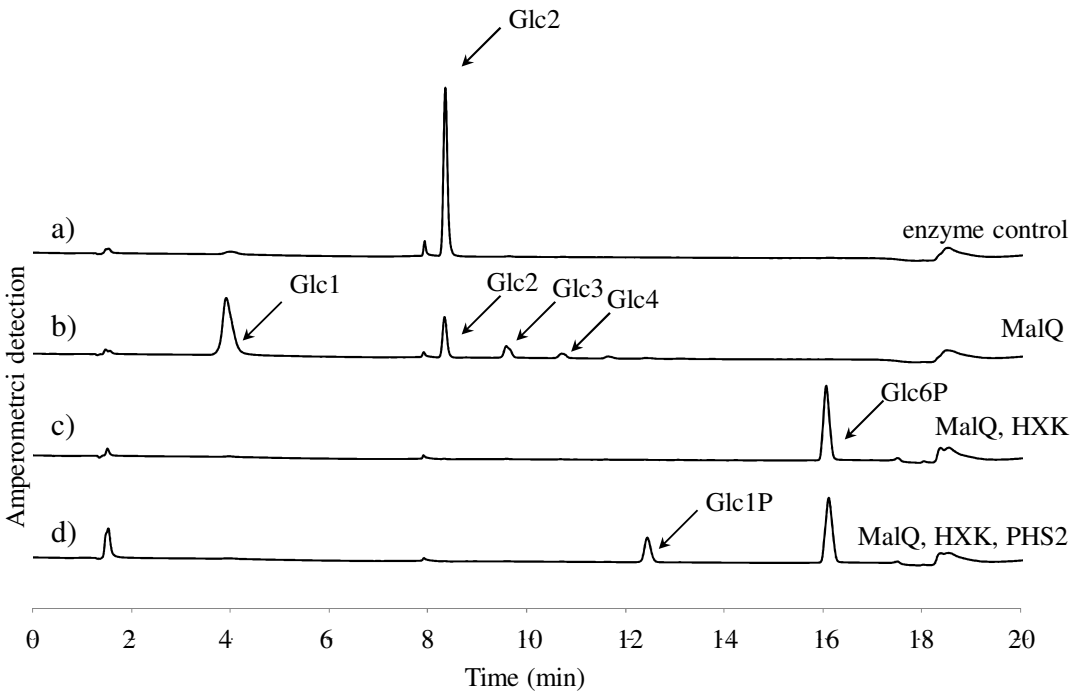

Figure 5.11 *In vitro* analysis of the action of MalQ, HXK and PHS2 on pure maltose

In a final volume of 100 µl, maltose (10 mM) was incubated for 30 min at 37°C with 0.1 µg of a) BSA b) MalQ c) MalQ and HXK (1.5 U) or d) MalQ, HXK and PHS2. Following incubation, the reaction mixtures were passed through a 10 kDa filter and the resulting filtrates were analysed by HPAEC-PAD.

Another group of enzymes that is capable of hydrolysing MOS are α-glucosidases. The Arabidopsis genome encodes five enzymes classified as α-glucosidases, at least some of which may be capable of hydrolyzing MOS to produce glucose. None of these, however, is predicted with confidence to be cytosolic. Nevertheless, analysing the glycosidic and amylolytic activity in extracts of *dpe2* MalQ lines could discover whether there may be any interfering enzyme activities in the cytosol.

5.3.3 The physiological importance of the modular domain arrangement in DPE2 for maltose metabolism

The complementation of *dpe2* knockout mutants with the simple bacterial MalQ was surprising. Neither the CBM20 tandem, nor the unique amino acid insertion of DPE2 seem to be required to effectively metabolise maltose in the plant since MalQ lacks all of these features. The two transgenic lines on which most of the work in this chapter was focussed (*dpe2* MalQ9 and *dpe2* MalQ11) grew much better than the *dpe2* control line. However, none of the lines that lack DPE2 and express MalQ grew as fast as the wt control line (Figure 5.2, A). This could be caused be a number of reasons.

Insufficient *dpe2* MalQ lines:

During this study, 12 independent lines of plants lacking DPE2 and expressing MalQ were initially chosen for starch and fresh weight analysis based on their ability to survive treatment with glufosinate (plants expressing MalQ contain a glufosinate resistance gene cassette). Most of the further work focussed on two lines, *dpe2* MalQ9 and *dpe2* MalQ11. These lines represented plants with the strongest growth amongst the transgenic lines. The subtle difference in growth between *dpe2* MalQ9 and the wt control line could be merely due to insufficient expression of MalQ in the plant. The gene encoding for MalQ has been optimised for expression in plants. Nevertheless, the expression of MalQ could still be limited due to poor codon bias or incorporation of the gene in an unfavourable region in the plant genome. Expanding the selection of *dpe2* lines expressing MalQ and screening these lines for the highest MalQ activity could yield lines that grow as well as the wt control line.

Sugar signalling:

There is ample evidence that mechanisms exist that sense and respond to sugar levels (Rolland et al., 2006). For instance, hexokinase1 (HXK1) has been shown to act as a glucose sensor in addition to metabolising glucose (Moore *et al*., 2003; Cho *et al.,* 2006). The Arabidopsis plants deficient in HXK1 (glucose insensitive 2 [*gin2*]) exhibits reduced vegetative growth. In a similar fashion a slight elevation of maltose might be sufficient to signal the plant an imbalance in carbon flux from starch. Maltose could act as a signalling molecule that provides a measure of the carbon flux at a specific time point. One potential candidate for maltose sensing in the cytosol could be the unique bifunctional enzyme fructose-6-phosphate,2-kinase; fructose-2,6-bisphosphatase (F2KP) (Nielsen *et al.,* 2004). This enzyme synthesises and hydrolyses fructose-

2,6-bisphosphate (Fru-2,6-P2), a central signalling molecule in primary carbohydrate metabolism in all eukaryotes. In plants, Fru-2,6-P2 inhibits fructose-1,6-bisphosphatase (F-1,6-BP), which catalyses the first essentially irreversible step of sucrose synthesis. Amongst all F2KP occurring in nature, the plant enzyme is the only representative that contains a long N-terminal extension to its catalytic domain. This extension harbours a CBM20 module (similar to the CBM20 tandem in DPE2) (Nielsen *et al.,* 2004). CBM20 modules have been shown previously to bind maltose on two different surface sites (Christiansen *et al.,* 2009b). Binding of maltose to F2KP could amend enzyme activity towards Fru-2,6-P2 degradation. The levels of Fru-2,6-P2 and hence the activation state of F-1,6-BP could thus be sensitive to the levels of maltose in the cytosol and therefore slow down sucrose synthesis via F6P. During the dark period, the sucrose levels in *dpe2* MalQ indeed are low and comparable to the *dpe2* control line (Figure 5.7, C). The small elevation of maltose during the dark period in *dpe2* MalQ9 could thus be sufficient to slow down plant growth.

A further mechanism for possible maltose sensing pathways involving β-amylases will be dicussed in Chapter 6.

Lack of CBM20 tandem and amino acid insertion:

The so called archaeplastida represent a major group of eukaryotes, comprising the land plants, green algae, red algae and the glaucophytes. Starch as storage polysaccharide (and consequently maltose metabolism) is present in all three archaeplastida lineages. DPE2 is localised in the cytosol of all archaeplastida. It is furthermore present in plasmodial slime molds and a few protist parasites like *Chlamydia* (Steichen *et al.,* 2008). The presence of a single *DPE2* gene encoding DPE2 in the genomes of this evolutionary diverse group of organisms points to an importance of the domain architecture of DPE2. MalQ does not possess any of the features found in DPE2, representing an archetypical GH77 enzyme in maltose metabolism. The subtle reduction in growth of plants lacking DPE2 and expressing MalQ suggest that certain features of DPE2 (e.g. CBM20 tandem, coiled coild domain, amino acid insertion) might be required for optimal wt like growth. If this is the case, differences in growth of wt and spe MalQ plants would be seen in other photoperiods. In an initial experiment, growth at 16-hour light/8-hour dark and 8-hour light/16-hour dark did not substantially disadvantage *dpe2* MalQ plants relative to wt plants (Figure 5.12). However, it remains possible that other environmental conditions will reveal a specific advantage of DPE2 over MalQ for plant growth. A few of these conditions will be further discussed in Chapter 6.

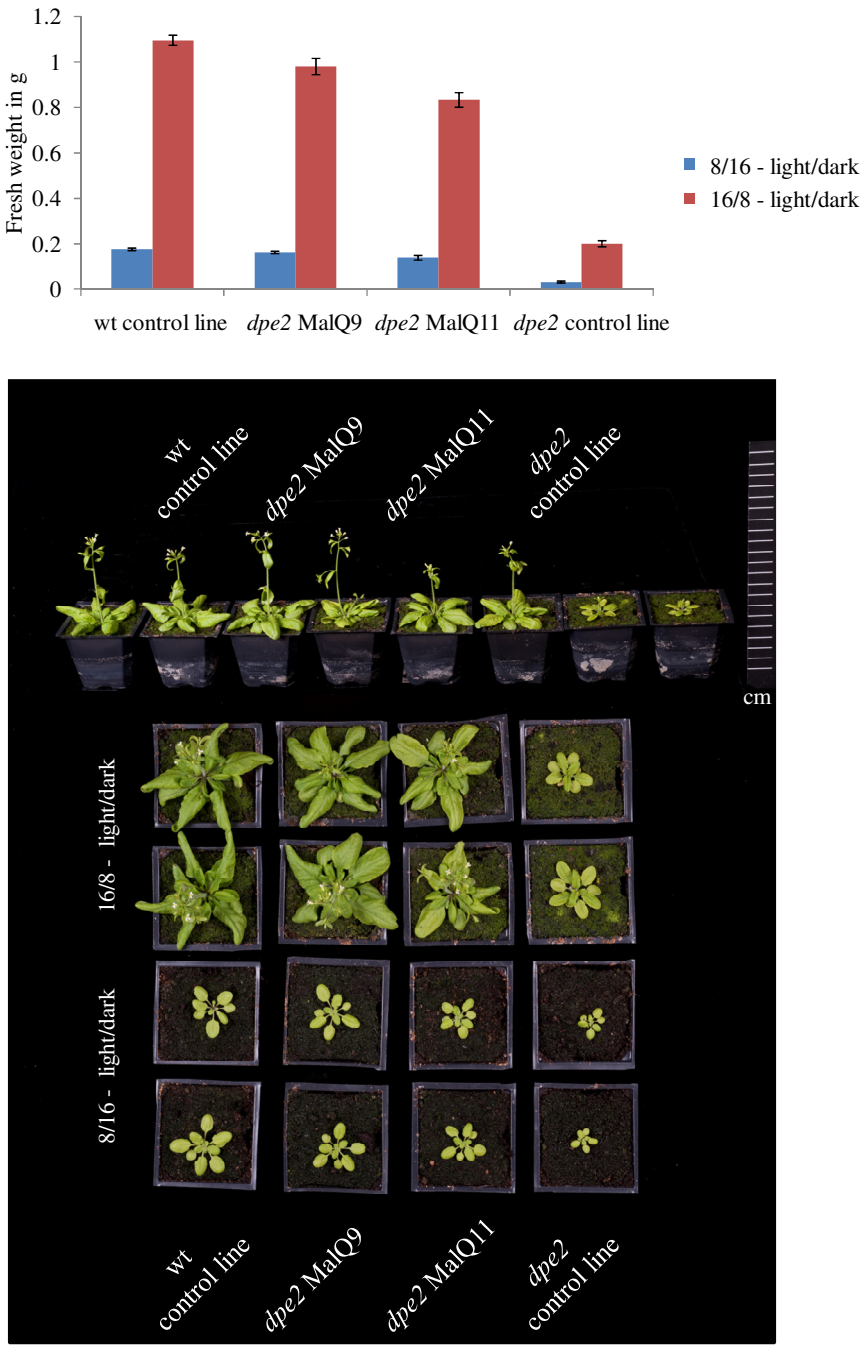

Figure 5.12 Phenotype of transgenic Arabidopsis lines grown at 16/8 and 8/16 photoperiods

Transgenic *dpe2* knockout mutant expressing MalQ and *dpe2* control and wt control were grown in two different photoperiods (16-hour light/8-hour dark and 8-hour light/16-hour dark). The photograph was taken 28 days after stratification. Values are means of measurements made on ten plants.

In summary, based on the data presented in this chapter MalQ seems to be able to complement the strong phenotype of plants that lack DPE2. Important metabolic markers of maltose metabolism like starch and maltose content as well as SHG composition mainly resemble wt character in *dpe2* MalQ lines. Work is being carried out to test the idea that this complementation is caused by bypassing the evolutionary conserved SHG pathway.

6 General Discussion and Outlook

The metabolism of maltose is an essential component of the major route of carbon from starch for plant growth and metabolism during the night in many plant species. DPE2 is the key enzyme in maltose metabolism in plants. In this thesis I compared the biochemical and enzymatic properties of DPE2 with its simpler homologue in *E. coli*, MalQ. I furthermore questioned the importance of the DPE2-SHG interaction for plant maltose metabolism in *Arabidopsis thaliana* by engineering a bypass to this pathway, by expressing MalQ in a *dpe2* knockout mutant. In this final chapter, I summarise the results of my work. Key findings are also illustrated in a model in Figure 6.1. Furthermore, I will set my results in a plant evolutionary context and outline arising questions that need to be addressed in future research.

6.1 DPE2 has unique structural and enzymatic properties

The metabolism of maltose in plants was proposed to require the transfer of a glucosyl unit from maltose by DPE2 onto SHG followed by its subsequent transfer onto orthophosphate by PHS2 (Fettke *et al.,* 2006a). The heterogeneous nature of SHG as well as its structural complexity hampers analysis of its interaction with DPE2 and PHS2. It was furthermore proposed that only a specific subfraction of SHG, termed SHG_{LI}, is used by DPE2 as acceptor substrate for glucosyl transfer from maltose (Fettke *et al.,* 2006a). This suggests that the activity of DPE2 on its acceptor substrate requires specific features of DPE2 and SHG that are currently unknown. My data in Chapter 3 however indicate that *in vitro*, DPE2 uses a broad range of acceptor substrates. Seemingly unrelated cell wall polysaccharides like RGI and carrageenans were substrates for DPE2. SHG_{LI} is thought to be cytosolic (Fettke *et al.,* 2005a) and is therefore spatially separated from cell wall polysaccharides. The composition of SHG however resembles that of arabinogalactans (AGs) (Fettke *et al.,* 2004). AGs are components found on the plasma membrane, in the wall, the apoplastic space and in secretions (eg stigma surface and wound exudates) of plant cells (Ellis *et al.,* 2010). My data therefore provide strong evidence that structural features of SHG, important for the interaction with DPE2, might resemble those of cell wall related polysaccharides like AGs.

The cytosolic phosphorylase (PHS2) was proposed to act downstream of DPE2 during the metabolism of maltose in plants (Fettke *et al.,* 2004). *In vitro*, PHS2 was shown to transfer a glucosyl residue, previously transferred onto SHG by DPE2, from SHG onto orthophosphate producing G1P (Fettke *et al.,* 2006a). Thus, DPE2 and PHS2 both interact with SHG, using it as

acceptor and donor substrate respectively. My data support this idea of a common acceptor substrate for DPE2 and PHS2. The substrate screen in Chapter 3 shows that PHS2 uses the same cell wall related polysaccharides as DPE2 as acceptor for glucosyl transfer from G1P *in vitro*. This suggests that there might be a similar carbohydrate-binding cleft at the protein surface of DPE2 and PHS2 that recognises complex glycan substrates like SHG. Future comparative structural analysis of potential surface binding sites in DPE2 and PHS2 could identify such binding clefts that are needed for interaction of both proteins with SHG.

The physiological function of the multimodular domain arrangement in DPE2 remains elusive. In Chapter 5 I have shown that a simple bacterial homologue of DPE2, MalQ from *E. coli*, is able to compensate for the lack of DPE2 in the *dpe2* mutant of Arabidopsis. MalQ lacks all of the additional structural features found in DPE2. This indicates that neither the CBM20 tandem nor the unique amino acid insertion are essential for maltose metabolism in plants (under the conditions tested). Data from Chapter 3 suggest that the CBM20 tandem provides a mean to bind to starch. However, there is no starch in the cytosol of plants. An alternative explanation could be that the CBM20 tandem in DPE2 is required for the interaction with SHG. However, based on my data from Chapter 4 and the literature (Steichen *et al.* (2008) as mentioned in Chapter 3) the function of the CBM20 tandem might lie in subsite restriction rather than in substrate binding. Future X-ray crystallographic analysis of DPE2 might therefore be the only means to decipher the exact function of the individual modules. A crystal structure of DPE2 could generate new hypotheses about the exact roles of the individual domains in DPE2 and how they interact with each other. These hypotheses could be tested by introducing mutant proteins into the plant.

6.2 Roles and specificities of DPE2 and MalQ

The provision of carbon for heterotrophic growth is fundamentally different in plants and bacteria. Whereas plants, like Arabidopsis, rely on carbon reserves acquired during the previous light period for heterotrophic growth in the dark, the growth of bacteria is dependent on carbon sources located outside the cell. Once a carbon source is found, highly specific ABC-type transporters in *E. coli* rapidly transport maltose and MOS into the cell (Dippel and Boos 2005). In the cytosol, MalQ starts acting on maltose and MOS which results in the production of Glc3 (Ehrmann and Boos 1987). Glc3 positively stimulates binding of MalT (transcriptional activator of MAL genes) to DNA. This suggests a function of MalQ not only in the metabolism of maltose but also in MAL gene regulation. A similar role for gene regulation by DPE2 in plants is hard to imagine. In contrast to MalQ, DPE2 does not seem to generate a unique small molecule

that could act as a specific signal in the same way as Glc3 in *E. coli*. Recently, however, two β-amylases were shown to be localised in the nucleus of Arabidopsis cells. BAM7 and BAM8 were shown to bind to Cis-regulatory elements via a DNA binding domain that is located at the N-terminus in both proteins (Reinhold *et al.,* 2011). The activity of the catalytic BAM domain (GH14) in BAM7 and BAM8 is three orders of magnitude lower than that of the full length chloroplastic isoforms BAM1 and BAM3. The full length BAM7 and BAM8 do not have any detectable activity at all (Reinhold *et al.,* 2011). Nevertheless, many of the amino acids lining the active site involved in substrate binding, including the catalytic residues, are conserved with respect to active BAMs (Fulton et al., 2008). One attractive idea is that the physiological role of the GH14 domain in BAM7 and BAM8 is to bind maltose. Depending on DPE2 activity, changes in maltose levels could therefore provide information about the flux from starch to sucrose to the cell nucleus. Binding of maltose to BAM7 and BAM8 could affect binding of the two BAMs to DNA and therefore trigger the down or up regulation of specific genes involved in carbon metabolism.

As discussed above and in Chapter 1, the metabolism of maltose in plants and bacteria like *E. coli* is very similar (Lu and Sharkey 2004, Lu and Sharkey 2006). Both pathways operate with the same set of enzymes, involving similar reactions. Nevertheless, data presented in Chapter 4 show that the manner in which DPE2 and MalQ metabolise maltose is very different. Whereas MalQ uses maltose as donor and acceptor of glucosyl unit and MOS transfer, DPE2 strictly uses maltose as glucosyl donor only. This is an important difference as it restricts DPE2 to catalyse a simple glucosyl transfer reaction, whereas MalQ is able to freely disproportionate maltose and larger MOS. This may also mean that DPE2 depends on SHG as an acceptor substrate *in vivo* since there are no MOS in the plant cytosol. MalQ in contrast, does not seem to rely on the presence of MOS. Data presented in Chapter 5 indicate that MalQ-catalysed maltose metabolism in *dpe2* plants expressing MalQ might bypass the SHG pathway. The ability of MalQ to directly disproportionate maltose derived from the chloroplast makes it potentially independent of an acceptor molecule like SHG.

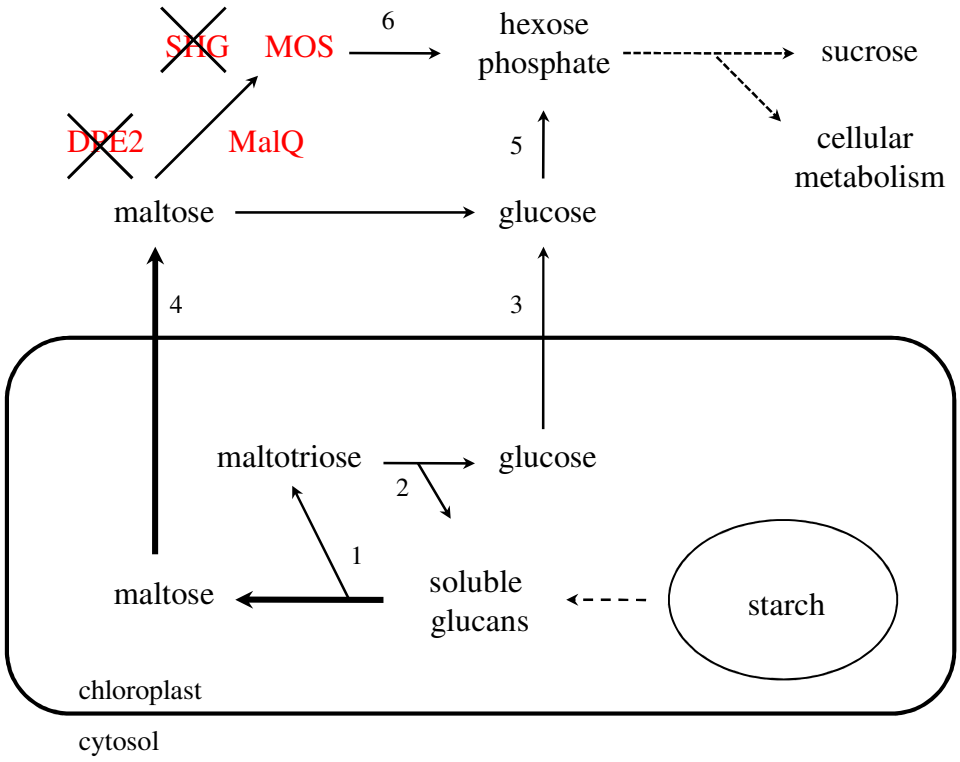

Figure 6.1 Proposed pathway of conversion of starch to sucrose at night in a transgenic *dpe2* Arabidopsis expressing MalQ

The pathway of maltose metabolism has been rerouted via MalQ. MOS are produced and serve as substrates for PHS2 which transfers glucose from MOS onto orthophosphate producing hexose phosphates. 1, β-amylase (BAM). 2, disproportionating enzyme 1 (DPE1). 3, glucose transporter (GlcT). 4, maltose transporter (MEX). 5, hexokinase (HXK). 6, PHS2

No obvious growth defects were observed in *dpe2* plants expressing MalQ, even when they were subjected to a range of photoperiods (Chapter 5, Figure 5.12). However, it cannot be excluded that altered biotic or abiotic conditions other than varying photoperiods can affect growth of *dpe2* MalQ plants. A recent study has shown that cold-induced freezing tolerance in plants is associated with an inactivation of DPE2 immediately after the plant has been subjected to freezing stress (within seconds). Upon freezing, the accumulation of maltose due to inactivation of DPE2 is thought to protect cells from freezing damage through the action of maltose as a cryoprotectant (Li *et al.,* 2011). Arabidopsis mutants that lack DPE2 exhibited increased tolerance to freezing stress when compared to wt plants. In future, similar freeze shock experiments with *dpe2* MalQ plants could help to test this idea about a specific role of DPE2 in tolerance to freezing in *Arabidopsis thaliana*.

6.3 Possible evolutionary origins of DPE2 and SHG

In considering the exact physiological function of DPE2 it is important to contemplate its possible evolutionary origins, as recently reviewed by Ball *et al.* (2011).

The commonly accepted endosymbiont theory states that an ancestor of present day cyanobacteria was internalized, probably through phagocytosis (Raven *et al.,* 2009) by a heterotrophic eukaryotic cell. This symbiont is the common ancestor for the three archaeaplastidic linkages: the Chloroplastida (green algae and land plants), the Rhodophyceae (red algae), and the Glaucophyta (glaucophytes). The common feature of these three lineages is the phototrophic life style and the ability to store carbon in the form of semicrystalline starch. The genomes of all archaeaplastidic organisms sequenced so far contain at least one copy of DPE2 and one copy of β-amylase. Other species like simple slime molds or bacterial pathogens such as Chlamydia also contain a single copy of each gene. The strict presence of both DPE2 and BAM thus seems to be common amongst archaeaplastidic and seemingly evolutionarily unrelated organisms (Deschamps *et al.,* 2008a). BAMs are enzymes with an inverting mechanism producing β-maltose from α-glucans (Thoma and Koshland 1960). Interestingly, DPE2 does not metabolise α-maltose *in vitro* (Weise *et al.,* 2005) or *in vivo* (Dumez *et al.,* 2006), but strictly uses β-maltose as substrate. The dependence of DPE2 on the β-anomer might be of physiological relevance. The interconversion of β-maltose to α-maltose is spontaneous (rate constant of 0.007 min^{-1})(Weise *et al.,* 2005). It is plausible that α-maltose, which is not metabolised in the cytosol of plants, could provide a signal for carbon status that influences gene expression. Currently there is no experimental evidence for this. Therefore it is of importance to investigate the maltose binding properties of the catalytic domain of the DNA binding BAMs (BAM7 and BAM8).

Recent evidence from genome sequencing of various organisms closely related to the common ancestor of the archaeplastidic lineage led to the suggestion that polysaccharide synthesis was ancestrally cytosolic (Deschamps *et al.,* 2008b). A complex series of interchanges of the glucan metabolism machinery was suggested to occur between the eukaryotic host cell (cytosol) and the endosymbiont (chloroplast) that led to the present arrangement in plants, where most glucans are metabolised in the chloroplast but some elements (SHG) remain in the cytosol (Figure 6.2). DPE2 is thought to originate from eukaryotic cells as part of machinery involved in glycogen metabolism (Figure 6.2).

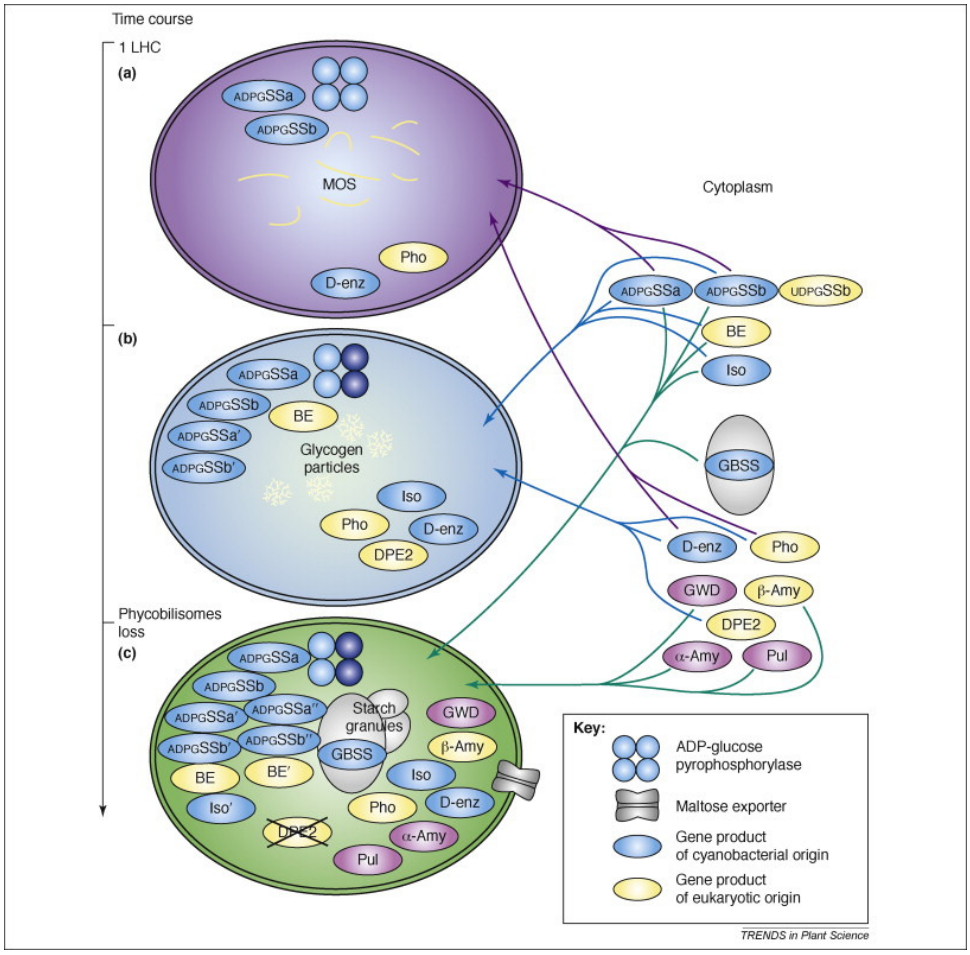

Figure 6.2 Starch metabolism rewiring during evolution of Chloroplastida (Figure from Deschamps *et al.* 2008)

The three panels represent plastids corresponding to three distinct stages of Chloroplastidae evolution. (a) The common ancestor of Rhodophyceae and Chloroplastida, containing simple light harvesting complex (phycobilisomes chlorophyll a) and cytosolic starch. (b) An intermediate stage of light harvesting complex diversification of an ancestor that still contains phycobilisomes and cytosolic starch in addition to more diverse chlorophyll-a- and chlorophyll-b-containing light harvesting complexes. (c) The 'final' stage of chloroplastidae evolution, where both with phycobilisomes and cytosolic starch have been lost. The colour of each enzyme represents its phylogenetic origin. Each arrow corresponds to stage-specific duplications of genes encoding the cytosolic paralogs concerned. The purple arrows represent those gene duplications encoding cytosolic paralogs that were required for the synthesis and degradation of a small pool of MOS (a). The blue arrows display those genes (including *DPE2*) encoding cytosolic paralogs that were required for the synthesis and degradation of an average-sized pool of glycogen in the plastid (b). Superscripts are used to symbolize the successive rounds of duplications and subfunctionalisations. The green arrows represent those gene duplications encoding cytosolic paralogs that were required for starch degradation.

The presence of DPE2 in non-photosynthetic organisms that metabolise glycogen (e.g. Dictyostelium and related slime molds) is consistent with this idea. Further investigation of the role of DPE2 in the metabolism of glycogen in these organisms would be valuable in understanding its origins.

There is also a possibility that SHG derived from the peptidoglycan layer of the cyanobacterial endosymbiont. During evolution, external surface layers (S-layers) and carbohydrate structures on the peptidoglycan layer would become obsolete as the symbiont evolved into a plant cell organelle which houses photosynthesis and many other fundamental intermediary metabolic reactions (McFadden 1999) (with the exception of glaucophytes that still contain a peptidoglycan layer). Their original function as protective coats or molecular sieves involved in cell adhesion and recognition was no longer needed in the protected environment of the new host. Some structures however might have gained a new function. Composition and linkage analysis of the active SHG Subfraction I (SHG_{LI}) in an earlier study could only account for around 80 mol % of the total composition (Fettke *et al.,* 2005a, Fettke *et al.,* 2005b). The remaining 20 mol % need to be further analysed but for now leave room for speculation. SHG might contain a yet unidentified phospholipid anchor (that could account for the missing 20 mol %) that attaches it at the outer membrane of the chloroplast. Thereby SHG would face the cytosolic compartment where it is acted on by DPE2 and PHS2.

Only a few cyanobacterial exopolysaccharides have been defined structurally, although some details of their composition are known. The sheaths of *Polymicrodon uncinatum* and *Nostoc commune* contain cellulose-like homoglucan fibrils which are cross-linked by minor monosaccharides (Hoiczyk 1998). Southerland et al. (1992) showed that *Anabaena flos-aquae* synthesizes two different polysaccharides: a xyloglucan containing glucose and xylose in a molar ratio of 8:1 and a more complex polysaccharide containing uronic acid, glucose, xylose, and ribose in the molar ratio of 10:6:1:1. None of these exopolysaccharides closely resemble the complexity of SHG. However, they might present the ancient basis that allowed for the establishment of a heterogeneous pool of SHG molecules in the cytosol of modern plants.

As outlined in Chapter 1 and Chapter 3, SHG is a very complex pool of molecules that possibly demands high costs of maintenance. It is therefore plausible to assume that SHG has other functions in addition to serving as acceptor molecules for DPE2 and PHS2 mediated glucosyl transfer. Other cellular functions of SHG in autotrophic tissues that have to be considered are for example involvement in cell wall metabolism. It is conceivable that SHG is part of a system that

coordinates or integrates carbon availability with cell wall metabolism. Consistent with this idea, a recent study by Fettke *et al.* (2010) has identified a third SHG_{LI} interacting protein (HIP 1.3). Arabidopsis mutants lacking this protein contain SHG with altered composition and severely reduced growth. The protein is predicted to be a nucleotide epimerase and therefore a potential candidate for the supply of sugar donors designated for SHG or cell wall related carbohydrate biosynthesis. UDP-galactose 4-epimerase could act on UDP-glucose, which is one precursor of sucrose synthesis in the plant cytosol. However, experiments so far have failed to detect any enzymatic activity with heterologously produced HIP 1.3 (Fettke *et al.,* 2010).

Further insights into the role and importance of SHG will require research on its structure, synthesis (and therefore interacting proteins) plus tools with which its amount and composition can be manipulated *in vivo*.

6.4 Conclusion

The results in this thesis present an advance and new leads in our understanding of maltose metabolism in *Arabidopsis thaliana*. My data indicate that the complexity of the domain architecture of DPE2 does not seem to be essential for plant growth under controlled environment conditions. Further research should focus on the structural elucidation of this pathway.

Appendix 1

This part of the appendix shows the protein purification procedure of truncated versions of the starch binding domain (CBM20 tandem domain) of DPE2 as well as MalQ and CBM20-MalQ. The purification procedures were similar to the ones described for DPE2 and PHS2 in Chapter 1. Proteins were produced in *E. coli* and purified with nickel IMAC followed by SEC. The protein preparations were judged highly pure by SDS PAGE and DLS analysis

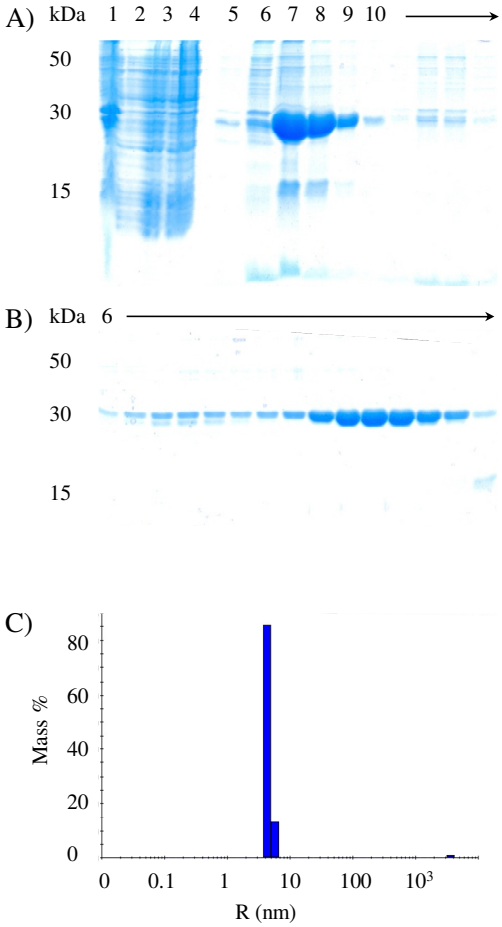

Figure Appendix 1.1 Purification of CBM20 tandem domain of DPE2 (in pET28a)

A and B) SDS PAGE analysis of fractions from nickel IMAC and SEC columns (10% acrylamide gel). Lane 1 and 2 are from uninduced, lane 3 and 4 are from IPTG induced bacteria. Lane 5 to 9 and Lane 10 onwards are from nickel IMAC and SEC columns.
C) DLS histogram of purified CBM20 tandem domain. The protein preparation (10mg·ml-1) was monitored for a period of 10 seconds at a laser intensity of 25% (which equalled approximately 3,000,000 counts per seconds). The histogram shows an average of 10 readings.

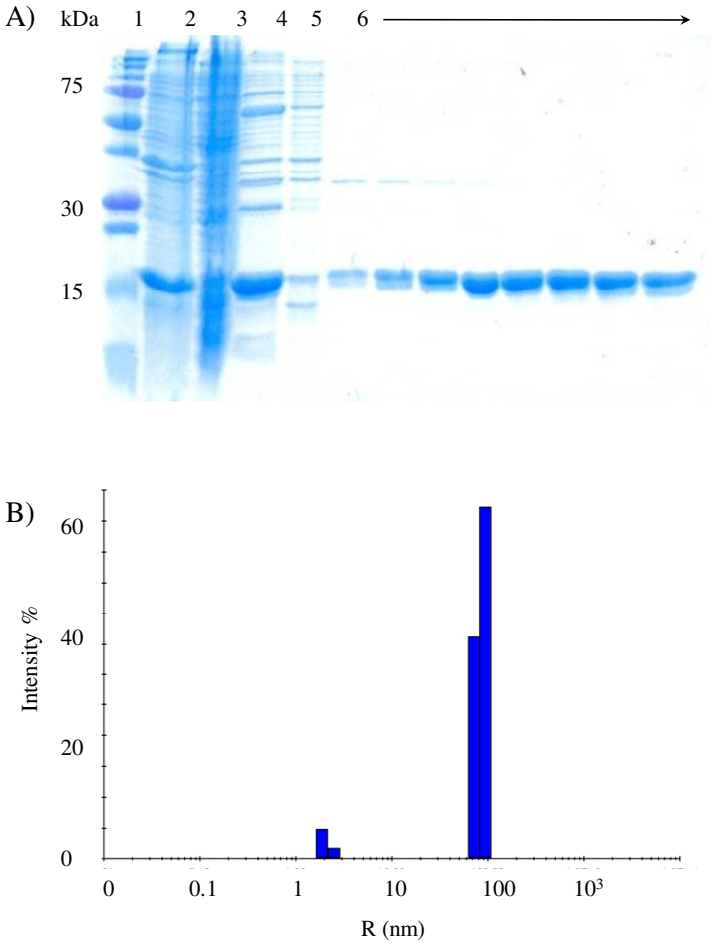

Figure Appendix 1.2 Purification of CBM20-1 (in pET28a)

A) SDS PAGE analysis of fractions from nickel IMAC and SEC columns (15% acrylamide gel). Lane 1 is molecular weight marker. Lane 2 is from induced bacteria. Lane 3 is from flow through nickel IMAC column. Lane 4 is from nickel IMAC. Lane 5 is from SEC void volume. Lane 6 onwards is from SEC column.
B) DLS histogram of purified CBM20-1. The protein preparation (10 $mg \cdot ml^{-1}$) was monitored for a period of 10 seconds at a laser intensity of 25% (which equalled approximately 3,000,000 counts per seconds). The histogram shows an average of 10 readings and shows the intensity. CBM20-1 is represented by the smaller peak at 2 nm.

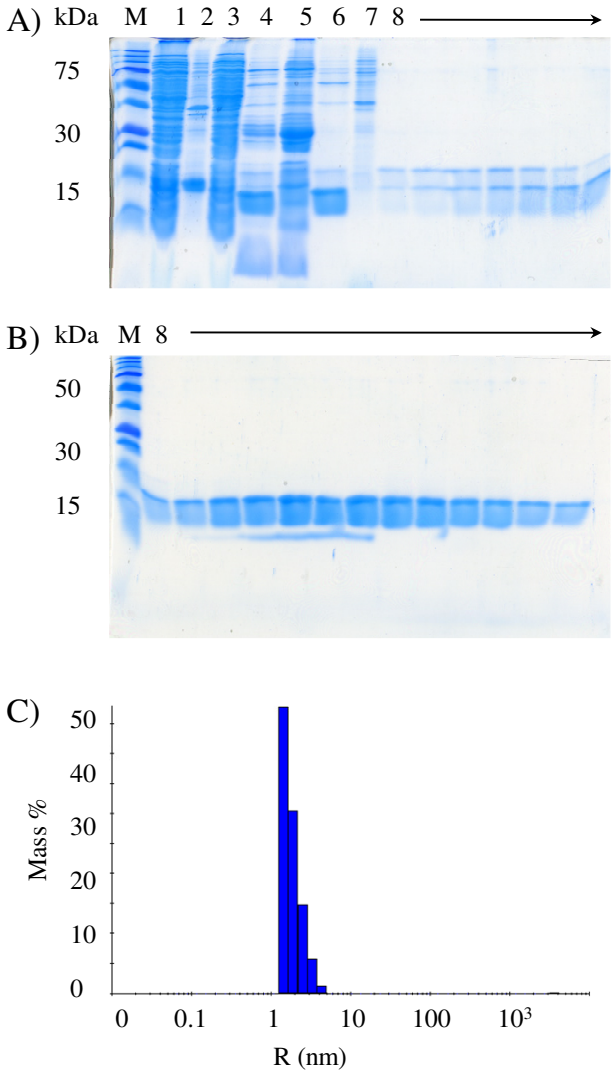

Figure Appendix 1.3 Purification of CBM20-2 (in pET151; TEC cut)

A and B) SDS PAGE analysis of fractions from nickel IMAC and SEC columns (15% acrylamide gel). M is molecular weight marker. Lane 1 is from induced sbacteria. Lane 2 is from first nickel IMAC. Lane 3 is flow through from second nickel IMAC column. Lane 4 is from second nickel IMAC. Lane 5 from bound protein to second nickel IMAC column. Lane 6 is from flow through of second nickel IMAC (containing TEV cut CBM20-2). Lane 7 is from SEC column void volume. Lane 8 and up is from SEC column (First few fractions contain both, TEV protease cut and uncut CBM20-2. Later fractions only contain the smaller –His_6 TEV protease cut CBM20-2).
C) DLS histogram of purified CBM20-2. The protein preparation (10 $mg \cdot ml^{-1}$) was monitored for a period of 10 seconds at a laser intensity of 25% (which equalled approximately 3,000,000 counts per seconds). The histogram shows an average of 10 readings.

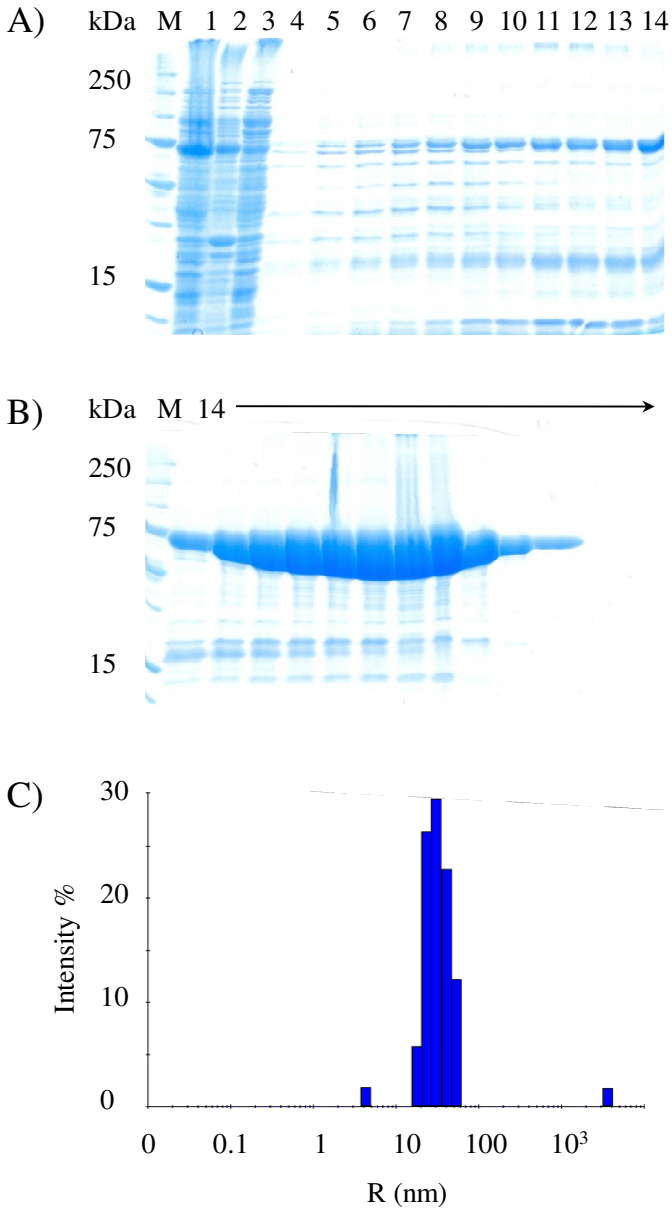

Figure Appendix 1.4 Nickel IMAC purification of MalQ (in pMAD145)

A and B) SDS PAGE analysis of fractions from nickel IMAC (10 % acrylamide gel). M is molecular weight marker. Lane 1 is induced sample of *E. coli* culture. Lane 2 flow through from nickel IMAC column. Lane 4 and up is from nickel IMAC column.
C) DLS histogram of purified MalQ. The protein preparation (10 $mg \cdot ml^{-1}$) was monitored for a period of 10 seconds at a laser intensity of 25% (which equalled approximately 3,000,000 counts per seconds). The histogram shows an average of 10 readings.

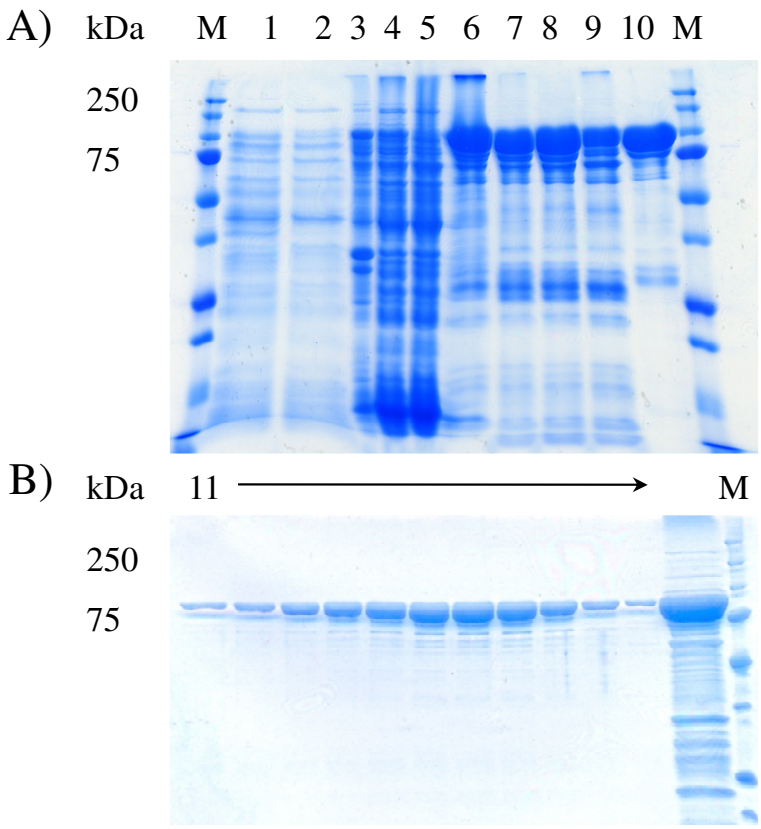

Figure Appendix 1.5 Purification of CBM20-MalQ (in pET151 TEV cut)

A and B) SDS PAGE analysis of chromatography fractions from nickel IMAC and SEC loaded on 12.5 % acrylamide gel. M is molecular weight marker. Lanes 1 and 2 are und induced and induced sample of *E. coli* culture. Lane 3 is pellet of protein extract. Lane 4 is supernatant of protein extract. Lane 5 is flow through. Lane 6 is from first nickel IMAC column. Lane 7 is from pellet after over night cleavage with TEV. Lane 8 is from supernatant after overnight cleavage with TEV. Lane 9 is from bound fraction of second nickel IMAC column. Lane 10 is cleaved protein (flow through from second nickel IMAC column). Lane 11 onwards is from SEC column.

Appendix 2

This part of the appendix contains data from the linkage analysis described in Chapter 4. I will provide a brief summary of the background and show the corresponding Gas Chromatography with Electron Impact Mass Spectrometry profiles (GC-EIMS) that were explained in Chapter 2 section 2.6.5. Typically, the disaccharides were collected from the HPAEC-PAD system and derivatised to form acid-stable methyl ethers. After that they were hydrolysed, reduced using $NaBD_4$, peracetylated, and the resulting Partially Methylated Alditol Acetates (PMAAs) were analyzed by GC-EIMS. *Myo*-inositol hexaacetate was present in all samples as an internal standard. The type of glycosidic linkage in the starting disaccharide follows from GC retention time of a particular PMAA species and from its characteristic fragmentation pattern in the EIMS.

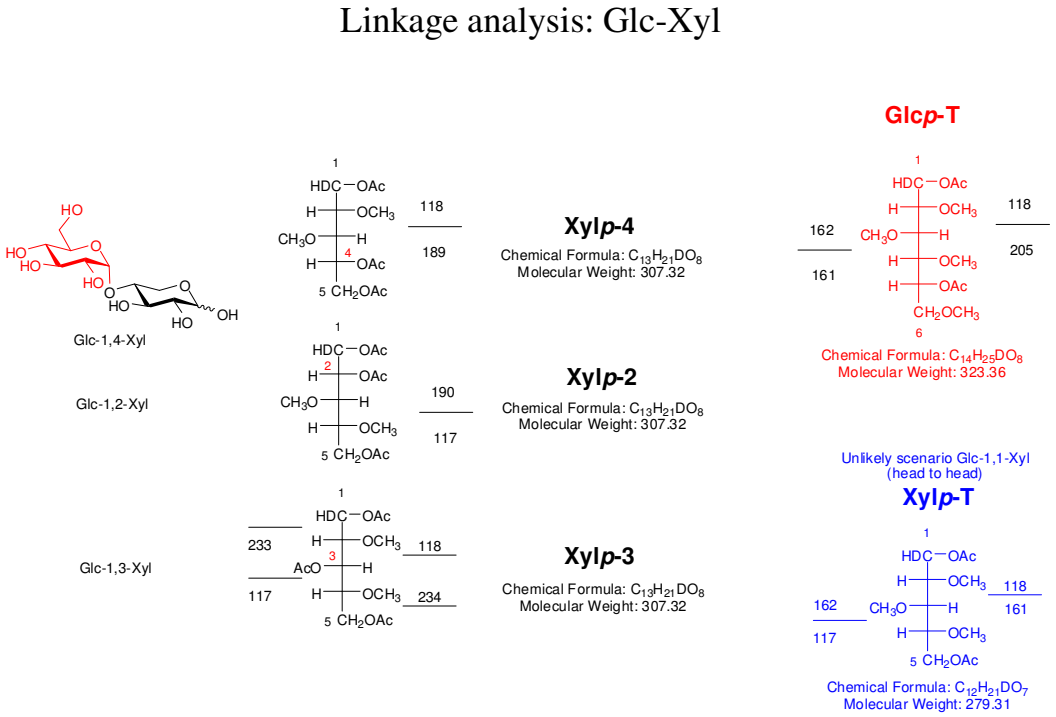

Figure Appendix 2.1 Expected fragmentation of Partially Methylated Alditol Acetates (PMAAs) derived from glycosidically linked xylose and a terminal glucose

The linkage of the disaccharide Glc-Xyl produced by MalQ and DPE2 in Chapter 4 is unknown. Outlined here are the expected fragmentation patterns of Partially Methylated Alditol Acetates (PMAAs) derived from glycosidically linked xylose and a terminal glucose.

Authentic sample: Glc-1,4-Xyl

Ref. No.	Structure	Amount	Glc*p*-T GC *Rf* [min]	Xyl*p*-4 GC *Rf* [min]	MIH GC *Rf* [min]
MRA67-6	α-Glc*p*-(1,4)-Xyl*p* (Birte)	5 µg	161, 162, 118, 205 11.471	118, 189 11.130	-
myo-inositol		2.5 µg			14.021

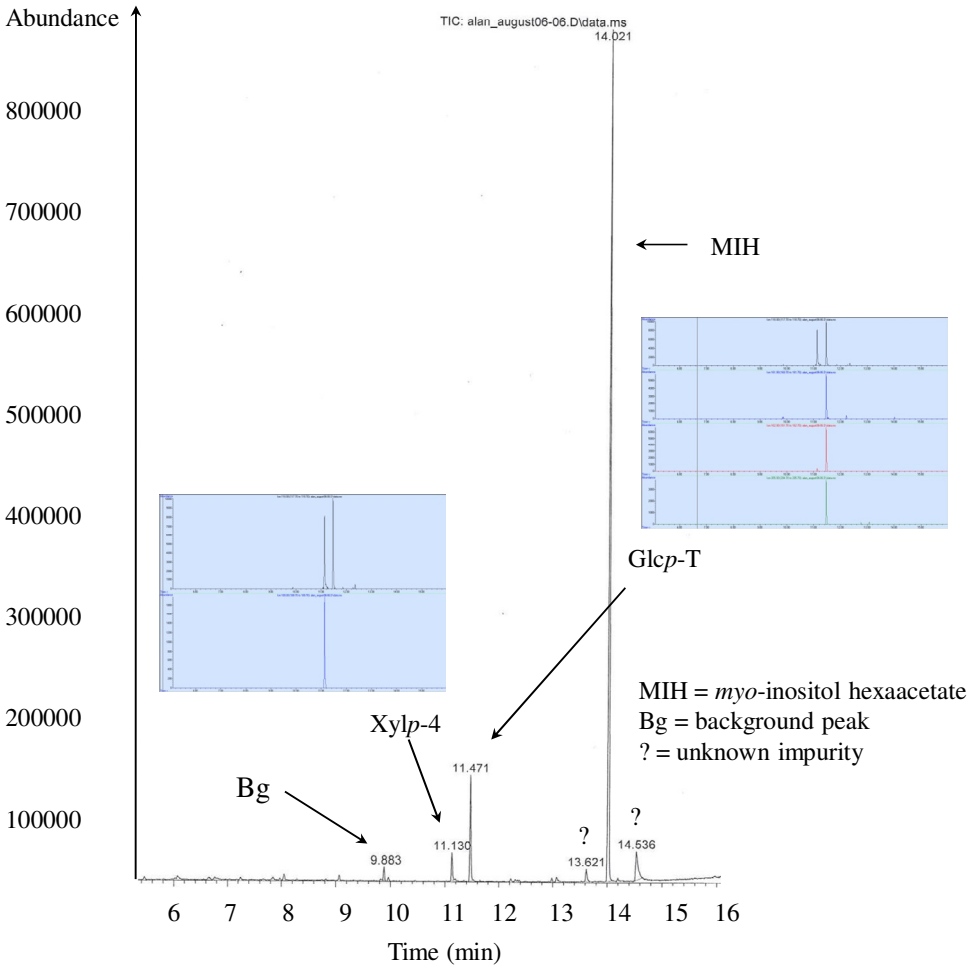

Figure Appendix 2.2 Linkage analysis of an authentic sample Glc-1,4-Xyl (Nakai *et al.,* 2010). GC-EIMS analysis of the corresponding PMAAs.

PMAAs are identified with Electron Impact Mass Spectrometry profiles (GC-EIMS). The x-axis indicates the retention time and the y-axis indicates the relative abundance of the respective PMAA peak. Automated search for EIMS fragments 118 and 189, characteristic for Xyl*p*-4, indicated GC peak with retention time 11.13 min (blue window). Terminal glucopyranose (Glc*p*-T) with fragmentation pattern "118, 161, 162, 205" was detected at 11.471 min in the GC.

Ref. No.	Structure	Amount	Glc*p*-T GC *Rf* [min]	Xyl*p*-4 GC *Rf* [min]	MIH GC *Rf* [min]
MRA68-1	α-Glc*p*-(?,?)-Xyl*p* DPE2	10 µg	161, 162, 118, 205 12.273	118, 189 11.813	- 15.334
MRA67-6 (standard)	α-Glc*p*-(1,4)-Xyl*p* (Birte)	5 µg	161, 162, 118, 205 11.471	118, 189 11.130	- 14.021
myo-inositol		5 µg			

Conclusion:
DPE2
Glc-1,4-Xyl

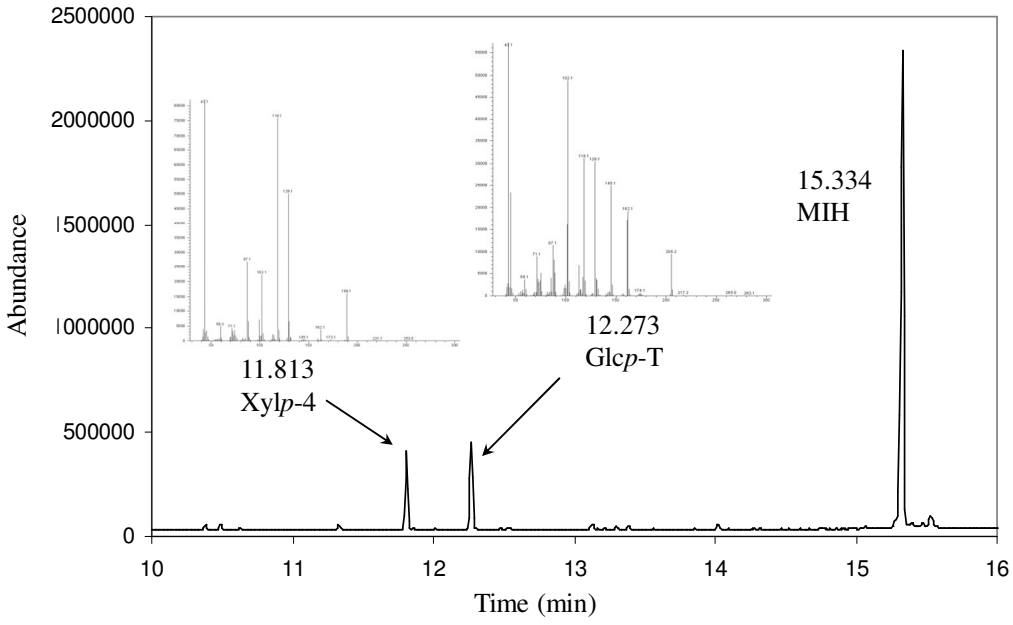

Figure Appendix 2.3 Linkage analysis of Glc-Xyl from DPE2 indicating Glc-1,4-Xyl. GC chromatogram and MS spectra corresponding to particular PMAAs.

The GC-EIMS data from Glc-Xyl formed by the action of DPE2 show the presence of Glc*p*-T and Xyl*p*-4 at retention times 12.273 min and 11.813 min, respectively, indicating a 1,4 glycosidic linkage.

Ref. No.	Structure	Amount	Glc*p*-T GC *Rf* [min]	Xyl*p*-4 GC *Rf* [min]	MIH GC *Rf* [min]
MRA68-4	α-Glc*p*-(?,?)-Xyl*p* MalQ	10 µg	161, 162, 118, 205 12.272	118, 189 11.812	- 15.329
MRA67-6 (standard)	α-Glc*p*-(1,4)-Xyl*p* (Birte)	5 µg	161, 162, 118, 205 11.471	118, 189 11.130	- 14.021
myo-inositol		5 µg			

Conclusion:
MalQ
Glc-1,4-Xyl

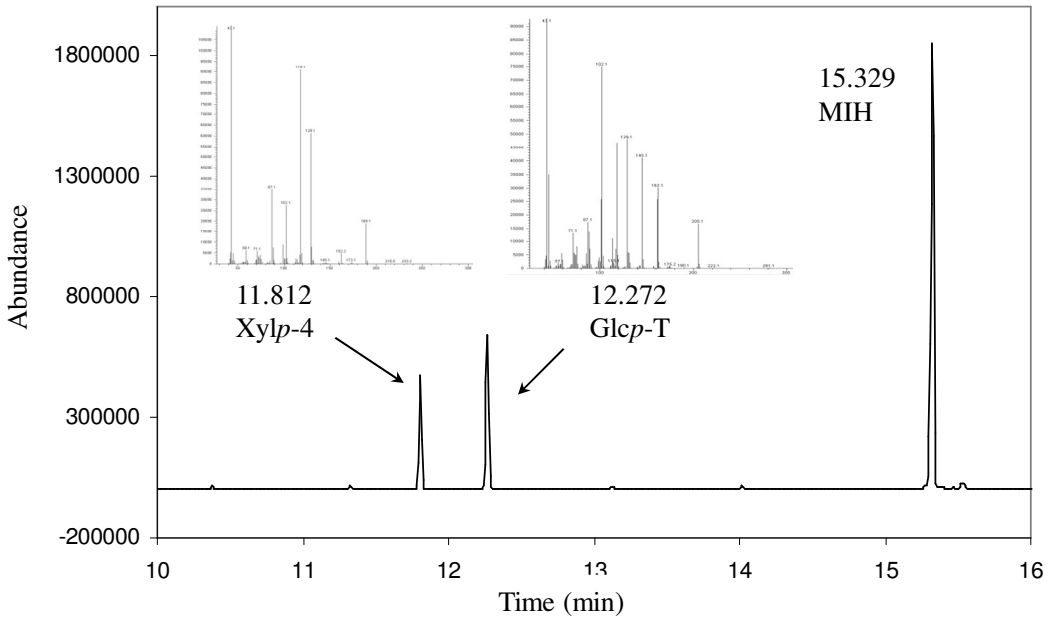

Figure Appendix 2.4 Linkage analysis of Glc-Xyl from MalQ

The GC-EIMS data of Glc-Xyl formed by the action of MalQ (Figure Appendix 2.4) show the presence of Glc*p*-T and Xyl*p*-4 at retention times 12.272 min and 11.812 min, respectively, indicating a 1,4 glycosidic linkage.

Linkage analysis: Glc-Glc

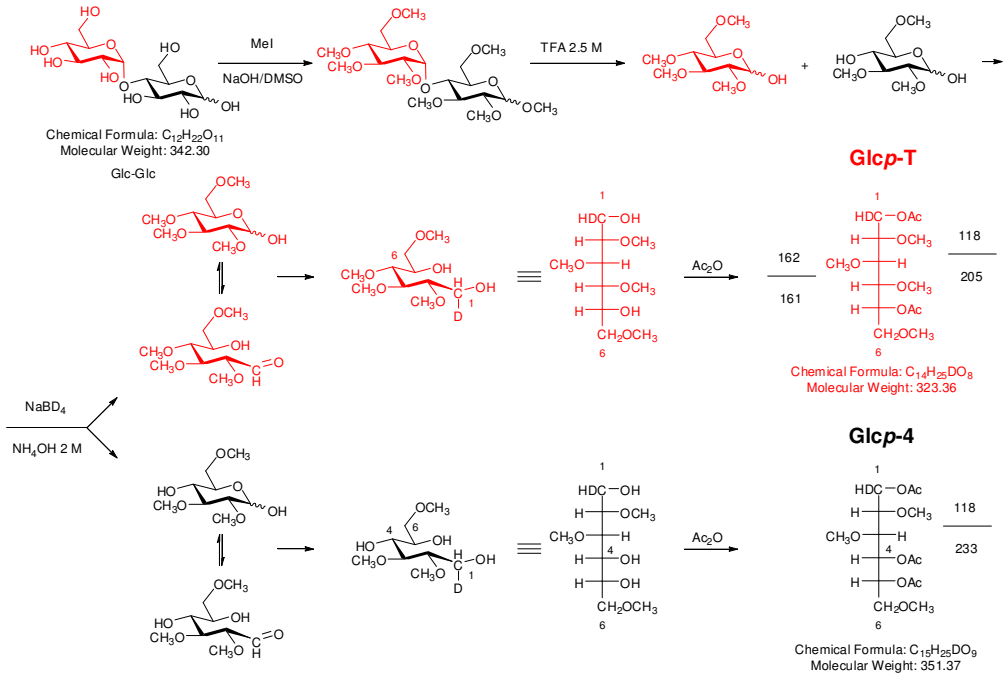

Figure Appendix 2.5

Expected fragmentation of Partially Methylated Alditol Acetates (PMAAs) derived from glycosidically linked glucose and a terminal glucose

The linkage of the disaccharide Glc-Glc produced by MalQ and DPE2 in Chapter 4 is unknown. Outlined here (Figure Appendix 2.5) are the expected fragmentation patterns of Partially Methylated Alditol Acetates (PMAAs) derived from glycosidically linked glucose and a terminal glucose.

Ref. No.	Structure	Amount	Glc*p*-T GC *Rf* [min]	Glc*p*-4 GC *Rf* [min]	MIH GC *Rf* [min]
MRA68-3	α-Glc*p*-(?,?)-Glc*p* MalQ	10 µg	161, 162, 118, 205 12.272	118, 233 13.302	- 15.321
myo-inositol		5 µg			

Conclusion:
MalQ
Glc-1,4-Glc

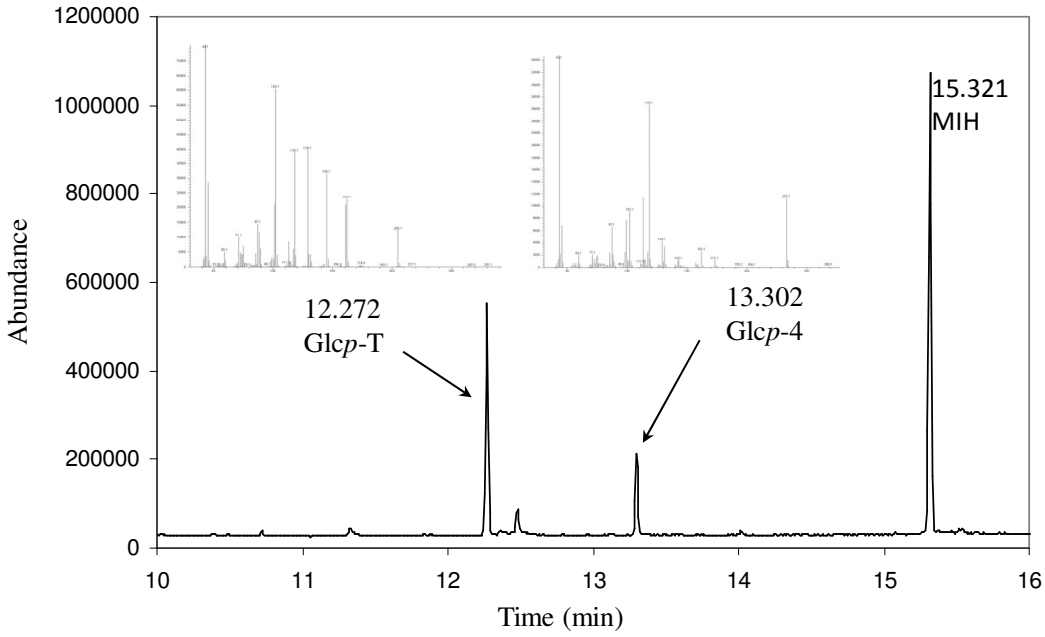

Figure Appendix 2.6 Linkage analysis of Glc-Glc from MalQ

The GC-EIMS data of Glc-Glc formed by the action of MalQ (Figure Appendix 2.6) show the presence of Glc*p*-T and Glc*p*-4 at retention times 12.272 min and 13.302 min, respectively, indicating a 1,4 glycosidic linkage.

Ref. No.	Structure	Amount	Glc*p*-T GC *Rf* [min]	Glc*p*-4 GC *Rf* [min]	MIH GC *Rf* [min]
MRA68-2	α-Glc*p*-(?,?)-Glc*p* DPE2	10 µg	161, 162, 118, 205 12.273	118, 233 13.303	- 15.322
myo-inositol		5 µg			

Conclusion:
DPE2
Glc-1,4-Glc

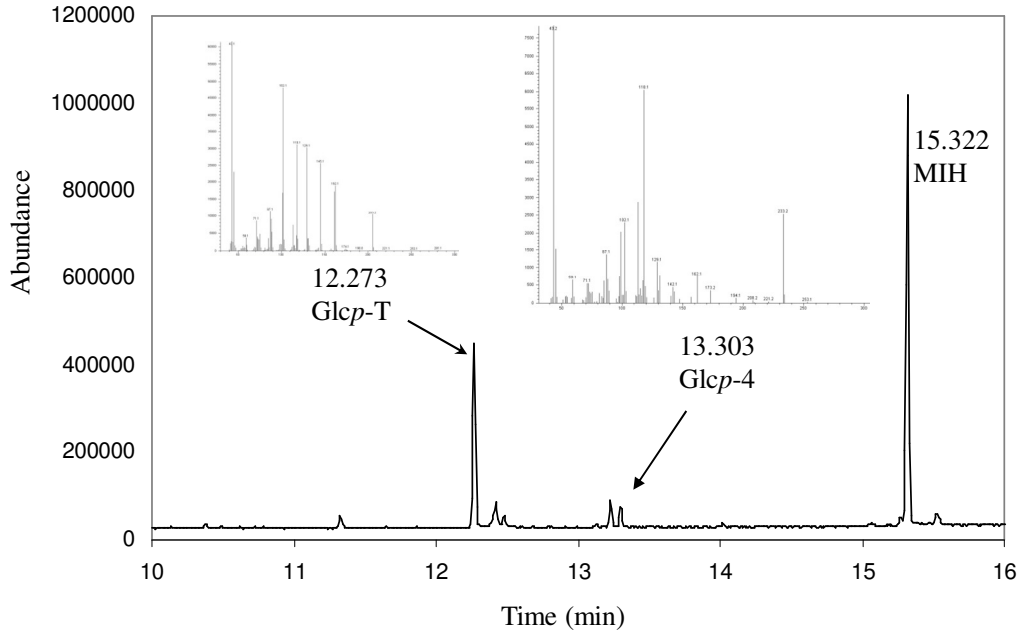

Figure Appendix 2.7 Linkage analysis of Glc-Glc from DPE2

The GC-EIMS data of Glc-Glc formed by the action of DPE2 (Figure Appendix 2.7) show the presence of Glc*p*-T and Glc*p*-4 at retention times 12.273 min and 13.303 min, respectively, indicating a 1,4 glycosidic linkage.

Appendix 3

The MalQ gene from *E. coli* MC 4100 (Lu *et al.,* 2006b) was optimised for expression in *Arabidopsis thaliana* by Geneart (Geneart number: 0918068). The following sequence alignment shows the optimised sequence aligned on top of the original bacterial sequence:

```
                10        20        30        40        50        60
103664 ATGGAAAGCAAACGTCTGGATAATGCCGCGCTGGCGGCGGGGATTAGCCCCAATTACATC
       ::::::   ::  : :: ::::: :: :: :: :: :: :: :::   :: :: ::::::
_      ATGGAATCTAAGAGACTCGATAACGCTGCTCTTGCTGCTGGAATTTCTCCTAACTACATC
                10        20        30        40        50        60

                70        80        90       100       110       120
103664 AATCCCCACGGTAAACCGCAGTCGATTAGCGCCGAAACCAAACGGCGTTTGCTTGACGCG
       ::  : :: :: :: :: :: :: ::    :: :: :: ::  :  : ::::: :: ::
_      AACGCTCATGGAAAGCCTCAATCTATCTCTGCTGAGACTAAGAGAAGATTGCTCGATGCT
                70        80        90       100       110       120

               130       140       150       160       170       180
103664 ATGCATCAACGTACCGCCACGAAAGTGGCGGTAACGCCAGTCCCGAATGTCATGGTTTAT
       :::::::::: : :: :: :: :: ::::: :: :: :: :: :: :: :: ::::: ::
_      ATGCATCAAAGAACTGCTACTAAGGTGGCAGTTACTCCTGTTCCTAACGTGATGGTGTAC
               130       140       150       160       170       180

               190       200       210       220       230       240
103664 ACCAGCGGCAAAAAAATGCCGATGGTGGTGGAGGGCAGCGGCGAATATAGCTGGCTGCTG
       :::   :: :: :::::::: :::::::: :: ::    :: :::::    ::::: ::
_      ACCTCTGGAAAGAAAATGCCTATGGTGGTTGAAGGATCTGGTGAATACTCTTGGCTTCTC
               190       200       210       220       230       240

               250       260       270       280       290       300
103664 ACCACCGAAGAAGGAACGCAGTACAAAGGCCATGTAACGGGGGGCAAAGCGTTCAATCTA
       :: :: ::::: ::::: :::::::: :: ::::: :: :: :: :: :: ::::: ::
_      ACTACTGAAGAGGGAACTCAGTACAAGGGACATGTTACTGGTGGAAAGGCTTTCAACCTT
               250       260       270       280       290       300

               310       320       330       340       350       360
103664 CCGACCAAGCTGCCGGAAGGTTATCACACGCTGACACTCACCCAGGACGACCAGCGCGCG
       :: :: ::::: :: :: :: :: :: :: :: :: ::::: ::::: :: ::  : ::
_      CCTACTAAGCTTCCTGAGGGATACCATACTCTTACTCTCACTCAGGATGATCAAAGAGCA
               310       320       330       340       350       360

               370       380       390       400       410       420
103664 CATTGCCGGGTGATTGTCGCCCCGAAACGCTGTTACGAACCGCAGGCGTTGCTGAATAAA
       :: ::: : :: :: :: :: :: ::  : ::::: :: :: :::::  :  :::: ::
_      CACTGCAGAGTTATCGTTGCTCCTAAGAGATGTTATGAGCCTCAGGCTCTTTTGAACAAG
               370       380       390       400       410       420

               430       440       450       460       470       480
103664 CAAAAGCTGTGGGGTGCCTGCGTTCAGCTTTATACGCTGCGATCGGAAAAAAACTGGGGT
       :::::::: ::::: :: :: :::::::::: :: ::  :::: ::::: ::::::::
_      CAAAAGCTTTGGGGAGCTTGTGTTCAGCTTTACACCCTCAGATCTGAAAAGAACTGGGGA
               430       440       450       460       470       480

               490       500       510       520       530       540
103664 ATTGGGGATTTTGGCGATCTCAAAGCGATGCTGGTGGATGTGGCAAAACGTGGCGGGTCG
       :: :: :::::::: ::::: :: :: ::::: :: ::::: :: ::  : :: :: ::
_      ATCGGAGATTTTGGAGATCTTAAGGCTATGCTCGTTGATGTTGCTAAGAGGGGAGGATCT
               490       500       510       520       530       540
```

```
              550       560       570       580       590       600
103664 TTCATTGGCCTGAACCCGATTCATGCGCTCTATCCGGCAAATCCGGAGAGCGCCACCGCA
       :::::::: :: ::::: :: ::::: :: ::::: :: ::::: :::   ::  :  :
_      TTCATTGGACTCAACCCTATCCATGCTCTTTATCCTGCTAATCCTGAGTCTGCTTCTCCT
              550       560       570       580       590       600

              610       620       630       640       650       660
103664 TACAGCCCGTCTTCTCGCCGTTGGCTGAATGTGATTTATATCGACGTTAACGCCGTTGAA
       :::   :: :: ::: :  : ::::: :: ::::: :: ::::: :::::::: :::::
_      TACTCTCCATCATCTAGAAGATGGCTCAACGTGATCTACATCGATGTTAACGCTGTTGAG
              610       620       630       640       650       660

              670       680       690       700       710       720
103664 GATTTCCATCTTAGCGAAGAGGCTCAGGCCTGGTGGCAGTTGCCGACCACGCAACAGACG
       ::::::::::    :::::::::: :: ::::::::  : :: :: :: ::::::::
_      GATTTCCATCTCTCTGAAGAGGCTCAAGCTTGGTGGCAACTTCCTACTACTCAACAGACT
              670       680       690       700       710       720

              730       740       750       760       770       780
103664 CTGCAACAGGCGCGCGATGCCGACTGGGTCGATTACTCCACGGTTACCGCCCTAAAAATG
       :: :: :: ::  : ::::: :: ::::: :: ::::: :: :::::::: :: :: :::
_      CTTCAGCAAGCTAGAGATGCTGATTGGGTGGACTACTCTACTGTTACCGCTCTTAAGATG
              730       740       750       760       770       780

              790       800       810       820       830       840
103664 ACAGCATTACGAATGGCGTGGAAAGGTTTCGCGCAACGTGATGATGAGCAGATGGCCGCG
       :: ::  :  ::::::: ::::: :: ::::: ::: : :::::::: :::::::: ::
_      ACTGCTCTCAGAATGGCTTGGAAGGGATTCGCTCAAAGGGATGATGAACAGATGGCTGCT
              790       800       810       820       830       840

              850       860       870       880       890       900
103664 TTTCGCCAGTTTGTTGCAGAGCAGGGCGACAGCCTGTTCTGGCAGGCAGCCTTTGATGCG
       ::  : :: :: ::::: :: ::::: :: :: :: :: :::::::: :: ::::::::
_      TTCAGACAATTCGTTGCTGAACAGGGTGATAGTCTTTTTTGGCAGGCTGCTTTTGATGCT
              850       860       870       880       890       900

              910       920       930       940       950       960
103664 CTACATGCCCAGCAAGTGAAAGAGGACGAAATGCGCTGGGGCTGGCCTGCATGGCCAGAG
       :: ::::: :: :::::::: :: :: :: ::::: ::::: :::::::: ::::: ::
_      CTCCATGCTCAACAAGTGAAGGAAGATGAGATGCGATGGGGATGGCCTGCTTGGCCTGAA
              910       920       930       940       950       960

              970       980       990      1000
103664 ATGTATCAGAACGTGGATTCACCAGAAGTGCGTCAGTTCT--------------------
       ::::: :::::::::::::: :: :::::  : :::::::
_      ATGTACCAGAACGTGGATTCTCCTGAAGTTAGACAGTTCTGCGAGGAACATAGAGATGAT
              970       980       990      1000      1010      1020
```

The optimisation of the gene sequence did not alter the amino acid sequence. Chapter 5 shows that MalQ is produced as active protein in Arabidopsis (Native PAGE) and that MalQ is also detectable with anti-MalQ antibodies via immunoblot.

Appendix 4

This part of the appendix summarises the data from the purification of polyclonal antibodies targeted against recombinant DPE2 and MalQ that were raised in rabbits by immunisation with purified protein preparations (DPE2 and MalQ).

The blood sera were used to purify anti-DPE2 and anti-MalQ antibodies. For this purpose, purified DPE2 and MalQ proteins were covalently coupled to aldehyde-activated beaded agarose (Piercenet Aminolink Plus) in columns. Glycine pH 2.5 eluted fractions were used to develop immunoblots of plant extracts from transgenic plant lines expressing or not expressing DPE2 and MalQ proteins.

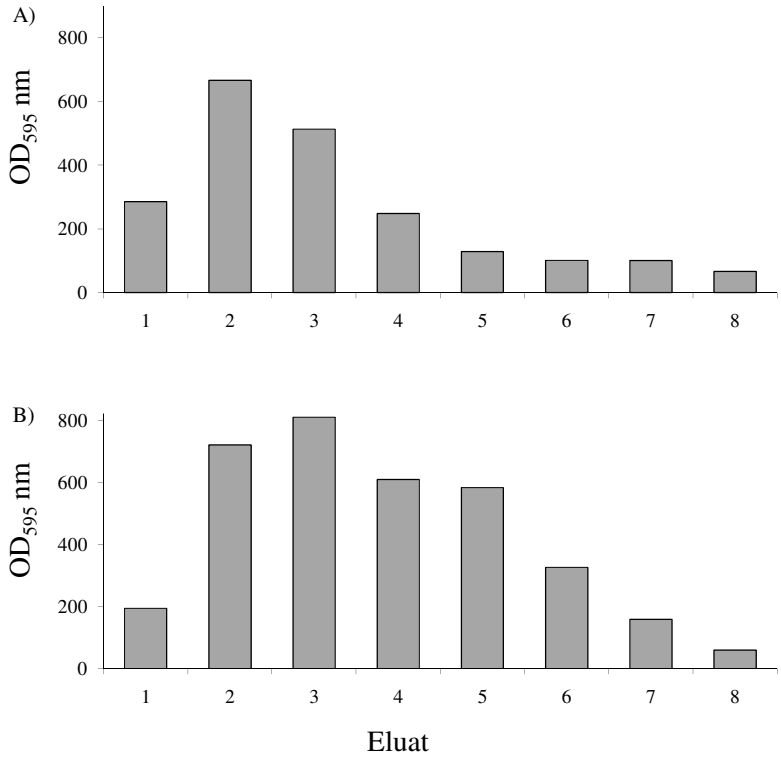

Figure Appendix 3.1 Purification profile of anti-MalQ and anti-DPE2 antibody

Fractions (0.5 ml – column volume 2.5 ml) were collected and the protein concentration was analysed via Bradford Protein Quantification assay. A) anti-DPE2 antibody eluate profile B) anti-MalQ antibody eluate profile. The same fractions were later used to evaluate the respective antibodies.

Fractions eluted from MalQ column as in Figure Appendix 3.1, A

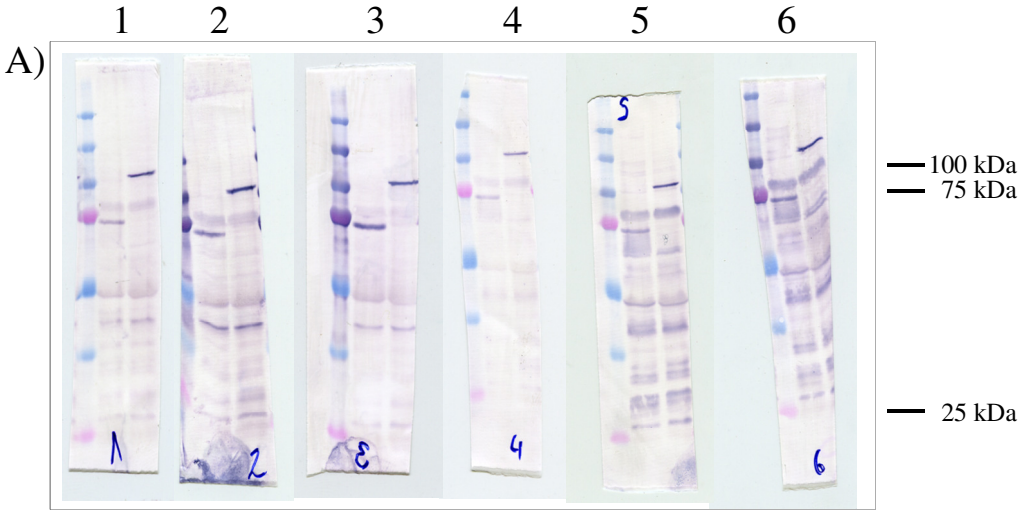

Fractions eluted from MalQ column as in Figure Appendix 3.1, B

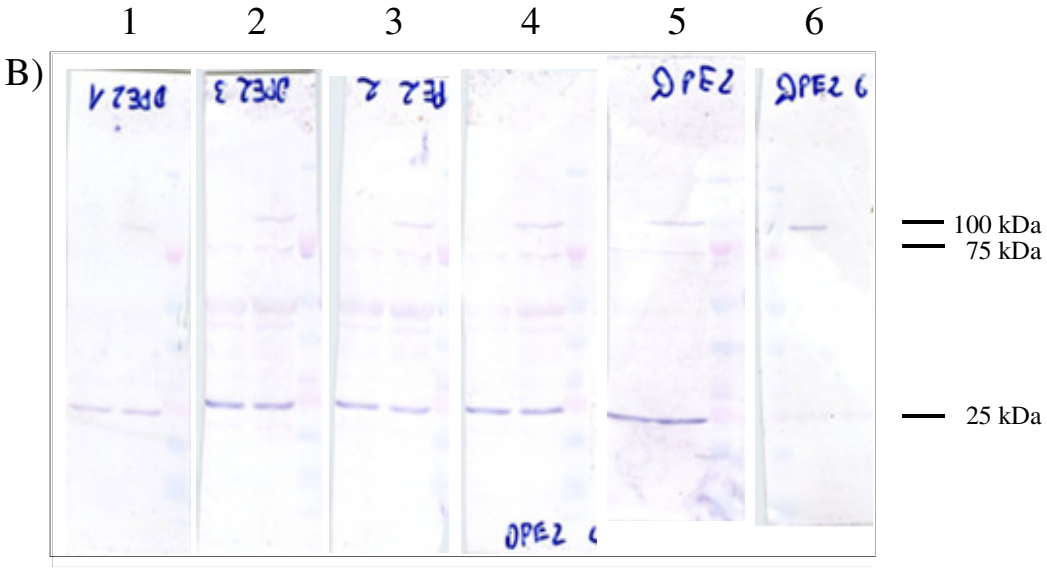

Figure Appendix 3.2 Immunoblot evaluation of anti-MalQ and anti-DPE2 antibody

Fractions collected from the MalQ and DPE2 affinity columns were evaluated on their ability to detect the target protein. A) MalQ immunoblot. MalQ and CBM20-MalQ are detected at 75 kDa and 100 kDa respectively. Plant extract of *dpe2* MalQ9 (first lane) and *dpe2* CBM20-MalQ8 (second lane) were used (1:3000 dilution of primary anti-MalQ antibody) B) DPE2 immunoblot. Plant extract of *dpe2* control (first lane) and wt control (second lane) were used (1:1000 dilution of primary anti-DPE2 antibody).

For immunoblots in this study I used fraction 3 from the anti-MalQ (Figure Appendix 3.2, A) antibody purification and fraction 6 from the anti-DPE2 antibody purification (Figure Appendix 3.2, B). The antibodies are stable at 4°C for 1 week and at -20°C for 3 months. After that time the antibody starts deteriorating and the dilution factor (initially 1:3000 for anti-DPE2 and 1:1000 for anti-MalQ antibody) has to be adjusted to ensure detection of the target protein during immunoblotting.

Bibliography

(HGP), T.H.G.P. (2000) Analysis of the genome sequence of the flowering plant *Arabidopsis thaliana*. *Nature*, **408**, 796-815.

Abdeen, A. and Miki, B. (2009) The pleiotropic effects of the bar gene and glufosinate on the Arabidopsis transcriptome. *Plant Biotechnol J*, **7**, 266-282.

Abe, A., Tonozuka, T., Sakano, Y. and Kamitori, S. (2004) Complex structures of *Thermoactinomyces vulgaris* R-47 alpha-amylase 1 with malto-oligosaccharides demonstrate the role of domain N acting as a starch-binding domain. *J Mol Biol*, **335**, 811-822.

Albenne, C., Skov, L.K., Mirza, O., Gajhede, M., Potocki-Veronese, G., Monsan, P. and Remaud-Simeon, M. (2002) Maltooligosaccharide disproportionation reaction: an intrinsic property of amylosucrase from Neisseria polysaccharea. *FEBS Lett*, **527**, 67-70.

Albrecht, T., Greve, B., Pusch, K., Kossmann, J., Buchner, P., Wobus, U. and Steup, M. (1998) Homodimers and heterodimers of Pho1-type phosphorylase isoforms in Solanum tuberosum L. as revealed by sequence-specific antibodies. *Eur J Biochem*, **251**, 343-352.

Alonso, M.D., Lomako, J., Lomako, W.M. and Whelan, W.J. (1995) A new look at the biogenesis of glycogen. *FASEB J*, **9**, 1126-1137.

Ardila, F.J. and Tandecarz, J.S. (1992) Potato Tuber UDP-Glucose:Protein Transglucosylase Catalyzes Its Own Glucosylation. *Plant Physiol*, **99**, 1342-1347.

Arora, K.K. and Pedersen, P.L. (1995) Glucokinase of Escherichia coli: induction in response to the stress of overexpressing foreign proteins. *Arch Biochem Biophys*, **319**, 574-578.

Ball, S.G. and Morell, M.K. (2003) From bacterial glycogen to starch: understanding the biogenesis of the plant starch granule. *Annu Rev Plant Biol*, **54**, 207-233.

Barends, T.R., Bultema, J.B., Kaper, T., van der Maarel, M.J., Dijkhuizen, L. and Dijkstra, B.W. (2007) Three-way stabilization of the covalent intermediate in amylomaltase, an alpha-amylase-like transglycosylase. *The Journal of biological chemistry*, **282**, 17242-17249.

Barnett, J.A. (1976) The utilization of sugars by yeasts. *Adv Carbohydr Chem Biochem*, **32**, 125-234.

Baroja-Fernandez, E., Munoz, F.J., Zandueta-Criado, A., Moran-Zorzano, M.T., Viale, A.M., Alonso-Casajus, N. and Pozueta-Romero, J. (2004) Most of ADP x glucose linked to starch biosynthesis occurs outside the chloroplast in source leaves. *Proc Natl Acad Sci U S A*, **101**, 13080-13085.

Baunsgaard, L., Lutken, H., Mikkelsen, R., Glaring, M.A., Pham, T.T. and Blennow, A. (2005) A novel isoform of glucan, water dikinase phosphorylates pre-phosphorylated alpha-glucans and is involved in starch degradation in Arabidopsis. *Plant J*, **41**, 595-605.

Beers, E.P., Duke, S.H. and Henson, C.A. (1990) Partial Characterization and Subcellular Localization of Three alpha-Glucosidase Isoforms in Pea (Pisum sativum L.) Seedlings. *Plant Physiol*, **94**, 738-744.

Berger, B., Wilson, D.B., Wolf, E., Tonchev, T., Milla, M. and Kim, P.S. (1995) Predicting coiled coils by use of pairwise residue correlations. *Proc Natl Acad Sci U S A*, **92**, 8259-8263.

Bernard, P., Gabant, P., Bahassi, E.M. and Couturier, M. (1994) Positive-selection vectors using the F plasmid ccdB killer gene. *Gene*, **148**, 71-74.

Bernstein, B.E., Michels, P.A., Kim, H., Petra, P.H. and Hol, W.G. (1998) The importance of dynamic light scattering in obtaining multiple crystal forms of Trypanosoma brucei PGK. *Protein Sci*, **7**, 504-507.

Bollag, D.M., Rozycki, M.D. and Edelstein, S.J. (1996) *Protein Methods* 2 edition edn. New York: Wiley-Liss.

Boos, W. and Shuman, H. (1998) Maltose/maltodextrin system of Escherichia coli: transport, metabolism, and regulation. *Microbiol Mol Biol Rev*, **62**, 204-229.

Bradford, M.M. (1976) A rapid and sensitive method for the quantitation of microgram quantities of protein utilizing the principle of protein-dye binding. *Anal Biochem*, **72**, 248-254.

Buleon, A., Colonna, P., Planchot, V. and Ball, S. (1998) Starch granules: structure and biosynthesis. *Int J Biol Macromol*, **23**, 85-112.

Buleon, A., Gallant, D.J., Bouchet, B., Mouille, G., D'Hulst, C., Kossmann, J. and Ball, S. (1997) Starches from A to C. Chlamydomonas reinhardtii as a model microbial system to investigate the biosynthesis of the plant amylopectin crystal. *Plant Physiol*, **115**, 949-957.

Buttrose, M.S. (1960) Submicroscopic development and structure of starch granules in cereal endosperms. *J Ultrastruct Res*, **4**, 231-257.

Buttrose, M.S. (1962) The influence of environment on the shell structure of starch granules. *J Cell Biol*, **14**, 159-167.

Cantarel, B.L., Coutinho, P.M., Rancurel, C., Bernard, T., Lombard, V. and Henrissat, B. (2009) The Carbohydrate-Active EnZymes database (CAZy): an expert resource for Glycogenomics. *Nucleic Acids Res*, **37**, D233-238.

Caspar, T., Huber, S.C. and Somerville, C. (1985) Alterations in Growth, Photosynthesis, and Respiration in a Starchless Mutant of Arabidopsis thaliana (L.) Deficient in Chloroplast Phosphoglucomutase Activity. *Plant Physiol*, **79**, 11-17.

Cheng, C., Mu, J., Farkas, I., Huang, D., Goebl, M.G. and Roach, P.J. (1995) Requirement of the self-glucosylating initiator proteins Glg1p and Glg2p for glycogen accumulation in Saccharomyces cerevisiae. *Mol Cell Biol*, **15**, 6632-6640.

Cheng, H., Rogers, J.A., Dunham, N.A. and Smithgall, T.E. (1999) Regulation of c-Fes tyrosine kinase and biological activities by N-terminal coiled-coil oligomerization domains. *Mol Cell Biol*, **19**, 8335-8343.

Chia, T., Thorneycroft, D., Chapple, A., Messerli, G., Chen, J., Zeeman, S.C., Smith, S.M. and Smith, A.M. (2004) A cytosolic glucosyltransferase is required for conversion of starch to sucrose in Arabidopsis leaves at night. *Plant J*, **37**, 853-863.

Chilton, M.D., Drummond, M.H., Merio, D.J., Sciaky, D., Montoya, A.L., Gordon, M.P. and Nester, E.W. (1977) Stable incorporation of plasmid DNA into higher plant cells: the molecular basis of crown gall tumorigenesis. *Cell*, **11**, 263-271.

Christiansen, C., Abou Hachem, M., Janecek, S., Vikso-Nielsen, A., Blennow, A. and Svensson, B. (2009a) The carbohydrate-binding module family 20--diversity, structure, and function. *FEBS J*, **276**, 5006-5029.

Christiansen, C., Hachem, M.A., Glaring, M.A., Vikso-Nielsen, A., Sigurskjold, B.W., Svensson, B. and Blennow, A. (2009b) A CBM20 low-affinity starch-binding domain from glucan, water dikinase. *FEBS Lett*, **583**, 1159-1163.

Critchley, J.H., Zeeman, S.C., Takaha, T., Smith, A.M. and Smith, S.M. (2001) A critical role for disproportionating enzyme in starch breakdown is revealed by a knock-out mutation in Arabidopsis. *Plant J*, **26**, 89-100.

Davies, G.J., Wilson, K.S. and Henrissat, B. (1997) Nomenclature for sugar-binding subsites in glycosyl hydrolases. *Biochem J*, **321 (Pt 2)**, 557-559.

Decker, K., Peist, R., Reidl, J., Kossmann, M., Brand, B. and Boos, W. (1993) Maltose and maltotriose can be formed endogenously in Escherichia coli from glucose and glucose-1-phosphate independently of enzymes of the maltose system. *J Bacteriol*, **175**, 5655-5665.

Delgado, I.J., Wang, Z., de Rocher, A., Keegstra, K. and Raikhel, N.V. (1998) Cloning and characterization of AtRGP1. A reversibly autoglycosylated arabidopsis protein implicated in cell wall biosynthesis. *Plant Physiol*, **116**, 1339-1350.

Deschamps, P., Haferkamp, I., d'Hulst, C., Neuhaus, H.E. and Ball, S.G. (2008a) The relocation of starch metabolism to chloroplasts: when, why and how. *Trends Plant Sci*, **13**, 574-582.

Deschamps, P., Moreau, H., Worden, A.Z., Dauvillee, D. and Ball, S.G. (2008b) Early gene duplication within chloroplastida and its correspondence with relocation of starch metabolism to chloroplasts. *Genetics*, **178**, 2373-2387.

Dhugga, K.S., Tiwari, S.C. and Ray, P.M. (1997) A reversibly glycosylated polypeptide (RGP1) possibly involved in plant cell wall synthesis: purification, gene cloning, and trans-Golgi localization. *Proc Natl Acad Sci U S A*, **94**, 7679-7684.

Dippel, R., Bergmiller, T., Bohm, A. and Boos, W. (2005) The maltodextrin system of Escherichia coli: glycogen-derived endogenous induction and osmoregulation. *J Bacteriol*, **187**, 8332-8339.

Dippel, R. and Boos, W. (2005) The maltodextrin system of Escherichia coli: metabolism and transport. *J Bacteriol*, **187**, 8322-8331.

Doyle, E.A., Lane, A.M., Sides, J.M., Mudgett, M.B. and Monroe, J.D. (2007) An alpha-amylase (At4g25000) in Arabidopsis leaves is secreted and induced by biotic and abiotic stress. *Plant, cell & environment*, **30**, 388-398.

Dumez, S., Wattebled, F., Dauvillee, D., Delvalle, D., Planchot, V., Ball, S.G. and D'Hulst, C. (2006) Mutants of Arabidopsis lacking starch branching enzyme II substitute plastidial starch synthesis by cytoplasmic maltose accumulation. *Plant Cell*, **18**, 2694-2709.

Earley, K.W., Haag, J.R., Pontes, O., Opper, K., Juehne, T., Song, K. and Pikaard, C.S. (2006) Gateway-compatible vectors for plant functional genomics and proteomics. *Plant J*, **45**, 616-629.

Edner, C., Li, J., Albrecht, T., Mahlow, S., Hejazi, M., Hussain, H., Kaplan, F., Guy, C., Smith, S.M., Steup, M. and Ritte, G. (2007) Glucan, water dikinase activity stimulates breakdown of starch granules by plastidial beta-amylases. *Plant Physiol*, **145**, 17-28.

Edwards, A., Borthakur, A., Bornemann, S., Venail, J., Denyer, K., Waite, D., Fulton, D., Smith, A. and Martin, C. (1999) Specificity of starch synthase isoforms from potato. *Eur J Biochem*, **266**, 724-736.

Ehrmann, M. and Boos, W. (1987) Identification of endogenous inducers of the mal regulon in Escherichia coli. *J Bacteriol*, **169**, 3539-3545.

Ellis, M., Egelund, J., Schultz, C.J. and Bacic, A. (2010) Arabinogalactan-proteins: key regulators at the cell surface? *Plant Physiol*, **153**, 403-419.

Fettke, J., Chia, T., Eckermann, N., Smith, A. and Steup, M. (2006a) A transglucosidase necessary for starch degradation and maltose metabolism in leaves at night acts on cytosolic heteroglycans (SHG). *Plant J*, **46**, 668-684.

Fettke, J., Eckermann, N., Kotting, O., Ritte, G. and Steup, M. (2006b) Novel starch-related enzymes and carbohydrates. *Cell Mol Biol (Noisy-le-grand)*, **52 Suppl**, OL883-904.

Fettke, J., Eckermann, N., Poeste, S., Pauly, M. and Steup, M. (2004) The glycan substrate of the cytosolic (Pho 2) phosphorylase isozyme from Pisum sativum L.: identification, linkage analysis and subcellular localization. *Plant J*, **39**, 933-946.

Fettke, J., Eckermann, N., Tiessen, A., Geigenberger, P. and Steup, M. (2005a) Identification, subcellular localization and biochemical characterization of water-soluble heteroglycans (SHG) in leaves of Arabidopsis thaliana L.: distinct SHG reside in the cytosol and in the apoplast. *Plant J*, **43**, 568-585.

Fettke, J., Hejazi, M., Smirnova, J., Hochel, E., Stage, M. and Steup, M. (2009a) Eukaryotic starch degradation: integration of plastidial and cytosolic pathways. *J Exp Bot*, **60**, 2907-2922.

Fettke, J., Malinova, I., Eckermann, N. and Steup, M. (2009b) Cytosolic heteroglycans in photoautotrophic and in heterotrophic plant cells. *Phytochemistry*, **70**, 696-702.

Fettke, J., Nunes-Nesi, A., Alpers, J., Szkop, M., Fernie, A.R. and Steup, M. (2008) Alterations in cytosolic glucose-phosphate metabolism affect structural features and biochemical properties of starch-related heteroglycans. *Plant Physiol*, **148**, 1614-1629.

Fettke, J., Nunes-Nesi, A., Fernie, A.R. and Steup, M. (2010) Identification of a novel heteroglycan-interacting protein, HIP 1.3, from Arabidopsis thaliana. *J Plant Physiol*, **168**, 1415-1425.

Fettke, J., Poeste, S., Eckermann, N., Tiessen, A., Pauly, M., Geigenberger, P. and Steup, M. (2005b) Analysis of cytosolic heteroglycans from leaves of transgenic potato (Solanum tuberosum L.) plants that under- or overexpress the Pho 2 phosphorylase isozyme. *Plant Cell Physiol*, **46**, 1987-2004.

Frandsen, T.P., Lok, F., Mirgorodskaya, E., Roepstorff, P. and Svensson, B. (2000) Purification, enzymatic characterization, and nucleotide sequence of a high-isoelectric-point alpha-glucosidase from barley malt. *Plant Physiol*, **123**, 275-286.

Fujii, K., Minagawa, H., Terada, Y., Takaha, T., Kuriki, T., Shimada, J. and Kaneko, H. (2005) Use of random and saturation mutageneses to improve the properties of Thermus aquaticus amylomaltase for efficient production of cycloamyloses. *Appl Environ Microbiol*, **71**, 5823-5827.

Fulton, D.C., Stettler, M., Mettler, T., Vaughan, C.K., Li, J., Francisco, P., Gil, M., Reinhold, H., Eicke, S., Messerli, G., Dorken, G., Halliday, K., Smith, A.M., Smith, S.M. and Zeeman, S.C. (2008) Beta-AMYLASE4, a noncatalytic protein required for starch breakdown, acts upstream of three active beta-amylases in Arabidopsis chloroplasts. *Plant Cell*, **20**, 1040-1058.

Gallagher, S.R. (2001) One-dimensional electrophoresis using nondenaturing conditions. *Curr Protoc Protein Sci*, **Chapter 10**, Unit 10 13.

Gibon, Y., Blasing, O.E., Palacios-Rojas, N., Pankovic, D., Hendriks, J.H., Fisahn, J., Hohne, M., Gunther, M. and Stitt, M. (2004) Adjustment of diurnal starch turnover to short days: depletion of sugar during the night leads to a temporary inhibition of carbohydrate utilization, accumulation of sugars and post-translational activation of ADP-glucose pyrophosphorylase in the following light period. *Plant J*, **39**, 847-862.

Gillmor, C.S., Poindexter, P., Lorieau, J., Palcic, M.M. and Somerville, C. (2002) Alpha-glucosidase I is required for cellulose biosynthesis and morphogenesis in Arabidopsis. *J Cell Biol*, **156**, 1003-1013.

Glaring, M.A., Baumann, M.J., Abou Hachem, M., Nakai, H., Nakai, N., Santelia, D., Sigurskjold, B.W., Zeeman, S.C., Blennow, A. and Svensson, B. (2011) Starch-binding domains in the CBM45 family--low-affinity domains from glucan, water dikinase and alpha-amylase involved in plastidial starch metabolism. *FEBS J*, **278**, 1175-1185.

Graf, A., Schlereth, A., Stitt, M. and Smith, A.M. (2010) Circadian control of carbohydrate availability for growth in Arabidopsis plants at night. *Proc Natl Acad Sci U S A*, **107**, 9458-9463.

Gruber, M., Soding, J. and Lupas, A.N. (2006) Comparative analysis of coiled-coil prediction methods. *J Struct Biol*, **155**, 140-145.

Hammond, J.B. and Preiss, J. (1983) Spinach Leaf Intra and Extra Chloroplast Phosphorylase Activities during Growth. *Plant Physiol*, **73**, 709-712.

Hanahan, D. (1983) Studies on transformation of Escherichia coli with plasmids. *Journal of molecular biology*, **166**, 557-580.

Hargreaves, J.A. and ap Rees, T. (1988) Turnover of starch and sucrose in the roots of *Pisum sativum. Phytochemistry*, **27**, 1627-1629.

Haselbarth, V., Schulz, G.V. and Schwinn, H. (1971) [Studies on amylomaltase. II. Molecular constants and activity of the enzyme]. *Biochim Biophys Acta*, **227**, 296-312.

Henrissat, B. and Davies, G.J. (2000) Glycoside hydrolases and glycosyltransferases. Families, modules, and implications for genomics. *Plant Physiol*, **124**, 1515-1519.

Hoiczyk, E. (1998) Structural and biochemical analysis of the sheath of Phormidium uncinatum. *J Bacteriol*, **180**, 3923-3932.

Hussain, H., Mant, A., Seale, R., Zeeman, S., Hinchliffe, E., Edwards, A., Hylton, C., Bornemann, S., Smith, A.M., Martin, C. and Bustos, R. (2003) Three isoforms of isoamylase contribute different catalytic properties for the debranching of potato glucans. *Plant Cell*, **15**, 133-149.

Iglesias, N., Abelenda, J.A., Rodino, M., Sampedro, J., Revilla, G. and Zarra, I. (2006) Apoplastic glycosidases active against xyloglucan oligosaccharides of Arabidopsis thaliana. *Plant Cell Physiol*, **47**, 55-63.

Izawa, H., Nawaji, M., Kaneko, Y. and Kadokawa, J. (2009) Preparation of glycogen-based polysaccharide materials by phosphorylase-catalyzed chain elongation of glycogen. *Macromol Biosci*, **9**, 1098-1104.

Janecek, S., Svensson, B. and MacGregor, E.A. (2007) A remote but significant sequence homology between glycoside hydrolase clan GH-H and family GH31. *FEBS Lett*, **581**, 1261-1268.

Jang, J.C. and Sheen, J. (1994) Sugar sensing in higher plants. *Plant Cell*, **6**, 1665-1679.

Jenkins, P.J. and Donald, A.M. (1995) The influence of amylose on starch granule structure. *Int J Biol Macromol*, **17**, 315-321.

Kaper, T., Leemhuis, H., Uitdehaag, J.C., van der Veen, B.A., Dijkstra, B.W., van der Maarel, M.J. and Dijkhuizen, L. (2007) Identification of acceptor substrate binding subsites +2 and +3 in the amylomaltase from Thermus thermophilus HB8. *Biochemistry*, **46**, 5261-5269.

Kaper, T., Talik, B., Ettema, T.J., Bos, H., van der Maarel, M.J. and Dijkhuizen, L. (2005) Amylomaltase of Pyrobaculum aerophilum IM2 produces thermoreversible starch gels. *Appl Environ Microbiol*, **71**, 5098-5106.

Knappe, S., Flugge, U.I. and Fischer, K. (2003) Analysis of the plastidic phosphate translocator gene family in Arabidopsis and identification of new phosphate translocator-homologous transporters, classified by their putative substrate-binding site. *Plant Physiol*, **131**, 1178-1190.

Kotting, O., Santelia, D., Edner, C., Eicke, S., Marthaler, T., Gentry, M.S., Comparot-Moss, S., Chen, J., Smith, A.M., Steup, M., Ritte, G. and Zeeman, S.C. (2009) STARCH-EXCESS4 is a laforin-like Phosphoglucan phosphatase required for starch degradation in Arabidopsis thaliana. *Plant Cell*, **21**, 334-346.

Kuriki, T. and Imanaka, T. (1999) The concept of the alpha-amylase family: structural similarity and common catalytic mechanism. *J Biosci Bioeng*, **87**, 557-565.

Laemmli, U.K. (1970) Cleavage of structural proteins during the assembly of the head of bacteriophage T4. *Nature*, **227**, 680-685.

Lammerts van Bueren, A., Ficko-Blean, E., Pluvinage, B., Hehemann, J.H., Higgins, M.A., Deng, L., Ogunniyi, A.D., Stroeher, U.H., El Warry, N., Burke, R.D., Czjzek, M., Paton, J.C., Vocadlo, D.J. and Boraston, A.B. (2011) The conformation and function of a multimodular glycogen-degrading pneumococcal virulence factor. *Structure*, **19**, 640-651.

Langeveld, S.M. (2002) Glucosylation activity and complex formation of two classes of reversibly glycosylated polypeptides. *Plant Physiol*, **129**, 278-289.

Lavintman, N. and Cardini, C.E. (1973) Particulate UDP-glucose: Protein transglucosylase from potato tuber. *FEBS Lett*, **29**, 43-46.

Lavintman, N., Tandecarz, J., Carceller, M., Mendiara, S. and Cardini, C.E. (1974) Role of uridine diphosphate glucose in the biosynthesis of starch. Mechanism of formation and enlargement of a glucoproteic acceptor. *Eur J Biochem*, **50**, 145-155.

Le Breton, Y., Pichereau, V., Sauvageot, N., Auffray, Y. and Rince, A. (2005) Maltose utilization in Enterococcus faecalis. *J Appl Microbiol*, **98**, 806-813.

Leemhuis, H., Dijkstra, B.W. and Dijkhuizen, L. (2002) Mutations converting cyclodextrin glycosyltransferase from a transglycosylase into a starch hydrolase. *FEBS Lett*, **514**, 189-192.

Leloir, L.F., De Fekete, M.A. and Cardini, C.E. (1961) Starch and oligosaccharide synthesis from uridine diphosphate glucose. *The Journal of biological chemistry*, **236**, 636-641.

Lengsfeld, C., Schonert, S., Dippel, R. and Boos, W. (2009) Glucose- and glucokinase-controlled mal gene expression in Escherichia coli. *J Bacteriol*, **191**, 701-712.

Leterrier, M., Holappa, L.D., Broglie, K.E. and Beckles, D.M. (2008) Cloning, characterisation and comparative analysis of a starch synthase IV gene in wheat: functional and evolutionary implications. *BMC Plant Biol*, **8**, 98.

Levander, F., Andersson, U. and Radstrom, P. (2001) Physiological role of beta-phosphoglucomutase in Lactococcus lactis. *Appl Environ Microbiol*, **67**, 4546-4553.

Li, T., Xu, S.L., Oses-Prieto, J.A., Putil, S., Xu, P., Wang, R.J., Li, K.H., Maltby, D.A., An, L.H., Burlingame, A.L., Deng, Z.P. and Wang, Z.Y. Proteomics analysis reveals post-translational mechanisms for cold-induced metabolic changes in Arabidopsis. *Mol Plant*, **4**, 361-374.

Li, T., Xu, S.L., Oses-Prieto, J.A., Putil, S., Xu, P., Wang, R.J., Li, K.H., Maltby, D.A., An, L.H., Burlingame, A.L., Deng, Z.P. and Wang, Z.Y. (2011) Proteomics analysis reveals post-translational mechanisms for cold-induced metabolic changes in Arabidopsis. *Mol Plant*, **4**, 361-374.

Lin, T.P., Caspar, T., Somerville, C.R. and Preiss, J. (1988a) A Starch Deficient Mutant of Arabidopsis thaliana with Low ADPglucose Pyrophosphorylase Activity Lacks One of the Two Subunits of the Enzyme. *Plant Physiol*, **88**, 1175-1181.

Lin, T.P., Spilatro, S.R. and Preiss, J. (1988b) Subcellular localization and characterization of amylases in Arabidopsis leaf. *Plant Physiol*, **86**, 251-259.

Lindeboom, N. (2004) Analytical, Biochemical and Physicochemical Aspects of Starch Granule Size, with Emphasis on Small Granule Starches: A Review. *Starch - Stärke*, **56**, 88-99.

Lloyd, J.R., Blennow, A., Burhenne, K. and Kossmann, J. (2004) Repression of a novel isoform of disproportionating enzyme (stDPE2) in potato leads to inhibition of starch degradation in leaves but not tubers stored at low temperature. *Plant Physiol*, **134**, 1347-1354.

Lloyd, J.R., Landschutze, V. and Kossmann, J. (1999) Simultaneous antisense inhibition of two starch-synthase isoforms in potato tubers leads to accumulation of grossly modified amylopectin. *Biochem J*, **338 (Pt 2)**, 515-521.

Lomako, J., Lomako, W.M. and Whelan, W.J. (1992) The substrate specificity of isoamylase and the preparation of apo-glycogenin. *Carbohydr Res*, **227**, 331-338.

Lomako, J., Lomako, W.M., Whelan, W.J., Dombro, R.S., Neary, J.T. and Norenberg, M.D. (1993) Glycogen synthesis in the astrocyte: from glycogenin to proglycogen to glycogen. *FASEB J*, **7**, 1386-1393.

Lu, Y. and Sharkey, T.D. (2004) The role of amylomaltase in maltose metabolism in the cytosol of photosynthetic cells. *Planta*, **218**, 466-473.

Lu, Y. and Sharkey, T.D. (2006) The importance of maltose in transitory starch breakdown. *Plant, cell & environment*, **29**, 353-366.

Lu, Y., Steichen, J.M., Weise, S.E. and Sharkey, T.D. (2006a) Cellular and organ level localization of maltose in maltose-excess Arabidopsis mutants. *Planta*, **224**, 935-943.

Lu, Y., Steichen, J.M., Yao, J. and Sharkey, T.D. (2006b) The role of cytosolic alpha-glucan phosphorylase in maltose metabolism and the comparison of amylomaltase in Arabidopsis and Escherichia coli. *Plant Physiol*, **142**, 878-889.

Ludewig, F., Sonnewald, U., Kauder, F., Heineke, D., Geiger, M., Stitt, M., Muller-Rober, B.T., Gillissen, B., Kuhn, C. and Frommer, W.B. (1998) The role of transient starch in acclimation to elevated atmospheric CO2. *FEBS Lett*, **429**, 147-151.

Lupas, A. (1996) Prediction and analysis of coiled-coil structures. *Methods Enzymol*, **266**, 513-525.

Lutken, H., Lloyd, J.R., Glaring, M.A., Baunsgaard, L., Laursen, K.H., Haldrup, A., Kossmann, J. and Blennow, A. (2010) Repression of both isoforms of disproportionating enzyme leads to higher malto-oligosaccharide content and reduced growth in potato. *Planta*, **232**, 1127-1139.

MacGregor, E.A., Janecek, S. and Svensson, B. (2001) Relationship of sequence and structure to specificity in the alpha-amylase family of enzymes. *Biochim Biophys Acta*, **1546**, 1-20.

Machovic, M., Svensson, B., MacGregor, E.A. and Janecek, S. (2005) A new clan of CBM families based on bioinformatics of starch-binding domains from families CBM20 and CBM21. *FEBS J*, **272**, 5497-5513.

Malinova, I., Steup, M. and Fettke, J. Starch-related cytosolic heteroglycans in roots from Arabidopsis thaliana. *J Plant Physiol*.

Malinova, I., Steup, M. and Fettke, J. (2011) Starch-related carbon fluxes in roots and leaves of Arabidopsis thaliana. *Plant Signal Behav*, **6**.

Marianayagam, N.J., Sunde, M. and Matthews, J.M. (2004) The power of two: protein dimerization in biology. *Trends Biochem Sci*, **29**, 618-625.

Martin, S.A. and Russell, J.B. (1987) Transport and phosphorylation of disaccharides by the ruminal bacterium Streptococcus bovis. *Appl Environ Microbiol*, **53**, 2388-2393.

Mason, J.M. and Arndt, K.M. (2004) Coiled coil domains: stability, specificity, and biological implications. *Chembiochem*, **5**, 170-176.

Matheson (1996) The chemical structure of amylose and amylopectin fractions of starch from tobacco leaves during development and diurnally-nocturnally. *Carbohydrate Res*, **282**, 247-262.

McCallum, C.M., Comai, L., Greene, E.A. and Henikoff, S. (2000) Targeting induced local lesions IN genomes (TILLING) for plant functional genomics. *Plant Physiol*, **123**, 439-442.

McFadden, G.I. (1999) Endosymbiosis and evolution of the plant cell. *Curr Opin Plant Biol*, **2**, 513-519.

Meyerowitz, E.M. (2001) Prehistory and history of Arabidopsis research. *Plant Physiol*, **125**, 15-19.

Moller, I., Sorensen, I., Bernal, A.J., Blaukopf, C., Lee, K., Obro, J., Pettolino, F., Roberts, A., Mikkelsen, J.D., Knox, J.P., Bacic, A. and Willats, W.G. (2007) High-throughput mapping of cell-wall polymers within and between plants using novel microarrays. *Plant J*, **50**, 1118-1128.

Munoz, F.J., Baroja-Fernandez, E., Moran-Zorzano, M.T., Alonso-Casajus, N. and Pozueta-Romero, J. (2006) Cloning, expression and characterization of a Nudix hydrolase that catalyzes the hydrolytic breakdown of ADP-glucose linked to starch biosynthesis in Arabidopsis thaliana. *Plant Cell Physiol*, **47**, 926-934.

Nahoum, V., Roux, G., Anton, V., Rouge, P., Puigserver, A., Bischoff, H., Henrissat, B. and Payan, F. (2000) Crystal structures of human pancreatic alpha-amylase in complex with carbohydrate and proteinaceous inhibitors. *Biochem J*, **346 Pt 1**, 201-208.

Nakai, H., Dilokpimol, A., Abou Hachem, M. and Svensson, B. (2010) Efficient one-pot enzymatic synthesis of alpha-(1-->4)-glucosidic disaccharides through a coupled reaction catalysed by Lactobacillus acidophilus NCFM maltose phosphorylase. *Carbohydr Res*, **345**, 1061-1064.

Nakamura, T., Yamamori, M., Hirano, H., Hidaka, S. and Nagamine, T. (1995) Production of waxy (amylose-free) wheats. *Mol Gen Genet*, **248**, 253-259.

Nielsen, T.H., Rung, J.H. and Villadsen, D. (2004) Fructose-2,6-bisphosphate: a traffic signal in plant metabolism. *Trends Plant Sci*, **9**, 556-563.

Niittyla, T., Messerli, G., Trevisan, M., Chen, J., Smith, A.M. and Zeeman, S.C. (2004) A previously unknown maltose transporter essential for starch degradation in leaves. *Science (New York, N.Y*, **303**, 87-89.

Nozue, K. and Maloof, J.N. (2006) Diurnal regulation of plant growth. *Plant, cell & environment*, **29**, 396-408.

Oakley, M.T., Bulheller, B.M. and Hirst, J.D. (2006) First-principles calculations of protein circular dichroism in the far-ultraviolet and beyond. *Chirality*, **18**, 340-347.

Okita, T.W., Greenberg, E., Kuhn, D.N. and Preiss, J. (1979) Subcellular localization of the starch degradative and biosynthetic enzymes of spinach leaves. *Plant Physiol*, **64**, 187-192.

Palmer, T.N., Ryman, B.E. and Whelan, W.J. (1976) The action pattern of amylomaltase from Escherichia coli. *Eur J Biochem*, **69**, 105-115.

Park, J.T., Shim, J.H., Tran, P.L., Hong, I.H., Yong, H.U., Oktavina, E.F., Nguyen, H.D., Kim, J.W., Lee, T.S., Park, S.H., Boos, W. and Park, K.H. (2011) Role of maltose enzymes in glycogen synthesis by Escherichia coli. *J Bacteriol*, **193**, 2517-2526.

Pitcher, J., Smythe, C., Campbell, D.G. and Cohen, P. (1987) Identification of the 38-kDa subunit of rabbit skeletal muscle glycogen synthase as glycogenin. *Eur J Biochem*, **169**, 497-502.

Przylas, I., Terada, Y., Fujii, K., Takaha, T., Saenger, W. and Strater, N. (2000a) X-ray structure of acarbose bound to amylomaltase from Thermus aquaticus. Implications for the synthesis of large cyclic glucans. *Eur J Biochem*, **267**, 6903-6913.

Przylas, I., Tomoo, K., Terada, Y., Takaha, T., Fujii, K., Saenger, W. and Strater, N. (2000b) Crystal structure of amylomaltase from thermus aquaticus, a glycosyltransferase catalysing the production of large cyclic glucans. *J Mol Biol*, **296**, 873-886.

Pugsley, A.P. and Dubreuil, C. (1988) Molecular characterization of malQ, the structural gene for the Escherichia coli enzyme amylomaltase. *Mol Microbiol*, **2**, 473-479.

Recondo, E. and Leloir, L.F. (1961) Adenosine diphosphate glucose and starch synthesis. *Biochem Biophys Res Commun*, **6**, 85-88.

Rees, N.J.K.a.T. (1983, b) Maltose metabolism by pea chloroplasts. *Planta*, **158**, 179-184.

Reinhold, H., Soyk, S., Simkova, K., Hostettler, C., Marafino, J., Mainiero, S., Vaughan, C.K., Monroe, J.D. and Zeeman, S.C. (2011) beta-amylase-like proteins function as transcription factors in Arabidopsis, controlling shoot growth and development. *Plant Cell*, **23**, 1391-1403.

Reissner, K.J. and Aswad, D.W. (2003) Deamidation and isoaspartate formation in proteins: unwanted alterations or surreptitious signals? *Cell Mol Life Sci*, **60**, 1281-1295.

Ritte, G., Heydenreich, M., Mahlow, S., Haebel, S., Kotting, O. and Steup, M. (2006) Phosphorylation of C6- and C3-positions of glucosyl residues in starch is catalysed by distinct dikinases. *FEBS Lett*, **580**, 4872-4876.

Ritte, G., Lloyd, J.R., Eckermann, N., Rottmann, A., Kossmann, J. and Steup, M. (2002) The starch-related R1 protein is an alpha -glucan, water dikinase. *Proc Natl Acad Sci U S A*, **99**, 7166-7171.

Roldan, I., Wattebled, F., Mercedes Lucas, M., Delvalle, D., Planchot, V., Jimenez, S., Perez, R., Ball, S., D'Hulst, C. and Merida, A. (2007) The phenotype of soluble starch synthase IV defective mutants of Arabidopsis thaliana suggests a novel function of elongation enzymes in the control of starch granule formation. *Plant J*, **49**, 492-504.

Sanger, F., Nicklen, S. and Coulson, A.R. (1977) DNA sequencing with chain-terminating inhibitors. *Proceedings of the National Academy of Sciences of the United States of America*, **74**, 5463-5467.

Schulze, W., Stitt, M., Schulze, E.D., Neuhaus, H.E. and Fichtner, K. (1991) A Quantification of the Significance of Assimilatory Starch for Growth of Arabidopsis thaliana L. Heynh. *Plant Physiol*, **95**, 890-895.

Schupp, N. and Ziegler, P. (2004) The relation of starch phosphorylases to starch metabolism in wheat. *Plant Cell Physiol*, **45**, 1471-1484.

Shure, M., Wessler, S. and Fedoroff, N. (1983) Molecular identification and isolation of the Waxy locus in maize. *Cell*, **35**, 225-233.

Singh, D.G., Lomako, J., Lomako, W.M., Whelan, W.J., Meyer, H.E., Serwe, M. and Metzger, J.W. (1995) beta-Glucosylarginine: a new glucose-protein bond in a self-glucosylating protein from sweet corn. *FEBS Lett*, **376**, 61-64.

Sivak, M.N., Wagner, M. and Preiss, J. (1993) Biochemical Evidence for the Role of the Waxy Protein from Pea (Pisum sativum L.) as a Granule-Bound Starch Synthase. *Plant Physiol*, **103**, 1355-1359.

Skurat, A.V., Dietrich, A.D. and Roach, P.J. (2006) Interaction between glycogenin and glycogen synthase. *Arch Biochem Biophys*, **456**, 93-97.

Smith, A.M., Denyer, K. and Martin, C.R. (1995) What Controls the Amount and Structure of Starch in Storage Organs? *Plant Physiol*, **107**, 673-677.

Smith, A.M. and Stitt, M. (2007) Coordination of carbon supply and plant growth. *Plant, cell & environment*, **30**, 1126-1149.

Smythe, C. and Cohen, P. (1991) The discovery of glycogenin and the priming mechanism for glycogen biogenesis. *Eur J Biochem*, **200**, 625-631.

Sonnhammer, E.L., Eddy, S.R. and Durbin, R. (1997) Pfam: a comprehensive database of protein domain families based on seed alignments. *Proteins*, **28**, 405-420.

Sorensen, I., Pedersen, H.L. and Willats, W.G. (2009) An array of possibilities for pectin. *Carbohydr Res*, **344**, 1872-1878.

Stanley, D., Rejzek, M., Naested, H., Smedley, M., Otero, S., Fahy, B., Thorpe, F., Nash, R.J., Harwood, W., Svensson, B., Denyer, K., Field, R.A. and Smith, A.M. (2011) The role of alpha-glucosidase in germinating barley grains. *Plant Physiol*, **155**, 932-943.

Steichen, J.M., Petty, R.V. and Sharkey, T.D. (2008) Domain characterization of a 4-alpha-glucanotransferase essential for maltose metabolism in photosynthetic leaves. *The Journal of biological chemistry*, **283**, 20797-20804.

Steup, M. (1981) Purification of chloroplast alpha-1,4-glucan phosphorylase from spinach leaves by chromatography on Sepharose-bound starch. *Biochim Biophys Acta*, **659**, 123-131.

Stitt, M., Bulpin, P.V. and ap Rees, T. (1978) Pathway of starch breakdown in photosynthetic tissues of Pisum sativum. *Biochim Biophys Acta*, **544**, 200-214.

Stitt, M. and Heldt, H.W. (1981) Physiological rates of starch breakdown in isolated intact spinach chloroplasts. *Plant Physiol*, **68**, 755-761.

Streb, S., Delatte, T., Umhang, M., Eicke, S., Schorderet, M., Reinhardt, D. and Zeeman, S.C. (2008) Starch granule biosynthesis in Arabidopsis is abolished by removal of all debranching enzymes but restored by the subsequent removal of an endoamylase. *Plant Cell*, **20**, 3448-3466.

Szmelcman, S., Schwartz, M., Silhavy, T.J. and Boos, W. (1976) Maltose transport in Escherichia coli K12. A comparison of transport kinetics in wild-type and lambda-resistant mutants as measured by fluorescence quenching. *Eur J Biochem*, **65**, 13-19.

Szydlowski, N., Ragel, P., Raynaud, S., Lucas, M.M., Roldan, I., Montero, M., Munoz, F.J., Ovecka, M., Bahaji, A., Planchot, V., Pozueta-Romero, J., D'Hulst, C. and Merida,

A. (2009) Starch granule initiation in Arabidopsis requires the presence of either class IV or class III starch synthases. *Plant Cell*, **21**, 2443-2457.

Tachibana, Y., Takaha, T., Fujiwara, S., Takagi, M. and Imanaka, T. (2000) Acceptor specificity of 4-alpha-glucanotransferase from Pyrococcus kodakaraensis KOD1, and synthesis of cycloamylose. *J Biosci Bioeng*, **90**, 406-409.

Taira, T., Uematsu, M., Nakano, Y. and Morikawa, T. (1991) Molecular identification and comparison of the starch synthase bound to starch granules between endosperm and leaf blades in rice plants. *Biochem Genet*, **29**, 301-311.

Thoma, J.A. and Koshland, D.E., Jr. (1960) Stereochemistry of enzyme, substrate, and products during beta-amylase action. *The Journal of biological chemistry*, **235**, 2511-2517.

Thompson, J., Gentry-Weeks, C.R., Nguyen, N.Y., Folk, J.E. and Robrish, S.A. (1995) Purification from Fusobacterium mortiferum ATCC 25557 of a 6-phosphoryl-O-alpha-D-glucopyranosyl:6-phosphoglucohydrolase that hydrolyzes maltose 6-phosphate and related phospho-alpha-D-glucosides. *J Bacteriol*, **177**, 2505-2512.

Tonozuka, T., Ohtsuka, M., Mogi, S., Sakai, H., Ohta, T. and Sakano, Y. (1993) A neopullulanase-type alpha-amylase gene from Thermoactinomyces vulgaris R-47. *Biosci Biotechnol Biochem*, **57**, 395-401.

Usadel, B., Blasing, O.E., Gibon, Y., Retzlaff, K., Hohne, M., Gunther, M. and Stitt, M. (2008) Global transcript levels respond to small changes of the carbon status during progressive exhaustion of carbohydrates in Arabidopsis rosettes. *Plant Physiol*, **146**, 1834-1861.

van de Velde, F., Peppelman, H.A., Rollema, H.S. and Tromp, R.H. (2001) On the structure of kappa/iota-hybrid carrageenans. *Carbohydr Res*, **331**, 271-283.

van de Velde, F., Rollema, H.S., Grinberg, N.V., Burova, T.V., Grinberg, V.Y. and Tromp, R.H. (2002) Coil-helix transition of iota-carrageenan as a function of chain regularity. *Biopolymers*, **65**, 299-312.

van der Leij, F.R., Visser, R.G., Ponstein, A.S., Jacobsen, E. and Feenstra, W.J. (1991) Sequence of the structural gene for granule-bound starch synthase of potato (Solanum tuberosum L.) and evidence for a single point deletion in the amf allele. *Mol Gen Genet*, **228**, 240-248.

Van Larebeke, N., Zaenen, I., Teuchy, H. and Schell, J. (1973) Circular DNA plasmids in Agrobacterium strains. Investigation of their role in the induction of crown-gall tumors. *Archives internationales de physiologie et de biochimie*, **81**, 986.

Wang, Q., Monroe, J. and Sjolund, R.D. (1995) Identification and characterization of a phloem-specific beta-amylase. *Plant Physiol*, **109**, 743-750.

Wattebled, F., Dong, Y., Dumez, S., Delvalle, D., Planchot, V., Berbezy, P., Vyas, D., Colonna, P., Chatterjee, M., Ball, S. and D'Hulst, C. (2005) Mutants of Arabidopsis lacking a chloroplastic isoamylase accumulate phytoglycogen and an abnormal form of amylopectin. *Plant Physiol*, **138**, 184-195.

Weber, A., Servaites, J.C., Geiger, D.R., Kofler, H., Hille, D., Groner, F., Hebbeker, U. and Flugge, U.I. (2000) Identification, purification, and molecular cloning of a putative plastidic glucose translocator. *Plant Cell*, **12**, 787-802.

Weise, S.E., Kim, K.S., Stewart, R.P. and Sharkey, T.D. (2005) beta-Maltose is the metabolically active anomer of maltose during transitory starch degradation. *Plant Physiol*, **137**, 756-761.

Weise, S.E., Weber, A.P. and Sharkey, T.D. (2004) Maltose is the major form of carbon exported from the chloroplast at night. *Planta*, **218**, 474-482.

Whelan, W.J. (1998) Pride and prejudice: the discovery of the primer for glycogen synthesis. *Protein Sci*, **7**, 2038-2041.

Whitmore, L. and Wallace, B.A. (2004) DICHROWEB, an online server for protein secondary structure analyses from circular dichroism spectroscopic data. *Nucl. Acids Res.*, **32**, W668-673.

Whitmore, L. and Wallace, B.A. (2008) Protein secondary structure analyses from circular dichroism spectroscopy: methods and reference databases. *Biopolymers*, **89**, 392-400.

Wiesmeyer, H. and Cohn, M. (1960) The characterization of the pathway of maltose utilization by Escherichia coli. II. General properties and mechanism of action of amylomaltase. *Biochim Biophys Acta*, **39**, 427-439.

Yariv, J., Lis, H. and Katchalski, E. (1967) Precipitation of arabic acid and some seed polysaccharides by glycosylphenylazo dyes. *Biochem J*, **105**, 1C-2C.

Yu, T.S., Kofler, H., Hausler, R.E., Hille, D., Flugge, U.I., Zeeman, S.C., Smith, A.M., Kossmann, J., Lloyd, J., Ritte, G., Steup, M., Lue, W.L., Chen, J. and Weber, A. (2001) The Arabidopsis sex1 mutant is defective in the R1 protein, a general regulator of starch degradation in plants, and not in the chloroplast hexose transporter. *Plant Cell*, **13**, 1907-1918.

Yu, T.S., Lue, W.L., Wang, S.M. and Chen, J. (2000) Mutation of Arabidopsis plastid phosphoglucose isomerase affects leaf starch synthesis and floral initiation. *Plant Physiol*, **123**, 319-326.

Zeeman, S.C., Kossmann, J. and Smith, A.M. (2010) Starch: its metabolism, evolution, and biotechnological modification in plants. *Annu Rev Plant Biol*, **61**, 209-234.

Zeeman, S.C., Northrop, F., Smith, A.M. and Rees, T. (1998a) A starch-accumulating mutant of Arabidopsis thaliana deficient in a chloroplastic starch-hydrolysing enzyme. *Plant J*, **15**, 357-365.

Zeeman, S.C., Smith, S.M. and Smith, A.M. (2007) The diurnal metabolism of leaf starch. *Biochem J*, **401**, 13-28.

Zeeman, S.C., Tiessen, A., Pilling, E., Kato, K.L., Donald, A.M. and Smith, A.M. (2002) Starch synthesis in Arabidopsis. Granule synthesis, composition, and structure. *Plant Physiol*, **129**, 516-529.

Zeeman, S.C., Umemoto, T., Lue, W.L., Au-Yeung, P., Martin, C., Smith, A.M. and Chen, J. (1998b) A mutant of Arabidopsis lacking a chloroplastic isoamylase accumulates both starch and phytoglycogen. *Plant Cell*, **10**, 1699-1712.

Zhang, X., Szydlowski, N., Delvalle, D., D'Hulst, C., James, M.G. and Myers, A.M. (2008) Overlapping functions of the starch synthases SSII and SSIII in amylopectin biosynthesis in Arabidopsis. *BMC Plant Biol*, **8**, 96.

Ziegler, P. and Beck, E. (1986) Exoamylase activity in vacuoles isolated from pea and wheat leaf protoplasts. *Plant Physiol*, **82**, 1119-1121.